Examination of molecular hydrogen (H$_2$) treatment and electromagnetic field (EMF) radiation effects on the growth of animal (zebrafish embryos) and plant (*Chlorella vulgaris*)

Zur Erlangung des akademischen Grades eines

DOKTORS DER NATURWISSENSCHAFTEN

(Dr. rer. Nat.)

von der KIT-Fakultät für Chemie und Biowissenschaften

des Karlsruher Instituts für Technologie (KIT)

KIT

Karlsruher Institut für Technologie

genehmigte

DISSERTATION

von

M. Sc. Rajalakshmi Punampalam

aus

Ipoh, Malaysia

Karlsruhe 2022

Dekan: Prof. Dr. Hans-Achim Wagenknecht
Referent: Prof. Dr. Anne S. Ulrich
Korreferent: Prof. Dr. Martin Bastmeyer
Tag der mündlichen Prüfung: 24.10.2022

Declaration

This work was carried out in the working group of Prof. Dr. Anne S. Ulrich at the Karlsruhe Institute of Technology (KIT), Institute of Organic Chemistry (Chair of Biochemistry) in the period from September 2019 to September 2022.

I hereby truthfully affirm that I have written this thesis independently, I have indicated all the aids used completely and accurately, I have marked everything that has been taken unchanged or with modifications from the work of others, and I have observed the KIT Rules for Safeguarding Good Scientific Practice as amended from time to time. Furthermore, I assure that the electronic version of this work corresponds to the written version and that the delivery and archiving of the primary data is secured at the Institute according to paragraph A (6) of the KIT Rules for Assuring Good Scientific Practice. This thesis has not been submitted in the same or similar form to any other examination authority.

Karlsruhe, 14th September 2022

Acknowledgements

List of abbreviations

2PG	Phosphoglycolate/ glycolate 2-phosphate
3PGA	Phosphoglycerate/ glycerate 3-phosphate
AC	Alternating current
ATP	Adenosine triphosphate
CAT	Catalase
CHT	Caudal hematopoietic tissue
COVID-19	Coronavirus disease 2019
DC	Direct current
dpf	Day(s) post-fertilization
ECM	Extracellular matrix
EMF	Electromagnetic field
GSH-Px/GPx	Glutathione peroxidase
HO-1	Heme oxygenase-1
hpa	Hour(s) post-amputation
hpf	Hour(s) post-fertilization
Lyz:DsRed	Lysozyme promoter gene: Discosoma species derived red fluorescent protein
NADPH	Nicotinamide adenine dinucleotide phosphate
NOX2	NADPH oxidase 2
RF	Radio-frequency
RFP	Red fluorescent protein
RNS	Reactive nitrogen species
ROS	Reactive oxygen species
RuBisCO	Ribulose-1,5-bisphosphate (rubp) carboxylase-oxygenase
SOD	Superoxide dismutase
WLAN	Wireless local area networks

List of figures

List of tables

Table of contents

1. Introduction

1.1 Introduction to molecular hydrogen

Hydrogen is a colourless, odourless, tasteless diatomic gas molecule which is explosive above 4.7% in presence of pure oxygen (O_2) gas[1]. Free H_2 is comparatively rare on earth as the atmosphere contains only 0.55 parts per million of H_2, however, H_2 constitutes nearly 75% of the universe's elemental mass as a component of water and organic compounds. H_2 was assumed to be less soluble in water for the past many years conversely it has been proven to dissolve in water up to 0.8 mM or 1.6 mg/L under room conditions. The solubility could be increased up to 4 mg/L using commercially available pressurized proton-exchange membrane (PEM) electrolysis devices[2]. Since the last 2 decades a large number of studies exploring the therapeutic and preventive effects of H_2 with more than 300 papers on medical beneficial effects of H_2 has been published[3]. Researchers further elucidated the beneficial role of H_2 as an antioxidant, anti-inflammatory, anti-apoptotic, anti-viral and anti-cancer mostly on rats, cell culture and also on plants [4–7]. Now researchers have started to use H_2 in clinical trials knowing the non-cytotoxicity property of molecular H_2 even at high concentrations[7,8]. In the year 2020, during the COVID-19 pandemic, a massive fatality was caused mainly due to respiratory failure. To combat the medical emergency, the Chinese Health Commission has indicated implementing inhalation of H_2 and O_2 gas mixture to pacify COVID-19 symptoms in the clinical trial[8,9]. Now fellow researchers begin to accept and recognise the H_2 research, and their biochemical reactivity, which persuaded scientists to manufacture more tools based on different principles to measure dissolved H_2 in water, blood and body tissue[10,11]. The discovery of dissolved H_2 measuring tools further exposed novel theories about the excretion of H_2 from the human body due to fermentation of carbohydrate by microbiota in stomach[12], which motivated the scientists to further elucidate the possible medicinal benefits of H_2 to humans and now to enhance animal stocks and plant crops[4,13–15].

Researchers discovered that eukaryotic algae such as *Chlamydomonas species* and *Chlorella vulgaris*, also archaea and bacteria produce H_2 to the atmosphere by respiration[16–18] but the possible role of H_2 in algae or generally in plants and animals was vague for many years until some researchers start to explore about the properties of the H_2 and their role in organisms' physiological activity. The hydrogenase enzyme is found in hydrogen-producing organisms to catalyse the proton and electron conversion into molecular H_2[19,20]. Although hydrogenase is not produced endogenously in human cells, the anaerobic organisms in the human digestive system break down carbohydrates, mainly the non-digestible polysaccharide fraction of plant

1

cells via hydrogenase and generate H_2[12,21]. Fermentation of non-digestible carbohydrates by human intestinal microbiota may produce more than 12 litres of H_2 per day under normal physiological conditions. This H_2 gas are eliminated through flatus or respiratory excretion once absorbed into the systemic circulation. The molecular H_2 will be reduced to HS^-, CH_4 and CH_3COO^- by dissimilatory sulphate reduction, methanogenesis and acetogenesis (eq. 1, 2 & 3) respectively, through microbiota metabolism in human body[22,23]. Hydrogen conversion equations respectively[22,23].

$$4\ H_2 + SO_4^{2-} + H^+ \rightarrow HS^- + 4\ H_2O \qquad \text{(eq. 1)}$$
$$4\ H_2 + CO_2 \rightarrow CH_4 + 2\ H_2O \qquad \text{(eq. 2)}$$
$$4\ H_2 + 2CO_2 \rightarrow CH_3COO^- + H^+ + 2\ H_2O \qquad \text{(eq. 3)}$$
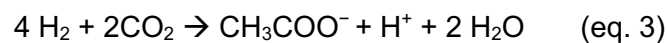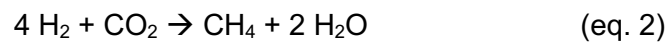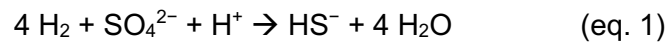
H_2 gas was first artificially produced in 1671 by Robert Boyle, when he plunged iron into diluted hydrochloric acid (HCl) and realised a new gas released with new chemical properties is actually H_2[24]. After more than a century, in 1783 another French researcher named this diatomic gas "hydrogen" which derived from the Greek word 'hydro' meaning water and 'genes' meaning creator when he discovered that water is produced when H_2 is burned with oxygen[25]. In 1920s German engineer, Rudolf Erren, was newly elucidated H_2 or H_2/O_2 mixture as a novel energy source for internal combustion engines of trucks and submarines due to its combustive property[26]. Henceforth, many researchers from the chemistry field focused on H_2 as an energy source. In the recent era, H_2 is still being explored to be a fossil fuel replacement due to the advantage of H_2 renewable carbon-free energy source has caught the attention of researchers and the public for a pollution-free environment[27]. The principle is H_2 and O_2 collision reaction releases water vapour by an exothermic reaction which generates heat energy[28]. Multiple methods were introduced by researchers to produce H_2, apart from water electrolysis and extraction from algae, the water-splitting technique with higher energy was demonstrated using EMF oscillation to break the covalent bond of the water molecule[28,29], another promising way to match the continuously growing demand for H_2 as renewable energy storage.

Apart from research of H_2 by engineers and chemist, the role of H_2 also investigated by Biologist. In 1928 Slyke et al. confirmed that H_2 gas dissolves in blood serum and cells at a temperature of 38°C by analysing the defibrinated ox blood[30]. Thereafter, biologists did not investigate much on H_2 for decades, until the biologists' attention falls again on H_2 to convert the smallest molecule into a pharmacologically beneficial substance. In 1975 Dole et al. were the first to propose that H_2 has an antioxidant property. Dole et al. made the debut that the antioxidant property of H_2 degenerated squamous cell carcinomas of hairless albino mice treated by hyperbaric H_2-therapy. They suggested that H_2 react with ·OH to produce water and

H· (eq. 4), which further scavenge by $\cdot O_2^-$ to harmless hydroperoxyl radical (HO_2^-) (eq. 5), also this sequence of reactions has prevented the unwanted reaction of $\cdot O_2^-$ with H_2O_2 which produces an aggressive and cancer-inducing $\cdot OH$ radical (eq. 6)[31–34].

$$H_2 + \cdot OH \rightarrow H_2O + H\cdot \qquad \text{(eq. 4)}$$

$$H\cdot + \cdot O_2^- \rightarrow HO_2^- \qquad \text{(eq. 5)}$$

$$\cdot O_2^- + H_2O_2 \rightarrow OH^- + \cdot OH + O_2 \qquad \text{(eq. 6)}$$
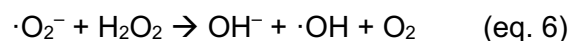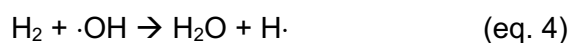
The finding by Dole et al. revokes the research on H_2. Molecular H_2 is now proven and widely accepted to have biochemical effects in both animals and plants. A recent study revealed that molecular H_2 may serve as a modulator of signal transduction in the human body that can control physiological activity, like other gaseous signaling molecules like nitric oxide, NO·, hydrogen peroxide, H_2O_2, and hydrogen sulphide, H_2S[35,36] however, the possible cellular level mechanism is still indefinite. In 2007, Ohsawa et al. published in *Nature Medicine* that oxidative stress damage, induced by brain ischemia-reperfusion, was suppressed by H_2-therapy in rats. Further explained that H_2 has a chemical reactivity that tends to quench the most aggressive and harmful reactive oxygen species (ROS) like hydroxyl radical (OH·) and peroxynitrite (ONOO·) while leaving the other ROS which involves in molecular signaling such as NO·, H_2O_2 and $\cdot O_2$ unscathed [7].

Ohsawa et al. supported the 5 decades ago described scavenging mechanism by Dole et al. H_2 molecule is expected to reduce $\cdot OH$ to produce water and hydrogen radical ($\cdot H$) (eq. 4) which is followed by a reaction with $\cdot O_2^-$ to convert the $\cdot H$ radical into subtle hydroperoxyl (HO_2^-) (eq. 5)[7,31,32]. However, a small group of researchers were cogitating the reaction of H_2 with $\cdot OH$ either producing the reactive atomic $\cdot H$ radical (eq. 4) or considerably producing a more reactive solvated electron (eq. 7) where both could induce severe oxidative damage as would the $\cdot OH$[37–39].

$$H_2 + {}^{\cdot}OH \rightarrow H_3O^+ + e^- \qquad \text{(eq. 7)}$$
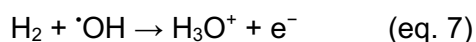
In a nutshell, although the benefits of H_2 were examined on various model organisms and observed the positive effect by many researchers from different parts of the world over the past decades and became more intense in the last 15 years, however, the possible molecular mechanism is still an unsolved mystery.

The $\cdot OH$ radical is highly cytotoxic species produced in inflamed tissues [3,7,40]. There is no known enzyme specifically suppress $\cdot OH$ and it reacts aggressively with the nearest nucleophilic biomolecules and induces oxidative damage[33]. Fenton/Weiss reaction is one of the main processes for the production of $\cdot OH$ in the cellular redox chemistry (eq. 8, 9 and 10)[33].

The ·OH is labelled to be a chain carrier since the ability to react with any organic species to propagate a reaction, however, chain termination occurs when two ·OH radicals combine to produce harmless H_2O_2, H_2O and O_2 (eq. 11 and 12)[33].

Fenton reaction:

$$Fe^{3+} + ·O_2^- \rightarrow Fe^{2+} + O_2 \qquad \text{(eq. 8)}$$

$$Fe^{2+} + H_2O_2 \rightarrow Fe^{3+} + OH^- + ·OH \qquad \text{(eq. 9)}$$
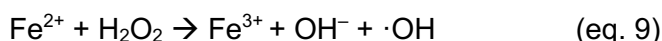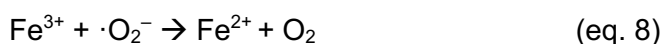
Fenton/Haber-Weiss reaction (later confirmed Fe^{3+} catalysed the overall reaction):

$$·O_2^- + H_2O_2 \xrightarrow{\text{catalyst, } Fe^{3+}} OH^- + ·OH + O_2 \qquad \text{(eq. 10)}$$
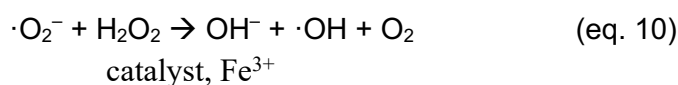
·OH radicals chain termination

$$·OH + ·OH \rightarrow H_2O_2 \qquad \text{(eq. 11)}$$

$$HO_2^- + ·OH \rightarrow H_2O + O_2 \qquad \text{(eq. 12)}$$
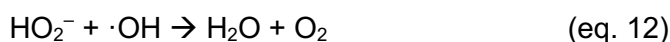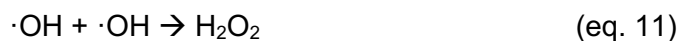
Superoxide anion ($·O_2^-$) also react with other radicals like nitric oxide (NO·) which contribute to the production of peroxynitrite (·ONOO), which is also a strong radical[41–43] (eq. 13).

$$·O_2^- + NO· \rightarrow ·OONO \qquad \text{(eq. 13)}$$

1.1.1 Hydrogen as a therapeutic agent

The accumulated evidence from a variety of therapeutic applications either by clinical trial or using experimental disease models indicated that molecular H_2 is a feasible and effective therapeutic agent. For the last 15 years, many researchers were trying to prove the benefits of molecular H_2 mainly as a potential antioxidant in preventive and therapeutic applications[3], which subsequently helps to overcome inflammatory conditions and apoptosis[4,44]. In 2001 Gharib et al. from France studied the benefits of H_2 on mice with liver inflamed by the parasite *Schistosoma mansoni* were supplemented with 0.8 atm H_2 for 2 weeks in a hyperbaric chamber, the combination of H_2/O_2 has shown alleviation of fibrosis in correlation to an increase in antioxidant enzyme activity[4]. In 2019, a clinical trial conducted on 82 patients with stage III and IV cancer treated by H_2 inhalation for 4 weeks reported of improvement in physical status among 41.5% of patients, mostly lung cancer patients in correlation with peroxidation[45,46]. In 2020 another clinical trial, peripheral blood cells quantification analysis

showed that H_2-rich water consumed for 4 weeks by healthy adults has built immunity to reduce inflammatory responses which eventually prevents apoptosis of peripheral blood cells in a correlation of increase in antioxidant potential[44]. A clinical trial with H_2-therapy became possible due to the non-cytotoxicity property of H_2[3,7,8]. Li et. al. from China used adult zebrafish as a model organism to study the possibility of molecular H_2 reflecting anti-viral properties. Spring viraemia of carp virus (SVCV) inflamed adult zebrafish were treated for 7 days with 0.7 ppm H_2-enriched water has reduced the average mortality rate by 40% associated with reduced ROS[15].
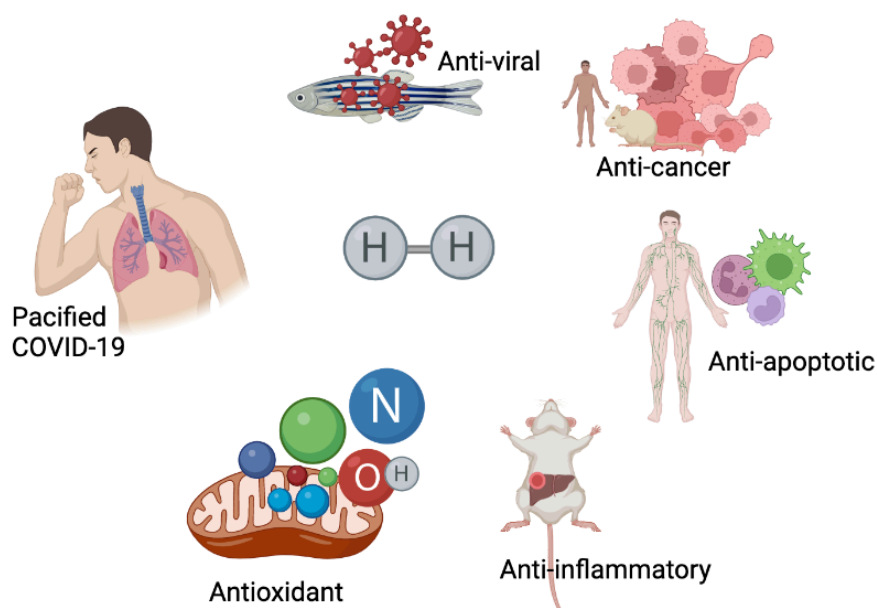
Fig. 1: The proposed beneficial effects of molecular hydrogen.
The beneficial properties of molecular hydrogen contribute to preventive and therapeutic applications in the medical field. Image created using BioRender.com.

Researchers further elucidated the beneficial role of H_2 as an antioxidant, anti-inflammatory, anti-apoptotic, anti-viral and anti-cancer mostly in rats, also in other different model animals, plants and cell culture[4–7]. Now researchers have started to use H_2 in clinical trials knowing the non-cytotoxicity property of molecular H_2 even at high concentrations[7,8]. The very small molecular size of H_2 allows rapid diffusion into tissues and cells, which makes it more efficient than other antioxidants and anti-inflammatory agents that are already available on the market[7].

1.1.2 Feasibility of molecular hydrogen in therapeutic applications

Hydrogen is a hydrophobic homonuclear molecule with a very small molecular size which facilitates the rapid diffusion of molecular H_2 through the skin, cell membrane and further into cell organelles easily[7]. There are several different methods of H_2 intake that have been

approached by researchers such as consuming H_2-enriched water, inhaling H_2 gas, taking an H_2 bath in H_2-enriched water, injecting H_2-enriched saline into veins, dropping H_2 saline onto the eyes or inducing the intestinal H_2 production by bacteria[12,14,44,47–49]. Nonetheless, it is very important to identify the most effective method to intake molecular H_2 for optimum results. On the other hand, some researchers assess the susceptibility of body tissue and the human physiological system to molecular H_2. In 2008, Hayashida et al. supplied rats with H_2 and reported that H_2 was detected in the arterial blood within 5 minutes after gas inhalation[47]. In 2014, Liu et al. reported that various organs in rat achieved H_2 saturation point within 5 minutes of treatment with H_2-rich saline solution by oral administration and within 1 minute by intravenous injection[50]. Then in 2019, Yamamoto et al. showed inhalation of 3% hydrogen gas by rat are believed to reach saturation within a few minutes into the body tissue, however, claimed that different organ has different absorption tendency. Liver tissue achieves the highest concentration of molecular H_2 compared to the brain, mesentery tissue, muscle tissue and kidney[6].

Meanwhile, in my study, I used the transcutaneous gas exchange method of application on zebrafish larvae for 3 hours on 3 consecutive days but the H_2 absorption rate and concentration of molecular H_2 in the tissue are not known. Nevertheless, researchers have described the effective transcutaneous gas exchange by fish larvae with oxygen (O_2) gas due to the larger surface-to-volume ratio will sufficiently drive passive diffusion of O_2 through epithelial cells, cell plasma and further into cell organelles by partial pressure (PO_2) gradients[51,52]. Therefore, H_2 with a much smaller molecular size compared to O_2 might diffuse into larvae tissue much easier compared to O_2 gas exchange.

1.1.3 The role of molecular hydrogen in higher and lower photosynthetic plants

Oxidative damages caused by ROS and the requirement for antioxidant for healthy growth is not only applied to animals but also to plants. There are several possible routes to induce oxidative stress in plants majorly divided by biotic and abiotic stress. Biotic stress provokes ROS accumulation by damage-inducing living organisms specifically bacteria, viruses, parasites, insects, nematodes and also weeds competing for nutrients with crops[53–55]. In contrast, abiotic stress is external interference caused by environmental factors including salt, soil, drought, heat and toxicity which could retard plant growth[36,40,56,57]. Plants respond to biotic and abiotic stresses through a defence mechanism classified as an innate and systemic response which regulates ROS generation and oxidative bursts occur[53,58]. Increases in intracellular ROS under such stress conditions are often accompanied by an increase in

antioxidant levels in cells however in antioxidants insufficiency condition, oxidative damage of proteins and other nutrients occur accompany by plant softening and eventually dying[59,60].

H_2 has been shown to have the potential to combat stress and manipulate plant growth. H_2 has the potential to contribute to crop enhancement[61]. Xu et al. reported that H_2-water pre-treated rice seeds have increased the antioxidant enzymes in cells and also observed to increase seed germination rate[56]. H_2 was also found to reduce metal toxicity and paraquat-induced oxidative stress[13,62–64]. Even though a direct contribution of H_2 combating pathogens was not reported but researchers have updated that H_2 can prolong the shelf life of fruits[54,65]. Molecular H_2 treated kiwifruit with 80% H_2-enriched water and fumigation with H_2 gas reduced rotting incidence, by reducing cell wall-degrading enzyme activity while increasing antioxidants activity to maintain radical-scavenging activity in kiwifruit, positive results are shown with other fruits too[54,55,65]. Phytologists concluded that molecular H_2 has a tendency to inhibit ethylene biosynthesis[65]. Ethylene is a gaseous plant hormone which involved in a signaling pathway where ethylene receptors activate transcription factors to induce ripening.

The potential of H_2 to regulate the cellular functions in plant cells involving both phytohormone signaling, metabolism and ROS-induced oxidative stress responses was observed by phytologists however the possible molecular mechanism involved is yet to be confirmed. Nevertheless, researchers proposed of reactive $\cdot OH$ could potentially be the target of H_2 [7,31,66,67]. It has long been known that ROS such as $\cdot O_2^-$, H_2O_2 and $\cdot OH$ are generated in stress-induced plant cells and could impact the intracellular and extracellular physiological activities[40,68]. The aggressive $\cdot OH$ radicals are known to lead to proteins, lipids, carbohydrates and DNA oxidation[34,69–71] which should be detrimental to cell function. Therefore, the scavenging activity of H_2 may prevent the harmful effects of $\cdot OH$, which may account for some of the observed effects. One of the significant actions of H_2 in animal biological systems is $\cdot OH$ scavenging activity[7,47,49] and a similar root action is expected to be involved in plants[13,72,73].

1.1.4 Reactive oxygen species (ROS) & Reactive nitrogen species (RNS)

Early in the 1950s, when O_2 was believed to be benign, Gerschman et al. were nominated for the Nobel prize in Physiology and Medicine for discovering O_2 toxicity which is interrelated to ROS and the underlying complications due to the deleterious effect of oxygen radicals[74]. Later Denham Harman explained how free radicals from the environment and internal metabolism induce damage to the cellular constituents[75]. Free radicals are atoms surrounded by electrons that orbit the atom in layers called shells. Basically, in typical stable atoms each shell is filled with an even number of electrons. An atom is considered unstable free radical when the

outermost shell has unpaired electrons[76]. The active free radicals are triggered to bind with other random atoms or molecules to steal electrons, in order to neutralise themselves by pairing the unpaired electrons. The O_2 molecule that lost an electron becomes oxygen radical with unpaired electrons and this will be an internal damage-causing chain reaction[77].

Free radicals in the biological system include hydroxyl ($\cdot OH$), superoxide ($\cdot O_2^-$), peroxynitrite ($\cdot ONOO$), nitric oxide ($NO\cdot$), nitrogen dioxide ($NO_2\cdot$), peroxyl ($ROO\cdot$) and lipid peroxyl ($LOO\cdot$) radicals meanwhile, hydrogen peroxide (H_2O_2), ozone (O_3), singlet oxygen ($^1O_2$), hypochlorous acid ($HOCl$), nitrous acid (HNO_2), dinitrogen trioxide (N_2O_3) and lipid peroxide ($LOOH$) are not free radicals but oxidants which easily lead to free radical reactions in living organisms called ROS or RNS[77]. In phenomena when free radicals and oxidants are generated in vast numbers initiating extreme deleterious reactions that severely alter the cell membranes and other structures such as proteins, lipids, lipoproteins and deoxyribonucleic acid (DNA)[33,70,78]. The condition worsens when cells are unable to neutralise the excessive free radicals formed. The imbalance between the formation and neutralization of ROS or RNS leads to oxidative damage[79,80].

The mitochondrial respiratory chain is one of the fundamental sources of ROS/RNS production. In the body, during normal cell metabolisms, the electron transfer reactions to generate cellular ATP in the inner mitochondrial membrane are possible to produce ROS/RNS as by-products. ROS/RNS are also introduced to living organisms from external sources such as pollution, radiation, cigarette smoke and medication too[81]. ROS/RNS play a dual role as both toxic and beneficial compounds. ROS at a low level can act as second messengers to activate signaling cascades involving inflammation, tissue regeneration, apoptosis, and other crucial intracellular pathways[79]. On the other hand, an overload of free radicals causes internal oxidative damage[32,35,82].

Generally, animals and plants have antioxidant defence systems complemented with antioxidant enzymes such as superoxide dismutase (SOD), catalase (CAT), glutathione peroxidase (GSH-Px) and heme oxygenase-1 (HO-1) in the cells to protect the biological systems from free radical toxicity[83,84]. The antioxidant enzymes catalyse the harmful radicals into harmless molecules. However, in extreme conditions, exogenous antioxidants such as vitamins, carotenoids, phenolic acid, flavonols and trace elements like zinc and selenium are necessary for animals and humans[85,86]. Antioxidants are molecules that prevent the oxidation of other stable molecules by donating an electron to unstable free radicals. Thereby, antioxidants reduce oxidative damage reactivity while not becoming a reactive free radical by themselves which ultimately terminates the radical chain reaction[87].

In the recent decade, molecular H_2 is started to be considered as a novel antioxidant though the suggested mechanism is still controversial. Most of the involved researchers are debating the possible direct scavenging reaction of H_2 with $\cdot OH$ radical[3,7,40], a highly cytotoxic species produced in inflamed tissues. There is no known enzyme specifically to deal with $\cdot OH$ and it reacts instantaneously with the nearest nucleophilic biomolecules[33]. H_2 is a proposed reductant that can penetrate the cell membrane and possibly neutralize the aggressive $\cdot OH$ and $\cdot ONOO$ while unaffected the $\cdot O_2^-$ and H_2O_2 which are claimed to maintain physiological function[7].

1.1.5   Water electrolysis

The pure H_2 or H_2/O_2 mixture is produced using a water electrolysis system. A typical Proton Exchange Membrane (PEM) electrolysis system is made with a negative cathode and a positive anode separated by a diaphragm. The transition of electric current through the water decomposes H_2O into H^+ and OH^- ions. The charged ions are attracted to the opposingly charged electrode where they are composed and liberated as gas. The chemical reaction at the anode and cathode produces O_2 and H_2, respectively. The O_2 and H_2 gas production which is separated by a diaphragm will be collected via separate output from the electrolyser. The PEM electrolysis technique with a diaphragm between the electrodes ensures the production of pure gases separately and also reduces unwanted secondary reactions[88–90].

Anode (positive electrode)   : $2\,H_2O \rightarrow O_2 + 4\,H^+ + 4e^-$

Cathode (negative electrode)   : $4\,H^+ + 4\,e^- \rightarrow 2\,H_2$

Overall reaction   : $2\,H_2O \rightarrow 2\,H_2 + O_2$
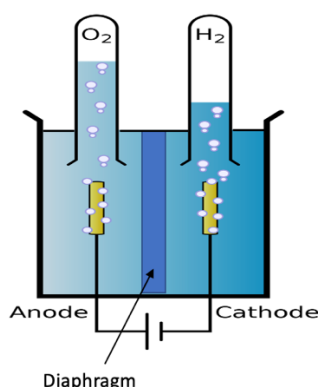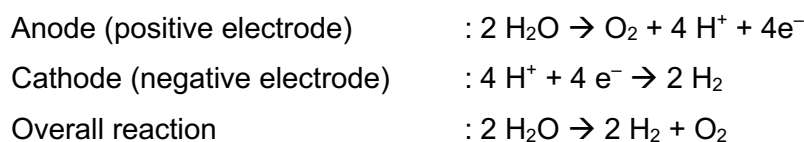
Fig. 2: PEM water electrolysis system.
Proton Exchange Membrane or Polymer Electrolyte Membrane (PEM) electrolysis system has an intermembrane to separate the different charge electrodes to generate pure O_2 and H_2 gas separately[91]. Image adapted from Nécropotame[92]

While the commercially available Brown's gas (BG) is also known as Oxy-hydrogen, HydrOxy or HHO gas. Brown's gas is first introduced as Brown's gas by a Bulgarian chemist named Yull Brown who received a patent for his invented electrolyser in 1977. The main difference from a conventional electrolyser is that Brown's gas generating electrolyser has only one gas output. The Brown's gas electrolyser is not equipped with an intermediate diaphragm to separate the cathode and anode electrodes therefore H_2/O_2 gas mixture is collected through a single output. Brown's gas electrolyser worked by the principle of a typical alkaline electrolysis system but with intercalated electrodes.
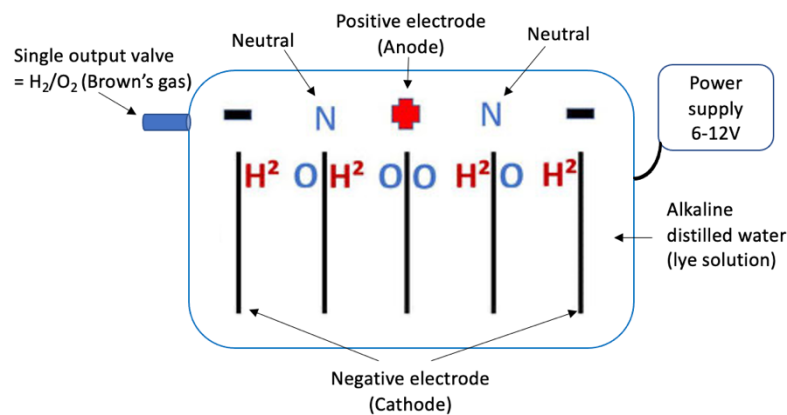
Fig. 3: The alkaline electrolysis with intercalated electrodes system (Brown's gas)
The principle of the formation of Brown's gas by an alkaline electrolysis system with an intercalated electrode. Image created using BioRender.com.

Brown's gas was first invented to work as high heat energy generating gas for metal welding purpose[91]. H_2-O_2 mixture or Brown's gas was introduced in heavy metal industries as industrial combustion support due to its combustible properties and fuel efficiency coupled with environmentally safe compared to ozone polluting carbon combustion[93]. In typical carbon combustion with the stream of air or O_2, sufficient heat is released for welding together with unwanted harmful by-products such as carbon monoxide (CO) and carbon dioxide (CO_2). Alternatively, H_2 burn in a stream of O_2 creating the same or more heat for welding in absence of toxic gas[91]. This attracted many scientists to replicate the device but later the benefit of this combination gas has been explored by medical researchers.

Fig. 4: The commercially available electrolysers in the market to generate Brown's gas.

Brown's gas is introduced as an emerging medical gas. The Brown's gas is suggested for inhalation via a nasal cannula or mask, allowing the Brown's gas to directly enter the respiratory system to overcome most of the free radical-induced diseases[93]. Researchers claimed that Brown's gas has an extraordinary structure of a combination of hydrogen and oxygen[94,95]. According to Santilli, the intercalated electrodes facilitate the transition of the conventional H-O-H species to a new (H×H)-O species ("x", denoting a new magnecular bond and "-" the conventional molecular bond) predicted due to the electric polarization of water[94]. A magnecular bond is a novel type of bond consisting of atoms held together by magnetic field attraction. Brown's gas is also claimed to be an "electrically expanded water" (ExW)[96] hence several creative structural orientations are assumed to be produced like OH_2 and H_2OH_2 species which are stated to be stably present in treated water only for a very short period[94,95].

1.2 Electromagnetic field (EMF) waves

Electromagnetic field (EMF) waves are a combination oscillation of an electric field and a magnetic field. The electric and magnetic fields oscillate in a plane that is perpendicular to the direction of propagation and also perpendicular to each other. EM waves travel through vacuum conditions at 3.00 x 10^8 ms, which is travelling at the speed of light. EM waves do not need a medium to transmit unlike other mechanical waves such as sound and water waves[97].
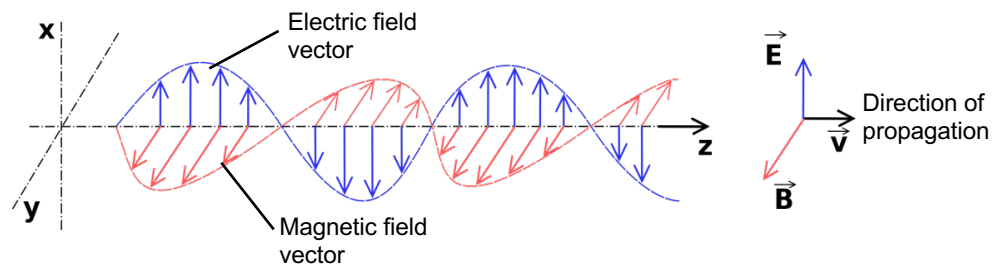
Fig. 5: EMF waves are a combination of the electric and magnetic fields.
The combination of the electric field, (E) together with the magnetic field, (B) going to a particular direction, (V) is electromagnetic field (EMF) wave propagation[98]. Image source from Emmanuel Boutet[99].

Generally, we are exposed to multiple radiations in everyday life, from naturally exposed sunlight to the home electric appliances such as television, radio, WLAN signals, microwave oven, mobile phones, and heat-generating radiators. The next intense radiation exposure source is medical diagnostic tools like X-rays and magnetic resonance imaging (MRI). While, the gamma-ray photons have the highest energy in the EM radiation spectrum, released from radioactive elements[100]. The radiation waves from gadgets and electric appliances have a much longer wavelength coupled with lower frequency waves imply a much lower intensity of radiation energy. Meanwhile, gamma-ray radiation has a way shorter wavelength with higher frequency waves delivering a higher intensity of radiation energy to the surroundings which is far more aggressive and harmful to the recipients due to its atomic ionising capacity[101]

Based on the World Health Organisation (WHO), EMFs are categorised into ionising and non-ionising radiation[102]. Ionising radiation is mid to high-frequency radiation which includes x-rays and gamma rays. Ionising radiation has strong energy to ionise an atom to be charged by removing a tightly bound electron from an atom. Earlier research studies have shown the side effects of human cell damage and the risk of cancer due to exposure to strong ionising radiations[102–104]. Whilst, the non-ionising radiation by a longer and lower frequency wavelength only produce thermal effects which cause tissue heating at short exposure however, may damage molecules and cells of living organisms at long exposure[105].
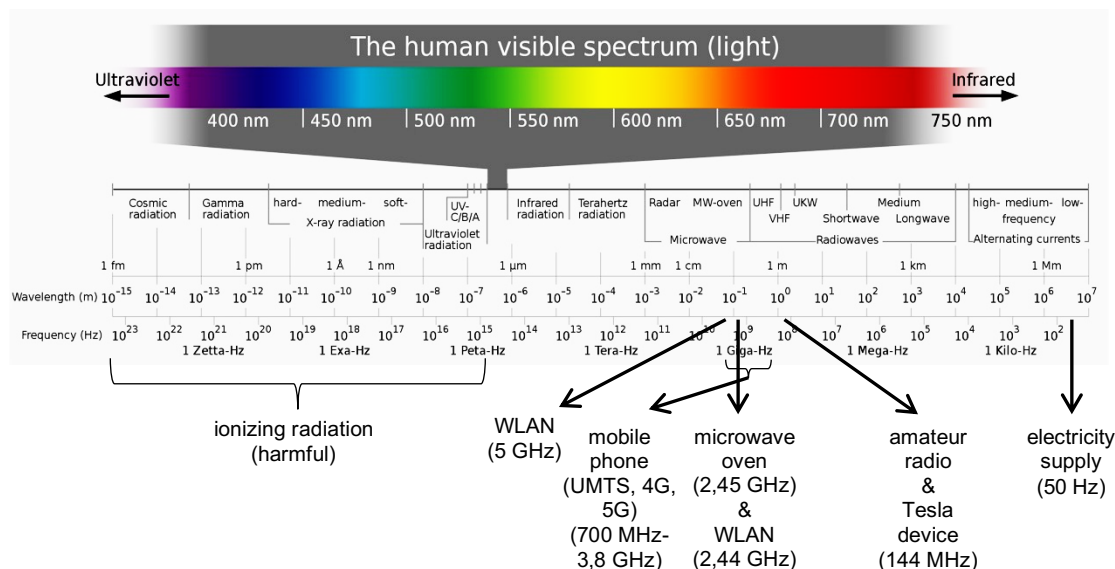
Fig. 6: Electromagnetic spectrum shows the frequencies of different sources.
The low-frequency (LF-EMF) radiation with long wavelengths comes from power lines, gadgets and electric appliances (non-ionising radiation) while the extremely short wavelengths with very high frequency (VHF-EMF) and intense radiation energy sources come from X-rays and gamma rays (ionising radiation). The image source from Horst Frank[106]

Although radiation effect is always seen as an unwanted side effect of using appliances, gadgets and medical diagnostic tools however EMF radiation is also seen as a treatment by many other researchers. In 1985, Anthony Barker from the University of Sheffield, UK first introduced transcranial magnetic stimulation (TMS) into medical practice for neuropsychological assessment[107]. In 2007, Markov investigated the benefits of pulsed electromagnetic field (PEMF) therapy which is a low-frequency electromagnetic signal to heal musculoskeletal disorders[108]. According to his research study, benefits of electromagnetic therapy were observed with radiation stimulation of less than 100 Hz with magnetic flux density between 0.1 mT and 30 mT[108]. In recent 15 years, there were many researchers reported successful treatment of musculoskeletal disorders, lower back pain and bone fracture conditions using electromagnetic field stimulation [109–112]. How electromagnetic radiation helps in tissue recovery is not known however there were proven studies that the wave oscillation stimulated by EMF may contribute to physiological activity changes. Researchers are still exploring and have indicated that the oscillations of intra- and intercellularly, and at more complex oscillatory behaviours at the tissue level which often facilitate the cascade messenger for gene regulation, tissue elongation and muscle fibril contraction based on studies carried out on *Drosophila*[113–116].

Conventional and alternative medicine has attracted scientists and clinicians to the potential benefit of using EMF for therapeutic purposes however the safety of magnetic and EM fields is still a very sceptical and controversial subject. Although there are publications of successful

therapy by EMF stimulation nevertheless, there are equally numerous undeniable adverse effects such as headache, cancer, teratogenic, gene mutation (genotoxic) or seizures that are also being published[103,117]. In March 2022, the Swiss expert group on EMF and non-ionising radiation (BERENIS) posted the reliability and acceptance of the publication on post-synaptic structure alteration and neurite outgrowth retardation in developing hippocampal neurons of early postnatal mice upon exposure to radio-frequency, 1850 MHz for 5 hours for 28 days[118,119].

Although some findings showed the principle of electromagnetic oscillation as a second messenger and are being practised in the medical line, but the EMF wave frequency and intensity generated may vary from one radiation device to another. According to Wang et al., the United States FDA database record indicates that only 31 electromagnetic devices for muscle therapy were initially approved between the years 2000 to 2018 however there are many more unrecognised devices in the market. Later MAUDE (Manufacturer and User Facility Device Experience) database revealed 61 reports of adverse effects of radiation-based therapy such as acute skin damage, skin burn, dyspigmentation, infection and scarring[110]. Even though, such a database from the European commission is not seen however there could be many unreported adverse effects from unregistered "self-healing" promoting devices.

In a nutshell, the potential hazards of EMF exposure remain unclear, also convincing evidence and consistent results are lacking. Therefore, elucidated the effects of EMF on tissue development and tissue regeneration on zebrafish larvae, also the effects on *Chlorella vulgaris* using Tesla oscillator device and a WLAN (wireless local area network) router.

1.2.1 Tesla oscillator device oscillates sine wave at 144 MHz

Tesla oscillator is a commercially available "health-promoting" device, that oscillates at a frequency of 144 MHz that has not stated approved by the FDA. A measurement of the radiation wave of the Tesla oscillator with an oscilloscope meter and Fourier transform analysis confirmed that the Tesla oscillator resonates with sine waves at 144 MHz radio-frequency.
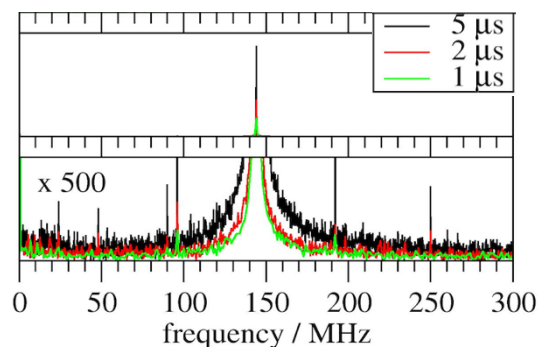
Fig. 7: The Tesla oscillator generates radiation frequency at 144 MHz.
The time traces of the Tesla oscillator radiation by Fourier transform analysis have confirmed the device generates a strong signal at 144 MHz.

The Tesla oscillator device is stated to be invented by an anonymous Russian researcher who uses this 144 MHz radio-frequency radiation to cluster the water molecules in a hexagonal structure. Drinking the structured water or called activated water is expected to improve blood flow and O_2 transport which is believed to enhance the health of humans, animals and plants[120]. However, this water structural modification assumption is not proven.

The device supplier also claimed that carrying Tesla oscillator handheld-antenna closer to the skin would accelerate skin repair, tissue regeneration and improvise the immune system in general[120]. In the year 2021, a private researcher from Wagenfeld, Germany, studied on Tesla oscillator device and concluded that single-time radiation of the Tesla oscillator on connective tissue fibroblasts for 30 minutes has the potential to improve cell regeneration and reduce superoxide anion radicals in inflammatory conditions. According to the paper, the migration of the cells closer from two separated tissue cells in a petridish was the only parameter taken to measure the cell regeneration[121]. Therefore, a more reliable measuring parameter is required to determine the capacity of the Tesla oscillator to induce tissue regeneration.
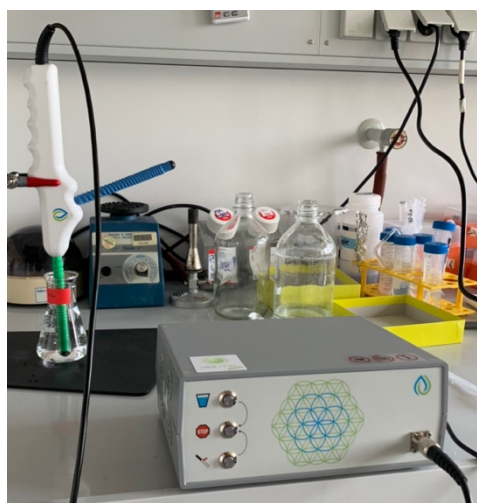
Fig. 8: Tesla oscillator device and usage.
The Tesla oscillator device radiates EMF upon connecting to the power supplier. The device is claimed to be beneficial for treating arthritis, limb oedema and injured skin including open wounds[120].

1.2.2 WLAN router oscillates pulsed waves at 5.0 GHz

Wireless local area networks (WLAN) commonly known as Wi-Fi, are formed by routers which connect directly with each other or via an entry point to a wired network, known as the access point (or "hot spot"). In order to establish a wireless network connection between routers with devices like a laptop, computer, printer, digital camera or video projector requires an antenna and a transmitter to transfer data. The most common WLANs operate at frequency bands of 2.4 GHz and recently begin to welcome 5 GHz for a faster connection network. Wireless networks use radio waves to connect WiFi-enabled devices to access the internet via a data connection[122]. The WLAN frequency used in this research is 5.0 GHz, operating at a RF/HF almost similar to mobile phones[123]. WLAN transmit data by a pulsed packet waveform, each pulse packed sine waves and shows a time gap between each packet. There is speculation among neurophysiologists that the pulsed wave by WLAN may interfere with the natural sine wave generated by cells and organs in the human body. However, the major alarming problem is using WLAN in daily life and exposure to HF-EMF in the long-term.

The possible health effects of RF/HF-EMF were considered in the epidemiological studies performed within the scope of the German Mobile Telecommunication Research Programme in order to establish statistical correlations between exposure and morbidity within the population[124]. The outcome of their study is no health damage occurs at usual WLAN radiation exposure however the effects of HF-EMF on biological organisms may differ such as inducing thermal effect on biological tissue. The fifth-generation (5G) telecommunications technologies, is the next controversial target achievement aimed by European countries however considering the possible development of higher frequency base stations and interrelated communication devices will increase the high-frequency radiation effect significantly[125]. Meanwhile, the scientific research study on the impacts of widely available 2.44 and 5.0 GHz of high-frequency WLAN routers doesn't make any better in long term exposure therefore it is still significant to determine the range of health deterioration with WLAN radiation.

1.2.3 Electromagnetic field to dissociate water molecules into molecular hydrogen

Since 1929 there were many attempts to dissociate water molecules, H_2O into H_2 and O_2 molecules by endothermic reaction ideally to store pure H_2 for future energy savings. Harold Clayton Urey who wins the Nobel Prize for the discovery of deuterium, ^2H, the heavy hydrogen, in 1934, also explored water vapour dissociation into hydrogen atoms, hydroxyl molecules and some unknown active species detected by an electric discharge in 1929[126,127]. Followed by his

attempt, for many decades there were numerous researchers attempting water dissociation by magnetic, electric, electrostatic or electromagnetic field waves radiation to store pure H_2[28,29,128,129].

The researchers explained that water dissociation is possible due to the conversion of irradiated EMF energy into kinetic energy of charged particles such as electrons and is expected to further convert into heat energy due to elastic collisions with adherent particles. According to Maehara et al. and a few more researchers, RF radiation of 13.56 MHz generates bubbles in water plasma, which is expected to produce H_2 and O_2 molecules or radicals such as ·OH and ·O_2[−28,29,126,128–130]. The presence of dissociated molecular H_2 is shown to be confirmed by a colourimetric assay of decolourising methylene blue[128].

1.3   Model Organisms

1.3.1   *Danio rerio* (Zebrafish)

Zebrafish or the scientific name *Danio rerio* is a teleost freshwater fish from the Cyprinidae family and is a vertebrate from the animal kingdom. Based on the human reference genome, zebrafish have approximately 70% of human common genes and 85% of the genes are associated with human diseases[131]. Zebrafish have been widely used as a model organism in variable aspects in research fields related to reproduction, stress, pathology, toxicology, immunology, genomics, nutrition also to manipulate growth factors[132–137].

Zebrafish have a short life cycle which is favourable for experimental purposes. The 1-hour post-fertilized embryo has 4 cells and further cell multiplication for the next 4 hours form blastodisc, a thin region of yolk-free cytoplasm atop of the egg[138]. Next, the embryo undergoes gastrulation to organise the cells into connected epithelial cells forming layers followed by epibolic movement of epithelial cell layers to form an enveloping layer. In the initial phase, the deep blastoderm cells move outwardly to intercalate with the more superficial cells which later move over the surface of the yolk to envelop it completely as a form of embryonic shield[139]. The embryonic shield eventually narrowing along the dorsal midline forms the precursor of the notochord in the somite stage within the next 16 hours. In vertebrates, somite is the crucial stage for outlining the vertebral column with skeletal muscle and skin. The extension in the epiblast brings the neural cells from all over the epiblast into the dorsal midline, where they form the neural keel and skin of the fish[139]. The organogenesis begins after the production of the nerve tube and differentiation of the germ layers. During organogenesis, the primary tissues differentiate into specific organs, especially the brain, eyes and intestine are expected

to develop earlier before the development of the liver, testes and heart[140]. The eggs are expected to be hatched into larva within 24 to 48 hours post-fertilisation. Zebrafish live for approximately 3 years on average and over 5 years maximally in laboratory conditions by gradual senescence. Zebrafish show ageing symptoms like spinal curvature, possibly due to muscle irregularities which is a typical ageing sign in most vertebrates including humans[141].
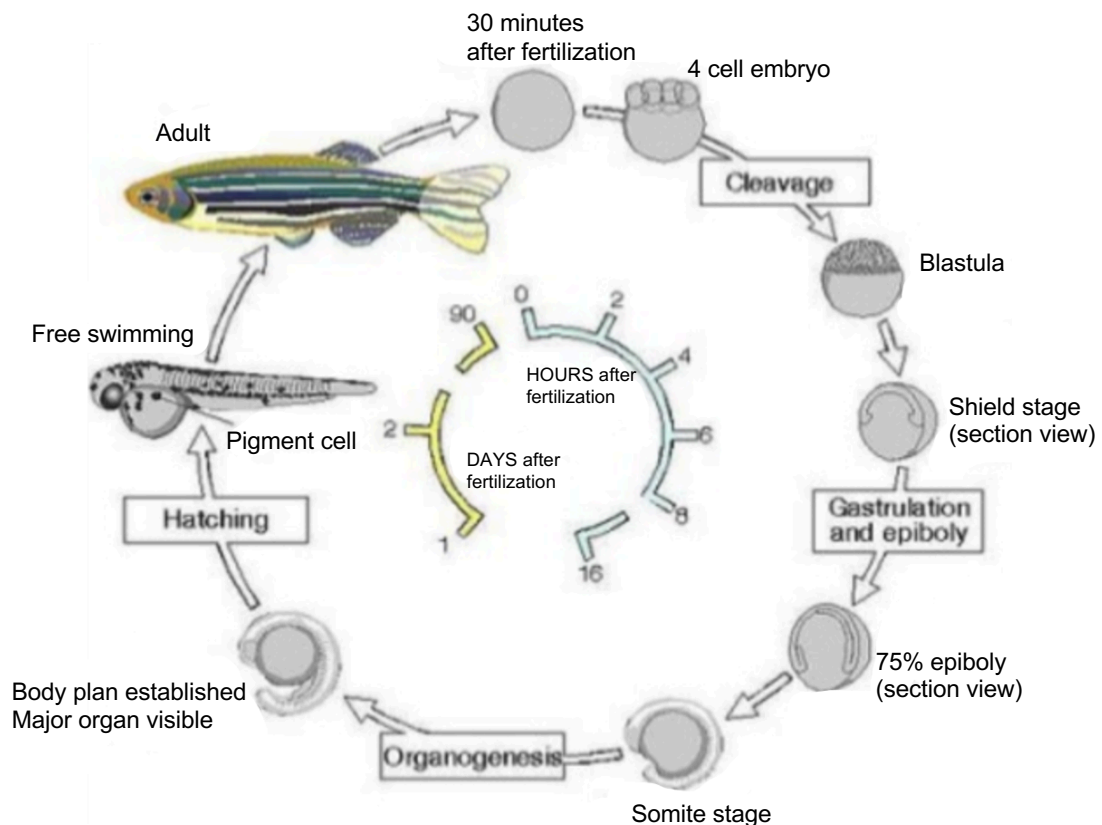
Fig. 9: Life cycle of the zebrafish.
Zebrafish develop from a one-cell zygote that sits on top of a large yolk cell and become blastula by rapid cell cleavage. Gastrulation begins at approximately 6 hours post-fertilisation followed by organogenesis to develop organs before hatching between day 1 to day 2. Zebrafish reach sexual maturity around 3 months post-fertilisation and live up to 5 years[139,140]. Image source from Indian institute of science education and research Bhopal[142].

Apart from the similarity with human genes, zebrafish is an economically perfect fit due to the large production of offspring from a single mating every week permits experiments to be carried out with high statistics. Zebrafish husbandry is relatively inexpensive raising procedure compared to other experimental animals like rats, mice and monkeys. Zebrafish larva is a suitable model organism to study pharmacological mechanisms and physiological activity due to its small size of less than 4 mm in length with optical transparency. These factors enable whole-mount, the entire fish on a microscopic slide with low-melt agarose for high-resolution imaging. The optical transparency of zebrafish larva allows *in vivo* study of immune cells in live intact larva without interfering the respiration and general development[43–145,154]. Zebrafish is also an easy organism to generate mutant strains including gene editing using CRISPR/Cas9

and exogenous transgene insertion to allow experimenters to test the role of specific genes and identify their specific regulators[135,143]. Zebrafish larva modelled experiments will be diet manipulation free since larvae do not require feeding until 7 days post-fertilization (dpf) due to the presence of the yolk sac for nutrition supply [144]. Apart from that, the ability of zebrafish to regenerate their dorsal, ventral and caudal fins makes zebrafish larvae ideal for studying fin tissue repair and regeneration processes. Larval zebrafish are also ideal for drug screening. Dissolving drugs or dispersing other therapeutic molecules into fish medium could easily diffuse into the body through the skin, as small molecules are well absorbed through larval skin[133].

1.3.2 *Chlorella vulgaris* (Microalgae)

Chlorella vulgaris is a green alga in the division of Chlorophyta[145]. In 1890, Martinus Willem Beijerinck discovered *C. vulgaris* as a eukaryotic unicellular alga and has a well-defined nucleus[145]. *C. vulgaris* belongs to the genus Chlorella, the name of the genus comes from the Greek word 'chloros' which means green and the Latin suffix 'ella' refers to its microscopic size. A typical *C. vulgaris* is a spherical microscopic cell with a diameter of 2.5 to 10 µm[146]. *C. vulgaris* is a photosynthetic alga with many structural elements similar to higher plants[147]. Therefore, *C. vulgaris* become an interesting lower plant to be used for research purposes including plant biochemical and physiological studies[148,149]. *C. vulgaris* is one of the most resistant plants against temperature and light fluctuation, pathogen attack and toxicity[149–151], apart from being easily cultured and harvested in the laboratory makes it the most feasible plant to study.

C. vulgaris reproduces asexually by mitosis of the matured parent cell. The daughter cells are liberated from the parent cell once matured enough to rupture the parental cell wall. The daughter cells are only enveloped by protoplast, but the thickness gradually increases as the cell matured. It has about 3 µm in diameter size and grows through photosynthesis by producing starch as an energy source. When the average diameter is between 8 to 10 µm, the nucleus and the chloroplast begin to split by mitosis. The daughter cells matured and split into another four daughter cells within the next 24 hours[146,152].
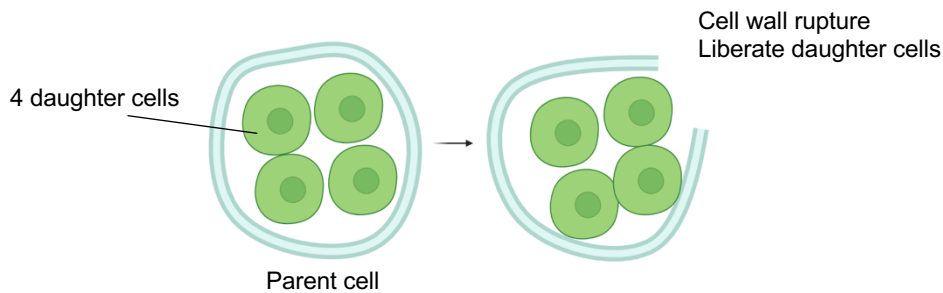
Fig. 10: Cell differentiation of *Chlorella vulgaris*.
The nucleus, chloroplast and protoplast of a matured cell divide when the cells in 8 -10 μm diameter size and further continue to undergo cell divisions to release four offspring from a single parent cell by cell wall rupture. The released 4 daughter cells enveloping their protoplasts are around 3 μm in diameter size[152]. Image created using BioRender.com.

C. vulgaris has almost a similar cell structure to higher plant cells. The well-known characteristic of matured *C. vulgaris* cells is having a rigid cell wall while the daughter cells have a more fragile wall called protoplast[163]. The cytoplasm is the gel-like substance confined within the barrier of the cell membrane and it is composed of water, soluble proteins and minerals. The cytoplasm also includes other organelles like vacuoles, Golgi body and mitochondrion to work as respiratory apparatus and for metabolism[158,163]. *C. vulgaris* has a single chloroplast with an enveloping membrane to confine a cluster of fused thylakoids where the dominant pigment chlorophyll is synthesised and store large protein content[167,168]. It also contains pyrenoid, starch and lipid droplets[169,170]. *C. vulgaris* synthesis own starch granules by photosynthesis and processes them by Calvin-cycle mechanism for energy production[169.] While the pyrenoid contains high levels of ribulose-1,5-bisphosphate (RuBP) carboxylase-oxygenase (RuBisCO) which is the centre for CO_2 fixation[170].
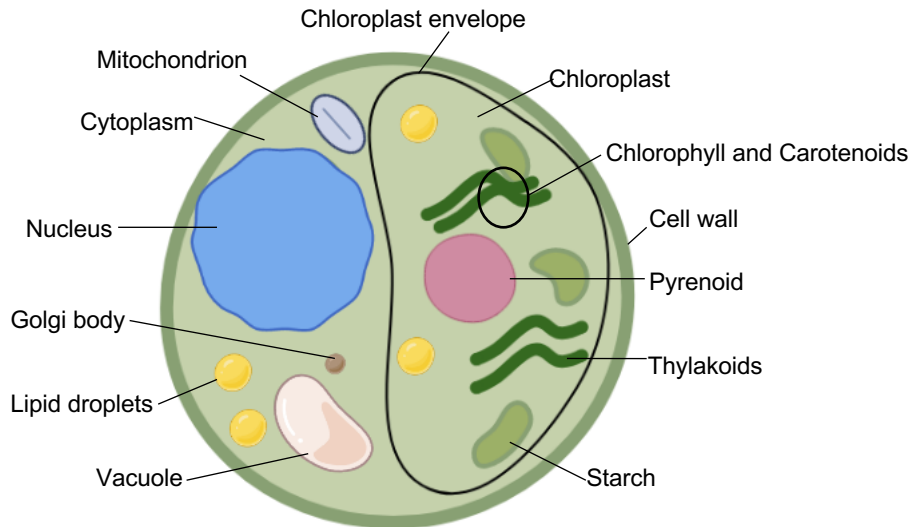
Fig. 11: *Chlorella vulgaris* cell structure representing different organelles. Image created using BioRender.com.

Pyrenoid is a microcompartment which accommodates Rubisco enzyme, unlike higher plants. In green algae, the Rubisco matrix is additionally surrounded by a starch sheath within the pyrenoid compartment to limit CO_2 leakage for maximal photosynthetic production[171]. Rubisco is an enzyme which is responsible for the fixation of carbon derived from atmospheric CO_2. Carbon fixation is a part of the Calvin cycle mechanism for starch (glucose) production which is essential for the growth of the organism[172]. Conversely, in PO_2 higher conditions, the O_2 substitutes CO_2 in the photosynthetic CO_2 fixation reaction, which is catalysed by Rubisco. The Rubisco catalytic reaction produces phosphoglycolate/ glycolate 2-phosphate (2PG), a toxic compound due to O_2 substitution[172,173]. In order to detoxify the 2PG, the plant cell is required to involve in a photorespiration cycle to replace 2PG with phosphoglycerate/ glycerate 3-phosphate (3PGA) in the cell. The recovery process consumes additional CO_2, ATP and NADPH. Since CO_2, ATP and NADPH are being used up to detoxify 2PG rather than producing new sugar molecules by Calvin cycle, hence the cell growth rate declines until the 2PG compound is complete removed[174]. The other main chain-event that occur in high O_2 condition together with photorespiration is photoinhibition. Photorespiration is well defined as the light-dependent consumption of O_2 and the production of CO_2. While, photoinhibition occurs when microalgae are exposed to high light intensities for a long period, which leads to ROS generation and induces cellular damage[175–177].
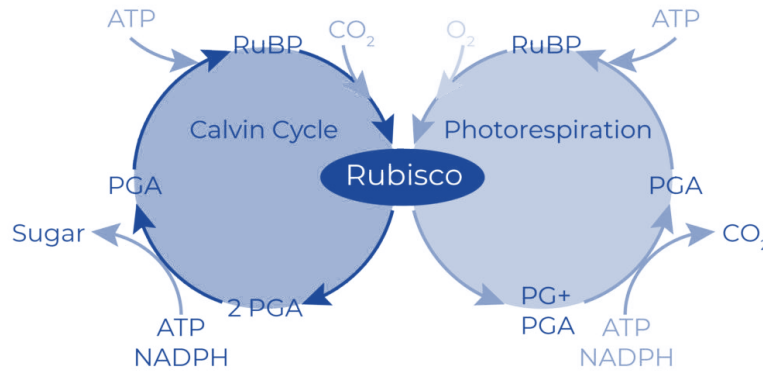
Fig. 12: The function of the Rubisco enzyme in *Chlorella vulgaris*.
Rubisco catalyses CO_2 into sugar via Calvin-cycle (carbon-fixation process) while Rubisco catalyses O_2 to produce 2PG, a toxic compound, via photorespiration at high PO_2 conditions. At atmospheric balanced conditions, Rubisco detoxifies 2PG via photorespiration by absorbing more CO_2 from the atmosphere, in addition to ATP and NADPH intake from extracellular matrix [175,177]. Image created using BioRender.com.

Microalgae in general is a very useful plant on earth. Microalgae were renowned for producing approximately half of the atmospheric O_2 on earth via photosynthesis and absorbing a massive amount of CO_2 as a major feed. *C. vulgaris* content variable nutritious bioactive compounds that are proposed to overcome cardiovascular diseases, hypertension and cancer, also as a collagen-synthesis inducer and immune system modulator[180–184]. *C. vulgaris* specifically has the tendency to produce a significant amount of lipid and H_2 gas which are both very useful for biodiesel production and as a clean combustion material, respectively, for future energy saving[185,186].

The use of algae for H_2 production has been extensively studied specifically with *C. vulgaris*[186,187]. *C. vulgaris* is an organism capable of using sunlight for water oxidation to release electrons and protons in photosystem II (PSII) which eventually transferred to ferredoxin in photosystem I (PSI). Second light absorption by the PSI reaction centre energizes the electron that is transferred to ferredoxin (Fd). Normally, ferredoxin carries electrons to an enzyme that reduces $NADP^+$ to NADPH, which involves CO_2 conversion to carbohydrates by a carbon-fixation reaction. Whereas under a long period of darkness, the ferredoxin transfers the electron accepted from the PSII process to the hydrogenase to reduce protons to molecular H_2. Hydrogenase catalytic reaction more efficiently generates H_2 when PSI receive light after a long period of darkness[33,188].
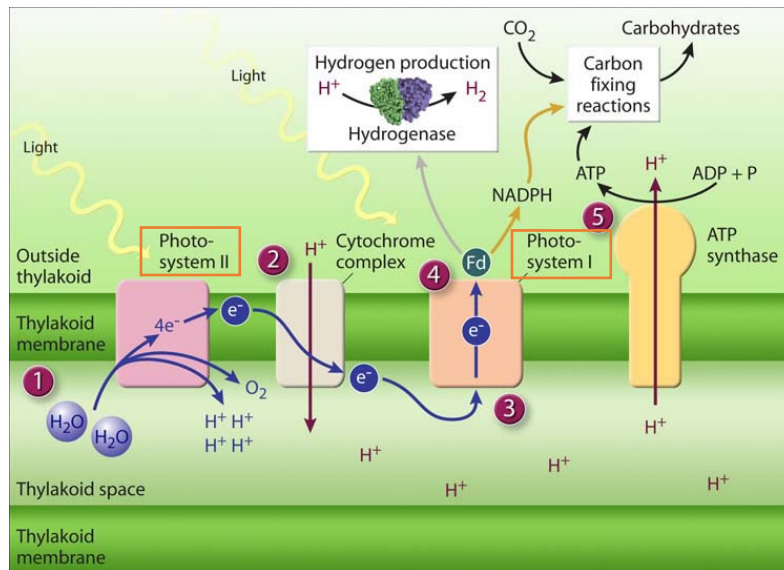
Fig. 13: Photosystem I (PSI) and Photosystem II (PSII) in *Chlorella vulgaris*.
PSI and PSII facilitate photosynthesis by light absorption as an energy source to convert carbon dioxide (CO_2) to carbohydrates. While in absence of light at PSI, ferredoxin transfer electron to the hydrogenase enzyme to reduce proton (H^+) to hydrogen (H_2) rather than transferring into the carbon fixing reaction to produce carbohydrate[33,189]. Image from US DOE[190]

1.4   Measuring parameter

In this thesis, the therapeutic effect of H_2 is to be determined. Therefore, different types of gases including N_2 and O_2 at different concentrations were used in comparison with H_2 and H_2-O_2 gas mixture. The therapeutic property of H_2 gas was determined by incubating the model organisms, zebrafish and *C. vulgaris* in H_2 enriched medium. The benefits of the therapeutic molecule were decided based on i) the regular development of the intact zebrafish larva ii) injured tissue regeneration of the zebrafish larva; iii) neutrophil recruitment at the injured site of the zebrafish larva; and iv) cell growth of *C. vulgaris*.

1.4.1 Measuring the growth of zebrafish larva

The overall development of zebrafish larvae is based on the nutrition supply contributed by its own yolk sac until 5 to 7 dpf[155,191], until the larvae develop the ability to hunt for food on their own[192]. Therefore, the larvae from 3-5 dpf stage get almost a similar amount of nutrients to multiply cells for regular tissue development. The larvae between 3-5 dpf stage will not go through large anatomy changes except for the swimming bladder development which enables it to swim, and also basic tissue development occurs including fin growth[193,194]. Therefore, in this research, it is very feasible to determine the therapeutic effect of molecular H_2 on intact zebrafish larvae by measuring the whole area of the caudal-fin fold. In this study, also assumed

that the rapid fin development indicates or represents an overall healthy development of the zebrafish larvae.

1.4.2 Measuring tissue regeneration of zebrafish larva

Zebrafish is a perfect model to study regeneration since the caudal-fin fold is easily accessible without causing a detrimental effect on the organism. The amputated tissue regeneration is easily followed in the live zebrafish larva by brightfield fluorescence microscopic imaging. In this study, the progression of amputated tissue growth was captured for 3 consecutive days and compared. The process of the amputated fin tissue restoration is called epimorphic regeneration and proceeds by i) rapid covering of the surface of the amputated site by wound epidermis; ii) de-differentiated mesenchymal cells appear; iii) cells near the amputation plane accumulate into a distinctive tissue called the blastema. Blastema formation comprises various cell de-differentiation, proliferation and re-differentiation to rebuild the missing fin structures; and iv) After blastema formation, appropriate tissues are newly formed from the blastema cells and reconstruct the original morphology[137,153]. Therefore, if the H_2 accelerates the fin regrowth, indicating the molecular H_2 may manipulate the epimorphic dynamic regeneration process. The elucidation of tissue repair and regeneration with molecular H_2 in zebrafish species if turns out to be a satisfactory outcome then expecting the molecular H_2 to equally benefit wound regeneration in humans as well.

1.4.3 Neutrophil count correlation to tissue regeneration

At the cellular level, the immune system is composed of two main arms which are adaptive immunity (revolving T cells and B cells) and innate immunity (revolving macrophages and neutrophils) bridged by dendritic cells. The caudal hematopoietic tissue (CHT) gives rise to macrophages and neutrophils in 2 dpf larvae. Since the adaptive immunity cells are not mature until 4 to 6 weeks post-fertilization, therefore studying innate immunity in isolation, without interference from adaptive immunity cells became possible in zebrafish larva[153,154]. On top of that, the neutrophils are often the first responders recruited to the injured site prior to macrophages arrival [196].

Recruited neutrophils execute the host-defence functions such as phagocytosis and degranulation[142,197]. In typical cases, researchers have shown the lifespan of neutrophils in zebrafish larvae is up to 5 days[198]. The recruited neutrophil closure was traditionally thought to occur through neutrophil apoptosis and clearance by macrophages[199]. However, Mathias et al. have shown that neutrophils display retrograde chemotaxis, back toward the vasculature

by *In vivo* time-lapse imaging in zebrafish larvae. The researchers have indicated that the reverse migration of neutrophils is a possible mechanism for resolved wound healing process, hence early disappearance of neutrophils is interrelated to the fast recovery of injury[154–156]. Therefore, the neutrophil fluctuation was quantified at 0.5, 3, 24 and 48 hours post-amputation to correlate the recovery rate of the injured tissue with the neutrophil count.

1.4.4 Measuring the growth of *Chlorella vulgaris*

The *C. vulgaris* matured cells differentiate into 4 daughter cells within 16-24 hours. A rapid increase in the cell density of *C. vulgaris* culture over time indicates an acceleration in cell development and cell differentiation. Therefore, the cell density is measured and further determine the healthy growth of the *C. vulgaris* cell by quantifying the molecular resources such as chlorophyll, protein and starch.

2. AIM OF STUDY

Molecular hydrogen (H_2) is not a commonly known therapeutic element in the medical line however there were many research on the application of H_2 as an anti-oxidant, anti-inflammatory, anti-apoptotic, anti-viral and anti-cancer in different model organisms for the past 15 years[7,15,31,44,49]. In the year 2020, during the COVID-19 pandemic, a massive fatality was caused mainly due to respiratory failure. To combat the medical emergency, the Chinese Health Commission has indicated implementing inhalation of H_2 and O_2 gas mixture to pacify COVID-19 symptoms in the clinical trial[8,9]. Thus, the aim of this work is to further elucidate if molecular H_2 has beneficial properties and shows a positive effect on the growth factors. The continuous research on molecular H_2 has invited variable water electrolysis systems into the market. In addition, there is also a modified alkaline water electrolysis system with intercalated electrodes in the market which produces H_2 and O_2 in a mixture called Brown's gas. This device supplier has claimed that Brown's gas has a "magic" component which contributes to "special" health-beneficial effects[93,96]. Therefore, the gas proportion and the effects of Brown's gas on organisms were studied to determine if there is any "magic" component or if Brown's gas delivers a beneficial effect due to the presence of H_2.

On top of that, Tesla oscillator with 144 MHz EMF radiation capacity which is commercially available as a "self-healing" device is used for the EMF radiation investigation. Tesla oscillator is used as an alternative modality to split the water molecules into H_2 and O_2 *in situ*[28,29] where the generated molecules were expected to influence the growth factor of the model organisms in this study. Additionally, the 144 MHz "special" radio-frequency wave is claimed to promote health by the device supplier[120,121]. Thus, the health-beneficial effects of the EMF stimulation on the model organisms were also elucidated. To determine if the molecular H_2 treatment and EMF stimulation contribute to the health beneficially, I monitored the growth response of animal (zebrafish embryos) and plant (*Chlorella vulgaris*) by further assessing five (5) different measuring parameters;

i)   the regular tissue development of intact-fin of the zebrafish embryo

ii)   the tissue regeneration of amputated-fin of the zebrafish embryo

iii)   the neutrophil count in fin-amputated zebrafish embryo

iv)   the cell density of *C. vulgaris* cell culture

v)   the quantification of bioactive compounds in *C. vulgaris* cell

3. Results

The concentration of dissolved gases in water is largely influenced by the gas proportion of atmospheric air. The proportion of dissolved gases such as O_2 and CO_2 is one of the important factors that contribute to the healthy growth of aquatic inhabitants like fish and microalgae. Many studies have been done by researchers, on how ambient gases like O_2 and CO_2 influence the physiological system in aerobic vertebrates and plants, respectively. Alternatively, this research work focus on the potential role of H_2 gas in organisms. Although, free H_2 is comparatively rare on earth as the atmosphere contains only 0.55 parts per million of H_2, however, H_2 constitutes nearly 75% of the universe's elemental mass as a component of water and organic compounds. Therefore, would be very beneficial for human and other living organisms if able to reveal the benefits of this largely available element. The potential beneficial role of molecular H_2 is examined by assessing the influence of H_2 in regular tissue development and tissue regeneration on intact and fin-amputated zebrafish larvae, respectively.

In the preliminary stage of the research, the zebrafish larvae were directly bubbled through with H_2 gas generated by a typical PEM water electrolysis system. The intact-fin and amputated fin analysis did not show a beneficial growth response instead morphological abnormalities such as oedema, notochord bending and heart bloating effects were seen (Fig. 14). The reason for the morphological abnormalities was not definite; either H_2 gas produced in a pressurized condition may cause suffocation to the larvae or the zebrafish larvae were affected by the aggressive agility during the direct-gas bubbling treatment. Therefore, I have decided to change the treatment method by pre-treat the fish medium (E3 medium) with H_2 gas prior to incubating the larvae in the medium. The medium pre-treatment with H_2 gas has refrained from any morphological deformities, instead, the H_2 infused medium aided to see a beneficial growth response.
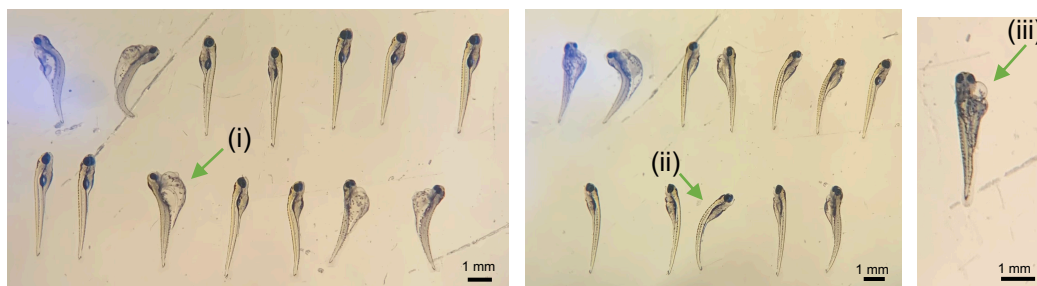
Fig. 14: Morphological deformities seen in direct-gas bubbled conditions.
Unhealthy sign of zebrafish larvae was seen due to direct-gas bubbling method such as (i) oedema, (ii) notochord bending and (iii) heart bloating. This could be due to unfavourable ambient condition such as extreme fluctuation of gas pressure in the medium might have caused suffocation to the larvae. A rapid movement of the larvae due to an aggressive bubbling effect also might cause damaging effects. Apart from that, generating H_2 enriched water using high pressurized PEM water electrolysis system might contribute to unpleasant high-pressure condition for the larvae. However, throughout this experiment with improvised procedures and standardized PEM electrolysis devices, all these possibilities are pulled out and such deformities are not observed in the currently pooled data.

The therapeutic effect of H_2 was also investigated in unicellular, photosynthetic *C. vulgaris*. The beneficial effect of molecular H_2 on *C. vulgaris* was evaluated based on the cell growth rate. The cell growth rate was determined by measuring the cell density at maximum absorbance of 750 nm (A_{750}). The *C. vulgaris* cultured with Bold's Basal medium (BBM) was also bubbled through directly with H_2 gas in the preliminary stage of the research. Since *C. vulgaris* has a high potential to increase the cell differentiation rate in a shaking condition hence a medium pre-treatment method was also implemented in the *C. vulgaris* growth evaluation study to avoid false results due to the overlay of agitation effect. However, the concentration of the infused gas and the impact on the readily dissolved O_2 in the medium were uncertain. Furthermore, the infused gas stability in the pre-treated medium is also unknown. Therefore, a saturation curve and desaturation curve were built to verify the gas saturation point and also to determine the stability of the infused gas in the pre-treated medium.

The gas saturation curve was built for each gas which have been used as a control in this study. In order to observe the definite effects of H_2 on zebrafish larvae and *C. vulgaris* cell culture, a few different gases such as air-saturated, N_2-saturated, H_2-O_2 gas mixture-saturated, Brown's gas-saturated, O_2-saturated and O_2 limitedly-infused (O_2-levelled) medium were used as controls. The saturation curve facilitates to identify of the duration taken by each device to generate the respective gases to reach the equilibrium condition. Confirming the equilibrium condition is essential to standardise the gas concentration in every experimental replication also gives an optimum possibility to observe any growth response. Moreover, different devices may generate gases at different flow rates and pressure therefore it's important that each medium is treated until the equilibrium concentration is achieved. The physicochemical

properties such as the concentration of the dissolved O_2, dissolved H_2 and the ORP value are measured from 0-40 minutes upon gas infusion to determine the gas saturation curve.

The zebrafish larvae from 3-5 dpf stage were used in this research study. The 3-5 dpf stage larva is expected to absorb the H_2, N_2, O_2, H_2-O_2 gas mixture and Brown's gas into systemic circulation by trans-cutaneous gas exchange since respiratory organs (gills) were not completely developed. The zebrafish larvae are known to absorb O_2 gas readily due to the small skin surface area against large volume of water which makes the gas diffusion through the skin, epithelial cells and further into organelles to be feasible[51], while the feasibility of molecular H_2 to be absorbed into larvae skin is unknown and unable to be measured with limited tools. However, it is known that molecular H_2 with hydrophobic properties and has a far smaller molecular size than O_2 which might enable it to be absorbed into cell organelles via skin much more efficiently than the O_2 molecule. Hence in this experiment, the larvae were exposed to the H_2 gas and the other controls by incubating the larvae in the gas saturated medium for 3 hours/day. Nevertheless, it is very uncertain of the concentration of the remaining infused gases in 3 hours incubation period.

Generally, the infused gases from external sources will not remain in the medium for a longer period as the gases tend to be volatile from the medium. However, this is not applicable to the dissolved O_2, CO_2 and N_2 gases which readily dissolve in water by rotation of the atmospheric air (78.08% of N_2, 20.95% of O_2, 0.93% of Ar, 0.036% of CO_2 and the remaining 0.004% is noble gases and trace gases). Therefore, the stability of the infused gas over time was measured until the medium reach equilibrium with atmospheric air. The measurement of the physicochemical properties such as the concentration of the dissolved O_2, dissolved H_2 and the ORP value aided to determine the gas volatility rate. Therefore, the gas volatility curve for H_2 gas and for each gas control (N_2, O_2, H_2-O_2 gas mixture and Brown's gas) were built based on the 3 listed physicochemical properties.

O_2 sensor electrode were used to measure the O_2 concentration and a colourimetric assay using methylene blue reagent was used in this study to determine the concentration of dissolved H_2 in the treated medium. The methylene blue reagent is commercially distributed in small plastic bottles, the decolourisation of one drop of the methylene blue reagent (17 mg or 23 μL) indicates the presence of 0.1 mg/L of H_2. Although the H_2 content in distilled water and E3 medium is successfully measured but the H_2 concentration in gas saturated BBM medium couldn't be measured. The methylene blue decolourisation could be interfered by other salt metal ions in the BBM medium for example, iron(ii), cobalt(ii) and manganate(vii) especially in presence of O_2 which possibly oxidise the leucomethylene back into methylene blue[157]. This

interference makes the dissolved H_2 measurement in the BBM medium with H_2 and H_2-O_2 gas mixture or Brown's gas to become impossible. Therefore, the presence of H_2 in the BBM medium was confirmed by comparing the ORP values of the BBM medium and the ORP values of the distilled water upon H_2 gas treatment. The ORP is the energy measurement in millivolts (mV) based on electrons' movement in the medium. The mildly salted E3 water and BBM water do not influence the ORP reading however the proportion changes of reducing agent (H_2) and oxidising agent (O_2) with high reduction and oxidation potential in the medium indeed influence the ORP values. The listed physicochemical properties such as the concentration of the dissolved O_2, dissolved H_2 and the ORP values in gas infused distilled water, E3 medium and BBM medium were determined and found to be almost similar. Thus, only the data collected by measuring the gas infused distilled water were presented here (Fig. 15 and Fig. 20) while, the saturation and volatility curve with E3 and BBM medium is attached in appendices (Fig. S1-Fig.S12).

On the other hand, a 144 MHz EMF wave generating Tesla oscillator device was used as an alternative modality to split the water molecules into H_2 and O_2 *in situ*[28,29] where the generated molecules were expected to influence the growth factor of the model organisms in this study. Maehara et al. and a few more other researchers in year 2000s have proposed the potential of radio-frequency EMF to split water molecules into H_2 and O_2. Further, the presence of dissociated molecular H_2 is shown to be confirmed by a colourimetric assay of decolourising methylene blue to leucomethylene blue by Maehara et al.[128,130]. However, in this study the measurement using O_2 and ORP electrode sensor, also using the colourimetric assay to determine the presence of dissociated H_2 and O_2 molecules in the radiated medium was unsuccessful. The probably dissociated H_2 and O_2 were untraceable however different aspects were monitored. The research was proceeded by monitoring the influence of EMF radiation on physiological activity as a second messenger which determined by the growth response.

Tesla oscillator is a commercially available "self-healing" device. The device supplier claimed that the exposure to the 144 MHz "special" radio-frequency wave enables the patients to heal from health complications such as skin inflammation, limb oedema and lower back pains[120]. In larger perception, conventional and alternative medicine have attracted scientists and clinicians to the potential benefits of using EMF for therapeutic purposes however the safety of magnetic and EM field exposure is still a very sceptical and controversial subject. Although there are publications of successful therapy by EMF stimulation[108,109,111,112], on the other hand, there are equally numerous publications on undeniable adverse effects due to EMF exposure such as headache, cancer, teratogenic, gene mutation (genotoxic) or seizures[103,117]. Hence, the development of the intact-fin larvae and regeneration of the amputated-fin larvae were

used as a parameter to study the effects of EMF radiation on health. The growth response by zebrafish larvae was compared upon treatment by a "health-promoting" Tesla oscillator (144 MHz) and the WLAN router that generates pulsed waves at 5 GHz frequency. A set of untreated larvae (control) was kept away from the Tesla and WLAN radiation radius to compare the EMF effects on larvae.

3.1   Gas saturation curve determination with gas infused distilled water

Gas saturation curves were determined based on O_2 concentration, H_2 concentration and ORP measurement. Fig. 15 shows the O_2 saturation curve of distilled water upon H_2 gas, N_2 gas, O_2 gas, H_2-O_2 gas mixture and Brown's gas infusion. The O_2 concentration in air saturated and untreated distilled water was also measured from 0-40 minutes however there is no obvious fluctuation of O_2 concentration. The O_2 concentration of air saturated water is very crucial to be determined here because, both the zebrafish larvae and *C. vulgaris* were incubated in an air compressor bubbled medium to represent a baseline in this overall study. Bubbling a medium with an air compressor may air-saturate the medium by rotating the ambient N_2 and O_2 from the atmosphere into the treated medium. However, the untreated control medium and air treated medium has almost similar amount of dissolved O_2 throughout the treatment period which shows that bubbling water with air compressor does not change the dissolved O_2 in the medium. Hence, air treated larvae will be a perfect baseline to make a comparison study of beneficial of H_2 to larvae.

Based on the untreated and air saturated medium, it is obvious that distilled water contains ~6.7 mg/L of O_2 at atmospheric equilibrium conditions. However, water has the capacity to further dissolve O_2 maximum up to ~30 mg/L by infusing of pure O_2 generated by PEM electrolysis system. The O_2 concentration could increase to the saturation point within 15 minutes. Meanwhile, distilled water treatment by different gases such as H_2 gas, N_2 gas, H_2-O_2 gas mixture and Brown's gas were also influence the solubility of dissolved O_2. Diffusion of gas such as pure H_2, will not only increases the solubility of the dissolved H_2 in the medium but also depletes the readily dissolved O_2 from the medium. The same phenomena were observed when diffuse pure N_2 gas into a medium where the readily dissolved O_2 being depleted. The H_2 and N_2 maximum saturated medium has lost 70% of the dissolved O_2 concentration which is from 6.7 mg/L to 1.8 - 2.0 mg/L.

The combination of H_2 and O_2 gas such as the H_2-O_2 gas mixture and Brown's gas infusion medium shows a different result. A typical PEM water electrolyser with diaphragm-separated electrodes breaks water molecules to generate 2 moles of pure H_2 with 1 mole of pure O_2 via

separate output. The separately generated H_2 and O_2 gases were mixed in the medium until the saturation point. The Brown's gas generated by an alkaline water electrolyser which is modified with intercalated anode and cathode electrodes is also expected to produce H_2 and O_2 gas as a mixture via a single output valve in this study. Since Brown's gas device suppliers and some researchers claimed of "magical" component in Brown's gas infused medium delivers medicinal benefits[93,94,96] hence the physicochemical properties of Brown's gas were compared with the H_2-O_2 gas mixture. H_2-O_2 gas mixture and Brown's gas saturation show that the dissolved O_2 concentration increases from 6.7 mg/L to 11.7 mg/L in both conditions. H_2-O_2 gas mixture and Brown's gas infusion introduce around 40% more O_2 into the medium. Further to study the therapeutic benefit of H_2 and O_2 in a mixture, an O_2-levelled condition was used as a compatible control to rule out the side-effects of high O_2 content in the medium. The O_2-levelled condition is created by infusion of a limited amount of O_2 gas until the medium reaches the desired 11.7 mg/L concentration of O_2. The O_2-levelled condition was achieved by pure O_2 infusion for in 1 min 45 seconds.
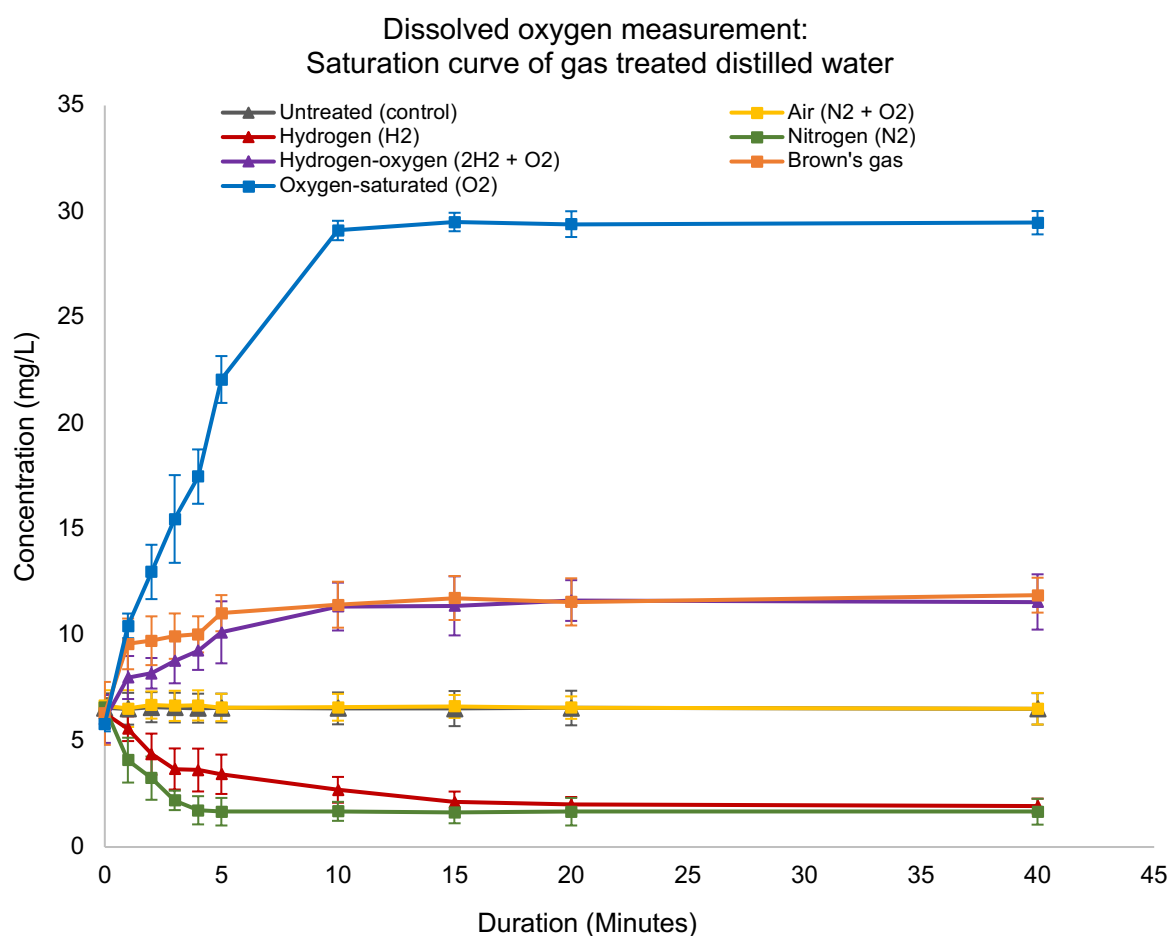
Fig. 15: Saturation curve for dissolved oxygen concentration.
Air, H_2, N_2, O_2, H_2-O_2 gas mixture and Brown's gas treated distilled water reach equilibrium conditions in a short period. O_2-levelled condition upon desirable O_2 infusion (11.7 mg/L concentration targeted, reached in 1 min 45 seconds).

The saturation curve for dissolved H_2 is only shown for H_2, H_2-O_2 gas mixture and Brown's gas infused medium because H_2 is not detectable in untreated or air saturated medium. The pure H_2 required a minimum of 15 minutes to reach the saturation point (~2.0 mg/L) in distilled water while the H_2-O_2 gas mixture and Brown's gas only required 5 minutes to reach the saturation point (0.8 mg/L) (Fig.16). The pure H_2 treated medium is able to retain almost 60% more dissolved H_2 concentration compared to the H_2-O_2 gas mixture and Brown's gas treated medium at equilibrium conditions. Since the H_2-O_2 gas mixture and Brown's gas generating devices diffuses a mixture of the H_2 and O_2 gas hence unable to dissolve a larger amount of H_2 into the medium. Based on the H_2-O_2 gas mixture generated by a typical PEM water electrolyser of 2:1 ratio of H_2 and O_2 diffusion observation showed a maximum concentration of 0.8 mg/L of H_2 (0.40 mM) with 11.7 mg/L of O_2 (0.37 mM). Meanwhile, Brown's gas saturated medium also showed the similar saturation of H_2 and O_2 gas as in H_2-O_2 gas mixture treated medium. This similarity indicates that most probably the Brown's gas and H_2-O_2 gas mixture are not difference gases.
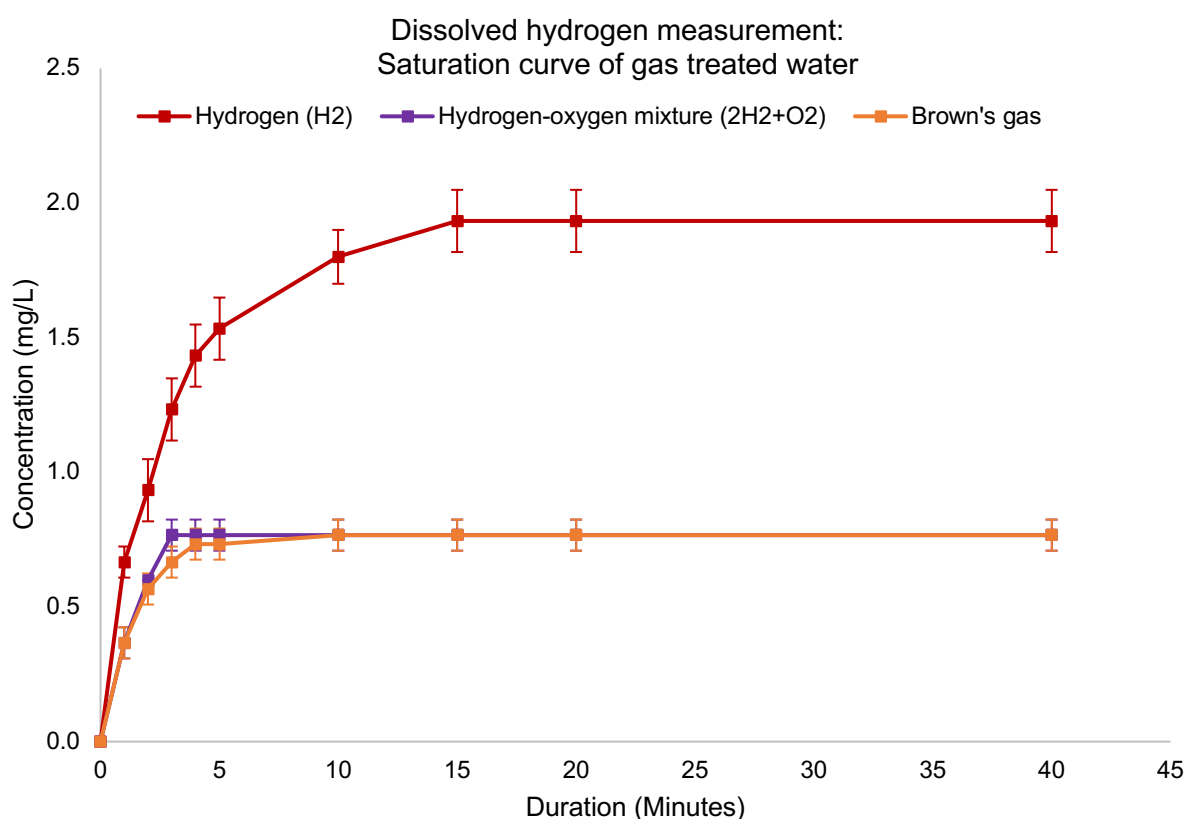
Fig. 16: Saturation curve for dissolved hydrogen concentration.
Pure H_2 gas able to retain a larger concentration in the medium compared to H_2-O_2 gas mixture and Brown's gas which only retain approximately 60% compared to pure H_2 at maximum saturation point.

The H_2 molecule has more reduction potential while the O_2 has more oxidation potential therefore elevation of either one of these molecules in higher proportion influenced the ORP value very distinctly. The increase of the H_2 proportion higher than the O_2 will show a more negative ORP value while a higher proportion of O_2 will show a more positive ORP value. The

33

untreated and air bubbled medium constantly shows a positive ORP value (+153 mV), this due to the presence of ~6.7 mg/L of dissolved O_2 in water in general (Fig. 17). The H_2 bubbled medium retains around 1.5 - 2.0 mg/L (0.74 - 1.0 mM) of H_2 while, depleting O_2 concentration to 2.0 mg/L (0.06 mM). The high concentration of reducing agent, H_2 in the medium signify the high reduction potential which influence the ORP value to be more negative (-560 mV) at saturation point. Meanwhile, the ORP value of pure N_2 treated water which also depletes O_2 to 1.8 mg/L (0.056 mM) has less negative ORP value (-194 mV) than H_2. This is because N_2 is not a reducing agent but an inert molecule. This condition explains that H_2 is a reactive element which has the potential to act as a good reducing agent to suppress stress-inducing oxidants compared to the N_2 molecule which is unreactive[43,158]. The O_2 infused medium elevated the dissolved O_2 concentration from 0.21 mM to 0.91 mM which elevated the ORP value from +153 mV to +291 mV. Meanwhile, the H_2 (0.4 mM) and O_2 (0.37 mM) combination gas including, the Brown's gas with similar physicochemical properties as the H_2-O_2 gas mixture is balanced the ORP value between -194 to -225 mV. Meanwhile, the O_2-levelled condition infused with limited O_2 achieve the desired condition with ORP value of + 175 mV which reached in 1 min 45 seconds.
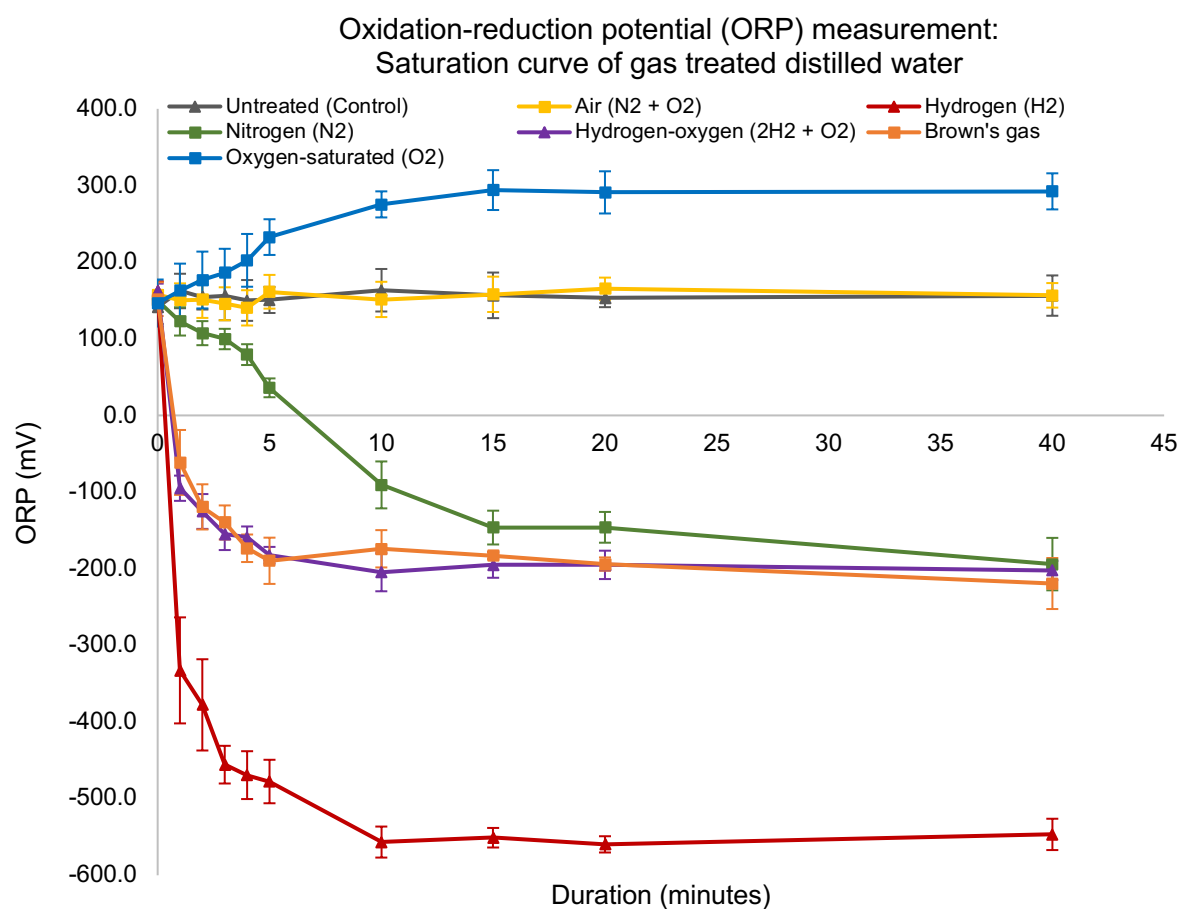
Fig. 17: Oxidation-reduction potential (ORP) of gases achieving saturation curve.
Air, H_2, N_2, O_2, H_2-O_2 gas mixture and Brown's gas treated medium with their respective ORP value as reaching equilibrium condition. O_2-levelled condition upon desirable O_2 infusion (+ 175 mV reached in 1 min 45 seconds).

Based on the dissolved H_2, dissolved O_2, and ORP values, it is obvious that gases reach saturation point within 10 – 15 minutes however to assure the medium reaches the saturation point the E3 medium for zebrafish larvae experiment and BBM medium for *C. vulgaris* experiment were pre-treated for 20 minutes to standardise the equilibrium concentration of dissolved H_2 and O_2.

3.2 Gas volatility curve determination with gas infused distilled water

Fig. 18-20 shows a time-dependent changes of the dissolved H_2 and O_2 in the gas infused medium. The infused gas (H_2, N_2, O_2, H_2-O_2 gas mixture and Brown's gas) from external sources other than the dissolved atmospheric air will eventually volatile from the treated medium after a certain period therefore it is essential to analyse the trend of gas volatility. The untreated and air saturated medium were included in the graph as a baseline to compare.

The O_2-levelled condition was achieved by treating the medium with pure O_2 up to 40% to match the dissolved O_2 level in the H_2-O_2 gas mixture and Brown's gas treated medium. The H_2-O_2 gas mixture, Brown's gas and O_2-levelled medium gained 40% additional O_2 upon treatment and lost 30% of dissolved O_2 in 30 minutes and return to atmospheric equilibrium condition in 2 hours. The O_2-saturated medium lost 27.0% of infused O_2 in 30 minutes and subsequently lost further 15% of O_2 in another 1.0 hours. Based on Fig. 18, the H_2 and N_2 treated medium which depletes 70% of O_2 from the medium will gain back 26% of O_2 from the atmospheric air in 20 minutes and 45% of O_2 in 30 minutes. The H_2 and N_2 treated medium reach equilibrium with the atmospheric condition in 6 hours.
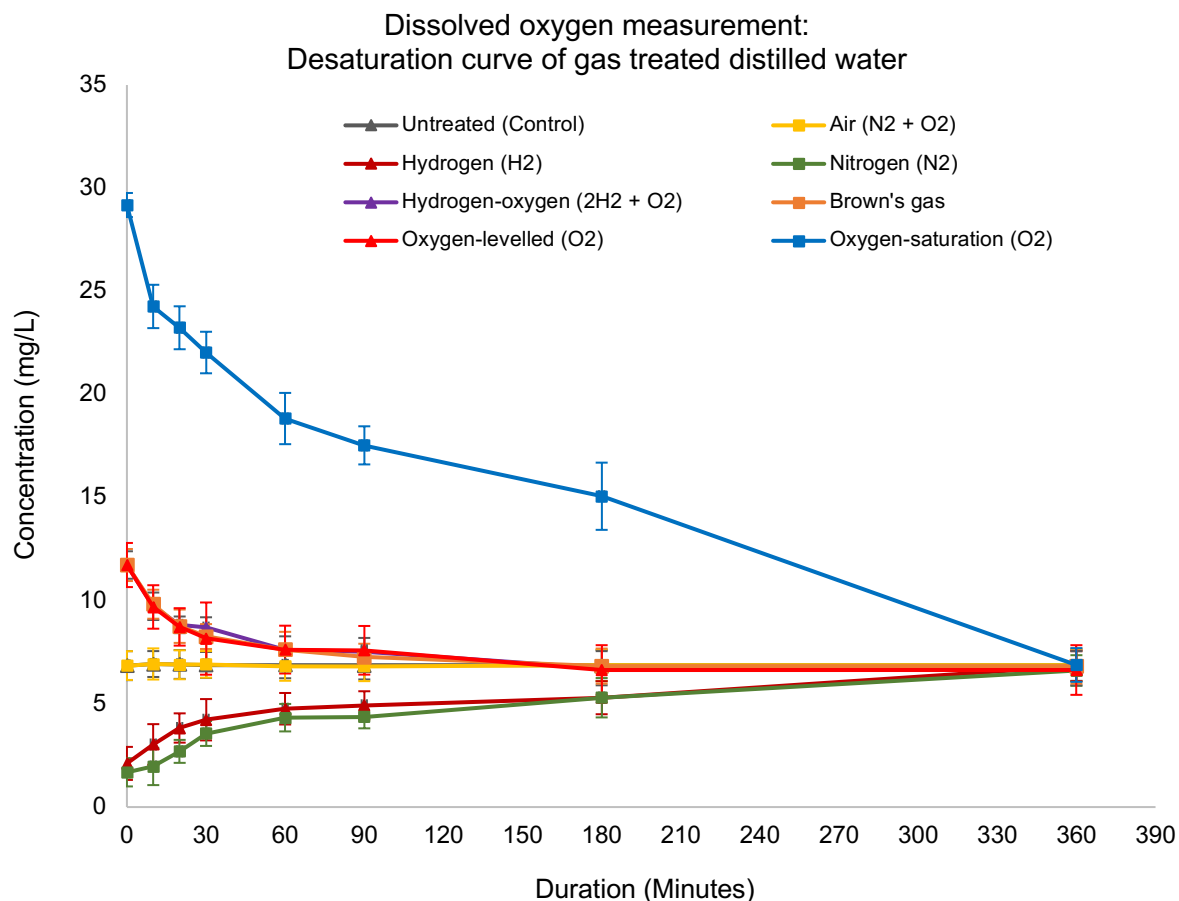
Fig. 18: Desaturation curve for dissolved oxygen concentration.
Time-dependent properties of dissolved oxygen in the treated medium. Air, H_2, N_2, O_2, H_2-O_2 gas mixture and Brown's gas treated distilled water reach atmospheric equilibrium condition in maximum of 6 hours.

Fig. 19 shows the gas volatility of dissolved H_2 from H_2, H_2-O_2 gas mixture and Brown's gas treated medium. The H_2 volatility is faster in pure H_2 treated medium compared to H_2 and O_2 mixture condition. The dissolved H_2 volatile 32% in 10 minutes and lost 53% in 30 minutes. While the H_2 infused medium reach atmospheric equilibrium condition in 60 minutes. While H_2-O_2 gas mixture and Brown's gas treated medium lost 12.5% of infused H_2 in 10 minutes and lost 38% in 30 minutes from the gas saturated medium. H_2-O_2 gas mixture and Brown's gas infused medium also reach atmospheric equilibrium condition in maximum 60 minutes. A high concentration of dissolved H_2 containing medium allows the gases to be volatile faster compared to the less gas saturated condition.
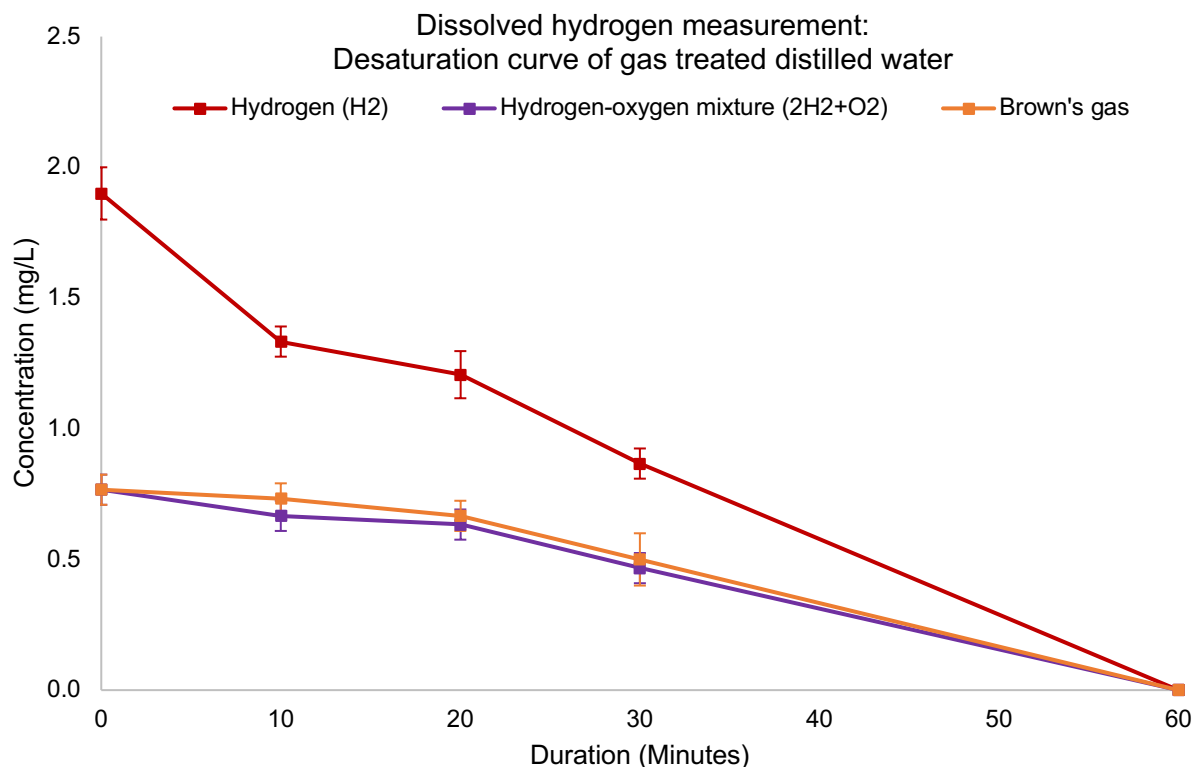
Fig. 19: Desaturation curve for dissolved hydrogen concentration.
Time-dependent volatility of dissolved hydrogen concentration in H_2, H_2-O_2 gas mixture and Brown's gas treated distilled water. The gas saturated medium reaches the atmospheric equilibrium condition in an hour.

Fig. 20 shows that the ORP value of H_2 treated medium became positive in 180 minutes upon desaturation of dissolved H_2 however took 6 hours to reach atmospheric equilibrium condition. Although the infused H_2 volatile within an hour however the H_2 desaturated medium required almost 6 hours to gain O_2 up to the atmospheric equilibrium condition. Containing lower dissolved O_2 in the medium will also lower the ORP value. The N_2 treated medium has less negative ORP value at saturation point compared to H_2 treated medium however N_2 treated medium also required more than 120 minutes to reach a positive ORP value and almost 6 hours to reach atmospheric equilibrium condition. Since the H_2-O_2 gas mixture and Brown's gas treated medium has almost same concentration of H_2 and O_2 therefore both gases infused medium has almost the same ORP values. The N_2 treated medium has almost similar ORP value with H_2-O_2 gas mixture treated medium at saturation point however the ORP value of the H_2-O_2 mixture gas infused medium increases (become more positive) faster and reached the atmospheric equilibrium condition by 180 minutes which is 2 times faster than H_2 and N_2 treated medium.
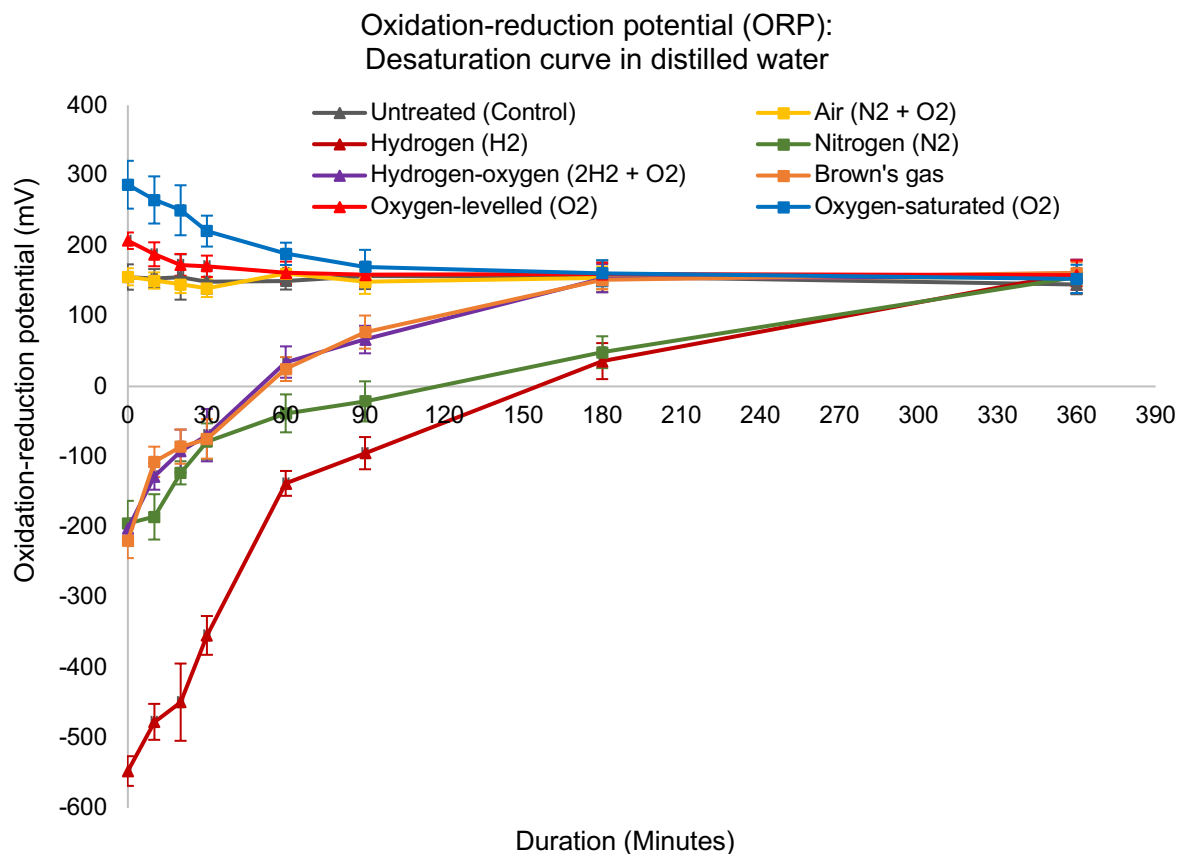
Fig. 20: Oxidation-reduction potential (ORP) of gas desaturation.
Air, H_2, N_2, O_2, H_2-O_2 gas mixture and Brown's gas treated medium with their respective ORP value as reaching atmospheric equilibrium condition.

The larvae were incubated in a pre-treated medium for 3 hours to ensure the larvae have absorbed sufficient infused H_2. The desaturation curves have confirmed that the infused gases are not stable for more than 30 minutes. Therefore, the medium incubated with the model organisms was changed every 30 minutes with freshly gas infused medium to see any possible beneficial effects. Table 1 shows the instrument/devices that used to generate distilled water, to generate gas and EMF wave generating devices with the maximum possible H_2 and O_2 concentration with their corresponding ORP values could be achieved using the respective devices as in the Table 1.

Table 1: The summarised table with distilled water, gas and EMF producing instruments/devices. The concentration of O_2, concentration of H_2 and the ORP values of untreated, air-saturated, H_2-saturated, O_2-saturated, H_2-O_2 gas mixture-saturated, N_2-saturated, Brown's gas-saturated and EMF treated medium is shown here together with the producing instruments/devices.
(Dissolved hydrogen, DH; dissolved oxygen, DO; oxidation-reduction potential, ORP)

Instruments/Devices	Images	Analysis results
Distilled water (Untreated water)		Untreated water DH: 0 mg/L DO: ~6.7 mg/L, 0.21 mM ORP: +153 mV
Air compressor Air (N_2 + O_2)		Air-saturated medium DH: 0 mg/L DO: ~6.7 mg/L, 0.21 mM ORP: +153 mV
Proton exchange membrane (PEM) water electrolysis Provides: hydrogen (H_2) and oxygen (O_2)		H_2 saturated medium DH: 1.6 - 2.0 mg/L, 0.79 - 1.0 mM DO: 2.0 mg/L, 0.06 mM ORP: - 560 mV O_2 saturated medium DH: 0 mg/L DO: 29.0 mg/L, 0.91 mM ORP: +290 mV $2H_2$ + O_2 saturated medium DH: 0.8 mg/L, 0.40 mM DO: 11.7 mg/L, 0.37 mM ORP: -206 mV

Nitrogen gas cylinder Provides: nitrogen (N$_2$)		N$_2$ saturated medium DH: 0 mg/L DO: 1.7 mg/L, 0.05 mM ORP: -194 mV
Alkaline water electrolysis with intercalated electrodes Provides: Brown's gas		Brown's gas saturated medium DH: 0.8 mg/L, 0.40 mM DO: 11.7 mg/L, 0.37 mM ORP: -219 mV
Tesla oscillator Provides: Electromagnetic field (EMF)		EMF treated medium DH: 0 mg/L DO: ~6.7 mg/L, 0.21 mM ORP: +153 mV
WLAN (wireless local area network) router Provides: Electromagnetic field (EMF)		EMF treated medium DH: 0 mg/L DO: ~6.7 mg/L, 0.21 mM ORP: +153 mV

3.3 Measuring parameter of gas and electromagnetic field (EMF) treatment on zebrafish embryos

The zebrafish larvae were exposed to experimental gases (H_2, N_2, O_2-levelled, O_2-saturated, H_2-O_2 gas mixture and Brown's gas) by incubating the larvae in a pre-treated E3 medium. The E3 medium is infused with gas before incubating the 3 dpf larvae for 30 minutes and replace the medium with another freshly gas infused medium to supply the larvae with maximum gas saturation for 6 times in a row, every 30 minutes. The gas treatment procedure was carried out for 3 consecutive days. The H_2 and H_2-O_2 gas mixture treated larvae growth rate were compared with their compatible controls as shown in Table 2 based on their comparable measured physicochemical properties such as the dissolved H_2 and O_2 concentration at equilibrium condition.

Apart from H_2 treatment, EMF radiation treatment effects are the next important observation made in this study. Untreated medium which kept away from 144 MHz Tesla oscillator and 5 GHz WLAN radiation radius were used as a control.

Table 2: The combination of gas treatment with compatible controls. The comparable conditions are prepared based on the measured physicochemical properties of each treated medium with respective gases at equilibrium conditions. (Dissolved hydrogen, DH; dissolved oxygen, DO)

Comparable conditions				
1	2	3	4	5
Oxygen concentration	Exploration	Hypoxia	Hyperoxia	EMF
Air (DO: ~6.7 mg/L)	Air (DO: ~6.7 mg/L)	Air (DO: ~6.7 mg/L)	Air (DO: ~6.7 mg/L)	Untreated (DO: ~6.7 mg/L)
N_2 (DO: 1.8 mg/L)	H_2 (DO: 2.0 mg/L) (DH: 1.6-2.0 mg/L)	N_2 (DO: 1.8 mg/L)	O_2-levelled (DO: 11.7 mg/L)	Tesla oscillator (sine wave) (DO: ~6.7 mg/L) (DH: 0.0 mg/L)
O_2-levelled (DO: 11.7 mg/L)	Brown's gas (DO: 11.7 mg/L) (DH: 0.8 mg/L)	H_2 (DO: 2.0 mg/L) (DH: 1.6-2.0 mg/L)	Brown's gas (DO: 11.7 mg/L) (DH: 0.8 mg/L)	WLAN (pulse wave) (DO: ~6.7 mg/L) (DH: 0.0 mg/L)
O_2-saturated (DO: ~29.0 mg/L)	H_2-O_2 gas mixture ($2H_2 + O_2$) (DO: 11.7 mg/L) (DH: 0.8 mg/L)		H_2-O_2 gas mixture ($2H_2 + O_2$) (DO: 11.7 mg/L) (DH: 0.8 mg/L)	

The therapeutic effects of molecular H_2 and EMF radiation on the zebrafish larvae was concluded by comparing with its compatible controls based on few measuring parameters such

as; i) the regular development of the zebrafish larvae by measuring the intact-caudal fin fold area ii) amputated-caudal fin tissue regeneration iii) quantification of neutrophils recruited to the amputated-fin site of the zebrafish larvae.

3.3.1 Measuring parameter of intact-fin growth and amputated-fin tissue regeneration on the zebrafish larvae.

The overall development of zebrafish embryo is based on the nutrition supply contributed by its own yolk sac until 5 to 7 dpf[159,160]. In additional, incubation of 3 dpf larvae in the gas pre-treated medium will allow gas diffusion into the larvae body through skin might also have influenced the larvae development including the growth of caudal fin-fold. Therefore, it is very feasible to determine the therapeutic effect of molecular H_2 on a healthy fish by measuring the whole area of the caudal-fin fold. The overall length of 3 dpf zebrafish larvae is about 4.3 mm while the caudal fin-fold part is about 0.36 mm long which is 8 – 8.5% of the overall skeletal structure. Thus, the rapid caudal fin-fold development upon treatment was assumed to represent an overall healthy development of the larvae within 3 - 5 dpf period.

While the amputated tissue regeneration is easily followed in live zebrafish larvae by brightfield fluorescence microscopic imaging. The progression of amputated tissue growth was captured for 3 consecutive days (3 - 5 dpf period) and compared with the controls. The caudal fin-fold of zebrafish larvae was amputated slightly below the notochord-end-point to have a defined reference-line to measure the fin area as described in Fig. 21 and Fig. 22. Also, it is crucial to not damage the notochord as it has a different recovery rate compared to the fin tissue.

Notochord end-point determine the reference-line

Area below reference-line measured to determine growth of whole fin area
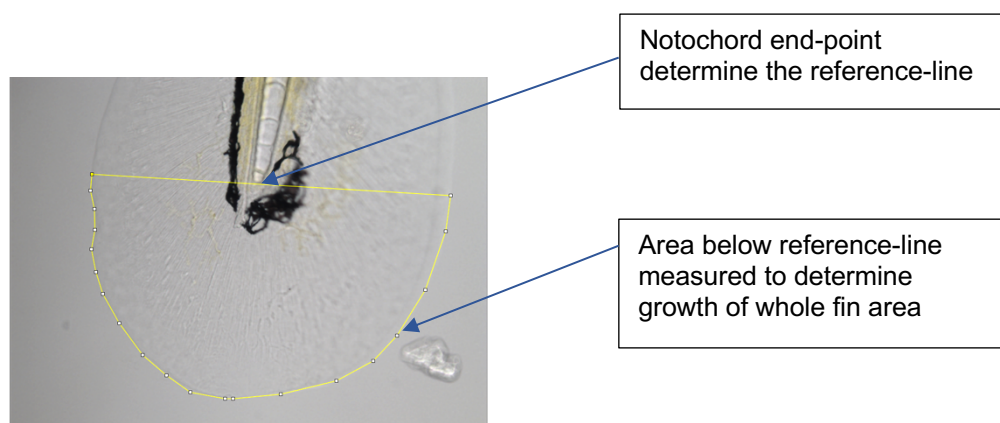
Fig. 21: The standard procedure to measure the intact caudal fin-fold of zebrafish larvae. The treated intact-larvae caudal fin measured from 3 days post-fertilized (3 dpf) to 5 days post-fertilized (5 dpf) from day 1 to day 3 to determine the fin development.
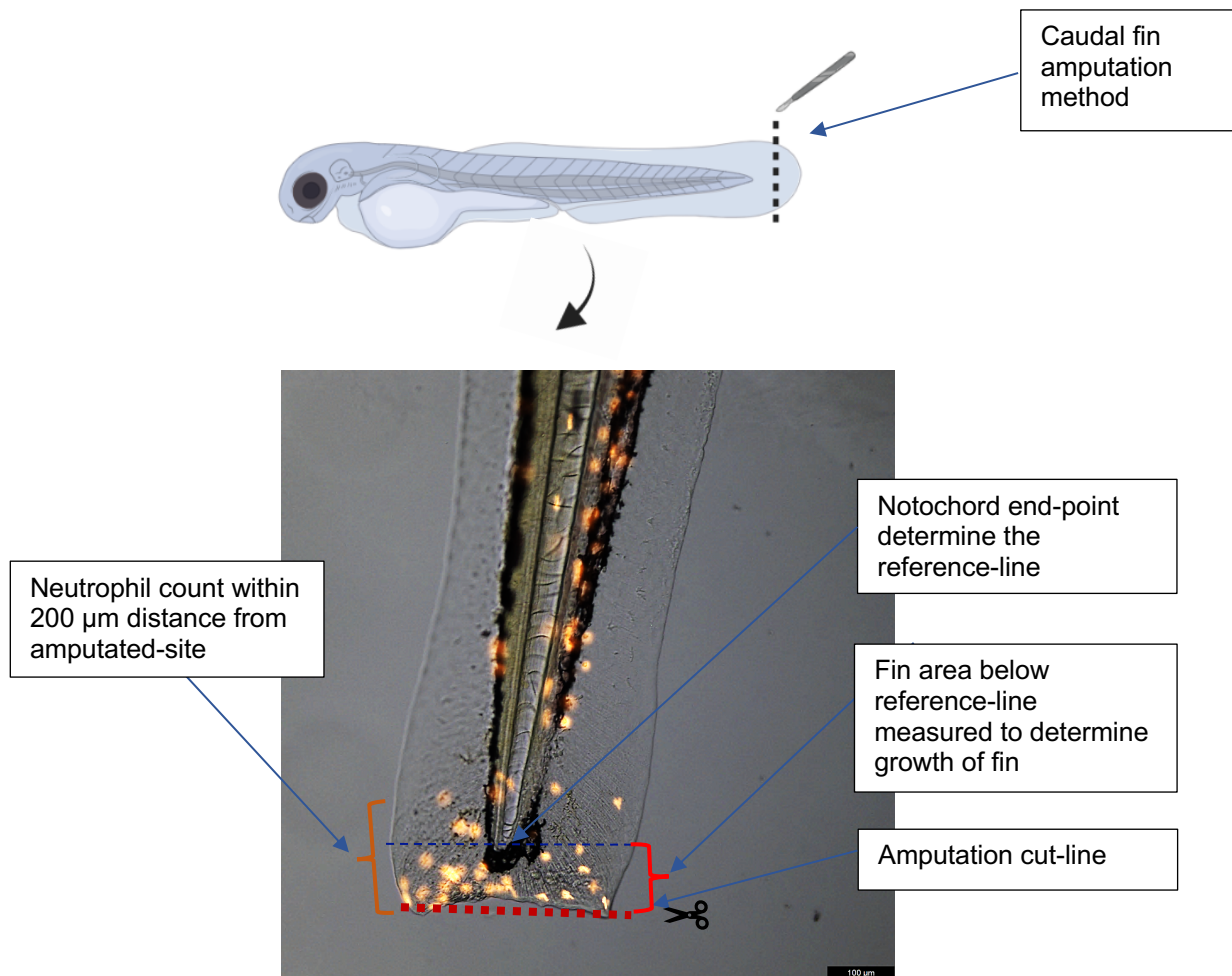
Fig. 22: The standard procedure to measure the amputated caudal fin-fold of zebrafish larvae.
Three days post-fertilized (3dpf) larvae were amputated slightly below the notochord end-point.
Defining the reference-line and cut-line of amputated larva to measure caudal fin area and quantify the
neutrophil cells. Image created using BioRender.com.

The Table 3 shows both the intact-fin and amputated fin of zebrafish larvae were measured
from Day 1 to Day 3. According to the standard procedure, the larvae samples were incubated
for 3 hours in a gas pre-treated E3 medium prior to caudal fin-fold amputation and imaging.
The zebrafish larvae with intact-fin were also treated with respective gases prior to immobilise
with agarose gel and continued by imaging. For EMF treatment effects observation, both the
intact and the fin-amputated zebrafish larvae were treated for 30 minutes twice/day prior to
imaging and amputation.

Table 3: The method of caudal fin-fold growth comparison from day 1 (3 dpf) to day 3 (5 dpf) of zebrafish larvae. Comparison of the intact-fin of larvae and amputated-fin of larvae from the same batch of fertilized embryos. (Hour(s) post-amputation, hpa; day(s) post-fertilization, dpf)

	Day 1 (0.5 hpa, 3 dpf)	Day 2 (24 hpa, 4 dpf)	Day 3 (48 hpa, 5 dpf)
Intact zebrafish larva caudal fin-fold (Whole fin area measured)			
Amputated larva caudal fin-fold (Area from reference-line to the cut-line measured)			
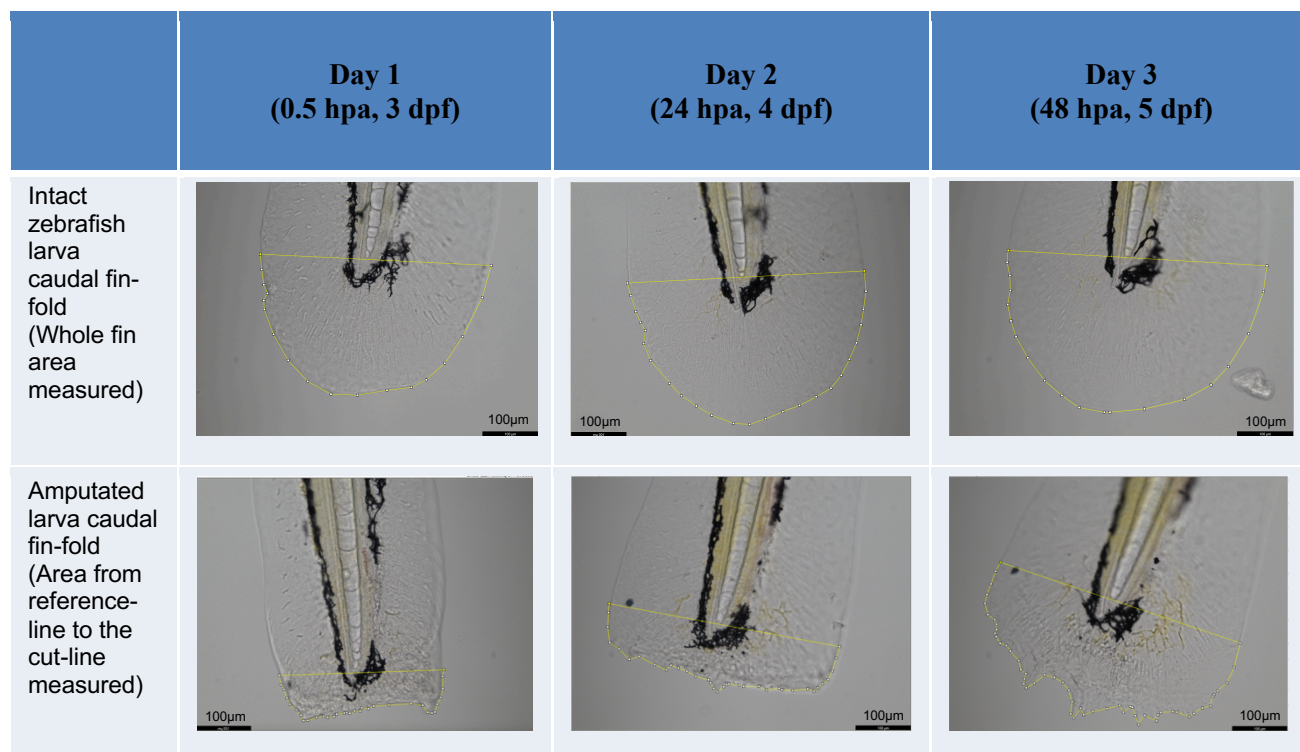
The growth rate of larvae varies in each experimental batch carried on different weeks, or even between each larva treated with the same gas under the same condition which depends on the respiration rate, metabolic rate also the overall health of the individual larvae. The different growth rates of larvae in each experiment from different batches could be manipulated by the room temperature of the day, the embryos hatching period upon post-fertilisation (dpf) or the growth factor regulating gene carried by larvae from different parents may vary. The embryos were collected from 3 to 4 pairs of parents therefore larvae are genetically varied. However, to minimise the variation, the controls and the specific gas treatments were carried out simultaneously.

3.3.2 Measuring parameter of neutrophil count at caudal fin-amputated site of zebrafish larvae to determine tissue repair

The caudal hematopoietic tissue (CHT) gives rise to macrophages and neutrophils in 2 dpf larvae. Since the adaptive immunity cells (T-cells and B-cells) are not mature until 4 to 6 weeks of post-fertilization, therefore studying innate immunity (neutrophils and macrophages) in isolation, without interference from adaptive immunity cells became possible in 3 dpf larval zebrafish[137,140]. Recruited neutrophils execute the host-defence functions such as phagocytosis and degranulation of antimicrobial or inflammatory cells[132,155,161]. It is known that

inflammatory conditions induce ROS production. At the same time, infiltration of neutrophils at the injured site is often interrelated to ROS signaling[162]. The neutrophils infiltration elevation is expected to see at high ROS conditions and the early disappearance of neutrophils probably indicates the fast recovery of injury[163,164] or might be due to suppression of ROS. Hence, in this study expected to observe if molecular H_2 or EMF treatment able to manipulate the neutrophils infiltration to the injured site.

The neutrophil fluctuation from 0.5 hpa, 3 hpa, 24 hpa and 48 hpa were quantified to determine the correlation to the recovery rate of the injured tissue. To define the mechanisms that regulate neutrophil-mediated inflammation *in vivo*, *lyzC:*DsRed transgenic zebrafish of neutrophils expressed by red fluorescent protein (RFP) under lysozyme C promoter drive myeloid-specific expression was used.
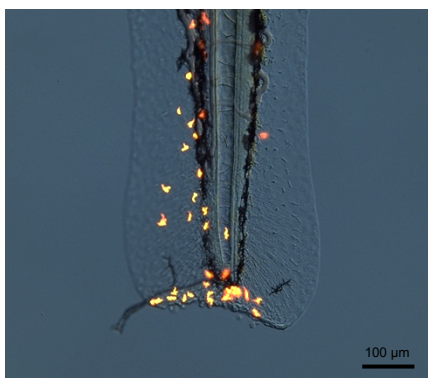
Fig. 23: Transgenic zebrafish Tg(*lyzC:DsRed*) allow neutrophil cell-specific visualization.
High-power image of transgenic neutrophils labelling the cytoplasm with RFP, demonstrating the dynamic structure of this leukocyte. Tail transection-induced inflammation causes a neutrophil influx to the injured site, visualized easily using fluorescent microscopic imaging.

While the amputated tissue regeneration is easily followed in the live zebrafish larva, the *in vivo* imaging and neutrophil count was determined by fluorescence microscopic imaging. The fluctuation of the neutrophil count at the injured site of amputated caudal fin-tissue was captured for 3 consecutive days beginning from 0.5, 3, 24 and 48 hpa (Table 4). Neutrophils recruited to the amputated-site of larvae were quantified upon providing H_2 or EMF treatment. The neutrophil count was compared with their compatible controls.

Table 4: The method of the neutrophil count at the injured site of amputated-fin from day 1 (3 dpf) to day 3 (5 dpf). Same batch of fertilized embryos used to measure the amputated-fin regeneration was also used to quantify the neutrophil count at the amputated-fin site. This helps to correlate the neutrophil count and wound healing with an acceleration of tissue re-growth on average. (Hour(s) post-amputation, hpa; day(s) post-fertilization, dpf)

Tg(*lyzC:DsRed*)	Day 1 (0.5 hpa, 3 dpf)	Day 1 (3 hpa, 3 dpf)	Day 2 (24 hpa, 4 dpf)	Day 3 (48 hpa, 5 dpf)
Neutrophils quantified within 200 µm distance above the cut-line	100µm	100µm	100µm	100µm
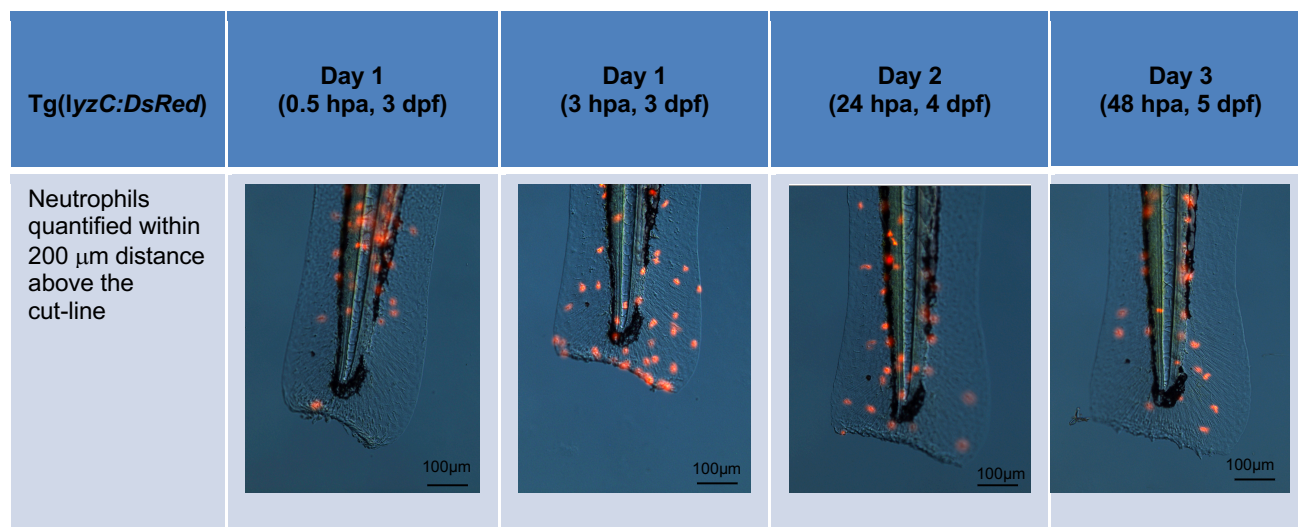
Statistical analyses were carried out using SPSS26. Data were tested for statistical significance using Welch's t-test of One-Way ANOVA. Post-Hoc multiple comparison with Gomes-Howell test. Data analysed by the mean difference is significant at the 0.05 level. The fin growth difference compared between the consecutive days of treatment from day 3 to day 1 is expressed by a stacked bar chart to represents the proportional growth of larvae in the first 24 hours (Day 2-Day1) and 48 hours (Day 3-Day 2) which contribute to the total growth of zebrafish larvae fin-area. The error bar represents the standard deviation of the growth of total larvae used in each experiment per condition. The neutrophil count results are expressed by a line graph of Mean ± S.D. for each experiment. All the graphs were prepared in Excel (Microsoft).

3.4 Comparison of air treated and untreated medium effects on growth of zebrafish larvae

The control in every gas treatment is air ($N_2 + O_2$) bubbled condition using an air compressor. The air compressor rotates the ambient atmospheric gases (78% of N_2 and 21% of O_2) into the medium. The physiochemical properties such as the dissolved O_2 and the ORP values do not vary between air bubbled and untreated medium, therefore, air bubbled medium is chosen as a compatible control in every experiment. The air treated medium is an important control to rule out the pre-agitation effect of medium which may infuse more ambient atmospheric gas into the medium during the treatment. The agitation effects of the medium prior to zebrafish larvae incubation are to be considered since the rest of the gases such as H_2, N_2, H_2-O_2 gas

mixture, Brown's gas, and O_2 are also being bubbled (cause agitation effect) into the medium from external sources such as gas cylinder or gas generating electrolysis devices.

Since air bubbled medium is used as a control rather than using an untreated E3 medium thus, a fin growth comparison study was done between the air treated and untreated larvae. The intact zebrafish larvae showed the average fin growth of air treated and untreated larvae are 20425 μm^2 and 20690 μm^2 while the growth rate/hour is 426 and 431 μm^2/hr, respectively (Fig. 24). The average growth difference of only 1.3%, statistically proved to be an insignificant difference in the overall growth rate between air ($N_2 + O_2$) treated and untreated larvae.
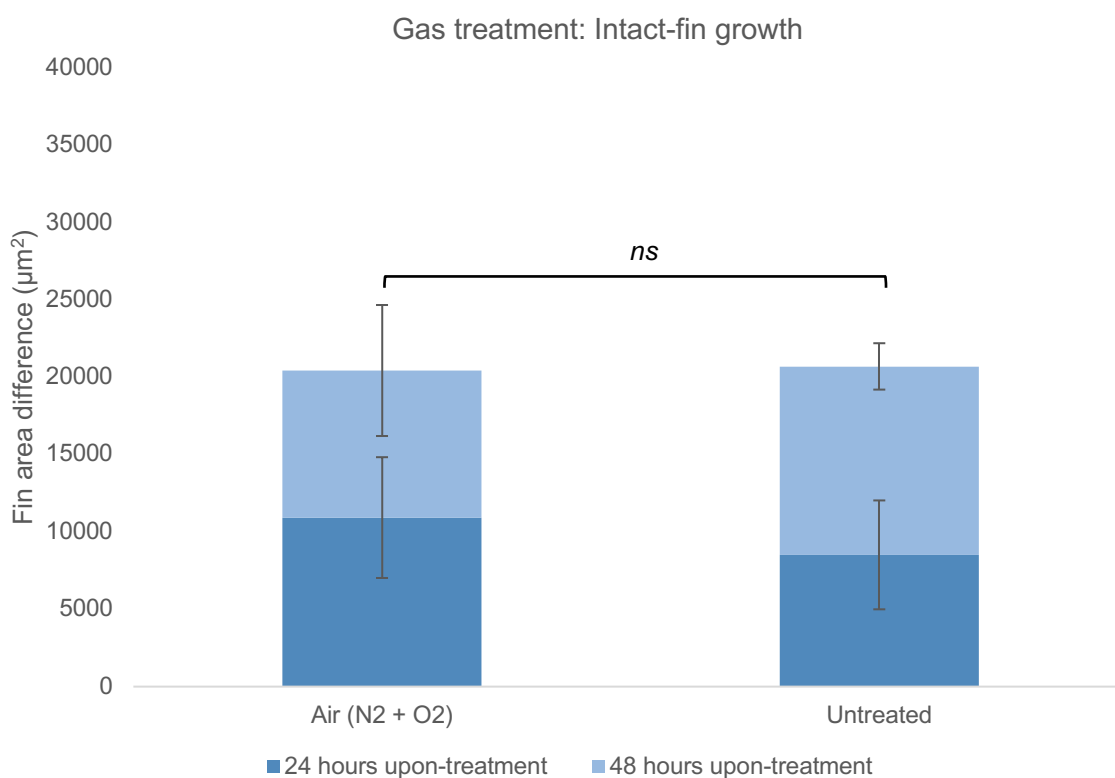
Fig. 24: The comparison of the intact-fin growth of air treated and untreated zebrafish larvae.
The intact fin-growth of 3 days post-fertilised zebrafish larvae incubated in the air ($N_2 + O_2$) treated and untreated E3 medium were imaged and measured over 48 hours. Statistically non-significant difference is indicated by (*ns*). Sample size (n=4 repetition, total 60 larvae) per condition. Data were analysed using the Welch's t-test by One-Way ANOVA.

Fig. 25 shows the re-growth of caudal fin-fold of amputated larvae which incubated in air bubbled medium and untreated medium. The air-treated and untreated intact-larvae has the average fin growth of 36412 μm^2 and 36140 μm^2 while the growth rate/hour is 759 and 753 μm^2/hr, respectively. The average growth difference of only 0.7% between air treated and untreated larvae is statistically proved to be insignificant difference. This helps to conclude that air-saturated medium does not contribute to any beneficial nor negative side effects to the treated larvae hence do not manipulate the results.

Apparently, the zebrafish larvae from both air bubbled and untreated medium indicates that, the amputated-fin grow more rapidly compared to the intact-fin. The amputated-fin of 3 dpf zebrafish larvae were observed to grow 40 - 45% faster compared to intact-fin fold development. The amputated-fin of zebrafish larvae may have some chemical gradient to regulate the growth factor gene to restructure the fin back to normal morphology therefore there is an additional acceleration of amputated-fin re-growth compared to intact-fin development. This has shown by Vieira et al. (2020) as a common chemical response in other self-regenerating species such as axolotl which accelerates the regeneration of its own limb upon amputation[165].
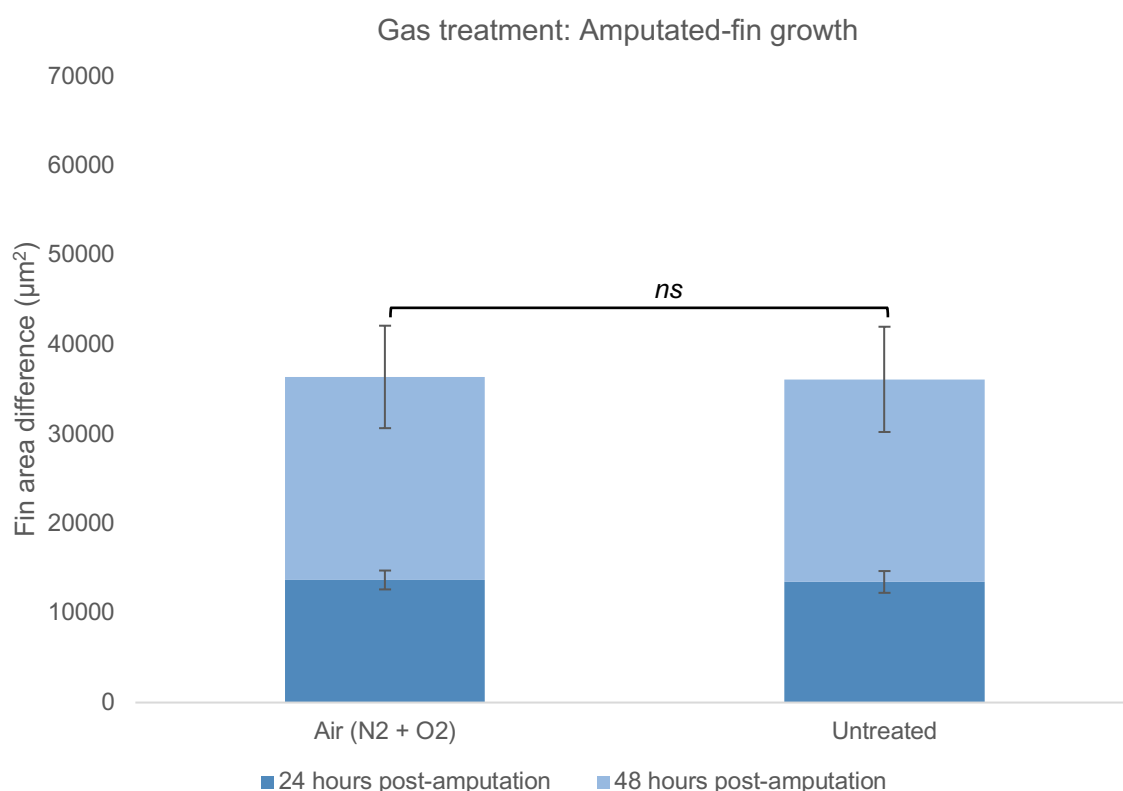
Fig. 25: The comparison of the amputated-fin growth of air treated and untreated zebrafish larvae. The amputated-fin regeneration of 3 days post-fertilised zebrafish larvae incubated in the air (N_2 + O_2) treated and untreated E3 medium were imaged and measured over 48 hours post-amputation. Statistically non-significant difference is indicated by (*ns*). Sample size (n=4 repetition, total 60 larvae) per condition. Data were analysed using the Welch's t-test by One-Way ANOVA.

The neutrophil infiltration is quantified in fin-amputated larvae since the neutrophils accumulate particularly at the tissue repair required sites. Neutrophils are the primary defense system which influx to the injured site immediately upon receiving cascade signaling from inflammatory conditions or regulated ROS[51,132,163]. In this study, the air treated and untreated larvae again have an insignificant difference in the number of recruited neutrophils to the injured site. At 3 hpa, the air treated larvae on average have 6.6 neutrophils while untreated have 8.7 neutrophils. The untreated larvae have recruited 24.5% more neutrophils compared to air

treated larvae however the standard deviation is in an overlapping range that makes the insignificant difference (*p*-value: 0.63). While, the neutrophil count comparisons between air treated and untreated zebrafish larvae observation at 0.5, 24 and 48 hpa showed not more than 11% difference (Fig. 26).
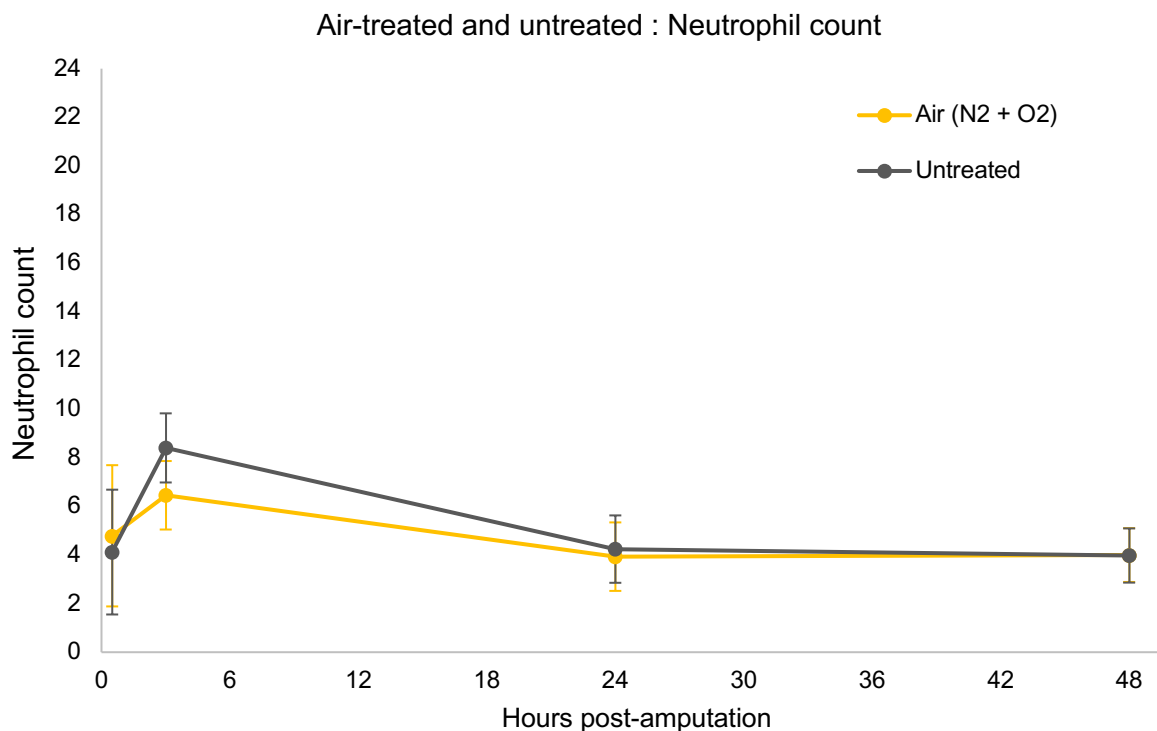
Fig. 26: The comparison of the neutrophil count at the amputated site of air treated and untreated zebrafish larvae. The comparison of the neutrophil count at the amputated site from 0.5 to 48 hours post-amputation (hpa) of larvae incubated in the air (N_2 + O_2) treated and untreated E3 medium shown insignificant difference. Sample size (n=4 repetition, total 45 larvae) per condition. The neutrophil count is expressed by Mean ± S.D. Data were analysed using the Welch's t-test by One-Way ANOVA.

3.5   Comparison of air, nitrogen, oxygen-levelled, oxygen-saturated medium effects on growth of zebrafish larvae

The air (N_2 + O_2) treated zebrafish larvae is a fair control to rule out the air-saturated condition which works as a baseline in this experiment. Apart from that, O_2-levelled condition and N_2-saturated condition are also essential controls which included in this experiment. The controls aid to see the definite effects of the beneficial gases such as H_2 and H_2-O_2 gas mixture. The pure H_2 treated medium tends to deplete the dissolved O_2 from the medium which could be partially harmful to the larvae therefore N_2 treatment was used as a control to rule out the effects of low O_2 in the medium. The H_2-O_2 gas mixture and Brown's gas treatment, not only introduces H_2 but also an additional 40% of O_2 into the medium. Thus, O_2-levelled condition is an essential control to rule out the effects of large O_2 concentration condition. At the same

time, also evaluated the side effects of O_2-saturated condition (hyperoxic condition) effects on zebrafish larvae intact-fin development and amputated-fin regeneration.

Fig. 27 shows the comparison of air, N_2, O_2-levelled and O_2-saturated medium effects on intact-fin of zebrafish larvae. The intact-fin of N_2 treated larvae develops at 317 μm^2/hour compared to air treated intact-fin grow at rate of 517 μm^2/hour while, O_2-levelled at 452 μm^2/hour and O_2-saturated at 408 μm^2/hour. The N_2 treated larvae have 38.7% lower growth rate than air treated larvae. The O_2-levelled and O_2-saturated condition treated intact-larvae showed 12.5% and 21.2% lower growth rate than air treated larvae.
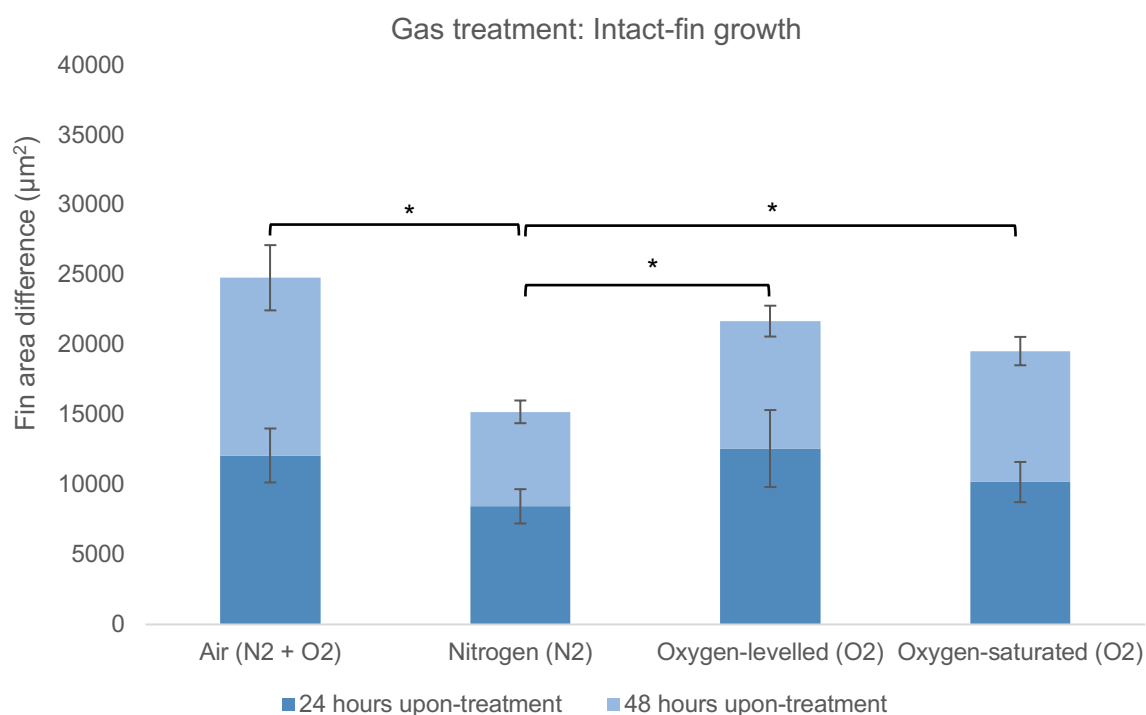
Fig. 27: The comparison of the intact-fin growth of air, nitrogen, oxygen-levelled and oxygen-saturated treated zebrafish larvae. The intact fin-growth of 3 days post-fertilised zebrafish larvae incubated in the air ($N_2 + O_2$), nitrogen (N_2), O_2-levelled and O_2-saturated treated E3 medium were imaged and measured over 48 hours. Statistically significant difference for total growth in 48 hours if $p < 0.05$, indicated by (*), the others are non-significant difference (*ns*). Sample size (n=4 repetition, total 62 larvae) per condition. Data were analysed using the Welch's t-test by One-Way ANOVA.

The amputated larvae fin regeneration also showed the same trend of growth as the intact-fin development. The N_2 treated larvae have the lowest amputated-fin growth rate. The N_2 treated larvae has 36.0% lower growth rate than air treated larvae (Fig. 28). The O_2-levelled and O_2-saturated condition treated larvae has 20.0% and 24.8% lower growth rate than air treated larvae. While, the N_2 treated larvae has 20.0% and 14.9% lower growth rate compared to O_2-levelled and O_2-saturated condition treated larvae.

In this set of experiment, the amputated-fin of air treated larvae regenerate at 824 μm^2/hour on average in 48 hours. The N_2, O_2-levelled and O_2-saturated condition treated fin-amputated larvae regenerate at lower rate of 528, 659 and 620 μm^2/hour, respectively, on average of total 48 hours of observation. Whether too low dissolved O_2 (~2.0 mg/L, 0.06 mM) or too high dissolved O_2 condition (11.7 to 29 mg/L, 0.37 - 0.91 mM), both seems equally did not benefit the larvae metabolic oxidation, hence inhibited the rate of intact-fin and amputated-fin growth. Nevertheless, N_2 has shown a significant growth retardation in both intact-fin and amputated-fin growth compared to air, O_2-levelled and O_2-saturated condition treated larvae.
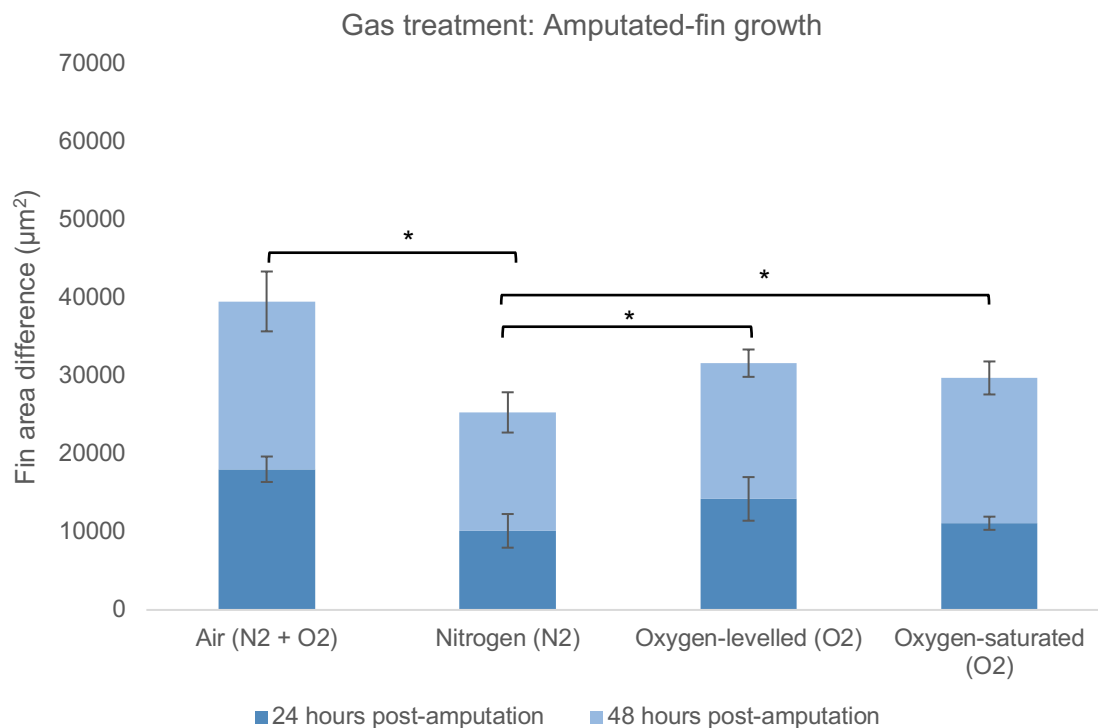
Fig. 28: The comparison of the amputated-fin growth of air, nitrogen, oxygen-levelled and oxygen-saturated treated zebrafish larvae. The amputated-fin regeneration of 3 days post-fertilised zebrafish larvae incubated in the air (N_2 + O_2), nitrogen (N_2), O_2-levelled and O_2-saturated treated E3 medium were imaged and measured over 48 hours post-amputation. Statistically significant difference for total growth in 48 hours if $p < 0.05$, indicated by (*), the others are non-significant difference (*ns*). Sample size (n=4 repetition, total 71 larvae) per condition. Data were analysed using the Welch's t-test by One-Way ANOVA.

In general, the neutrophils are found to be recruited highest at 3 hpa before the neutrophils retrograde back to vascular or the neutrophils going through cell death by apoptosis. Fig. 29 showed the N_2 treated larvae has the largest number of neutrophils accumulated at the injured site compared to air, O_2-levelled and O_2-saturated condition treated larvae. The N_2 treated larvae on average has 44.1%, 55.2%, 47.0% and 41.7% higher neutrophils than air-treated larvae at 0.5, 3, 24 and 48 hpa, respectively. While, the O_2-levelled and O_2-saturated condition treated larvae has 38.1% and 51.0% higher neutrophil count at 3 hpa compared to air treated larvae. However, at 48 hpa, the larvae incubated in air, O_2-levelled and O_2-saturated condition treated larvae have insignificant difference in neutrophil count while N_2 treated larvae still have

significantly high number of neutrophils at fin-amputated site. This indicates a very slow wound healing process occurring in N_2 treated larvae which may be the cause for the massive neutrophil recruitment to continue the tissue repair process.
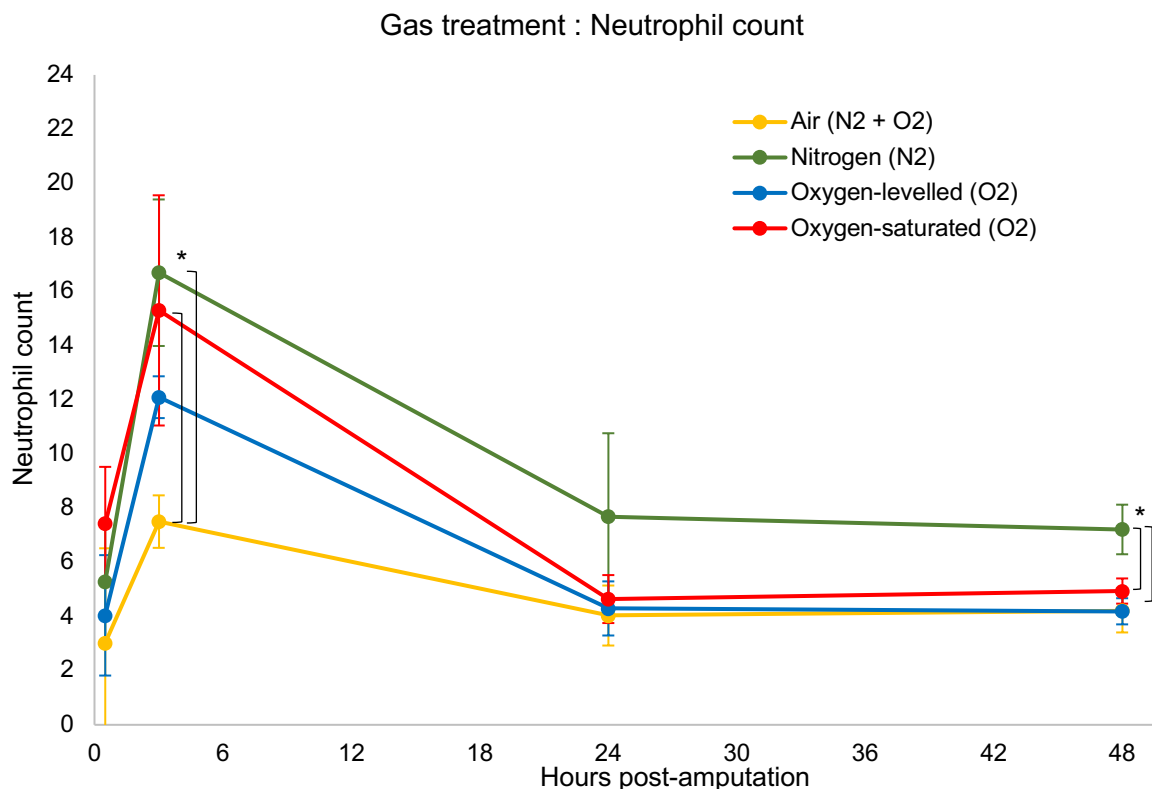
Fig. 29: The comparison of the neutrophil count at the amputated site of air, nitrogen, oxygen-levelled and oxygen-saturated treated zebrafish larvae. The comparison of the neutrophil count at the amputated site from 0.5 to 48 hours post-amputation (hpa) of larvae incubated in the air ($N_2 + O_2$), nitrogen (N_2), O_2-levelled and O_2-saturated treated E3 medium shown significant differences at 3 and 48 hpa. Statistically significant difference for neutrophil count if $p < 0.05$, indicated by (*), the others are non-significant difference (*ns*). Sample size (n=4 repetition, total 65 larvae) per condition. The neutrophil count expressed by Mean ± S.D. Data were analysed using the Welch's t-test by One-Way ANOVA.

3.6 Comparison of air, hydrogen, hydrogen-oxygen gas mixture and Brown's gas infused medium effects on growth of zebrafish larvae

In the exploration of different H_2 concentration effects on growth response of zebrafish larvae were incubated in H_2, H_2-O_2 gas mixture and Brown's gas enriched medium meanwhile, the air treated larvae were used as a control. The H_2 treated larvae were exposed to 2.0 mg/L of H_2 and 2.0 mg/L of O_2. The H_2-O_2 gas mixture and the Brown's gas treated larvae were exposed to 0.8 mg/L of H_2 and 11.7 mg/L of O_2. The H_2-O_2 gas mixture and the Brown's gas treated larvae were exposed to 60% lesser H_2 and 83% more O_2 concentration compared to the pure H_2 treated larvae.

The intact zebrafish larvae from H_2 treated medium have 25.1% higher total growth rate than the control (air-treated) in 48 hours of observation (Fig. 30). The H_2-O_2 gas mixture and the Brown's gas treated larvae were seen to develop the intact-fin 9.5% and 10.5%, respectively, larger than the air-treated larvae. The intact zebrafish larvae incubated in H_2 has grown at 663 μm^2/hour compared to H_2-O_2 gas mixture and the Brown's gas treated larvae grow at 548 and 555 μm^2/hour, respectively. H_2-O_2 gas mixture and the Brown's gas treated larvae showed 17.3% and 16.3% lower growth rate compared to the pure H_2 treated larvae, respectively, in 48 hours.
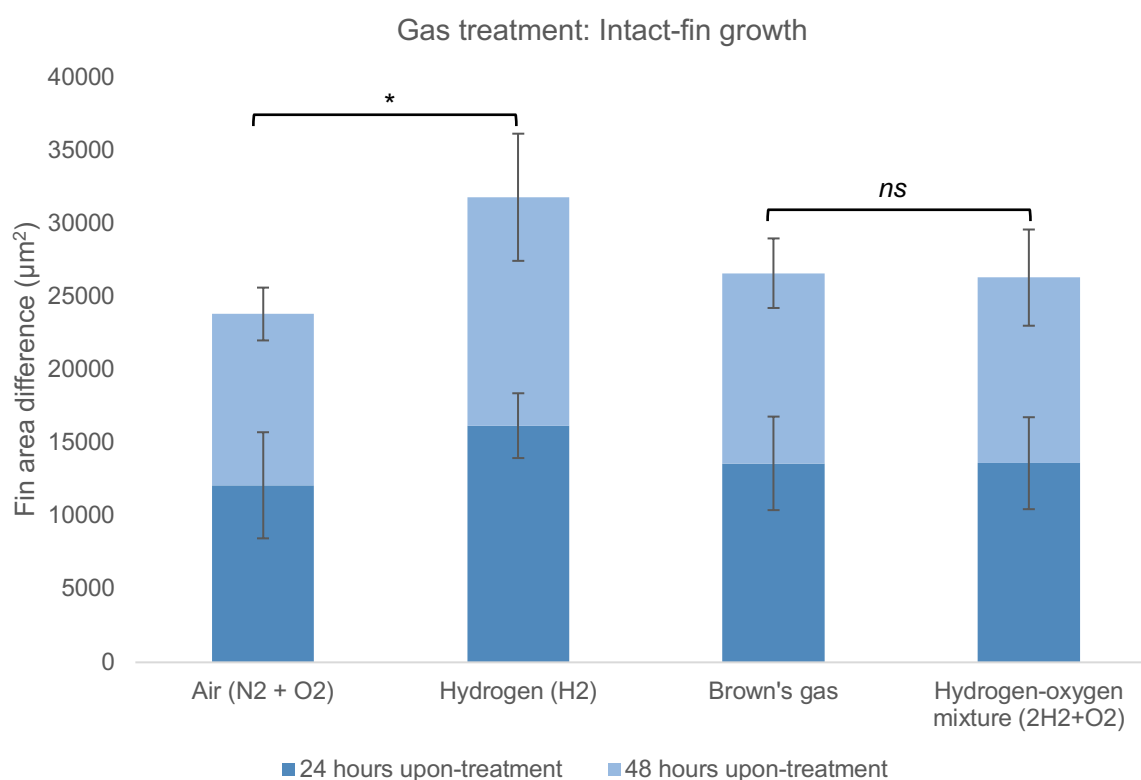
Fig. 30: The comparison of the intact-fin growth of air, hydrogen, hydrogen-oxygen gas mixture and Brown's gas treated zebrafish larvae. The intact fin-growth of 3 days post-fertilised zebrafish larvae incubated in the air (N_2 + O_2), hydrogen (H_2), H_2-O_2 gas mixture ($2H_2$+O_2) and Brown's gas treated E3 medium were imaged and measured over 48 hours. Statistically significant difference for total growth in 48 hours if $p < 0.05$ indicated by (*), the others are non-significant difference (*ns*). Sample size (n=6 repetition, total 104 larvae) per condition. Data were analysed using the Welch's t-test by One-Way ANOVA.

Based on the caudal fin-amputated assay, the H_2 treated larvae showed the largest re-growth compared to air, H_2-O_2 gas mixture and the Brown's gas treated larvae. The H_2 treated larvae regenerate the amputated fin 56104 μm^2 in 48 hours of observation while the air (control), H_2-O_2 gas mixture and the Brown's gas treated larvae regenerate 43528, 48792 and 48718 μm^2 (Fig. 31). The amputated-fin of pure H_2 treated larvae regenerate 22.4% faster than air treated larvae. The amputated-fin of H_2-O_2 gas mixture and the Brown's gas treated larvae both regenerate around ~11% faster than air treated larvae and ~13% slower than pure H_2 treated larvae. This indicates that a high concentration of H_2 in a treated medium enables the larvae

to grow significantly faster than air treated larvae, regardless of a low proportion of O_2 concentration in the medium. Since 2.0 mg/L of O_2 is still considered an adaptable O_2 concentration for zebrafish larvae[166] therefore the respective model organism able to reflect a positive effect of the absorbed molecular H_2. Well, the H_2-O_2 gas mixture and the Brown's gas treated larvae also have reflected slightly better intact-fin development and amputated-fin regeneration compared to the air treated larvae in presence of 0.8 mg/L of dissolved H_2, though significant difference were not seen.
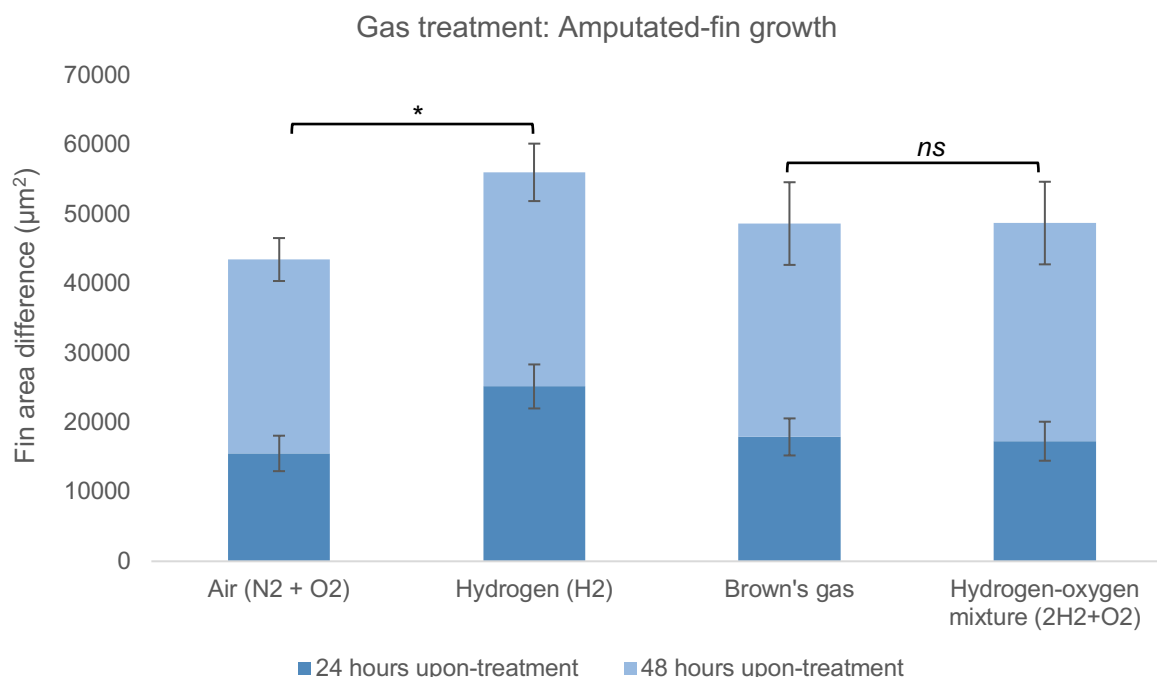
Fig. 31: The comparison of the amputated-fin growth of air, hydrogen, hydrogen-oxygen gas mixture and Brown's gas treated zebrafish larvae. The amputated-fin regeneration of 3 days post-fertilised zebrafish larvae incubated in the air (N_2 + O_2), hydrogen (H_2), H_2-O_2 gas mixture ($2H_2$+O_2) and Brown's gas treated E3 medium were imaged and measured over 48 hours post-amputation. Statistically significant difference for total growth in 48 hours if $p < 0.05$, indicated by (*), the others are non-significant difference (*ns*). Sample size (n=6 repetition, total 115 larvae) per condition. Data were analysed using the Welch's t-test by One-Way ANOVA.

The neutrophil recruitment rate in fin-amputated larvae did not show a significant difference between air, H_2, H_2-O_2 gas mixture and the Brown's gas treated larvae (Fig. 32). However, on average at 48 hpa, the pure H_2, H_2-O_2 gas mixture and Brown's gas treated larvae showed 38.3%, 23.4% and 29.0% lower neutrophil count than in the air-treated larvae, respectively. The presence of 2.0 to 0.8 mg/L of H_2, might have accelerated the wound healing and tissue re-epithelization of amputated-fin of zebrafish larvae compared to the air treated larvae on average. Thus, the H_2 absorbed larvae, may not send signal for neutrophils recruitment at 48 hpa. The air treated larvae which still recruited a larger number of neutrophils, probably still required the assistance of immune cells (neutrophils) at 48 hpa to overcome the inflammatory condition at the amputated site.
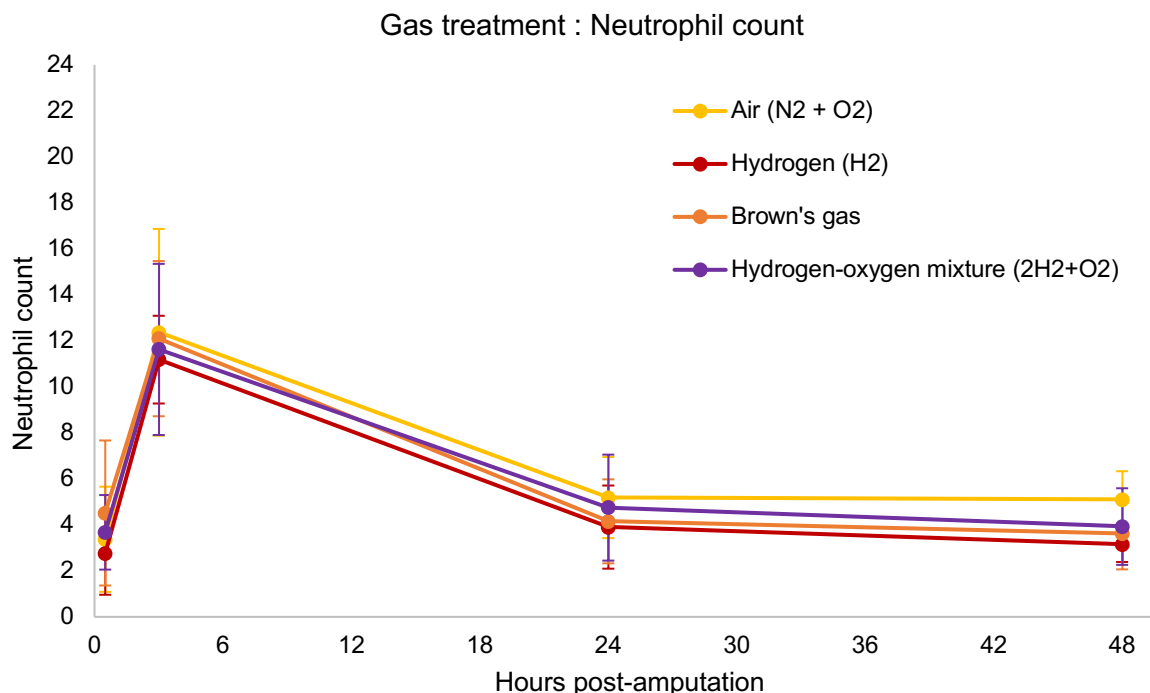
Fig. 32: The comparison of the neutrophil count at the amputated site of air, hydrogen, hydrogen-oxygen gas mixture and Brown's gas treated zebrafish larvae. The comparison of the neutrophil count at the amputated site from 0.5 to 48 hours post-amputation (hpa) of larvae incubated in the air (N_2 + O_2), hydrogen (H_2), H_2-O_2 gas mixture ($2H_2$ + O_2) and Brown's gas treated E3 medium showed insignificant difference. Sample size (n=6 repetition, total 105 larvae) per condition. The neutrophil count is expressed by Mean ± S.D. Data were analysed using the Welch's t-test by One-Way ANOVA.

3.7   Comparison of air, nitrogen and hydrogen gas infused medium effects on growth of zebrafish larvae

The growth rate of intact-fin and amputated-fin of zebrafish larvae were compared upon incubation in air (N_2 + O_2), N_2 and H_2 treated medium. Since the H_2 and N_2 saturated medium depletes approximately 70% of the dissolved O_2 concentration hence N_2 is used as a compatible control to study the benefits of H_2. Depletion of dissolved O_2 as low as ~2.0 mg/L (0.06 mM) in both H_2 and N_2 pre-treated medium may induce a mild hypoxic condition for the Zebrafish larvae. This hypoxic condition may slow down the metabolism rate and energy production for aerobic vertebrates like zebrafish. The low metabolic oxidation could eventually retard the overall zebrafish larvae growth factor including intact-fin development, also amputated-fin regeneration due to a constrained wound healing mechanism. However, the H_2 treated larvae showed significantly higher average growth rate compared to the N_2 treated larvae.

The intact-fin growth of air, N_2 and H_2 treated larvae samples increases continuously from 0.5 to 48 hpa (Fig. 33). The intact zebrafish larvae incubated in the air, N_2 and H_2 pre-treated medium showed 20986, 16892 and 30639 µm^2 average fin growth upon 48 hours of

observation. The intact zebrafish larvae incubated in N_2 have 19.5% lower growth rate compared to air treated larvae while, the H_2 treated larvae have 31.5% of higher growth rate compared to air treated larvae. The N_2 treated intact larvae have 45.0% lower growth rate compared to H_2 treated larvae upon 48 hours of observation, although both H_2 and N_2 treated larvae have almost the same O_2 concentration level. The H_2 treated larvae have the highest caudal fin growth rate (638 μm^2/hour) followed by air (437 μm^2/hour) and N_2 (352 μm^2/hour) treated larvae on average of 48 hours. This indicates that the ~1.0 mM of molecular H_2 in the medium has the potential to accelerate the overall fin development of intact zebrafish larvae.
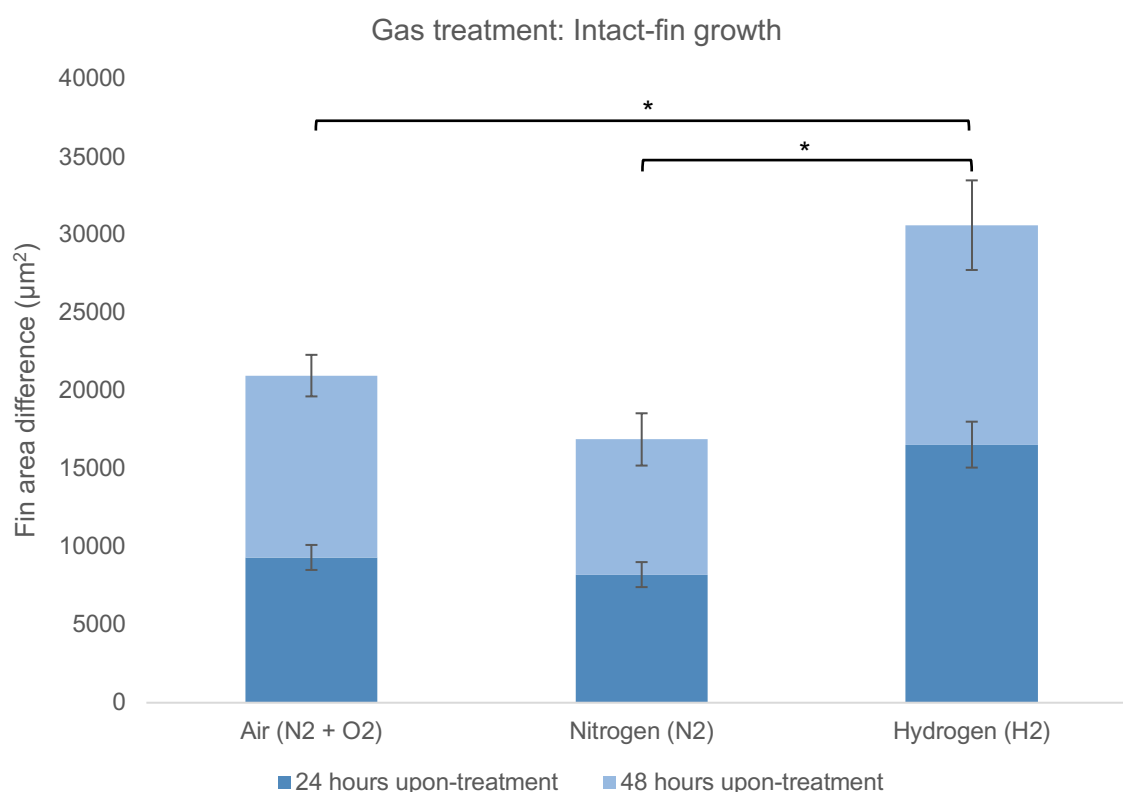
Fig. 33: The comparison of the intact-fin growth of air, nitrogen and hydrogen treated zebrafish larvae. The intact fin-growth of 3 days post-fertilised zebrafish larvae incubated in the air (N_2 + O_2), nitrogen (N_2) and hydrogen (H_2) treated E3 medium were imaged and measured over 48 hours. Statistically significant difference for total growth in 48 hours if $p < 0.05$, indicated by (*), the others are non-significant difference (*ns*). Sample size (n=6 repetition, total 105 larvae) per condition. Data were analysed using the Welch's t-test by One-Way ANOVA.

While the fin-amputated zebrafish larvae from the air, N_2 and H_2 pre-treated medium has 36676, 29176 and 47388 μm^2 average fin growth upon 48 hours of observation (Fig. 34). In overall 48 hours, the fin-amputated zebrafish larvae incubated in N_2 treated medium has 20.4% lower growth rate compared to larvae from air treated medium. While H_2 treated larvae have 22.6% higher growth rate than air treated larvae. Meanwhile, the N_2 treated fin-amputated larvae showed 38.4% lower growth rate compared to H_2 treated larvae.

The air treated larvae grow at 764 μm^2/hr compared to the fin-amputated larvae from N_2 and H_2 pre-treated medium grows at rate of 608 and 987 μm^2/hr in 48 hpa observation. Based on

the intact-fin and amputated-fin analysis, the results shows that the H_2 treated larvae grow 22-32% and 38-45% faster than air treated and N_2 treated larvae which indicate that the ~1.0 mM of molecular H_2 benefits both the intact-fin development in healthy zebrafish larvae as well as accelerates the fin regeneration of fin-amputated zebrafish larvae on average though a statistically significant difference compared to the controls is not seen in amputated-fin re-growth data.
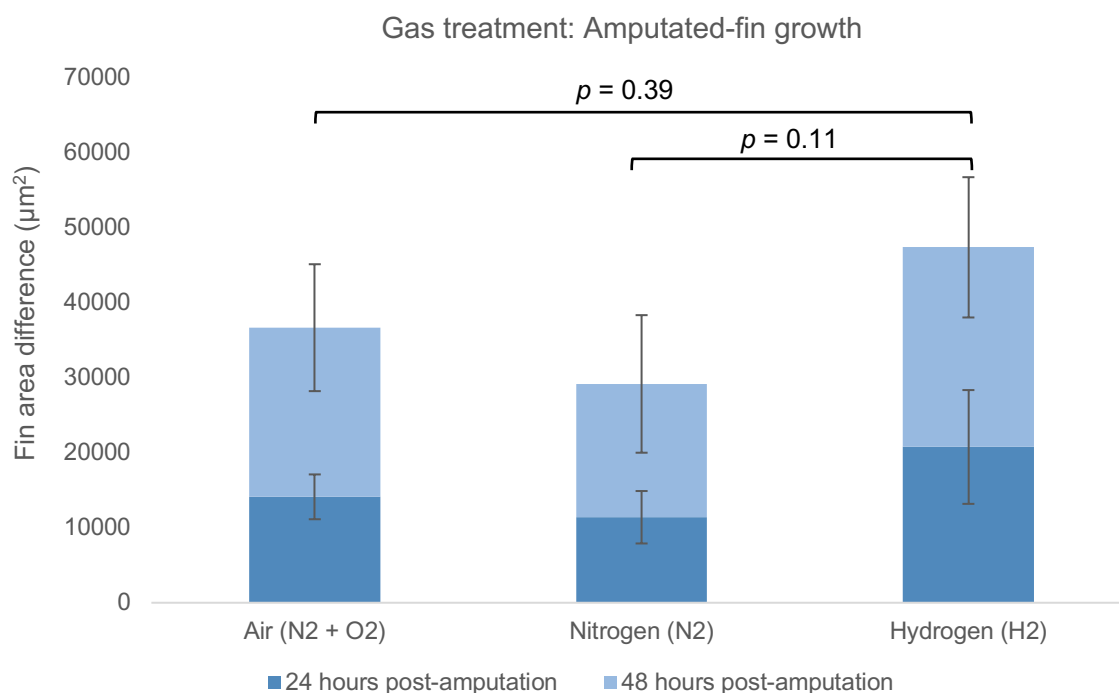
Fig. 34: The comparison of the amputated-fin growth of air, nitrogen and hydrogen treated zebrafish larvae. The amputated-fin regeneration of 3 days post-fertilised zebrafish larvae incubated in the air (N_2 + O_2)**,** nitrogen (N_2) and hydrogen (H_2) treated E3 medium were imaged and measured over 48 hours post-amputation. Statistically significant difference for total growth in 48 hours if *p* < 0.05, indicated by (*), the others are non-significant difference (*ns*). Sample size (n=6 repetition, total 110 larvae) per condition. Data were analysed using the Welch's t-test by One-Way ANOVA.

The neutrophil influx rate in fin-amputated larvae is different on average between air, N_2 and H_2 treated samples from 0.5 hpa to 48 hpa. The N_2 treated larvae have the largest number of neutrophils accumulated at the amputated-fin area (Fig. 35). N_2 treated larvae have in a range of 15.8 to 35.2% higher neutrophil count while H_2 treated larvae have in a range of 4.6 to 31.7% lesser neutrophils than air treated larvae, respectively, in overall from 0.5 hpa to 48 hpa observation. At 48 hpa, the N_2 treated larvae still have 6.4 average neutrophil count, which is 22.0% and 46.7% more neutrophils than air treated and H_2 treated larvae, respectively. Meanwhile, the air and H_2 treated larvae has only 5.0 and 3.4 average number of neutrophils, respectively, at the injured site. Moreover, the neutrophil count of N_2 treated larvae showed significantly lower number of neutrophil infiltrations compared to H_2 treated larvae.

The large number of neutrophils might indicate that the injured site is still undergoing wound healing mechanism and required the presence of neutrophils for phagocytosis of dead cells.

Phagocytosis is an essential process for a complete tissue repair before tissue regeneration takes place[164,167]. Meanwhile, the low neutrophil count in H_2 treated larvae might indicate low signaling from ROS to regulate the neutrophils to the injured site. Low neutrophil count at 48 hpa may indicate that the H_2 treated larvae might undergo a rapid wound healing and further continued by re-epithelization of amputated tissue sooner compared to air and N_2 treated larvae. The rapid wound healing cascade mechanism might not signal more neutrophils to the injured site[155].
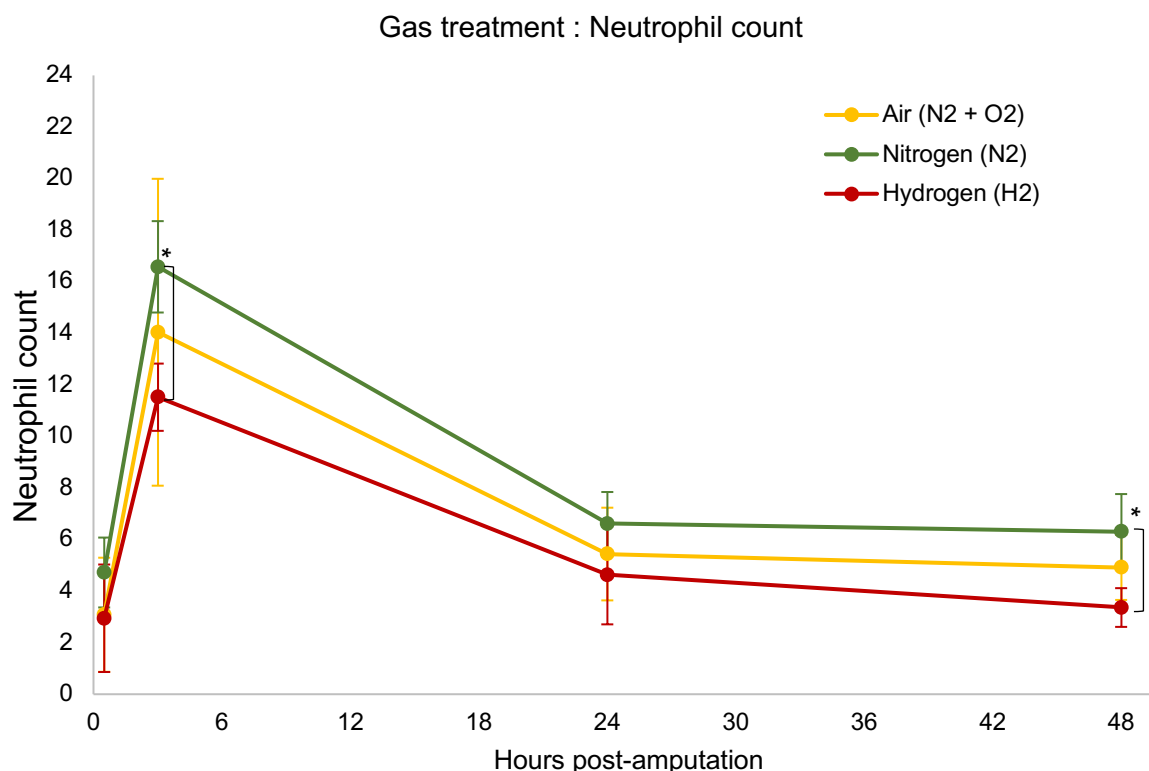
Fig. 35: The comparison of the neutrophil count at the amputated site of air, nitrogen and hydrogen treated zebrafish larvae. The comparison of the neutrophil count at the amputated site from 0.5 to 48 hours post-amputation (hpa) of larvae incubated in the air ($N_2 + O_2$) nitrogen (N_2) and hydrogen (H_2) treated E3 medium. Statistically significant difference for neutrophil count if *p* < 0.05, indicated by (*), the others are non-significant difference (*ns*). Sample size (n=6 repetition, total 102 larvae) per condition. The neutrophil count is expressed by Mean ± S.D. Data were analysed using the Welch's t-test by One-Way ANOVA.

The H_2 treated and N_2 treated medium has O_2 depleted condition which is 70% lower O_2 content compared to air treated medium. The low O_2 content in the E3 medium causes some obvious behavioural changes to the N_2 treated larvae (Fig. 36). The zebrafish larvae in N_2 treated medium are found to move towards surface of the water for better respiration support compared to larvae from H_2 treated medium which remain immersed in the medium without any behavioural changes. The behavioural changes such as moving towards the water surface may be due to suffocation counteract caused by low O_2 content in the medium however similar behavioral changes are not observed in H_2 treated larvae which equally has ~0.06 mM dissolved O_2 concentration. This may indicate that molecular H_2 might be supporting the

metabolic oxidation regardless of the low concentration of O_2 molecule in the systemic circulation.
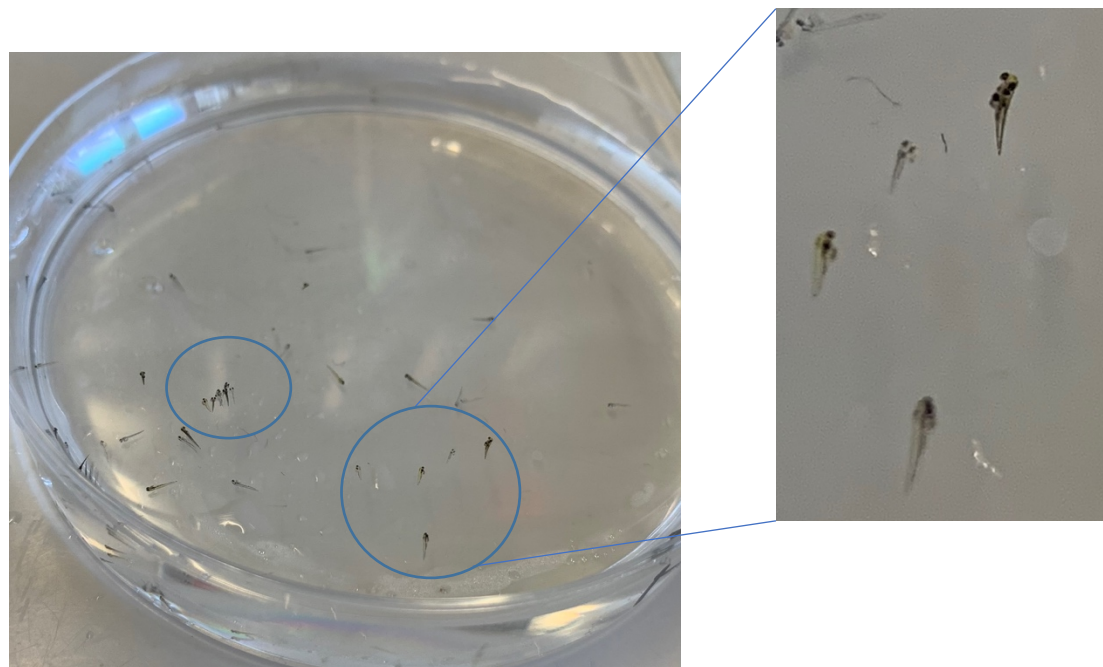
(A) Larvae in nitrogen gas (N_2) infused E3 medium

(B) Larvae in hydrogen gas (H_2) infused E3 medium

Fig. 36: The abnormal behavioural changes in low O_2 concentration medium. (A)&(B) The image of zebrafish larvae in the N_2 medium showed an abnormal behaviour of moving towards the surface of water most probably gasping for some O_2 gas however the same behavioural changes in H_2 treated zebrafish larvae were not observed.

Even though, the hypoxic condition effect is easily seen in the initial stage of the experiment on N_2 treated larvae, where an obvious behavioural change was detected (Fig. 36). However, both H_2 and N_2 treated larvae did not show any obvious structural deformities at 2.0 - 1.8 mg/L of dissolved O_2 concentration level (Fig. 37). This is most probably because the low O_2 (~2.0 mg/L) condition is yet considerably adaptable by zebrafish larvae although not providing an optimum growth condition as described by Strecker et. al.[166].

(A) Hydrogen (H$_2$) treated larvae

(B) Nitrogen (N$_2$) treated larvae

Fig. 37: Morphological deformities are not seen in the hydrogen and nitrogen treated larvae.
(A) & (B): Larvae growing in low O$_2$ concentration may experience structural deformities however neither the H$_2$ treated nor N$_2$ treated larvae for 3 hours on 3 consecutive days under low O$_2$ conditions do not reflect any morphological deformities but only growth retardation observed in N$_2$ treated larvae.

3.8   Comparison of air, oxygen-levelled, hydrogen-oxygen gas mixture and Brown's gas infused medium effects on growth of zebrafish larvae

In this part of study, the 3 dpf larvae were treated with air, O$_2$-levelled, H$_2$-O$_2$ gas mixture and Brown's gas to compare the tissue development of intact-fin and tissue regeneration of amputated-fin. Brown's gas is generated by an alkaline electrolysis with intercalated electrodes (modified electrolyser). Brown's gas is claimed to have a "magical" component which delivers medicinal benefits by some researchers and this modified electrolyser suppliers[93,94,96]. Therefore, the "special" beneficial effects of Brown's gas are determined by comparing the growth response with H$_2$-O$_2$ gas mixture treated larvae. Since the gas saturation curve and gas desaturation curve (Fig. 15 - Fig. 20) has made very clear that Brown's gas reacts exactly like H$_2$-O$_2$ gas mixture, hence further growth response analysis will make explicit if Brown's gas has any "special" health beneficial component. The H$_2$-O$_2$ gas mixture treated medium retains 0.8 mg/L (0.4 mM) of H$_2$ and 11.7 mg/L (0.37 mM) of O$_2$ in the medium. Therefore, a O$_2$ concentration standardized condition were prepared as a second control by infusing limited O$_2$ into the medium. The O$_2$-levelled condition is infused with 11.7 mg/L of O$_2$ became the second control in this comparison study to rule out the possible side effects from the mild hyperoxic condition due to introducing 40% higher O$_2$ into medium compared to the air treated condition.

The intact-fin area of air, O_2-levelled, H_2-O_2 gas mixture and Brown's gas treated larvae growth increases over time on average however, O_2-levelled condition treated intact-larvae showed mild retardation on fin growth compared to air-treated larvae (Fig. 38). Based on the total growth in 48 hours of observation, the O_2-levelled treated intact-larvae showed 12.1% lower growth rate than air while, 20.4% and 21.3% lower growth rate than H_2-O_2 gas mixture and Brown's gas treated larvae, respectively. The H_2-O_2 gas mixture and Brown's gas treated larvae showed 9.5% and 10.5% of higher growth rate than air treated intact-fin larvae. Meanwhile, the H_2-O_2 gas mixture (548 μm^2/hour) and Brown's gas (555 μm^2/hour) treated larvae showed only 1.1% difference in the growth rate and statistically showed insignificant difference (p = 0.43).

Fig. 38: The comparison of the intact-fin growth of air, oxygen-levelled, hydrogen-oxygen gas mixture and Brown's gas treated zebrafish larvae. The intact fin-growth of 3 days post-fertilised zebrafish larvae incubated in the air (N_2 + O_2), O_2-levelled, H_2-O_2 gas mixture ($2H_2$+O_2) and Brown's gas treated E3 medium were imaged and measured over 48 hours. Statistically significant difference for total growth in 48 hours if $p < 0.05$, indicated by (*), the others are non-significant difference (*ns*). Sample size (n=6 repetition, total 105 larvae) per condition. Data were analysed using the Welch's t-test by One-Way ANOVA.

The amputated-fin growth of O_2-levelled condition treated larvae is 22.9% lower than air treated larvae based on 48 hours of average growth rate (Fig. 39). On the other hand, the H_2-O_2 gas mixture and Brown's gas treated larvae both has 31.1% higher growth rate compared to O_2-levelled condition treated larvae. The H_2-O_2 gas mixture and Brown's gas treated larvae on average has a larger growth rate of 1016 and 1015 μm^2/hour followed by air with 907 μm^2/hour and the lowest growth rate of 699 μm^2/hour with O_2-levelled condition treated larvae. Both intact-fin larvae and amputated-fin larvae treated by either H_2-O_2 gas mixture and Brown's gas showed significant difference compared to O_2-levelled condition.
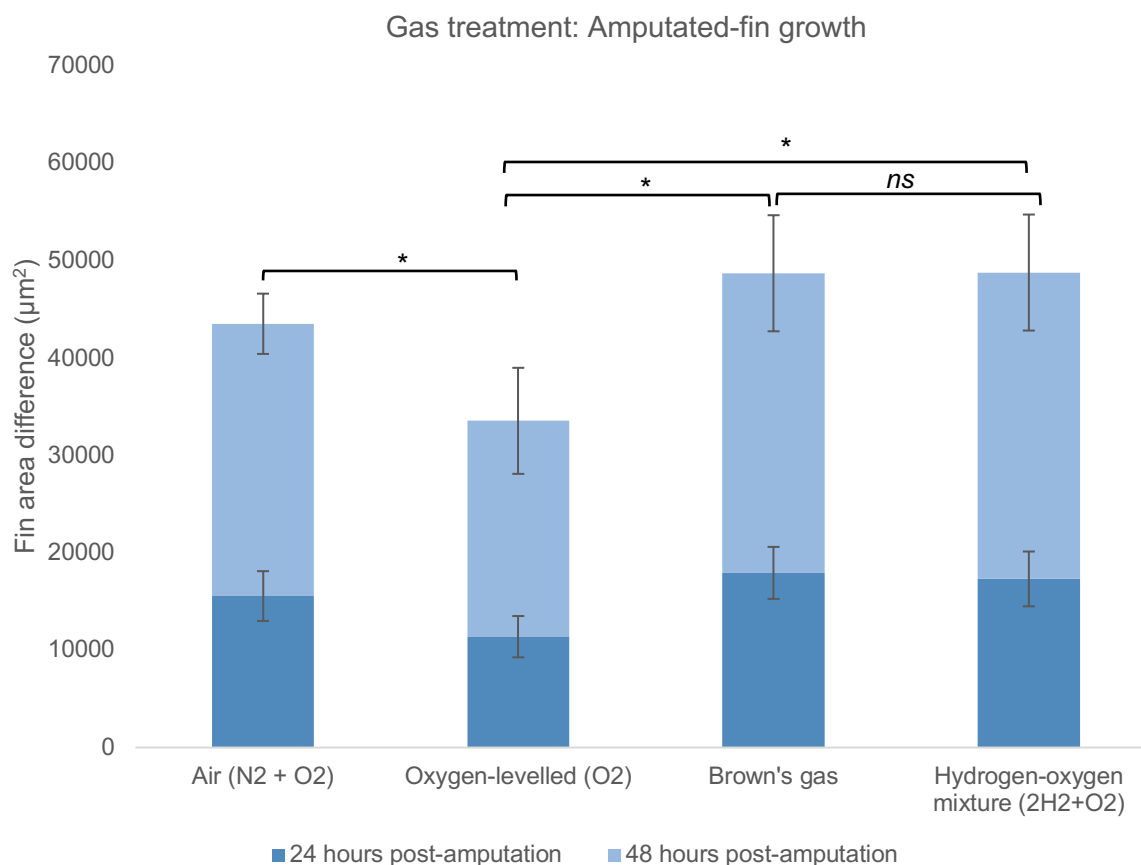
Fig. 39: The comparison of the amputated-fin growth of air, oxygen-levelled, hydrogen-oxygen gas mixture and Brown's gas treated zebrafish larvae. The amputated-fin regeneration of 3 days post-fertilised zebrafish larvae incubated in the air ($N_2 + O_2$), O_2-levelled, H_2-O_2 gas mixture ($2H_2+O_2$) and Brown's gas treated E3 medium were imaged and measured over 48 hours post-amputation. Statistically significant difference for total growth in 48 hours if $p < 0.05$, indicated by (*), the others are non-significant difference (*ns*). Sample size (n=6 repetition, total 118 larvae) per condition. Data were analysed using the Welch's t-test by One-Way ANOVA.

The neutrophil influx rate in fin-amputated larvae is high in O_2-levelled conditions with 15.7%, 18.0% and 14.6% more neutrophils compared to air, H_2-O_2 gas mixture and Brown's gas, respectively, at 3 hpa. At 48 hpa the O_2-levelled condition and air treated still has 23 -27% higher neutrophils compared to H_2-O_2 gas mixture and Brown's gas treated larvae (Fig. 40). However, the data is not consistent enough to show a significant difference.

Gas treatment : Neutrophil count
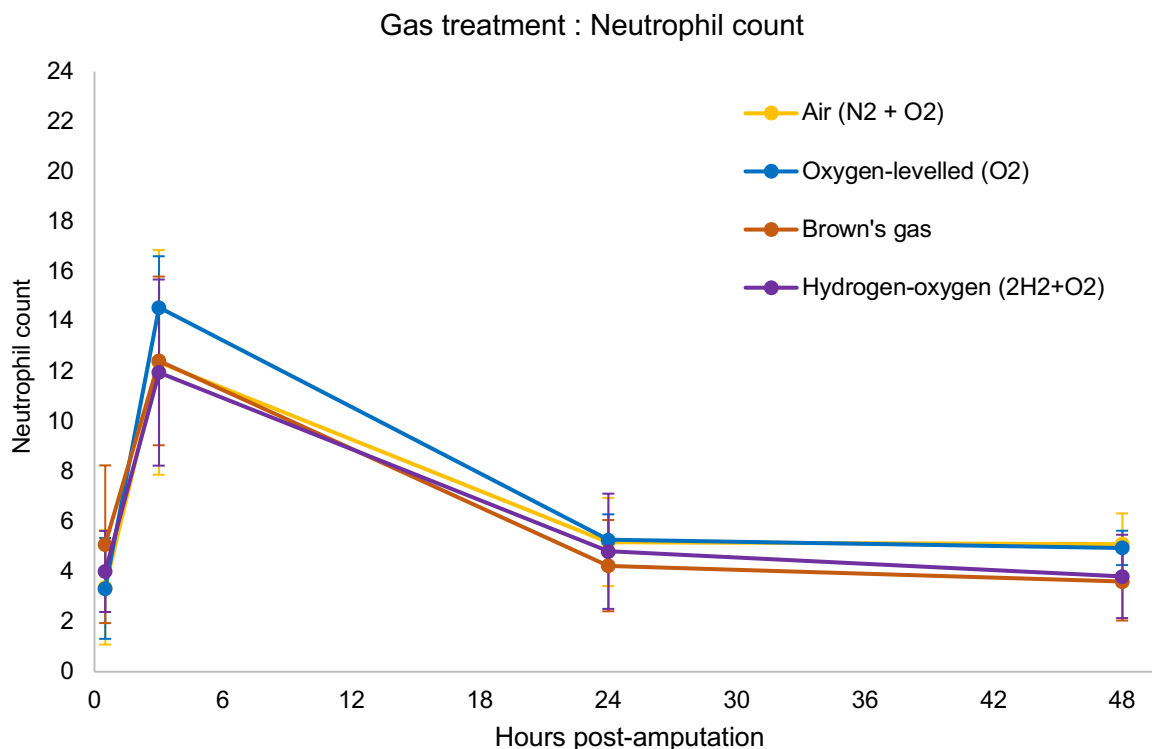
Fig. 40: The comparison of the neutrophil count at the amputated site of air, oxygen-levelled, hydrogen-oxygen gas mixture and Brown's gas treated zebrafish larvae. The comparison of the neutrophil count at the amputated site from 0.5 to 48 hours post-amputation (hpa) of larvae incubated in the air ($N_2 + O_2$), O_2-levelled (O_2), H_2-O_2 gas mixture ($2H_2 + O_2$) and Brown's gas treated E3 medium shown insignificant difference. Sample size (n=6 repetition, total 105 larvae) per condition. The neutrophil count expressed by Mean ± S.D. Data were analysed using the Welch's t-test by One-Way ANOVA.

3.9 Electromagnetic fields radiation effects on growth of zebrafish larvae

The commercially available "health-promoting" handheld-antenna, oscillates at a frequency of 144 MHz named Tesla oscillator is used for EMF radiation investigation. According to the Tesla oscillator device manual, this handheld-antenna can be used by patients for "self-healing" such as for skin inflammation, limb oedema and lower back pains[120]. Hence, the development of intact-fin larvae and regeneration of amputated-fin larvae observation were used as a parameter to study the effects of EMF radiation on health. The growth response of zebrafish larvae was compared upon exposure to 144 MHz EMF frequency wave generated by Tesla oscillator and 5 GHz frequency wave generated by WLAN router. A set of untreated larvae (control), was kept away from the Tesla and WLAN radiation radius to compare the EMF effects on larvae.

To analyse the benefits of Tesla oscillator radiation, 3 dpf zebrafish larvae were treated with the radiation-antenna for 30 minutes, twice a day by an hour pause. Generally, radiation may increase the kinetic energy to the adjacent molecules which eventually increases the

surrounding temperature upon extreme collision. The high thermal effect may give a false result, in this study. Therefore, the temperature fluctuation was handled by increasing the total volume of E3 medium in the container containing the zebrafish larvae. Also, to avoid temperature fluctuation, the duration and frequency of the treatment were minimized. This precaution methods, help to not increase the temperature of the treated medium more than ~1.5 ºC.

The intact-larvae exposed to EMF radiation generated by Tesla oscillator (144 MHz) exhibited much lower growth rate compared to untreated (control) and WLAN (5 GHz) treated larvae (Fig. 41). The Tesla oscillator radiation exposed larvae grow at 326 μm^2/hour in 48 hours of observation while, untreated and WLAN treated larvae grow at 488 and 483 μm^2/hour. The Tesla oscillator treated intact-larvae grow 33.2% and 32.5% significantly slower than untreated and WLAN treated larvae. The WLAN treated larvae is only reflected 1.2% slower intact-fin development compared to untreated larvae which is an insignificant difference (p=0.99).
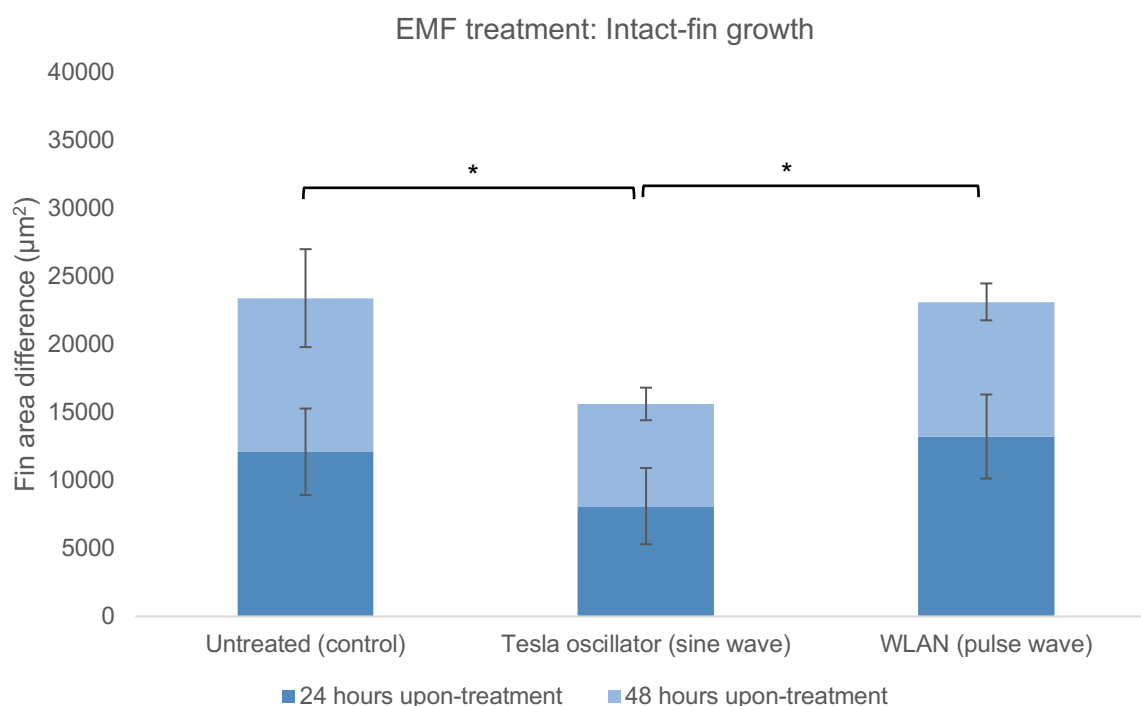
Fig. 41: The comparison of the intact-fin growth of untreated and EMF (Tesla oscillator and WLAN) radiation exposed larvae. The intact fin-growth of 3 days post-fertilised untreated (control) zebrafish larvae were compared to Tesla oscillator and WLAN electromagnetic field (EMF) radiation exposed larvae were imaged and measured over 48 hours. Statistically significant difference for total growth in 48 hours if $p < 0.05$, indicated by (*), the others are non-significant difference (*ns*). Sample size (n=5 repetition, total 82 larvae) per condition. Data were analysed using the Welch's t-test by One-Way ANOVA.

For the fin-amputated larvae, the Tesla oscillator radiation exposed larvae were also having difficulty to regenerate. The Tesla oscillator treated larvae grow 12.7% slower than untreated larvae and 13.2% slower than WLAN treated larvae (Fig. 42). Tesla oscillator radiation exposed larvae grow at 773 μm^2/hour in 48 hours of observation while untreated and WLAN treated larvae grow at 886 and 891 μm^2/hour. However, the Tesla oscillator treated fin-amputated larvae did not show a significant difference compared to untreated and WLAN treated larvae. The WLAN treated larvae showed only 0.5% slower growth compared to untreated larvae which is insignificant difference.
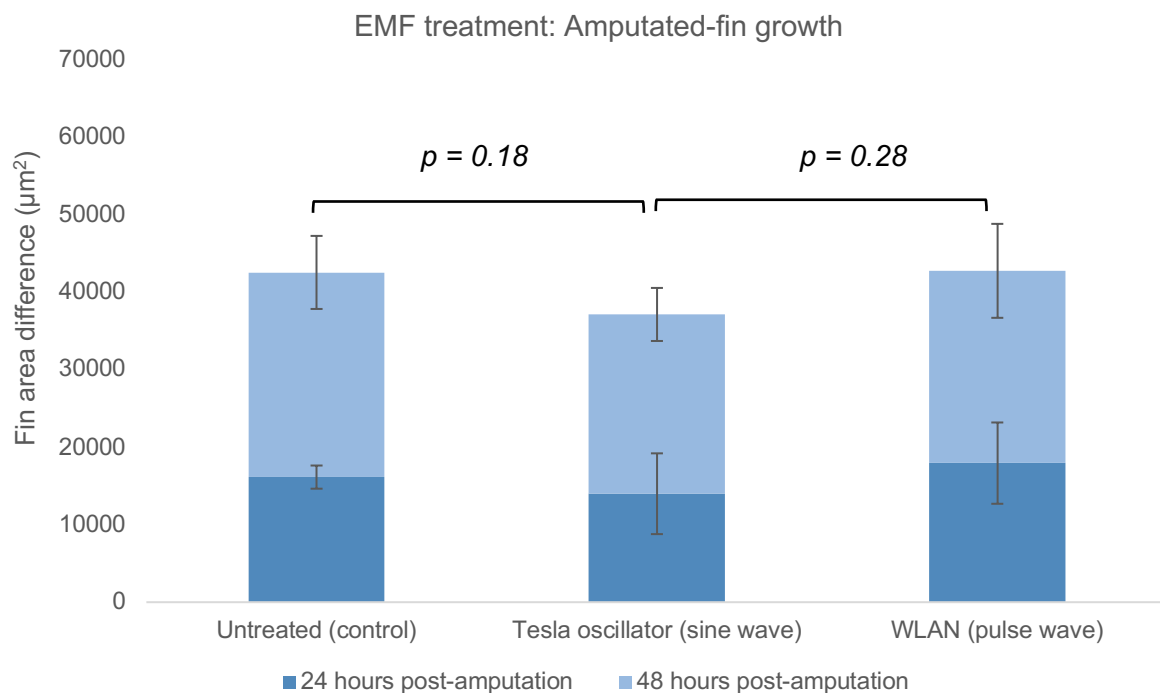
Fig. 42: The comparison of the amputated-fin growth of untreated and EMF (Tesla oscillator and WLAN) radiation exposed larvae. The amputated-fin growth of 3 days post-fertilised untreated (control) zebrafish larvae were compared to Tesla oscillator and WLAN electromagnetic field (EMF) radiation exposed larvae were imaged and measured over 48 hours post-amputation. Statistically significant difference for total growth in 48 hours if $p < 0.05$, indicated by (*), the others are non-significant difference (*ns*). Sample size (n=5 repetition, total 100 larvae) per condition. Data were analysed using the Welch's t-test by One-Way ANOVA.

The neutrophil infiltration in fin-amputated larvae is significantly high for Tesla oscillator treated larvae at 3 hpa compared to untreated and WLAN treated larvae (Fig. 43). The Tesla treated larvae have 39.0% more neutrophil infiltration at injured site compared to untreated and 28.4% more than WLAN treated larvae at 3 hpa. At 48 hpa, the Tesla treated larvae still have 21.6% and 28.4% higher neutrophil count compared to untreated and WLAN exposed larvae, respectively, however statistically there is no significant deference.

EMF treatment : Neutrophil count
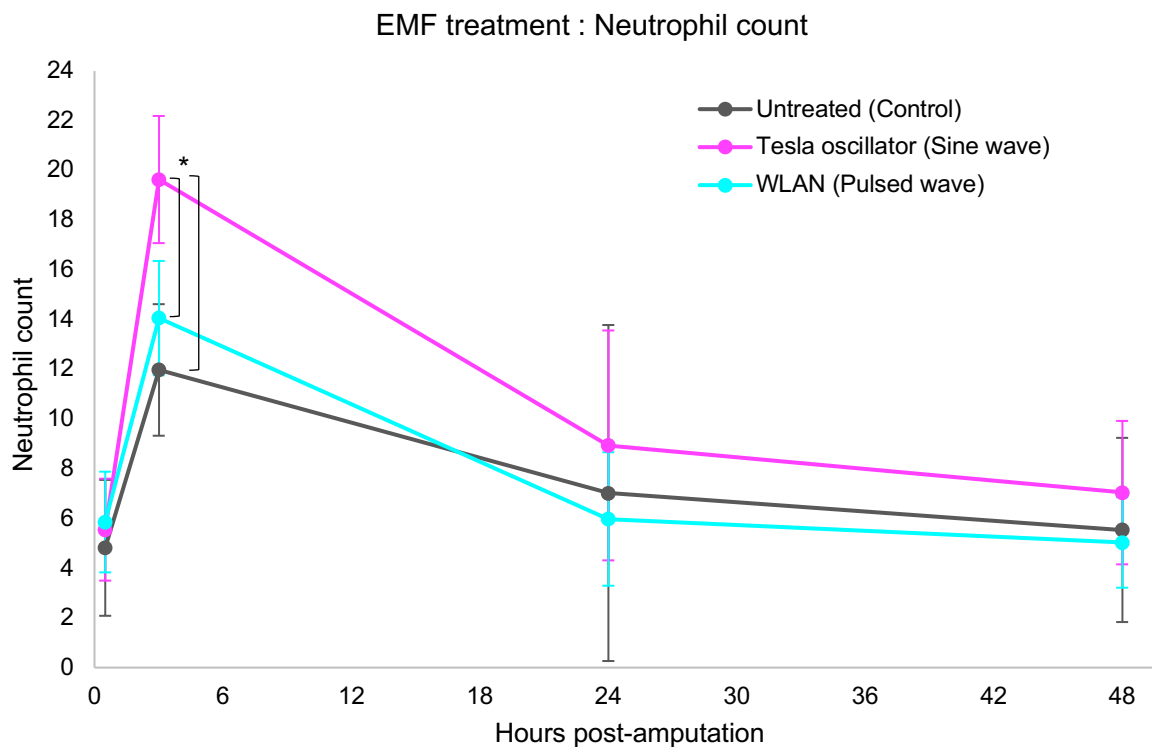
Fig. 43: The comparison of the neutrophil count at the amputated site of untreated and EMF (Tesla oscillator and WLAN) radiation exposed larvae. The comparison of the neutrophil count at the amputated site from 0.5 to 48 hours post-amputation (hpa) of untreated (control) zebrafish larvae were compared to Tesla oscillator and WLAN electromagnetic field (EMF) radiation exposed larvae showed significant difference at 3 hpa. Statistically significant difference for neutrophil count if $p < 0.05$, indicated by (*), the others are non-significant difference (*ns*). Sample size (n=5 repetition, total 94 larvae) per condition. The neutrophil count is expressed by Mean ± S.D. Data were analysed using the Welch's t-test by One-Way ANOVA.

The Tesla oscillator generated EMF radiation induces growth retardation in both intact and amputated-fin growth of zebrafish larvae. However, referring to Fig. 44, observing the agarose whole mounted larvae shows no obvious morphological deformities in Tesla oscillator radiated larvae.

Fig. 44: Morphological deformities are not seen in the Tesla oscillator (EMF) treated larvae.
The image taken upon 48 hours of radiation treatment by Tesla oscillator (1 hour/day for for 3 consecutive days). EMF radiation by Tesla oscillator induces growth retardation however morphological deformities in the overall structure are not visible.

3.10   Effects of gas treatment on the growth of *Chlorella vulgaris* cell culture

C. vulgaris matured cells differentiate into 4 daughter cells and liberate the daughter cell by breaking the cell wall of parent cells within the next 16 to 24 hours duration. The acceleration of *C. vulgaris* matured cells to differentiate into 4 daughter cells indicates the rapid development of *C. vulgaris* (Fig. 45). Thus expected the cell density of *C. vulgaris* culture increases over time to indicate a healthy development. The *C. vulgaris* culture growth rate was determined by absorbance reading at OD_{750}, which aid to determine the quantification of particles because 750 nm wavelength is out of chlorophyll light absorbance interference range therefore the cell density reading could not be influenced by chlorophyll accumulation in the cells. The harvested cell culture was further macerated using French press to quantify the bioactive content such as chlorophyll, protein and starch.

(A)   **(B)**
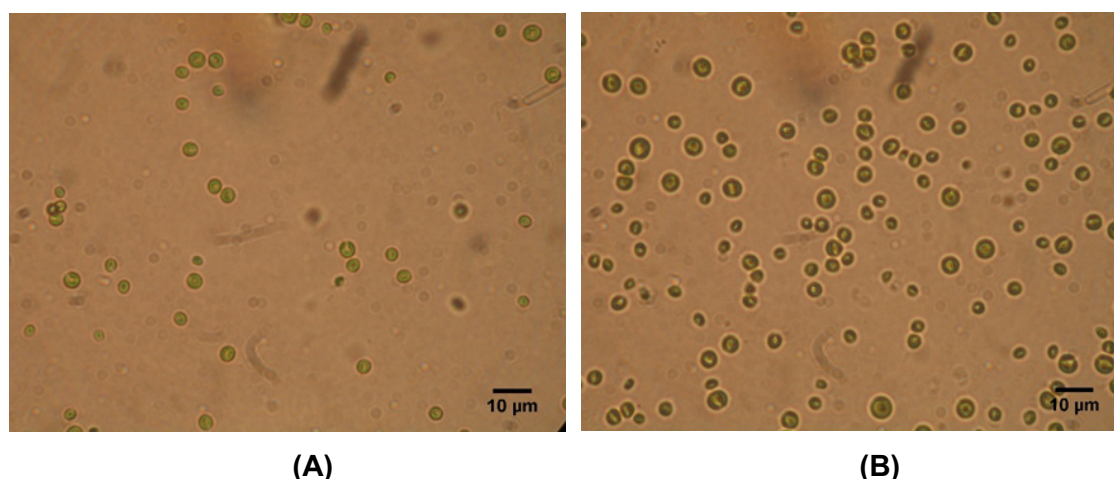
Fig. 45: *Chlorella vulgaris* observed under microscope at 10X lens objective.
(A) The cell density of *C. vulgaris* in the 1-week-old cell culture in control. (B) The cell density of *C. vulgaris* in the 4-week-old cell culture in control. Image (A) and (B) shows the unicellular cell matured and differentiate faster over time unlike higher plants which takes longer to observe the growth.

3.10.1 *Chlorella vulgaris* growth effect upon gas direct-treatment

In order to evaluate the influence of H_2 gas on the growth rate of the plant, we have chosen the photosynthetic *C. vulgaris*, a unicellular microalga to study the effects. Different gases were used including pure H_2 gas to make a comparison study such as Air, N_2, H_2-O_2 gas mixture, Brown's gas, O_2 and a pair of flasks with *C. vulgaris* culture were kept untreated to compare and rule out the bubbling effect on *C. vulgaris* culture. The H_2 gas treated medium has ~60% or 1.2 mg/L more dissolved H_2 and ~80% or 9.5 mg/L lesser dissolved O_2 compared to the H_2-O_2 gas mixture and Brown's gas treated condition however both samples showed almost a similar growth rate (Fig. 46). Brown's gas treated culture shows only 2% better growth rate compared to H_2 treated culture. The N_2 gas treated medium does not contain dissolved H_2,

however, has almost the same amount of dissolved O_2 compared to the H_2 gas treated medium. The growth density comparison study indicates that the N_2 treated sample has 7% more growth rate compared to the H_2 gas treated sample. While the air treated *C. vulgaris* culture, which is not exposed to dissolved H_2 and maintains a standard dissolved O_2 concentration of ~6.7 mg/L has the highest growth rate compared to H_2, N_2, H_2-O_2 mixture, Brown's gas, O_2 treated and untreated culture with 23%, 17%, 23%, 21%, 36% and 28%, respectively, lower than air treated *C. vulgaris* culture. The O_2 treated and untreated *C. vulgaris* culture showed 17% and 6%, respectively, lower growth rates compared to the H_2 gas treated sample. The untreated *C. vulgaris* has lower growth due to the absence of agitation or shaking hence the cell growth and differentiation of cells are being retarded. Meanwhile, the O_2 treated *C.vulgaris* culture growth deteriorates due to inhibition from starch formation at high O_2 concentration which interferes with the Rubisco enzyme in the CO_2 fixation mechanism in Calvin-cycle.
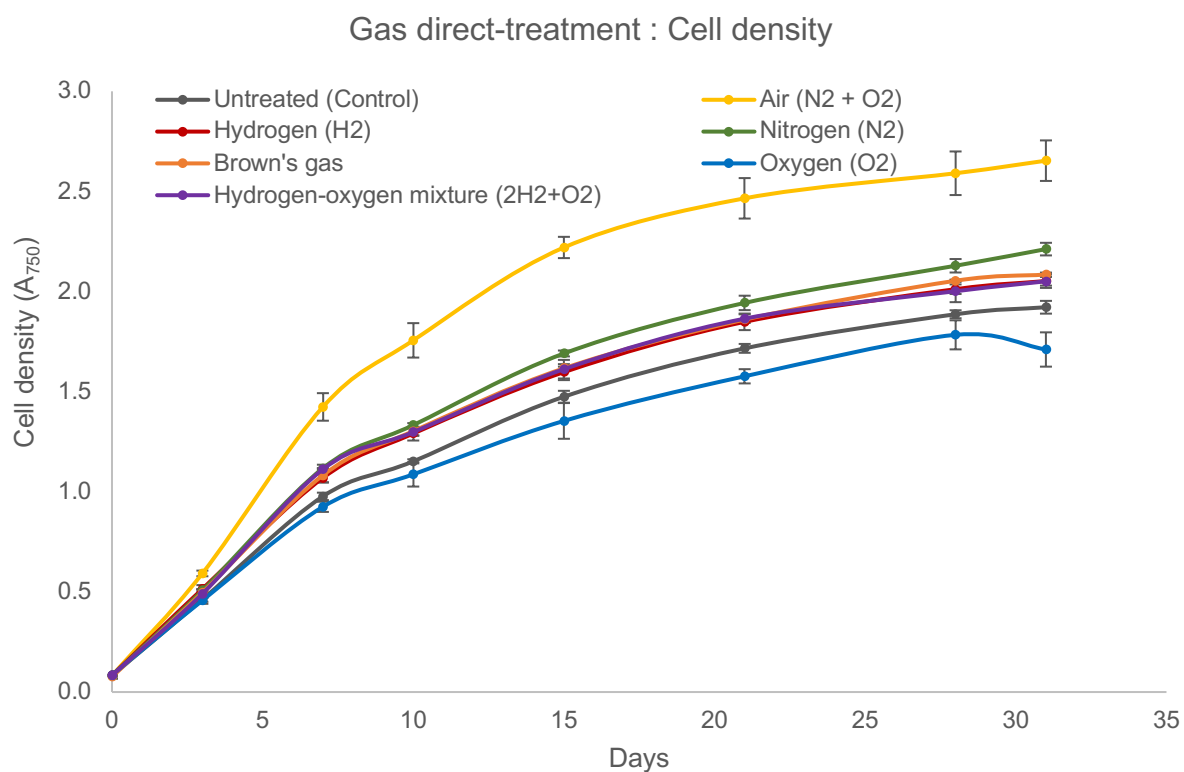
Fig. 46: The effect of different gases by direct-gas treatment on cell growth rate of *Chlorella vulgaris.* The cell growth rate of *Chlorella vulgaris* culture were determined by absorbance measurement at OD_{750}. The absorbance (OD_{750}) is expressed by Mean ± S.D.

Fig. 47 shows that cell culture of *C. vulgaris after* 4 weeks of treatment with different gases. The green colour reflected by *C. vulgaris* is the colour of chlorophyll accumulated in the cells therefore, the falcon tubes with the darkest colour reflection may give an approximate indication that the particular falcon may contain a high density of *C. vulgaris* cells. For example,

the untreated and the O_2 treated *C. vulgaris* showed to have the lowest cell density in Fig. 46 and both the cell culture reflected the lightest green colour reflection in Fig. 47.

Fig. 47: Image of direct-gas treated *Chlorella vulgaris* culture.
Each gas treatment has 2 flasks of culture. The *C. vulgaris* cell culture treatment including Untreated (control), Air, H_2, N_2, H_2-O_2 gas mixture, Brown's gas and O_2.

3.10.1.1 Dry weight of *Chlorella vulgaris* cell culture by direct gas treatment

On the cell culture harvesting day, 2 mL of cell culture are freeze dried overnight by lyophilize method before weighing the dry weight of *C. vulgaris* cell. The cell density of air treated samples is the highest followed by N_2, Brown's gas, H_2-O_2 mixture, H_2 treated, untreated culture and O_2 treated culture which is confirmed by dry weight analysis (Fig. 48). The air, N_2 and Brown's gas treated sample have 32%, 12% and 5%, respectively, more dry weight compared to H_2 gas treated *C. vulgaris* culture while the O_2 and untreated sample have 19% and 10% lower dry weight than H_2 treated sample. The H_2 and H_2-O_2 gas mixture treated sample has almost the same dry weight.

Gas direct-treatment: Dry weight of *Chlorella vulgaris*
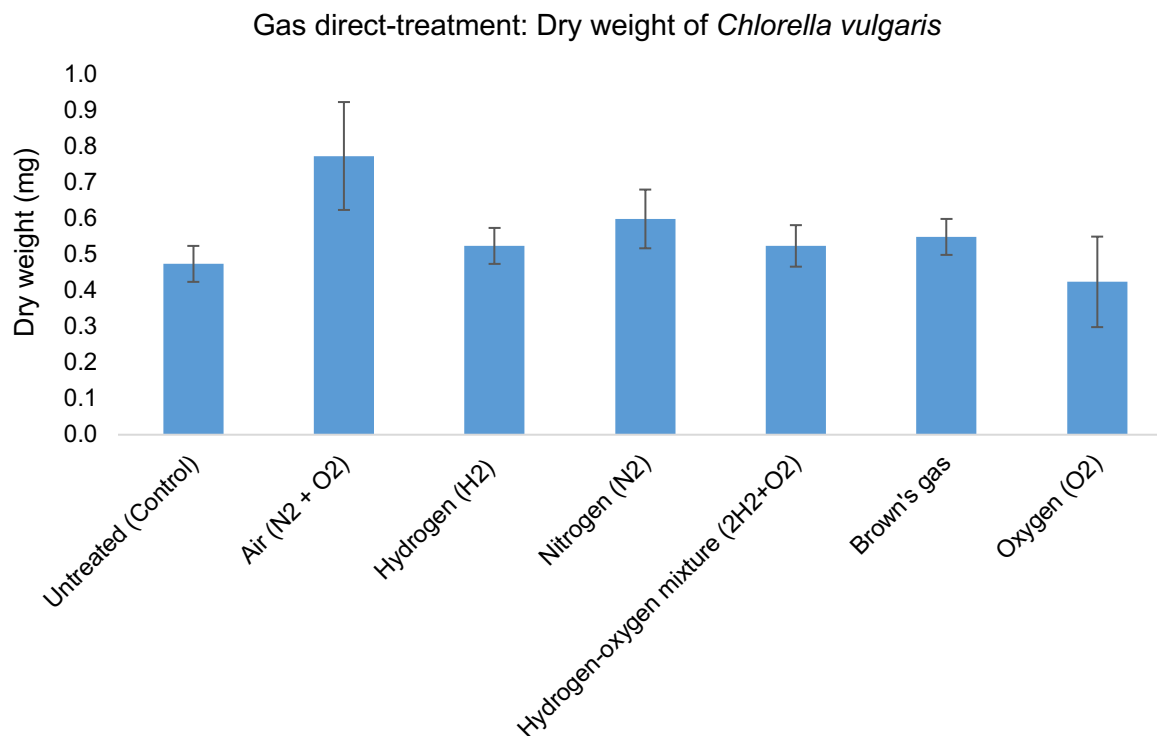
Fig. 48: Dry weight of direct-gas treated *Chlorella vulgaris* culture. The different gas treated cell cultures harvested and dry weight measured to confirm the *Chlorella vulgaris* culture density. The weight expressed by Mean ± S.D.

Since *C. vulgaris* has high potential to increase the cell differentiation rate in a shaking condition hence a medium pre-treatment method was implemented in *C. vulgaris* growth evaluation study to avoid false results due to overlay of agitation effect. However, the chlorophyll, protein and starch quantification analysis for direct-gas treatment were done to see if there are any abnormal changes. The *C. vulgaris* culture treated by air, H_2, N_2, O_2, H_2-O_2 gas mixture and Brown's gas did not indicate any obvious difference in the quantification of chlorophyll, protein and starch. The bioactive compound analysis results are attached at the appendices (Fig. S13 – Fig. S15).

3.10.2 *Chlorella vulgaris* growth effect upon gas pre-treatment

In general, microalgae grow faster in agitated conditions for example microalgae cultured on shaker. Therefore, there would be a high possibility that the effects of gases to be overlayed by the effect of *C. vulgaris* cell agility. In order to evaluate the influence of the gases without influence from other external factors, the *C. vulgaris* culture was centrifuged at a lower spin (4500 rpm) at a lower temperature (4 ºC) for a very short period (3 minutes) to avoid the cell walls from breaking but to separate the medium gently from *C. vulgaris* cells culture. The separated supernatant was infused with Air, H_2, N_2, H_2-O_2 gas mixture, Brown's gas, and O_2 before incubating the *C. vulgaris* cells back into the medium.

In the first 8 days of treatment, the *C. vulgaris* growth density is deteriorating in every *C. vulgaris* cell culture most probably due to the poor adaptation to the gas treatment method including repetitive centrifugation and shifting cells from one container to another which may add stress to the cells however from day 8 to day 19, for another 11 days, the *C. vulgaris* culture started to grow progressively (Fig. 49). As observed in the direct treatment, the air treated sample has the highest growth rate while the O_2 treated sample has the lowest growth density. Meanwhile, the H_2, N_2, H_2-O_2 mixture and Brown's gas treated *C. vulgaris* showed almost the similar cell density. Furthermore, the air and untreated *C. vulgaris* culture has better cell growth rate compared to H_2, N_2, H_2-O_2 mixture and Brown's gas treated samples. This gives an impression that H_2 do not contribute to any beneficial effects on the *C. vulgaris* cell growth.

In the pre-treatment method, air treated culture showed only 8% better growth rate compared to untreated culture have clearly indicated that air treated culture grows better in direct treatment due to agitation effects. While H_2, N_2, H_2-O_2 gas mixture, Brown's gas and O_2 treated culture grow 17%, 14%, 17%, 14% and 24% slower than air treated (control) culture, respectively. The O_2 treated culture growth is largely retarded due to high saturation of O_2 in *C. vulgaris* culture inhibits the photosynthesis reaction.
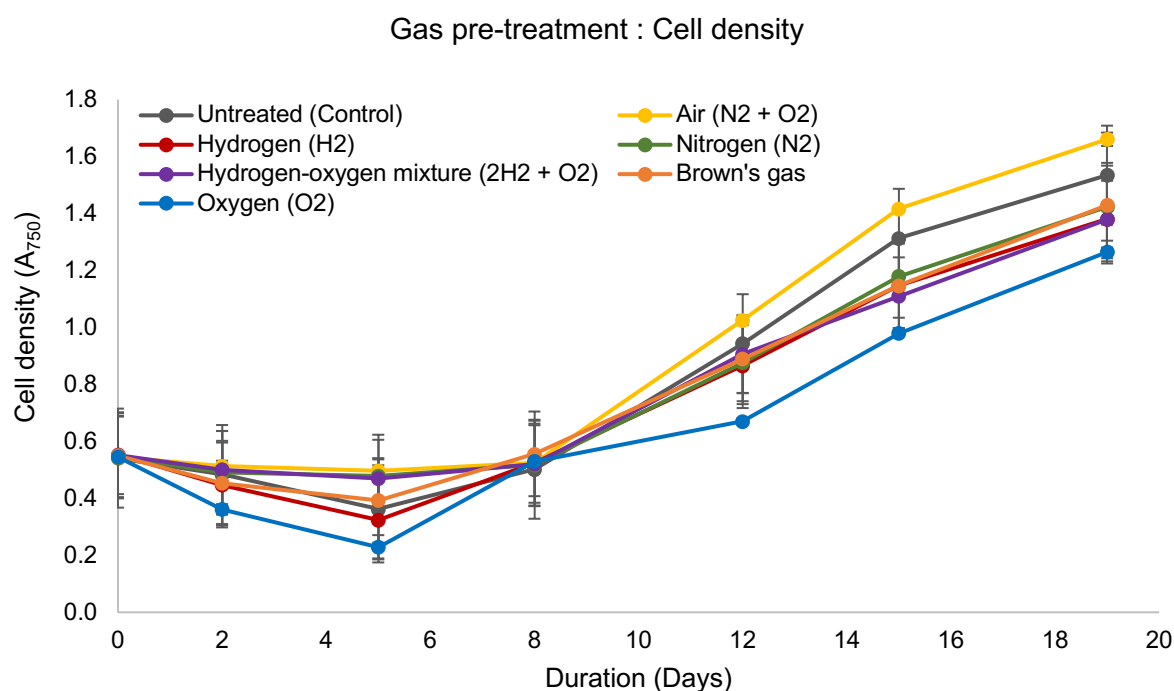
Fig. 49: The effect of gases on *Chlorella vulgaris* by medium pre-treatment. The BBM culture medium infused with different gases prior to incubation of the *Chlorella vulgaris* cells. The growth rate of *Chlorella vulgaris* culture over days was determined by absorbance measurement at OD_{750}. The absorbance (OD_{750}) is expressed by Mean ± S.D.

Fig. 50 shows the flasks containing *C. vulgaris* cell culture, the colour intensity of cells between untreated control, air treated, H_2, N_2, H_2-O_2 gas mixture and Brown's gas treated sample does not show an obvious colour intensity difference however the O_2 treated sample shows slightly a lower colour intensity by eye view which indicates could be a lower number of healthy cells in O_2 treated sample.
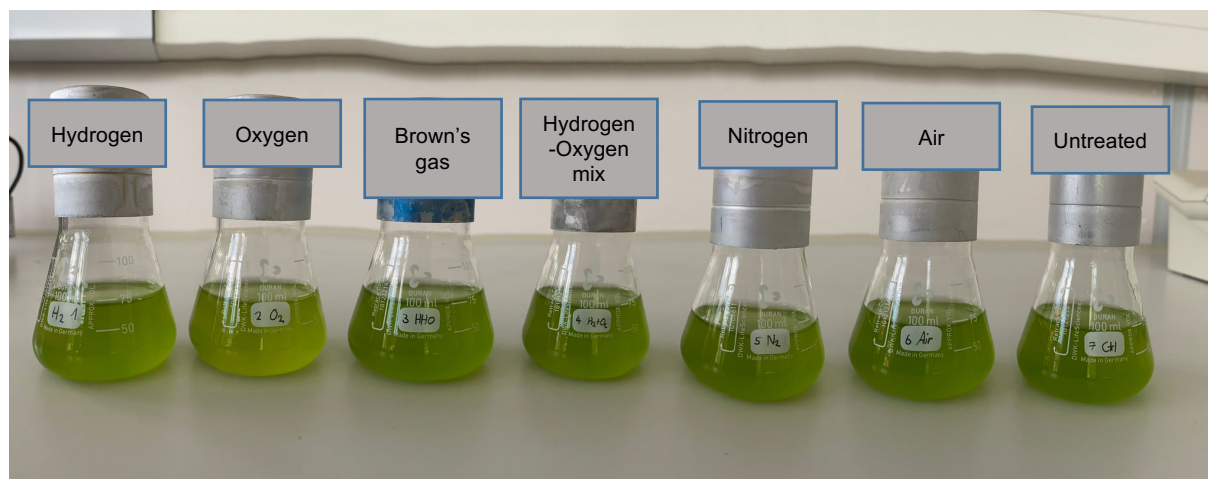
Fig. 50: Image of *Chlorella vulgaris* culture by pre-treatment method.
The *C. vulgaris* cell culture treatment including Untreated (control), Air, H_2, N_2, $2H_2$+O_2, Brown's gas and O_2.

3.10.2.1 Dry weight of *Chlorella vulgaris* cell culture by medium gas pre-treatment

On the cell culture harvesting day, 2 mL of cell culture was freeze dried overnight by lyophilize method before weighing the dry weight of *C. vulgaris* cell. The cell density of air-treated samples and untreated control showed the highest dry weight content compared to H_2, N_2, H_2-O_2 gas mixture and Brown's gas treated cell culture. The O_2 treated *C. vulgaris* cell culture has the lowest dry weight mass (Fig. 51). The air treated and untreated *C. vulgaris* cell culture has almost similar cell density and dry weight mass. Meanwhile, H_2, N_2, H_2-O_2 gas mixture and Brown's gas have almost the same quantity of cell density as well as the dry weight mass.

Gas pre-treatment: Dry weight
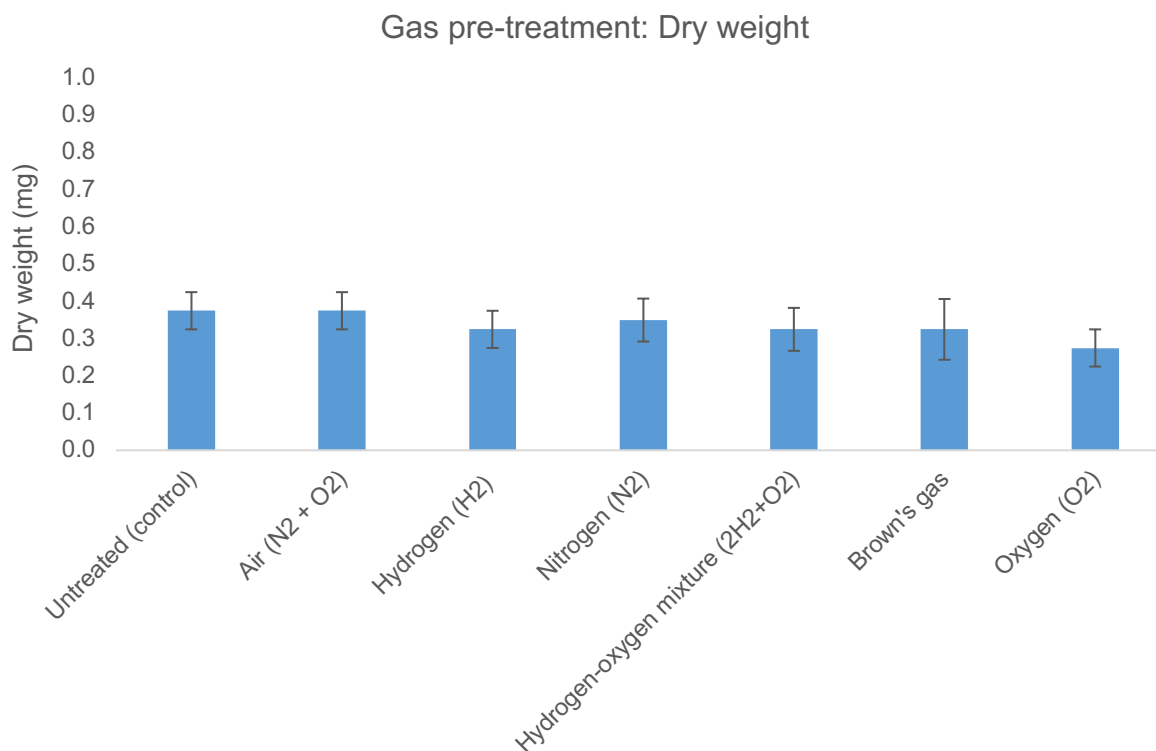
Fig. 51: Dry weight of medium pre-treated *Chlorella vulgaris* culture.
The different gas treated cell cultures harvested and dry weight measured to confirm the *Chlorella vulgaris* culture density. The value expressed by Mean ± S.D.

3.10.2.2 Bioactive compound analysis of *Chlorella vulgaris* cell culture by medium gas pre-treatment: Chlorophyll, protein and starch content

The chlorophyll content in air treated, untreated, H_2, N_2, H_2-O_2 gas mixture, Brown's gas and O_2 treated *C. vulgaris* culture content almost the same amount regardless of pre-treatment with different gases (Fig. 52). The concentration of chlorophyll of all different gas treatment is within the range of 9.4 - 9.9 µg/mL.
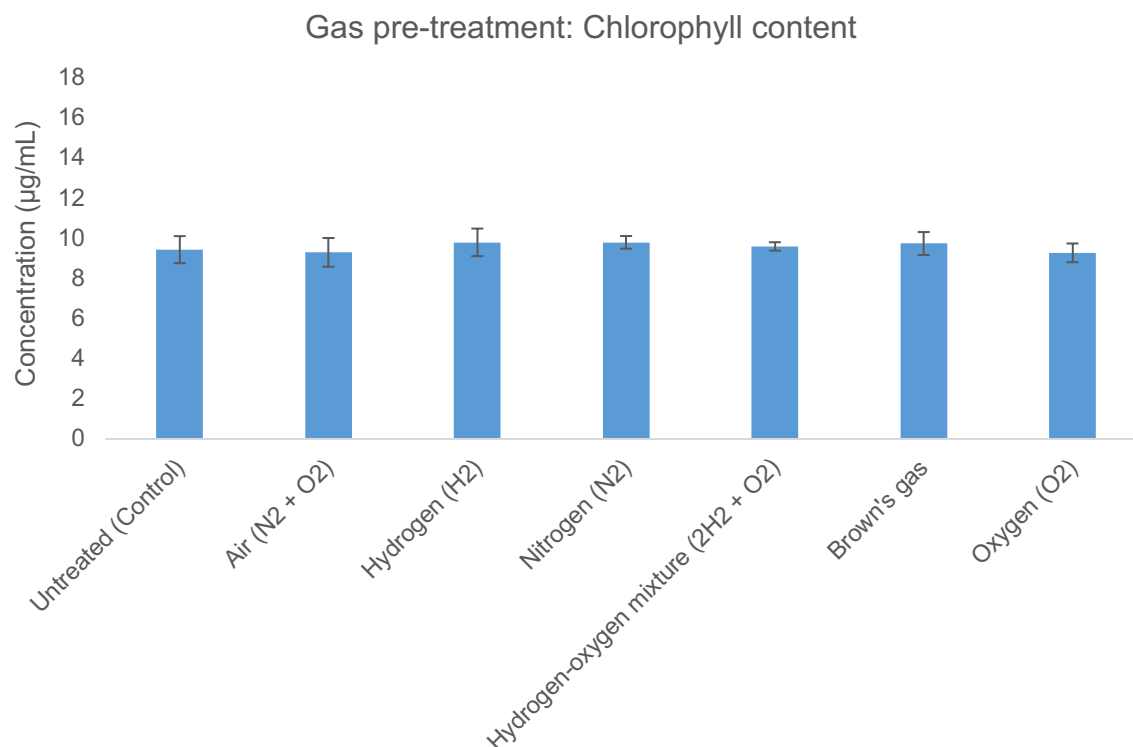
Fig. 52: Chlorophyll quantification of medium pre-treated *Chlorella vulgaris* culture. The different gas pre-treated cell culture harvested, absorbance measured at OD_{665} and OD_{652} to confirm the chlorophyll content in *Chlorella vulgaris* cell culture. The value expressed by Mean ± S.D.

The protein content in air treated, untreated, H_2, N_2, H_2-O_2 gas mixture, Brown's gas and O_2 treated *C. vulgaris* culture content almost the same amount of protein regardless of pre-treatment with different gases (Fig. 53). The quantification of protein from *C. vulgaris* culture from different gas treatment is within the range of 42 - 45 µg/mL. The pre-treatment of *C. vulgaris* culture medium with different gases did not either enhance the protein synthesis or reduces.
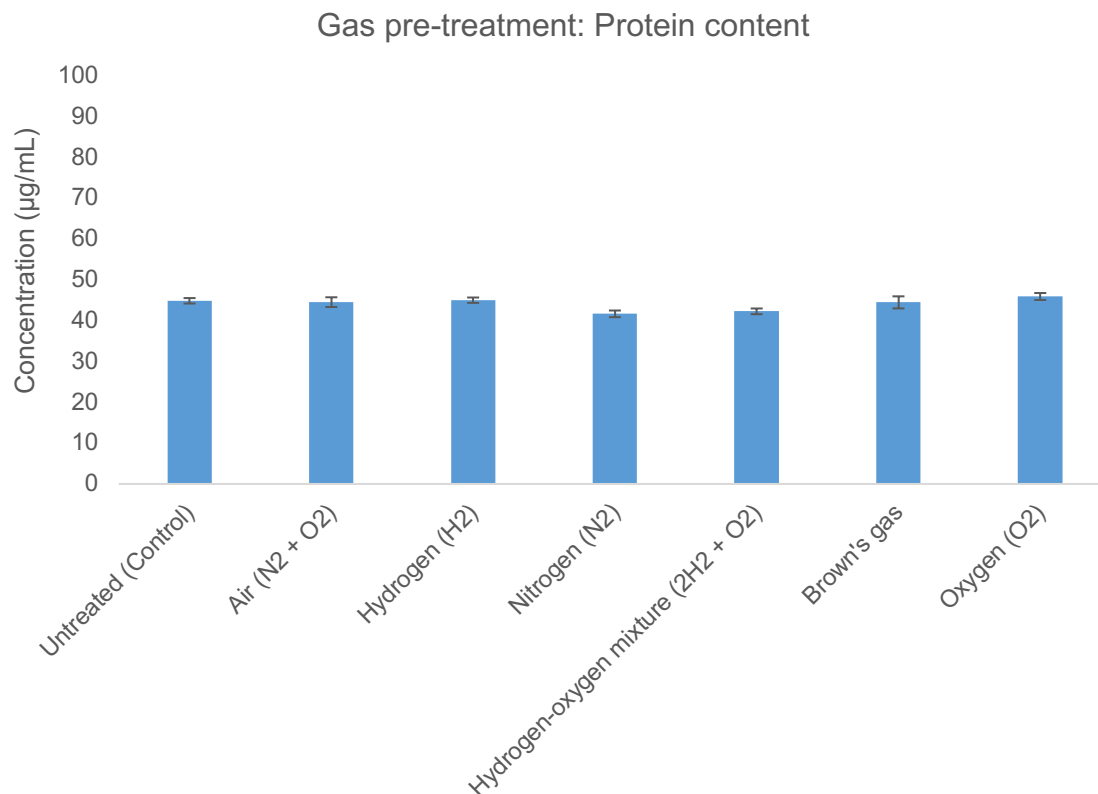
Fig. 53: Protein quantification of medium pre-treated *Chlorella vulgaris* culture. The different gas pre-treated cell culture harvested, absorbance measured at OD_{590}/OD_{450} and compared with BSA standard curve to confirm the protein content in *Chlorella vulgaris* cell culture. The value expressed by Mean ± S.D.

The starch content in air treated, untreated, H_2, N_2, H_2-O_2 gas mixture, Brown's gas and O_2 treated *C. vulgaris* culture contain almost the same amount of starch regardless of pre-treatment with different gases (Fig. 54). The quantification of starch of all different gas treatment is within the range of 100 - 120 mg/L.

Gas pre-treatment: Starch content
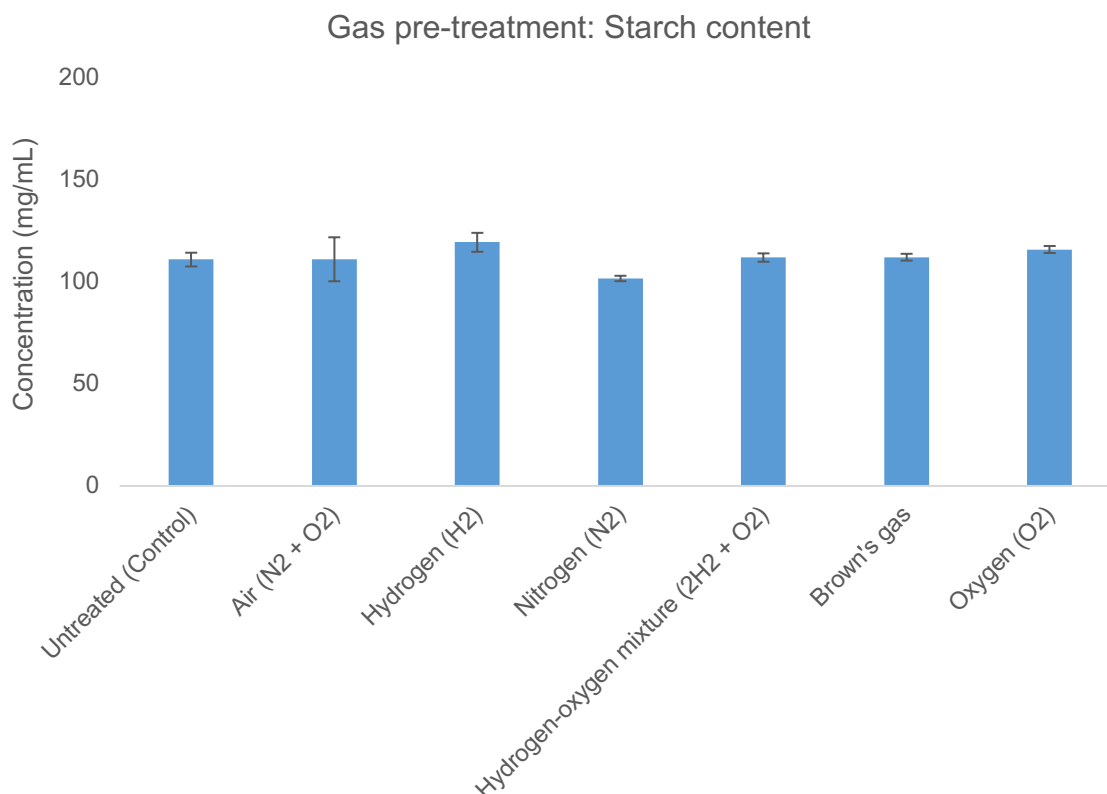
Fig. 54: Starch quantification of medium pre-treated *Chlorella vulgaris* culture.
The different gas pre-treated cell culture harvested, absorbance measured at OD_{625} and compared with the starch standard curve to confirm the starch content in *Chlorella vulgaris* cell culture. The value expressed by Mean ± S.D.

3.11 Electromagnetic fields radiation treatment on *Chlorella vulgaris* cell culture

C. vulgaris cell growth rate was observed for 28 days upon radiation to evaluate if EMF waves accelerate the cell differentiation of *C. vulgaris*. The untreated, Tesla oscillator and WLAN radiation exposed *C. vulgaris* cell culture did not show any difference in the cell density upon continuous measurement of absorbance at 750 nm (Fig. 55). Therefore, initially assumed that Tesla oscillator and WLAN radiation at 144 MHz and 5 GHz frequency, respectively, do not cause any side effects to *C. vulgaris* cell culture although treated for 5 days in a week for 4 weeks. However, the bioactive compound quantification for protein and starch showed a negative impact of EMF treatment.
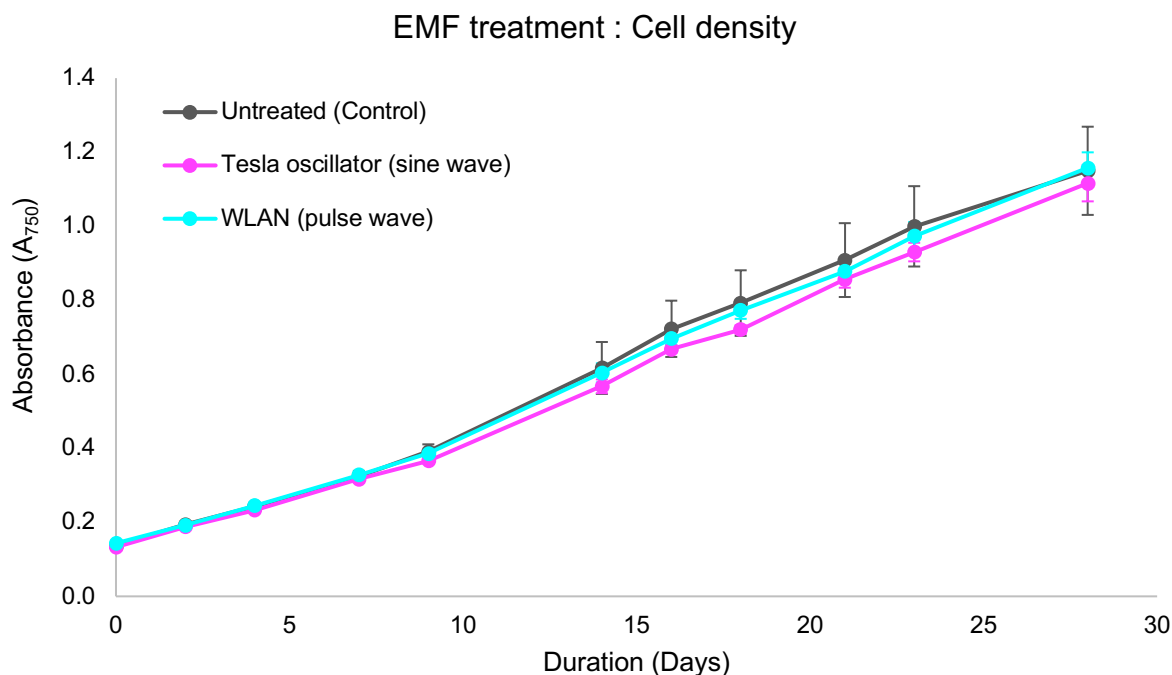
Fig. 55: The effect of EMF treatment on cell growth rate of *Chlorella vulgaris*.
The effect of electromagnetic field (EMF) by Tesla oscillator and WLAN radiation on the cell growth rate of *Chlorella vulgaris* culture were determined by absorbance measurement at OD_{750}. The absorbance (OD_{750}) is expressed by Mean ± S.D.

Fig. 56 shows pair of falcon tubes containing *C. vulgaris* cell culture treated by Tesla oscillator and WLAN radiation, as well as a pair of falcons contain untreated culture. The colour density of *C. vulgaris* cell culture between untreated control, Tesla oscillator and WLAN radiation treated sample does not show an obvious difference in colour intensity by eye view.
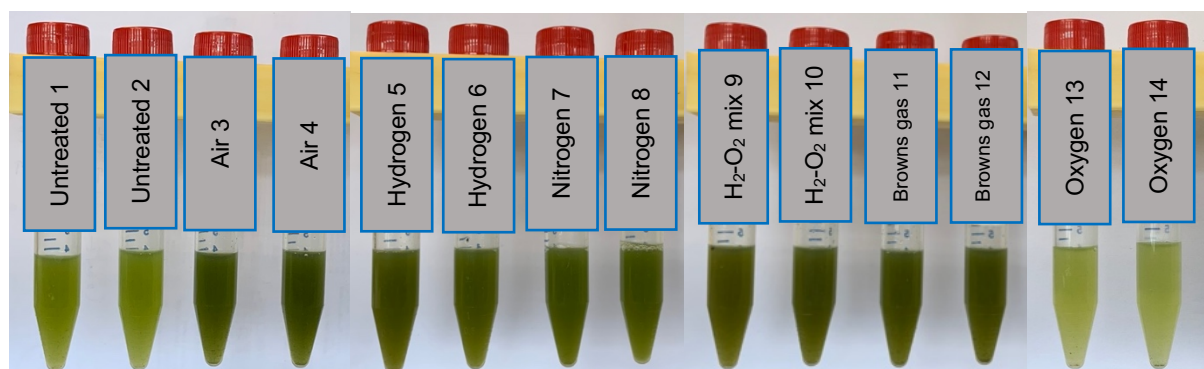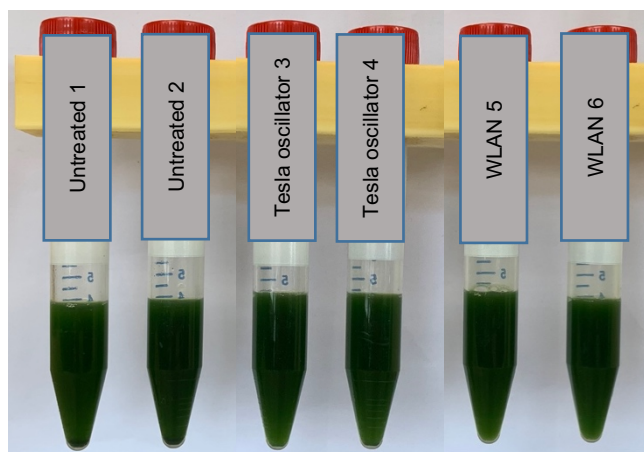

Fig. 56: Image of EMF treated *Chlorella vulgaris* culture.
Each gas treatment has 2 flasks of culture. The *C. vulgaris* cell culture treatment including Untreated (control), Tesla oscillator and WLAN.

3.11.1 Dry weight of electromagnetic field (EMF) treated *Chlorella vulgaris* cell culture

On the cell culture harvesting day, 2 mL of cell culture are freeze dried overnight by lyophilize method before weighing the dry weight of *C. vulgaris* cell. The cell density of *C. vulgaris* culture of untreated (control), Tesla oscillator and WLAN radiation exposed culture did not show an obvious difference as well as the dry weight of the lyophilised *C. vulgaris* culture, also did not show any difference (Fig. 57).
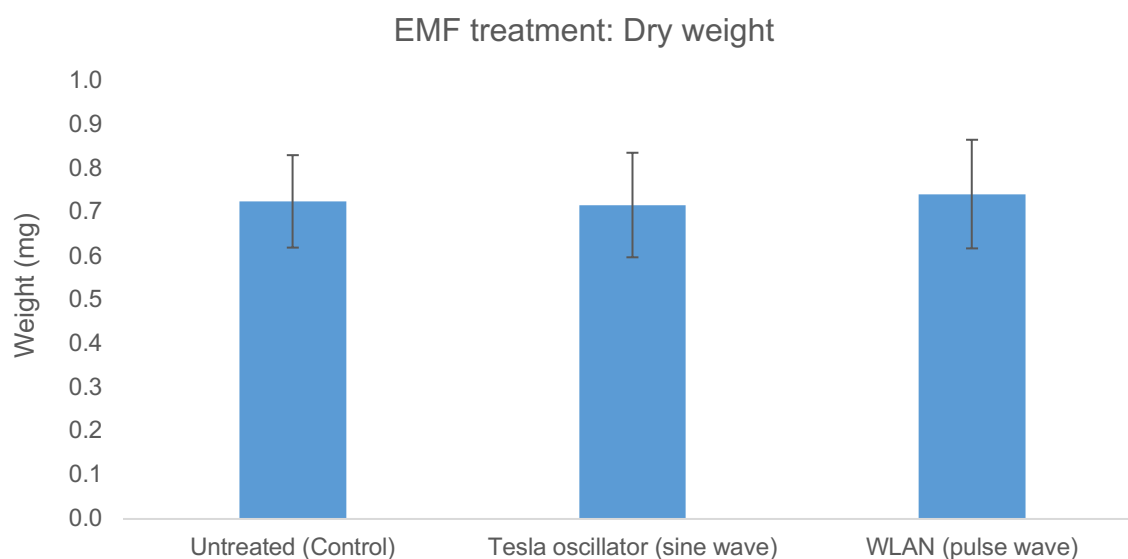
Fig. 57: Dry weight of EMF treated *Chlorella vulgaris* culture.
The untreated, Tesla oscillator and WLAN treated *Chlorella vulgaris* cell culture harvested on the last day of treatment. The dry weight of each *Chlorella vulgaris* cell culture was measured to confirm the growth rate. The value expressed by Mean ± S.D.

3.11.2 Bioactive compound analysis of electromagnetic field treated *Chlorella vulgaris* cell culture: Chlorophyll, protein and starch content

The chlorophyll content in untreated (control), Tesla oscillator and WLAN radiation treated *C. vulgaris* culture equally contain almost the same amount of chlorophyll regardless of the radiation effect (Fig. 58). The concentration of chlorophyll in untreated and different frequency of EMF treatment is within the range of 8.8 - 9.4 µg/mL.
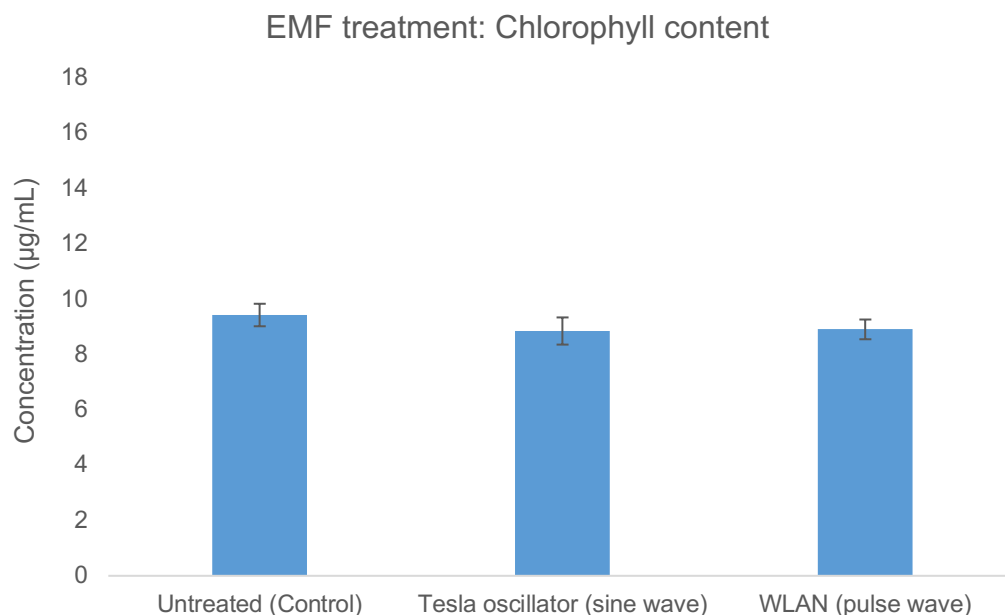
Fig. 58: Chlorophyll quantification of EMF treated *Chlorella vulgaris* culture.
The untreated, Tesla oscillator and WLAN treated *Chlorella vulgaris* cell culture harvested on the last day of treatment. The absorbance was measured at OD_{665} and OD_{652} to confirm the chlorophyll content in each *Chlorella vulgaris* cell culture. The value expressed by Mean ± S.D.

The protein quantification of untreated *C. vulgaris* culture is 48.63 µg/mL while the protein content in Tesla oscillator and WLAN radiated *C. vulgaris* culture is lower which is 38.15 µg/mL and 40.32 µg/mL, respectively (Fig. 59). The protein content analysis upon radiation shows 21.6% and 17.1% of lower protein content for Tesla oscillator and WLAN radiation exposed culture, respectively, compared to untreated *C. vulgaris* culture. Even though the cell density and chlorophyll content are the same among radiation exposed samples and untreated samples, however, the quantification of protein showed a sign of protein deterioration in radiation-exposed *C. vulgaris* culture.

EMF treatment: Protein content
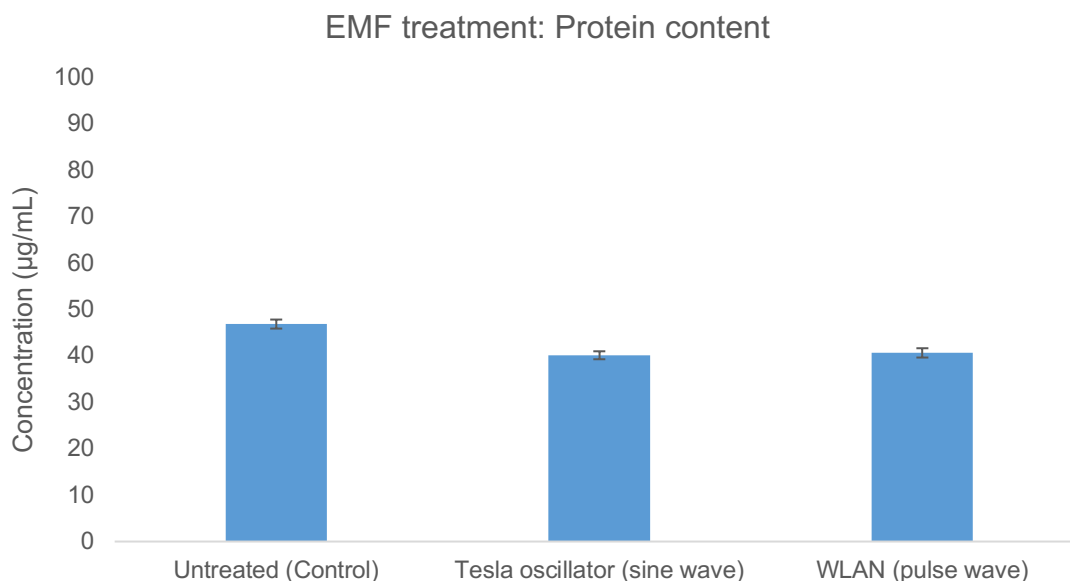
Fig. 59: Protein quantification of EMF treated *Chlorella vulgaris* culture.
The untreated, Tesla oscillator and WLAN treated *Chlorella vulgaris* cell culture harvested on the last day of treatment. The absorbance was measured at OD_{590}/OD_{450} and compared with BSA standard curve to confirm the protein content in each *Chlorella vulgaris* cell culture. The value expressed by Mean ± S.D.

The starch content of untreated *C. vulgaris* culture is 112.57 mg/mL while the starch content in Tesla oscillator and WLAN radiated *C. vulgaris* culture is slightly lower, 69.78 and 75.01 mg/mL, respectively (Fig. 60). The starch content analysis upon radiation shows 38.01% and 33.37% of lower starch content for Tesla oscillator and WLAN radiated culture, respectively, compared to untreated *C. vulgaris* culture. Tesla oscillator EMF radiated with 144 MHz sine wave with higher input energy may increase the radiation intensity and have further affected the starch production or deteriorated the stored starch due to long term (4 weeks) exposure to radiation. Meanwhile, the WLAN radiation at 5 GHz with lower input energy also largely affected the starch content in the *C. vulgaris* culture cell.
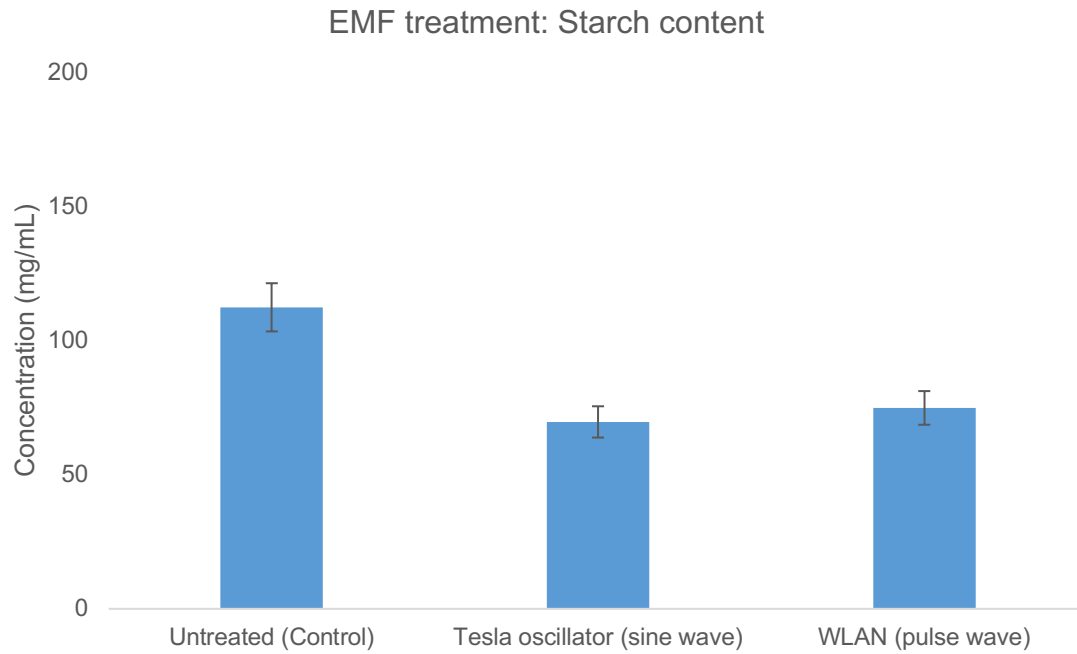
Fig. 60: Starch quantification of EMF treated *Chlorella vulgaris* culture.
The untreated, Tesla oscillator and WLAN treated *Chlorella vulgaris* cell culture harvested on the last day of treatment. The absorbance was measured at OD_{625} and compared with the starch standard curve to confirm the starch content in each *Chlorella vulgaris* cell culture. The value expressed by Mean ± S.D.

4. Discussion

4.1 Hydrogen gas treatment effects on tissue development and tissue regeneration of zebrafish embryos.

Ohsawa et al. published in *Nature Medicine* that oxidative stress damage, induced by brain ischemia-reperfusion, was suppressed by H_2-therapy in rats. Ohsawa et al. further explained that H_2 has a chemical reactivity that tends to quench the most aggressive and harmful ROS like hydroxyl radical (OH·) and peroxynitrite (ONOO·) while leaving the other ROS which involves in molecular signaling such as NO·, H_2O_2 and $·O_2^-$ unscathed[7]. The property of H_2 unscathed harmless oxidants indicates that H_2 may combat ROS without disturbing the redox homeostasis[7,162]. Thus, the aim of this work is to further elucidate if the molecular H_2 has therapeutic properties and if shows a positive effect on the growth factors. In addition, also studied the therapeutic effects of Brown's gas (H_2/O_2 mixture) generated by alkaline hydrolysis with intercalated electrodes. In this study, the beneficial effects of molecular H_2 and Brown's gas were determined by measuring a few different parameters including intact caudal fin-fold development of zebrafish larva, tissue regeneration of amputated-fin and neutrophil count at tissue amputated site.

The growth analysis was proceeded with 3 dpf intact-larvae, incubated for 3 hours for 3 consecutive days in H_2 enriched medium and the development of fin-fold was measured by brightfield microscopic imaging. In general, a 3 dpf zebrafish larvae is about 4.3 mm in length and the caudal fin will be approximately 8% of the total length therefore, a well-developed caudal fin tissue may reflect an overall healthy development of zebrafish larvae. Simultaneously, another set of larvae was treated with H_2 enriched medium prior to caudal fin-amputation and microscopic imaging. In this study, the zebrafish larvae were pre-treated with molecular H_2 prior to fin-amputation to load the organism with sufficient H_2. The pre-treatment method was implemented so that the molecular H_2 could act as an antioxidant to immediately suppress the ROS which might be generated upon amputation. To see the optimum effects of molecular H_2, the larvae were continued treated on day 2 and day 3 with H_2 enriched medium. The amputated-fin tissue regeneration was measured for 3 consecutive days as described in Table 3 and further quantified the recruited neutrophils at the amputated site at 0.5, 3, 24 and 48 hpa to analyse the correlation of amputated-fin regeneration rate with tissue repair activity induced by neutrophils.

Zebrafish larva (3 dpf) is the perfect model to analyse tissue growth to determine the molecular H_2 therapeutic effects. This is due to an easy access to the caudal-fin fold of zebrafish larva and the fin tissue ability to rapidly regenerate upon amputation via wound healing responses without causing a detrimental effect. As well as, the tissue repair responses by the dynamic progression of the neutrophil which acts as the first defence immune cell is observable via the fluorescence microscopic imaging of transgenic line Tg(*lyzC*:DsRed). The process of the amputated fin tissue restoration is called epimorphic regeneration and proceeds by i) rapid covering of the surface of the amputated site by wound epidermis; ii) de-differentiated mesenchymal cells appear; iii) cells near the amputation plane accumulate into a distinctive tissue called the blastema; iv) After blastema formation, appropriate tissues are newly formed from the blastema cells and reconstruct the original morphology[139,153]. Therefore, if the molecular H_2 accelerates the fin re-growth, indicating the molecular H_2 may manipulate the epimorphic dynamic regeneration mechanism.

To confirm the positive effects of H_2 treated larvae, a few compatible controls were arranged such as air ($N_2 + O_2$) which represents a normoxic condition and the pure N_2 treated larvae to represent a mild hypoxic condition. The pre-agitation of E3 medium with air ($N_2 + O_2$) may not introduce a new reactive gas molecule but only the ambient gas from the surrounding atmosphere which aid to rule out the effects of air saturated condition on the zebrafish larvae. Meanwhile, pure H_2 infused medium tends to deplete the readily dissolved O_2 from the medium to allow 1.0 mM of H_2 saturation. Therefore, inert N_2 gas infused medium will be a compatible control because N_2 gas also tends to deplete the readily dissolved O_2 from the medium to reach the equilibrium condition. However, the inert N_2 gas is unable to influence the biochemical reactivity of zebrafish larvae but N_2 as an additional control helps to understand the effects of low O_2 concentration on fin growth. Rule out the side effects of low O_2 condition using N_2 (control), allowing us to further understand the beneficial effect of molecular H_2 on tissue growth.

The comparison study of air, N_2 and H_2 treated zebrafish larvae showed that molecular H_2 significantly accelerates regular tissue development of intact-fin, and also increases the fin-regeneration of amputated-fin on average. The H_2 treated larvae which were exposed to 1.0 mM of H_2 and 0.063 mM of O_2 has 31.5% and 45.0% of higher tissue development of intact-fin meanwhile 22.6% and 38.4% of higher tissue regeneration of amputated-fin compared to air and N_2 treated larvae, respectively. This indicates that 1.0 mM of dissolved H_2 in the medium able to accelerate both tissue development and tissue regeneration on average. N_2 is an inert gas and is not supposed to interfere with the tissue growth factor, however, N_2 depletes ~70% (6.7 mg/L to 1.8 mg/L) of dissolved O_2 concentration inducing a mild hypoxic condition which

could be the reason for growth retardation. A similar level of growth retardation was expected from H_2 treated larvae due to a low O_2 concentration as N_2 treated condition, on the contrary, H_2 treated larvae exhibited the highest tissue development and tissue regeneration rate compared to the controls.

The beneficial effect of H_2 is still observable regardless of low O_2 content, this is due to the adaptability of zebrafish larvae to low O_2 conditions. Strecker et al. explained that zebrafish embryo development was not affected by O_2 concentration between 7.15 to 3.33 mg/L, whereas at concentrations between 3.0 to 2.0 mg/L minor developmental retardations might be observed, yet without any pathological consequences[166] . However, exposing zebrafish embryo to lower than 0.88 mg/L of dissolved O_2 may lead to hypoxia lethal[166,168]. In this research study, the O_2 concentration was not brought any lower than 1.8 mg/L. Referring to Fig. 37, observing the agarose whole mounted larvae, both H_2 and N_2 treated larvae do not show any obvious structural deformities. However, the hypoxic condition effect is easily seen in the initial stage of treatment on N_2 treated larvae (Fig. 36), where an obvious behavioural change was detected. The N_2 treated larvae were seen to move vertically towards the surface of water most probably as a sign of O_2 suffocation condition whereas, H_2 treated larvae did not show any behavioural changes although exposed to equally low O_2 condition.

Jonz et. al. explained the sensing of hypoxic and hyperoxic conditions occurs to maintain a sufficient gas exchange across the skin or gills, through a specialized chemoreceptor cell. The chemoreceptor cell may induce metabolic changes at the cellular level, which regulate the physiological response[169]. The low O_2 condition affects the larvae's physiological and immune responses, making them more susceptible to infection and low health recovery. Nishikawa et al. also have shown the deprivation of O_2 induces oxidative stress which may cause internal damage to the organism[78,158]. The exact mechanism of how a low O_2 condition (hypoxic) regulates ROS generation and ROS signaling pathway remains unclear. However, based on my current study, molecular H_2 treated zebrafish larvae have shown a better fin-growth compared to the control (O_2-levelled) regardless of being in a low O_2 atmosphere. This phenomenon suggests that the trans-cutaneous intake of molecular H_2 might be able to reverse the negative effects of low dissolved O_2 conditions by balancing healthy redox homeostasis. Nonetheless, the molecular level mechanism of how molecular H_2 compensates the basic need of larvae for O_2 without any health deterioration is not understood.

Though zebrafish larvae showed healthy growth in H_2 enriched medium regardless of low O_2 concentration, however, zebrafish being an aerobic vertebrate may achieve further advantages if H_2 is administered together with O_2. This mixture can be generated either by conventional

electrolysis of water, or from Brown's gas (alkaline electrolysis with intercalated electrodes). Researchers claim that Brown's gas has a "magic" component which contributes to "special" health-beneficial effects. Therefore, the physicochemical properties and the therapeutic effect of Brown's gas were studied and compared with H_2-O_2 gas mixture generated by typical PEM water electrolysis system. This experimental comparison aid to confirm if there is any "magic" component or Brown's gas delivers beneficial effects due to the presence of H_2 molecule. Based on the physicochemical property analysis (O_2 concentration, H_2 concentration and ORP), it became very explicit that treating a medium with a PEM water electrolysis system (H_2-O_2 gas mixture) and alkaline electrolysis with intercalated electrodes system (Brown's gas) showed a similar property. Analysis showed that, both the H_2-O_2 gas mixture and Brown's gas treated medium, have approximately 40% of higher dissolved O_2 than a normoxic condition with an additional 0.8 mg/L of H_2. Based on the physicochemical property analysis, it gives an impression that H_2-O_2 gas mixture and Brown's gas are not varied.

H_2-O_2 gas mixture and Brown's gas treated larvae is further elucidated to understand if the 0.8 mg/L of H_2 may be the reason for the beneficial therapeutic effects of Brown's gas. To determine the therapeutic effects of the Brown's gas, a proper control was prepared. Since the H_2-O_2 gas mixture and Brown's gas diffuse 40% more O_2 than untreated condition therefore an O_2-levelled condition (increased O_2 concentration to 40%, 11.7 mg/L) is used as a one of the controls to rule out the side effects of high dissolved O_2 condition to zebrafish larvae. An O_2-levelled is considered a mild hyperoxic condition for zebrafish larvae. Thus, 40% of higher O_2 concentration is not an optimum growth condition however, behavioural changes are observed neither in H_2-O_2 gas mixture, Brown's gas nor in the control (O_2-levelled condition). Instead, both H_2-O_2 gas mixture and Brown's gas treated larvae showed significantly higher growth compared to O_2-levelled (control) condition treated larvae (Fig. 38 and Fig. 39). The H_2-O_2 gas mixture and Brown's gas treated either fin-intact or fin-amputated larvae, both has shown significantly higher growth compared to the O_2-levelled condition treated larvae. The H_2-O_2 gas mixture and Brown's gas both showed ~21% and ~31% higher growth rate of intact-fin and amputated-fin compared to the O_2-levelled condition treated larvae. An additional of 0.8 mg/L of dissolved H_2 contributed by H_2-O_2 gas mixture and Brown's gas is seemed to be sufficient to show a beneficial effect on the growth factors of zebrafish larvae. Indeed 0.8 mg/L (0.4 mM) of molecular H_2 is able to manipulate the negative effect of high O_2 concentration which has retarded the growth in control (O_2-levelled). Meanwhile comparing the therapeutic effect of the H_2-O_2 gas mixture and Brown's gas on tissue growth of intact and amputated-fin showed insignificant difference. Apparently, the fin-growth analysis has showed the absence of any special "magic" component in the Brown's gas. The Brown's gas showed positive effect on growth as much as H_2-O_2 gas mixture. Therefore, concluded that the Brown's gas' "special"

health beneficial effect which is claimed by the device suppliers or researchers is may be due to the presence of an addition 0.8 mg/L of H_2 and most probably not related to any "magic components".

Meanwhile, the growth retardation observed in the O_2-levelled (control) condition may be due to the side effect induced by the an additional 40% of O_2 concentration supply. A mild hyperoxia condition may induces oxidative stress and could lead to oxygen toxicity[74,136,169]. It is known that hyperoxia could induce mitochondrial apoptosis, tissue growth arrest, and oxidative stress via the formation of ROS[82,170]. High O_2 metabolism induces mass ROS generation which disrupts the balance between oxidants and antioxidants[171]. In general, the metabolism of O_2 in mitochondria inevitably leads to the production of ROS that are highly reactive and promptly induce oxidative stress by chemical modifications of protein, lipid, and nucleic acid which can be protected by endogenous antioxidant[172]. However, a very high O_2 diffusion into the tissue cells beyond the mitochondrial capacity may causes metabolic disorder where a massive ROS generated without sufficient antioxidants to suppress. The excessively produced ROS will amplify the decline of molecular fidelity associated with slow tissue repair which may subsequently slows down the basic cell development of larvae[82,172,173]. However, neither H_2-O_2 gas mixture nor Brown's gas showed the side effects of high O_2 concentration on larvae fin-growth, instead exhibited a significantly higher growth rate compared to the control (O_2-levelled).

The third measuring parameter in this study is to determine the neutrophil count at fin-amputated site. Neutrophils are produced by the caudal hematopoietic tissue (CHT) together with macrophages in 2 dpf larvae [174]. Neutrophils are highly motile phagocytic cells that play a critical role in the immune response and wound healing. Since the adaptive immunity cells (T-cells and B-cells) are not mature until 4 to 6 weeks post-fertilization, therefore the inflammation and wound healing occurring in zebrafish larvae is due to respondent of neutrophils and macrophages only, without the influence from adaptive immunity cells[137,138]. On top of that, neutrophils are often the first responders infiltrate the damaged tissue before the arrival of macrophages[174]. Following fin-amputation, neutrophils migrate to their site of action along a chemical gradient of chemokines released by infectious agents or other inflammatory cells[132,175,176]. Neutrophils contain cytoplasmic granules containing numerous proteolytic and hydrolytic enzymes to eliminate the dead cells in internal vacuoles called phagosomes as a part of the wound healing response[163,167]. Therefore, the neutrophils accumulate at the injured site to remove dead cells and allow rejuvenation of tissues by regeneration of new cells.

During neutrophil phagocytosis activity, neutrophils are shown to consume large amounts of O_2 and further strongly activate NADPH oxidase (NOX2) activity[173]. NOX2 assembles in the membrane of neutrophils and catalyses the reduction of O_2 to $\cdot O_2^-$ radicals. Superoxide dismutase (SOD), the antioxidant protein catalyses the dismutation of $\cdot O_2^-$ to H_2O_2, which is subsequently detoxified to O_2 and water by catalase (CAT) or glutathione peroxidase (GPx)[87,177]. An excess of H_2O_2 degrades methaemoglobin to release iron ions that are possible to react with H_2O_2 to form an aggressive radical species $OH\cdot$[37,39,77]. Although neutrophils play an important role in the tissue repair process, they also generate ROS and secrete proteases, which could degrade the extracellular matrix (ECM) and exacerbate the post-injury inflammatory response[176,178,179] which may delay the re-epithelization and tissue regeneration of amputated-fin of zebrafish larvae. For this reason, timely neutrophil clearance is crucial to prevent further tissue damage[164,180]. Excessive activation or ineffectual clearance can lead to cell lysis and tissue damage[164].

Air, N_2 and H_2 treated larvae are observed to start to induce neutrophil infiltration within 30 minutes upon amputation. In general, a massive number of neutrophil accumulations were observed at the amputated site within 3 hpa. Eventually, the recruited neutrophils were expected to undergo apoptosis or retrograde back into the vascular system therefore the number of neutrophils is observed to decrease from 3 hpa to 24 hpa and, almost disappear by 48 hpa[175]. Meanwhile, the H_2 treated larvae showed 18.0% and 30.5% lower number of neutrophils accumulation compared to air and N_2 treated larvae, respectively, at 3 hpa observation. This trend of neutrophil infiltration is consistent also at 48 hpa where, the H_2 treated larvae showed 29.3% and 43.4% lower number of neutrophil accumulation compared to air and N_2 treated larvae, respectively (Fig. 35). The neutrophil count statistical analysis showed H_2 has significantly lower number of neutrophil recruitments at 3 and 48 hpa compared to in N_2 treated larvae. Meanwhile, comparing the H_2-O_2 gas mixture and Brown's gas with their compatible controls (air and O_2-levelled condition) also showed 23-27% lower number of neutrophil infiltrations at 48 hpa compared to the controls on average though unable to confirm with statistical difference.

The low neutrophil count in H_2 or H_2/O_2 treated larvae indicates the possibility that, molecular H_2 absorbed through the zebrafish larvae skin further into the systemic circulation, cells and organelles may have neutralised the $OH\cdot$ produced as a part of the phagocytosis process. This mode of action may inhibit from further oxidative stress damage at the amputated site as described by Ohsawa et. al.[7]. Inhibiting oxidative damage by combating the $OH\cdot$ radicals also might inhibit a massive infiltration of neutrophils to the amputated-site. Inhibiting the recruitment of neutrophils may shorten the tissue repair mechanism by not provoking pro-

inflammatory mechanism. A rapid tissue repair may induce a dynamic tissue regeneration which accelerates new tissue formation and restructure the amputated-fin morphology.

In a nutshell, vertebrates generate ROS in both low (hypoxic) and high O_2 (hyperoxic) condition. The ROS generation could be one the reason for the zebrafish larvae growth retardation such as in the N_2-treated condition or O_2-levelled treated condition. However, the H_2 exposed larvae were not prone to growth retardation regardless of O_2 proportion in the medium. This indicates that most probably, the exposure of the larvae to either low or high content of O_2 level in combination with a certain proportion of H_2 concentration could be able to balance the redox potential of the metabolic oxidation in mitochondria without exhibiting any side effects. The regulation of reducing and oxidising agents such as molecular H_2 and O_2, could influences the oxidation-reduction potential which is crucial to maintain a balance redox homeostasis[79]. Imbalance of redox potential intracellularly may exhibit high production of ROS. Although ROS beneficially participate in various cellular signaling pathways but excessive ROS undeniably induce severe cell oxidative damage in animals. The intracellular ROS levels are dependent on the dynamic balance between ROS generation and elimination which seemed to be beneficially moderated by molecular H_2.

4.2   Electromagnetic field radiation effects on tissue development and regeneration of zebrafish embryo

In this research study, I also examined if EMF treatment contributes to any beneficial effects to zebrafish larvae. Initially, EMF generating Tesla oscillator device was used as an alternative modality to split the water molecules into H_2 and O_2 *in situ*[28,29] where the generated molecules were expected to influence the growth factor of the zebrafish larvae. The presence of the dissociated molecular H_2 and O_2 were measured upon EMF radiation by colourimetric assay (methylene blue kit) and O_2 electrode sensor, respectively, as described by Maehara et. al.[130]. The analysis of EMF treated medium showed a negative result, I unable to detect any difference in H_2 and O_2 concentration compared to the EMF treated and untreated medium. Therefore, in this research, not able to determine if the 144 MHz Tesla oscillator and 5.0 GHz WLAN radiation able to dissociate water into H_2 and O_2. The potential of EMF to split the water molecule was not further examined but the possibility of the 144 MHz EMF wave to influence the growth response by acting as a second messenger was further investigated.

In a larger perception, conventional and alternative medicine have attracted scientists and clinicians to the potential benefits of using EMF for therapeutic purposes however the safety of magnetic and EM fields exposure is still a very sceptical and controversial subject.

Researchers have suggested of using magnetic or EMF waves to influence physiological activity in a beneficial way. In the year 2007, Markov showed pulsed electromagnetic field (PEMF) therapy with a low-frequency electromagnetic signal enable to heal musculoskeletal disorders[108] . In recent 15 years, there were many researchers reported successful treatment of musculoskeletal disorders, lower back pain and bone fracture conditions using EMF stimulation [109–112]. However, none of the research able to explain the cellular level mechanism. In earlier studies, EMF irradiation was shown to regulate gene expression which evolves cellular physiological processes, signal transduction and immune responses[181,182], however, on the other hand, other researchers also reported of insignificant differences in gene expression profiles upon EMF radiation[183,184]. Likewise, publications have proposed EMF indeed promote cell proliferation[148,185,186], whereas others have indicated that EMF exposure inhibits cell proliferation [105,187]. Thus, so far, the potential benefits or hazards of EMF exposure remain unclear, also convincing evidence and consistent results are lacking.

Therefore, to determine the effects of EMF on tissue growth, a commercially available EMF generating device named Tesla oscillator was used. The Tesla oscillator is a "health-promoting" handheld-antenna, generates 144 MHz sinusoidal wave. According to the Tesla oscillator device manual, this handheld-antenna can be used by patients for "self-healing" such as for skin inflammation, limb oedema and lower back pains[120]. The Tesla oscillator device supplier has claimed that the "special" radiation frequency of 144 MHz sine wave is able to beneficially regulate the physiological activity. Hence, investigated if radiation treatment by Tesla oscillator may positively influence the intact caudal fin-fold development, tissue regeneration of amputated-fin and wound healing by quantifying the neutrophil count at tissue amputated site of zebrafish larvae. The zebrafish larvae intact-fin area and amputated-fin area re-growth were measured upon EMF treatment and compared with the untreated larvae which were placed out of the radiation field radius. Since human are exposed to WLAN radiation in daily life for almost 24 hours/day and have the concern of possible side effects from long radiation exposure thus the impact of 5.0 GHz WLAN radiation on zebrafish larvae was also observed in this study.

To analyse the therapeutic effect of EMF, 3 dpf zebrafish larvae were treated by Tesla oscillator radiation-antenna for 30 minutes, twice a day by an hour pause. In the EMF experiment, temperature could be a major reason to manipulate the results. Tesla oscillator which is supplied by 12 V of input energy may amplify the device heat release or could also amplify the radiation intensity[102,119]. The EMF radiation by high intensity may induce extreme molecule collision due to high kinetic energy conversion which may increase the surrounding temperature. The high thermal effect may give a false result, in this study. Therefore, the

temperature fluctuation was handled by increasing the total volume of E3 medium in the container containing the zebrafish larvae. Also, to avoid temperature fluctuation, the duration and frequency of the treatment are minimized. This precaution methods, helped to not increase the temperature of the treated medium more than ~1.5 °C. While WLAN router being supplied by 0.8 V does not receive large input energy therefore the EMF radiation by WLAN possibly generated at lower intensity. Also, an increase of temperature of the WLAN router device itself or increase of the surrounding temperature is not observed upon 5 GHz WLAN radiation. Thus, WLAN treatment was carried out for 3 hours/day without a pause.

The EMF radiation analysis by Tesla oscillator with 144 MHz showed, a delay or retardation in the tissue growth of both intact-fin and amputated-fin larvae on average. The Tesla oscillator treated intact-larvae grow 33.2% and 32.5% significantly slower than untreated and WLAN treated larvae, respectively (Fig. 41). Meanwhile, the fin-amputated larvae treated with Tesla oscillator grow 12.7% and 13.2% slower on average than untreated and WLAN treated larvae (Fig. 42). However, a statistically significant difference for Tesla oscillator treatment was only seen in intact-fin growth analysis. The EMF radiation with 5 GHz WLAN does not show any obvious difference in growth assays neither for intact-fin nor for amputated-fin growth compared to the untreated zebrafish larvae.

Further analysis of neutrophil count showed that Tesla oscillator treated larvae have 39.0%, 21.4% and 21.3% more neutrophil count on average on 3, 24 and 48 hpa, respectively, compared to untreated larvae. However, statistically, there is no significant difference in the neutrophil count upon Tesla oscillator radiation compared to untreated larvae in the 24 and 48 hpa. WLAN radiation did not show any obvious difference in the neutrophil count analysis compared to the untreated larvae.

The 144 MHz frequency wave generated by the Tesla Oscillator lies in the radio frequency range while the WLAN radiation frequency of 5.0 GHz lies in the microwave radiation range however, the strength of the energy transmitter may manipulate the intensity of the radiation. The Tesla oscillator with 12 V energy transmission is higher amplitude compared to 0.8 V received by WLAN hence, Tesla oscillator may imply more intense radiation which may cause deteriorating effects to zebrafish larvae compared to those larvae treated by WLAN radiation.

The growth retardation upon radiation by Tesla oscillator (144 MHz) may be due to ROS production and possibly have induced oxidative stress damage. Generally, the exposure to EMF has been claimed to cause an increase in free radical production in the cellular environment by researchers[75]. Xu et al. have shown that RF-EMF induced DNA damage in

hamster lung cells and Human skin fibroblasts (HSFs) cell culture, who also indicated of a slight increase in cellular ROS level in the affected cells[188]. According to Schuermann et. al., EMF impairs the antioxidant defence mechanisms by causing overproduction of ROS, resulting in oxidative stress damage[189]. According to Maehara et al. and a few more researchers, RF radiation of 13.56 MHz initiates water dissociation which is expected to produce radicals such as $\cdot OH$ and $\cdot O_2^-$ [28,29,126,128–130]. Therefore, if 144 MHz frequency radiation by Tesla oscillator may have dissociated water into aggressive radicals such as $\cdot OH$ hence, could be a reason to stimulate oxidative stress damage in zebrafish larvae. The production of aggressive $\cdot OH$ may subsequently retards the tissue proliferation in intact-fin and tissue regeneration of amputated-fin. Apart from the growth factor, massive production of ROS such as $\cdot O_2^-$ and H_2O_2, due to radiation could involve in signaling cascade to recruit a large number of neutrophils to the injured site as what have been observed in Tesla oscillator treated larvae (Fig. 43).

The Tesla oscillator which claimed to provide health beneficial effect by the device supplier is not true based on the fin-growth analysis on zebrafish larvae. However, a different radiation frequency with controlled input energy and radiation intensity may reflect a different impact on zebrafish larvae. In addition, this radiation treatment was only given for 3 consecutive days from 3-5 dpf zebrafish larvae hence insufficient time was given to zebrafish larvae to adapt to EMF radiation treatment. Therefore, in this study also expected the retardation of tissue growth may be due to the radiation cell shock counteracts which could lead to cell cycle arrest. Overall, it is been confirmed that the 144 MHz radiation by the Tesla oscillator did not show a beneficial effect either on tissue development or tissue regeneration. There is no negative effect of WLAN radiation was observed, at least in the short-investigated time frame.

4.3 Hydrogen gas treatment effects on cell growth of *Chlorella vulgaris*

Chlorella vulgaris species is a fast-differentiating, photosynthetic, unicellular green microalga which is used as a model organism to understand the beneficial effects of the molecular H_2 on photosynthetic plants. The beneficial effect of molecular H_2 on *C. vulgaris* was evaluated based on the cell growth rate. The cell growth rate was determined by measuring the cell density at maximum absorbance of 750nm. The wavelength of 750nm is out of chlorophyll's light absorption spectra, this assures that the cell density of *C. vulgaris* culture measurement is not influenced by the colour intensity of chlorophylls. Initially, *C. vulgaris* culture was bubbled by H_2 gas directly for 30 minutes twice/day. The effects of molecular H_2 are compared with other directly bubbled gas including air ($N_2 + O_2$), N_2, O_2, H_2-O_2 gas mixture, Brown's gas treated and a pair of untreated *C. vulgaris* culture.

The direct-gas treatment method shows that the air treated *C. vulgaris* cell density is higher than H_2, N_2, O_2, H_2-O_2 gas mixture, Brown's gas and untreated culture by 23%, 17%, 36%, 23%, 21% and 28%. Although the air treated medium and untreated medium has almost similar dissolved O_2 concentration but the untreated *C. vulgaris* culture showed growth retardation. This is because microalgae generally differentiate faster with an additional bubbling effect for example microalgae on shaker will grow faster with additional agitation compared to those in a stagnant medium[190,191]. Since in the direct treatment condition the air treated culture experience agitation twice a day for 30 minutes compared to the untreated culture therefore the air bubbled culture grow faster than the untreated culture. This fast-growing effect in air treated conditions, opens the possibility that the positive effects of molecular H_2 are not able to be seen in directly bubbled culture due to the overlay effect of cell culture agitation.

Since a positive effect of H_2 treatment is not seen on *C. vulgaris* culture by direct-gas bubbling method therefore, a new treatment method was implemented on *C. vulgaris* cells to rule out the agitation effect. The *C. vulgaris* cells were centrifuged at a lower speed (4500 rpm) for a shorter time (5 mins) to separate the *C. vulgaris* cells from the medium. The separated medium was bubbled with respective gases prior to mixing the bubbled medium with *C. vulgaris* cells. The pre-treatment of BBM medium aid to see if molecular H_2 enhance the *C. vulgaris* growth rate without an overlay of agitation effect. Nevertheless, the air treated and untreated *C. vulgaris* have higher cell density compared to H_2, N_2, O_2, H_2-O_2 gas mixture and Brown's gas treated *C. vulgaris* culture. Meanwhile, the H_2, N_2, H_2-O_2 gas mixture and Brown's gas treated *C. vulgaris* have almost similar cell density. The H_2 treated *C. vulgaris* cells culture also did not show any beneficial effects on the chlorophyll, protein and starch production. This shows molecular H_2 as well as other combinations of dissolved H_2 and O_2 do not bring any benefits to the *C. vulgaris* cell growth.

4.4 Electromagnetic field radiation effects on cell growth of *Chlorella vulgaris*

In order to conduct an investigation of EMF effects, plants seemed to be more sensitive and reliable compared to animals. In this study, treatment was given consistently for 28 days to *C. vulgaris* cell culture compared to zebrafish larvae were only treated for 3 days. The advantage of EMF treatment on plants including microalgae is being immobile while treating which keeps a constant orientation in the EMF. Also, the unicellular *C. vulgaris* is spherical in shape, about 2 -10 µm diameter size has a high surface area exposed to the ratio of EMF. Besides that, there is a high possibility for the EMF waves to penetrate the thin cell wall of *C. vulgaris* to efficiently affect intercellularly[192]

The EMF treatment examination was carried out with Tesla oscillator radiating 144 MHz for 30 minutes, twice a day. While, another set of *C. vulgaris* cell culture was exposed to 5.0 GHz of WLAN radiation for 3 hours continuously per day. In this research study, the 144 MHz radio frequency radiation at higher input energy (12 V), is expected to cause more intense radiation and induce aggressive oxidative stress compared to 5.0 GHz WLAN with lower input energy (0.8 V). Further to elude the thermal effects, a large volume of cell culture of 120 mL was used to avoid temperature shoot-up during radiation treatment thus, an increase of temperature not more than ~1.5 °C was maintained.

Tkalec et al. and a few other researchers, indeed have reported that plants involve in molecular responses to EMF of even a small amplitude and reflected by alterations of their developmental system[192–198] however the molecular level mechanisms are unknown. EMF radiation is expected to interfere with intercellular signals that coordinate cell growth and cell division however, the EMF radiated *C. vulgaris* culture did not show an obvious growth difference compared to untreated *C. vulgaris* cell culture. The cell density measurement at OD_{750} and, chlorophyll measurement at OD_{665} and OD_{652} did not show much difference between EMF treated and untreated. Plant growth inhibition due to EMF exposure from a range of 400 MHz to 900 MHz[195,197], as well as 2.0 - 2.5 GHz WLAN/cell phone radiation[196,199–203], has been reported in multicellular plants and seedlings such as *Myriophyllum aquaticum*, duckweed, mung bean, wheat and maize by researchers. However, in this study, growth retardation was not observed in *C. vulgaris* cell culture at 144 MHz Tesla or 5.0 GHz WLAN radiation.

Meanwhile, the quantification of protein and starch showed that EMF treated *C. vulgaris* cell culture, either by Tesla oscillator or WLAN radiation both showed a lower bioactive compound content compared to untreated *C. vulgaris* cell culture. The protein content analysis by OD_{590}/OD_{450} upon long consecutive days of radiation showed protein reduction by 21.6% and 17.1% for Tesla oscillator and WLAN radiated culture, respectively, compared to untreated *C. vulgaris* culture. Although the cell density and chlorophyll content are not affected but the quantification of protein showed a sign of protein deterioration in radiation-exposed *C. vulgaris* culture. The quantification of starch of Tesla oscillator and WLAN radiated culture is 38.0% and 33.4% lower than untreated *C. vulgaris* culture, respectively. Tesla oscillator generated radiation at 144 MHz wave frequency with higher input energy may increase the radiation intensity and severely affected the starch production or deteriorated the stored starch due to 28 days of long-term radiation exposure. Meanwhile, the WLAN radiation at 5 GHz with lower input energy is also seen affected the starch content in the *C. vulgaris* culture cell. This shows that radiation including a lower amplitude could easily affect the protein and starch content in *C. vulgaris* cell culture.

The slight reduction of protein and starch measured in *C. vulgaris* cell upon Tesla oscillator and WLAN radiation, in my study could be due to the ROS activity. EMF exposure is known to alter the activity of several antioxidant enzymes such as peroxidase (GPx), catalase (CAT) and superoxide dismutase (SOD), including elevated ROS metabolism[204] that increases the production of $\cdot O_2^-$ and H_2O_2 radicals[194,204]. According to Halgamuge et al., the EMF radiation is expected to modify the development of plants[205] since EMF radiation could lead to ROS induced lipid peroxidation hence alter the cell membrane[194,204,206]. This ROS activity could eventually manipulate the bioactive content including protein and starch. ROS activity is also interrelated with protein damage in plant cells[196,207,208], however, a decrease in protein content may result from an increase in protein degradation or due to a decrease in protein synthesis which is indefinite. Meanwhile, starch content depletion upon exposure to 900 MHz EMF has been reported by Kumar et al. and Kouzmanova et al. [209,210]. Kumar et al. have further suggested that starch content depletion could be due to inhibition of the Krebs cycle and pentose phosphate pathway (PPP) where the starch formation is being interfered negatively upon exposure to radiation[210].

5. SUMMARY

In this study, the beneficial effects of molecular hydrogen (H_2) and electromagnetic field (EMF) stimulation have been analysed and demonstrated by observing the influence on the regular tissue development of intact-fin and tissue regeneration of amputated-fin of zebrafish larvae using neutrophil expressed transgenic line Tg(*lyzC*:DsRed). Zebrafish larva is a perfect model to study tissue regeneration since the caudal-fin fold is easily accessible and its ability to rapidly regenerate the fin via wound healing responses without causing a detrimental effect on the organism. Furthermore, the tissue repair responses by neutrophils in zebrafish larva can be monitored via *in vivo* imaging. The beneficial effect of molecular H_2 is also investigated on *Chlorella vulgaris*. *C. vulgaris* species is a fast-differentiating, photosynthetic, unicellular green microalga. The beneficial effect on *C. vulgaris* cell is determined based the cell density and bioactive compounds quantification.

The pre-treatment of medium with pure H_2 generated by PEM water electrolysis system saturates ~1.0 mM (1.6 - 2.0 mg/L) of H_2 enriched medium. The H_2 treated larvae have 29.0% and 43.0% of higher tissue growth of intact-fin meanwhile 21.0% and 38.0% of higher tissue regeneration of amputated-fin compared to air and N_2 treated larvae, respectively, on average. The neutrophil count at the fin-amputated site of zebrafish larvae has shown that molecular H_2 treated larvae have significantly lower neutrophil count at 3 and 48 hpa compared to the control (N_2-treated). In this study, further confirmed that H_2 generated together with O_2 by PEM water electrolysis system saturates the medium by 0.4 mM (0.8 mg/L). The H_2-O_2 gas mixture treated larvae showed significantly higher intact-fin development and amputated-fin regeneration compared to the control (O_2-levelled). Meanwhile, Brown's gas generated by an alkaline water electrolysis system with intercalated electrodes which is claimed to have "magical" components and "special" beneficial health effects by the researchers[93–95], has similar H_2 and O_2 proportion as H_2-O_2 gas mixture. The Brown's gas treated larvae also showed significantly higher intact-fin development and amputated-fin regeneration compared to the control (O_2-levelled). However, the beneficial health response stimulated by the Brown's gas is most probably due to the presence of 0.4 mM of dissolved H_2 in the Brown's gas enriched medium.

In other respect, the EMF radiation was expected to dissociate water into H_2 and O_2 but this is not able to be determined. Nevertheless, Tesla oscillator with 144 MHz EMF indeed regulated the growth response negatively, in zebrafish larvae. The Tesla oscillator causes tissue growth retardation in both intact-fin and amputated-fin of zebrafish larvae. The Tesla oscillator radiation exposed intact-fin and amputated-fin grow 33.2% and 12.7% slower on average

compared to the untreated larvae, respectively. The Tesla oscillator treatment also induced a constantly higher number of neutrophils on 3, 24 and 48 hpa larvae compared to the controls on average. Meanwhile, WLAN radiation does not show any impact on larvae.

On the other hand, the molecular H_2 as well as H_2-O_2 gas mixture and Brown's gas, do not bring any benefits to the *C. vulgaris* cell growth density or to the quantification of bioactive compounds such as chlorophyll, protein and starch. While the EMF treatment for 28 days on *C. vulgaris* cell culture showed an obvious negative result. Even though the cell density and chlorophyll content were not affected but the quantification of protein is reduced by 21.6% and 17.1% for Tesla oscillator and WLAN radiation exposed culture compared to the untreated *C. vulgaris* cell culture, respectively. Meanwhile, the quantification of starch of Tesla oscillator and WLAN radiation exposed culture were 38.0% and 33.37% lower than untreated *C. vulgaris* culture, respectively.

6.　Materials

6.1　Devices and measuring instruments

Autoclave	VX-95 (Systec GmbH)
	2540 EL (Systec GmbH)
Bunsen burner	Schütt Flammy S (Schütt Labortechnik GmbH)
Centrifuge rotors	JA-14 (Beckmann Coulter GmbH)
	19776-H (Sigma-Aldrich GmbH)
Centrifuges	Biofuge fresco (Heraeus Instruments)
	Sigma 3-18k (Sigma-Aldrich GmbH)
	MiniSpin plus (Eppendorf AG AG)
Clean bench	Herasafe 12 (Heraeus Instruments GmbH)
Electrolyser	PEM electrolyser H2/O2 65 PHYWE (Prof. Posten Clemens)
	AquaVolta® Nafion 117 - H2 generator 300 mL/min (Yasin Akgün)
	AquaVolta® - H2 generator 600 mL/min (Yasin Akgün)
	Aquacure-Brown's gas (George Wiseman)
	Recure-Brown's gas (Jürgen Jansen)
	Abgas engel-Brown's gas (Hans J. Wochian)
French pressure cell press	SLM-Aminco Instruments FA-078
Heat block	HB-2 (Wealtec Corporation)
	SBH200D (Stuart)
Ice machine	EF 103 easy-fit (Scotsman Ice Systems)
Illuminator	KIT Inhouse manufactured (a.k.a Prof. Posten Clemens)
Incubator	Incucell (MMM Medcenter Einrichtungen GmbH)
Lyophiliser	Alpha 1-4 LSC (Martin Christ GmbH)
	Alpha 2-4 LD (Martin Christ GmbH)
Magnetic stirrer with hotplate	IKAMAG RCT (IKA-Werke GmbH)
Microscopes:	
Light microscope	Axioskop 40
Fluorescence microscope	Leica DFC7000 T
Zoom stereomicroscope	Nikon SMZ 645
Microwave	M1712N (Samsung)
ORP sensor	SenTix ORP redox electrode (Ag/AgCl) (WTW GmbH)
Oscilloscope	Agilent/HP/Keysight 54835A Infiniium 1GHz 4GSA/S
Galvanic oxygen sensor	CellOx 325 (WTW GmbH)
pH electrode	SenTix 41 with temperature sensor (WTW GmbH)
Pipette:	
0.5-10 µL, 2-20 µL, 10-100 µL,	Reference (Eppendorf AG)
50-200 µL, 100-1000 µL,	Reference (Eppendorf AG)
Pipette: 1-5 mL	Finnpipette (Thermo Scientific)
Radiation device	Tesla oscillator 144 MHz (Bernard Pietsch)
Scales	PB3001 (Mettler Toledo GmbH)
	Kern PLJ-G (Kern & Sohn GmbH)
	CP64 (Sartorius Mechatronics AG)

	M2P (Sartorius Mechatronics AG)
Shaker	Heidolph Unimax 1010
	VWR Standard Orbital Shaker 5000
Spectrophotometer:	
UV-Vis Spectrometer	Ultrospec 6000
UV-Vis Spectrophotometer	SmartSpec 300 Plus (BioRad)
Tecan - Plate Reader	Spark Cyto
Ultra-pure water system	Milli-Q (Merck Millipore)
Universal meter	WTW MultiLine P4
	WTW pH 315i
Vortex	Genie K-550-GE (Bender und Hobein AG)
Water bath	SC100 (Thermo Fisher Scientific Inc.)
WLAN router	AC 1900 Dual Band 802.11ac Gigabit Router (ASUS)

6.2 Consumables

Aluminium foil	Carl Roth GmbH
Cover slip glass (7.5mm x 12mm x 0.06mm)	Marienfeld GmbH
Disposal nitrile gloves	LLG Labware
Disposal cuvette	Sarstedt AG & Co
Falcon-Tubes (Centrifuge tubes: 15 ml, 50 ml)	Sarstedt AG & Co
Meliseptol® rapid	B. Braun Melsungen AG
Microplate, 24-Well, sterile	VWR GmbH
Microscopic non-adhesion slides (76mm x 26mm x 1mm)	Thermo Fisher Scientific Inc.
Microscopic adhesion slides - SuperFrost Plus (76mm x 26mm x 1mm)	Thermo Fisher Scientific Inc.
Parafilm	Bemis Company Inc.
Pasteur-Pipetten	VWR GmbH
Petridish	Greiner Bio-One GmbH
Pipette tips (10 µl, 200 µl, 1000 µl)	Sarstedt AG & Co
Pipette tip (5 ml)	Thermo Fisher Scientific Inc.
Precision wipes Kimtech Science	Kimberly-Clark
Quartz Cuvette (10 mm)	Hellma® Analytics
Reaction tubes (0,5 ml, 1,5 ml, 2 ml)	Eppendorf AG
Reaction tubes with safe-lock (0,5 ml, 1,5 ml, 2 ml)	Eppendorf AG
Universal indicator-paper (pH 1-14)	Carl Roth GmbH
Weighing paper MN 226	Macherey-Nagel
Weighing pans	Carl Roth GmbH

6.3   Chemicals

Anthrone powder	Carl Roth GmbH
Boric acid	Carl Roth GmbH
Bovine serum albumin	Sigma-Aldrich GmbH
Calcium chloride dihydrate	Appli Chem
Cobaltous nitrate hexahydrate	Carl Roth GmbH
Copper sulfate pentahydrate	Carl Roth GmbH
Dipotassium hydrogen phosphate	Carl Roth GmbH
EDTA dipotassium dihydrate	Carl Roth GmbH
Ethanol	Fisher Scientific
Ferrous sulphate heptahydrate	Sigma-Aldrich GmbH
HEPES (4-(2-hydroxyethyl)-1-piperazineethanesulfonic acid)	Sigma-Aldrich GmbH
Low melting agarose gel	Sigma-Aldrich GmbH
Magnesium sulphate	Carl Roth GmbH
Magnesium sulphate-Heptahydrate	Merck
Manganese (II) chloride tetrahydrate	Carl Roth GmbH
Methanol	Actu-All Chemicals
Methylene blue-platinum reagent	Aquacentrum
Potassium chloride	Carl Roth GmbH
Potassium dihydrogen phosphate	Carl Roth GmbH
Potassium hydroxide	Carl Roth GmbH
ROTI®Nanoquant	Carl Roth GmbH
Sodium chloride	Carl Roth GmbH
Sodium molybdate dihydrate	Carl Roth GmbH
Sodium nitrate	Carl Roth GmbH
Starch powder	Carl Roth GmbH
Sulphuric acid 95%	KIT chemicals
Tricaine methanesulphonate (TMS222)	Sigma-Aldrich GmbH
Zinc sulphate heptahydrate	Carl Roth GmbH

6.4 Culture medium and solution

Bold's Basal Medium (BBM)	Content
$NaNO_3$	2.94 mM
$MgSO_4•7H_2O$	0.30 mM
$CaCl_2•2H_2O$	0.17 mM
NaCl	0.43 mM
K_2HPO_4	0.43 mM
KH_2PO_4	1.29 mM
$K_2EDTA.2H_2O$	0.17 mM
H_3BO_3	0.19 mM
$ZnSO_4.7H_2O$	0.03 mM
$MnCl_2.4H_2O$	0.007 mM
$FeSO_4.7H_2O$	0.02 mM
$Co(NO_3)_2.6H_2O$	0.002 mM
$CuSO_4.5H_2O$	0.006 mM
$Na_2MoO_4.2H_2O$	0.005 mM
KOH	0.06 mM
H_2SO_4	0.02 mM

Zebrafish embryo (E3) medium	Content
NaCl	5 mM
KCl	0.17 mM
$CaCl_2.2H_2O$	0.33 mM
$MgSO_4$	0.33 mM
1M HEPES (4-(2-hydroxyethyl)-1-piperazineethanesulfonic acid) pH 7.5	2 mM

7.   Methods

7.1   Gas infused medium preparations

Hydrogen Gas (H_2)

H_2 gas is generated by proton exchange membranes (PEM) water electrolysis system with different charge electrodes separated by a membrane to produce pure H_2 separately at the cathode is bubbled into E3 or BBM medium.

Oxygen gas (O_2)

O_2 gas is generated by a PEM water electrolysis system with different charge electrodes separated by a membrane to produce pure O_2 gas separately at the anode is bubbled into E3 or BBM medium.

Hydrogen-oxygen gas mixture (H_2-O_2)

H_2-O_2 gas is generated by a PEM water electrolysis system with different charge electrodes separated by a membrane to produce a 2:1 ratio of pure H_2 to pure O_2 separately. The pure H_2 and pure O_2 bubbled together into E3 or BBM medium until saturation point.

Brown's gas

Brown's gas is a gaseous mixture generated by alkaline water (lye solution) electrolysis system with a modified device with intercalated electrodes that generates a 2:1 ratio of H_2 to O_2 (66% and 33%, respectively) dissolves in the lye solution and is allowed to volatile and to be transferred into a wash bottle containing distilled water via a hose. The H_2 and O_2 are again allowed to be volatile and transferred into a second wash bottle containing distilled water via a hose for a double washing system before bubbled into E3 or BBM medium for experimental purposes. Double washing of H_2 and O_2 gaseous mixture in distilled water is to avoid introducing the lye solution into the experimental setup.

Nitrogen Gas (N_2)

Nitrogen gas is regulated through a gas-compressed cylinder.

Air

An air compressor is used to bubble the medium with ambient atmospheric air at STP.

7.2   Electromagnetic field radiation devices

Tesla Oscillator

This RF-EMF wave radiation antenna has one strong signal with a frequency of 144 MHz which was used to treat the model organisms. A measurement of the radiation frequency of Tesla oscillator with an oscilloscope and Fourier transform confirmed that the Tesla oscillator resonates sine waves at 144 MHz frequency. A borosilicate glass test tube was used as a shield around the antenna to protect the organisms from possible direct electric current or thermal effects. Tesla oscillator power supply AC/DC adaptor 60W; Input/output: AC100-240 V/ DC 12V, 5A. A complete Tesla oscillator set including a handheld-antenna with a power supply was provided by Wassermatrix AG[120].
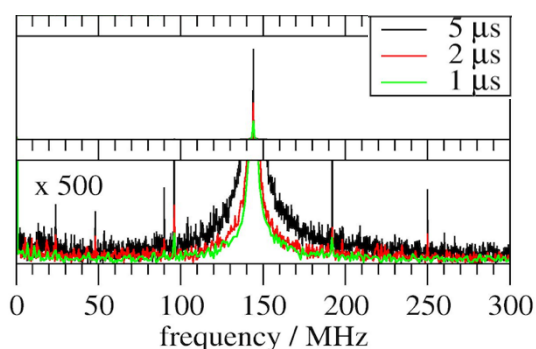
Fig. 61: Frequency of electromagnetic fields radiation device determined. The time traces of the Tesla oscillator radiation, exported from the oscilloscope meter and Fourier Transform analysis confirmed the device has a strong signal at 144 MHz.

Wireless local area networks (WLAN)

The WLAN used in this research is 5.0 GHz radiation signal, operating at a radio-frequency almost similar to mobile phones. In order to establish a wireless network connection between routers with devices like a laptop, computer, printer, digital camera or video projector requires an antenna and a transmitter to transfer data. The most fastest connection network WLANs operate at frequency bands of 5.0 GHz as a pulsed packet waveform. AC 1900 Dual Band 802.11ac Gigabit Router (ASUS) was used to generate the 5 GHz signal.

7.3   Physicochemical property measurement

7.3.1 Determination of the dissolved hydrogen concentration by colourimetric assay

Methylene blue dissolved in an ethanol solvent was used to measure the dissolved H_2 in the treated medium by a redox potential principle. Methylene blue is an oxidizing agent known to react with molecular H_2 in the presence of platinum to produce colourless leucomethylene blue, the reduced form of methylene blue. The titration method of methylene blue (blue) to leucomethylene blue (colourless) with H_2 treated medium was used to determine the concentration of dissolved H_2. One drop (17 mg or 23 µL) of decolourised methylene blue indicates the presence of 0.1 mg/L of dissolved H_2 in the treated medium (distilled water, E3 or BBM). The dissolved H_2 saturation increases maximum 1.6-2.0 mg/L (0.8-1.0 mM) when the medium (distilled water, E3 and BBM) is infused with H_2 gas until the equilibrium.
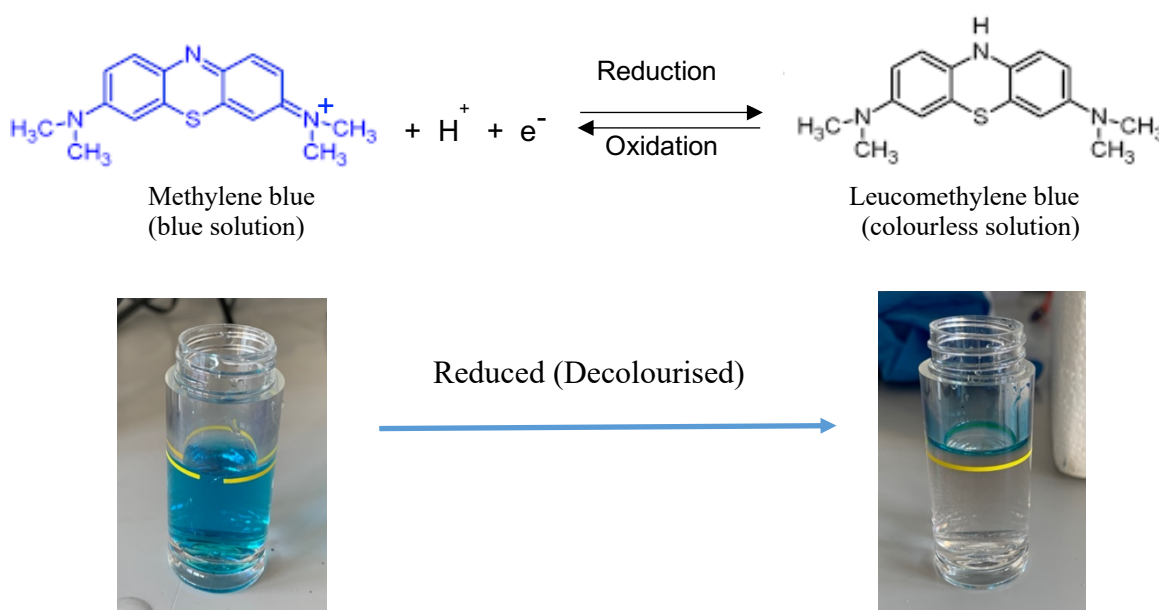
Fig. 62: Methylene blue titrated to leucomethylene blue. The equation above shows a reversible reduction of methylene blue into leucomethylene blue in presence of molecular H_2.

7.3.2 Determination of the dissolved oxygen concentration

The WTW MultiLine P4 universal meter with WTW CellOx 325-3 oxygen sensor was used to measure the dissolved oxygen (DO) concentration in the treated liquid medium. The oxygen sensor gives a reading of distilled water to be ~6.7 mg/L (0.21 mM) at normal atmospheric conditions. The dissolved O_2 saturation increases maximum to ~29 mg/L (0.91 mM) when the medium (distilled water, E3 and BBM) is infused with O_2 gas until the equilibrium.

7.3.3 Determination of the oxidation-reduction potential

The WTW MultiLine P4 universal meter with WTW SenTix oxidation-reduction potential (ORP) combination electrode (platinum electrode, Ag/AgCl system) was used to measure the ORP of the treated medium. The ORP is measured in millivolts (mV) and the higher the dissolved O2 (oxidising agent) present in the medium, the ORP value will become more positive (+Ve) while in the presence of a higher proportion of dissolved H2 (reducing agent) in the medium, the ORP value will become more negative (-Ve).

7.4   Microscopic imaging

7.4.1 Fluorescence microscopy

Zebrafish larvae anaesthetized with tricaine (TMS222) were embedded in 5% low melting agarose gel on adhesion-superfrost plus microscopic slide for direct imaging. The 5% low melting agarose gel holding zebrafish larvae will partially solidify within 3-5 minutes. Images were taken maximum within 10 minutes to avoid the agarose gel from drying out. Larvae fin imaging was performed on a Leica DFC7000 T fluorescence microscope equipped with a x20 objective lens by brightfield microscopic imaging. While the *in vivo* imaging of transgenic larvae Tg(*lyzC***:**DsRed), neutrophils expressed by RFP were monitored at 475-595 nm.

7.4.2 Light microscopy

5 µL of microalgae culture cells were placed on normal microscopic slides and spread the cells to a thin layer using the coverslip to avoid overlay of cells for direct imaging. Brightfield imaging was performed on a Carl Zeiss Axioskop 40 light microscope equipped with a x10 objective lens.

7.5 Zebrafish measuring parameters and treatments

7.5.1 Zebrafish husbandry

In this experimental study, zebrafish larvae Tg(*lyzC*:DsRed) transgenic line of neutrophils expressed by red fluorescent protein (RFP) under lysozyme C promoter drive was used. The adult zebrafish were maintained in dechlorinated tap water at 26.5 - 28 °C in a flow-through system under a 14:10 hours light:dark cycle. A maximum of 50 fish per tank with 3L water while the pH of the system water is checked daily and maintained between pH 6.8-7.5. The fish tank water passes through a UV disinfection filter before being circulated back into the tank to control biological contaminants. The adult fish were fed with brine shrimp (Artemia nauplii) thrice daily. The zebrafish embryos were collected by in-crossing parental stock maintained at the fish facility of Karlsruhe Institute of Technology - European Zebrafish Resource Centre (KIT-EZRC). The male and female adult zebrafish were separated by a net in the late evening, and the separating net will be removed the next day morning to allow mating and egg laying. After the adult female zebrafish laid eggs, the 1 hpf embryos were collected and rinsed with E3 water. The collected embryos were transferred into a 100 x 25 mm petri dish, filled up with an E3 medium. Each petri dish is occupied by 50 -100 embryos/40 mL E3 medium, kept in the incubator for 72 hours at 27-28.5°C until the larvae hatched and became 3-day post-fertilised larva. The unfertilized and dead embryos will be removed and the medium will be changed between the incubation period to avoid medium toxicity. The zebrafish larvae were treated from 3 dpf stage until 5 dpf stage therefore does not require to feed the larvae during the entire experimental period.

7.5.2 Zebrafish fin development assay (intact caudal fin-fold)

The treated intact-larvae were anaesthetized with 0.4 mM Tricaine before mounting with 5% low-melting agarose for immobilization of the specimen. The low-melting agarose was diluted to 5% with distilled water and boiled using microwave oven until the solution become clear

then transferred the liquid agarose into a 2.0 mL reaction tube before being stored in the fridge at 2-5 °C. Pre-warm the agarose to 80 °C on a heating block then cool down to ~42 °C before embedding the larvae into the agarose, as temperature above 43 °C will be detrimental to the larvae. The larva was immobilized on an adhesion microscopic slide by agarose mounting containing 0.3 mM Tricaine for direct imaging. A brightfield image was taken with 20x objective lens using Zeiss Leica DFC7000 T fluorescence microscope at 0.5 hpa, 24 hpa and 48 hpa. ImageJ analysis software tool was used to measure the whole caudal fin-fold area of the whole larvae intact-fin.

7.5.3 Zebrafish fin clipping assay (amputated caudal fin-fold)

The treated larva was anaesthetized with 0.4 mM Tricaine before the caudal fin-fold amputation. The anaesthetized larva was placed on a wet non-adhesion microscopic slide to amputate the caudal fin with a scalpel under a stereomicroscope. The caudal fin of the larva was amputated slightly below the notochord endpoint which is the reference point during the fin area measurement and also to avoid damaging the notochord. The amputated larva was immobilized on an adhesion microscopic slide by mounting with agarose containing 0.3 mM Tricaine for direct imaging. A brightfield image was taken with 20x objective lens using Zeiss Leica DFC7000 T fluorescence microscope at 0.5 hpa, 24 hpa and 48 hpa. ImageJ analysis software tool was used to measure the re-growing caudal fin area of the amputated-fin. The increases of the area size below the notochord reference-line at every 24 hours intervals will determine the growth rate of the amputated caudal fin.

7.5.4 Zebrafish neutrophil count assay

In this experimental study, zebrafish larvae Tg(*lyzC*:DsRed) transgenic line of neutrophils expressed by red fluorescent protein (RFP) under lysozyme C promoter drive was used to assess the injury response by neutrophils. The neutrophil infiltration to the amputated site upon amputation from 0.5, 3, 24 and 48 hours post-amputation was quantified to determine the correlation of the recovery rate of the injured tissue. The amputated-fin imaging together with RFP expressed neutrophil cell was taken in combination of brightfield and fluorescence light at 475-595 nm by Zeiss Leica DFC7000 T fluorescence microscope. ImageJ analysis software tool was used to quantify the neutrophils within the range of 200 μm above the larvae fin cut-line. The larvae fin re-growth rate of the amputated-fin was correlated with the neutrophil count to understand the influence of treatment on the tissue repair process.

7.5.5 Zebrafish larvae gas treatment

The E3 medium is pre-treated with gas prior to incubate the larvae. The comparable conditions were categorised into a few combination setups based on the physicochemical properties of each treated E3 medium at equilibrium conditions. The O_2-levelled condition is upon standardising the O_2 level according to the 2:1 ratio of H_2 to O_2 bubbled condition meanwhile O_2-saturated condition is O_2 infused into the E3 medium until reaches an equilibrium condition. The Untreated, air-treated, N_2-treated and O_2-levelled conditions are the comparable controls to rule out the side effects from medium pre-agitation, also to rule out too low and too high O_2 composition conditions.

The 3 dpf stage larvae were separated into two groups which are unamputated and amputated to observe the tissue development of intact-fin and tissue re-growth rate of amputated-fin of zebrafish larvae. The 3 dpf stage larvae were treated by incubating in gas infused medium for 3 hours on Day 1 before fin amputation and imaging, then on Day 2 and Day 3 at the age of 4 dpf and 5 dpf, respectively were incubated in gas infused E3 medium before imaging. The larvae were expected to absorb the dissolved gases in the medium by a trans-cutaneous gas exchange therefore 80 mL of E3 medium was bubbled with respective gases for 20 minutes until the medium reach the maximum saturation condition prior to incubating the larvae. In the H_2-O_2 gas mixture setup, the O_2-levelled (control) medium was prepared by bubbling the 80 mL of E3 medium with pure O_2 for 105 seconds. 40 mL of gas infused E3 medium were transferred into 2 sets of 100 X 25 mm petri dish containing 15 larvae in each set. The infused gas tends to be volatile 40-60% within 30 minutes from the treated E3 medium therefore the larvae were incubated into freshly gas infused E3 medium every 30 minutes for 6 times continuously to maintain the concentration of infused gas in the E3 medium at a relatively high level. In order to be consistent, the E3 medium of untreated larvae was also replaced accordingly with a fresh E3 medium. The treated larvae both amputated and unamputated larvae will be mounted with 5% low-melting agarose to immobilise the larvae on an adhesion microscopic slide prior to imaging on Day 1. The larvae will also be incubated in a gas-infused E3 medium for 3 hours prior to mounting with agarose on Day 2 and Day 3. The larvae will be extracted from the agarose gel and transferred into a petri dish containing untreated fresh E3 medium upon imaging on Day 1 and Day 2. The petri dish was kept in an incubator overnight at a temperature of 27.5-28 °C. On Day 3, the imaged larvae will be euthanised.

Day 1

| Respective gas infused into E3 medium for 20 mins | Larvae incubated in freshly gas infused E3 medium for 30 mins, 6 times in a row | Two group of larvae prepared: Unamputated & Anesthetized and amputated |

| Extracted from agarose and incubated at 28°C overnight in untreated E3 medium | Imaging | Anesthetized and mounted |

Day 2 & Day 3

| Respective gas infused into E3 medium for 20 mins | Larvae incubated in freshly gas infused E3 medium for 30 mins, 6 times in a row | Anesthetized and mounted |

| Extracted and incubated at 28°C overnight in untreated E3 medium on Day 2. Euthanised on Day 3 | Imaging |
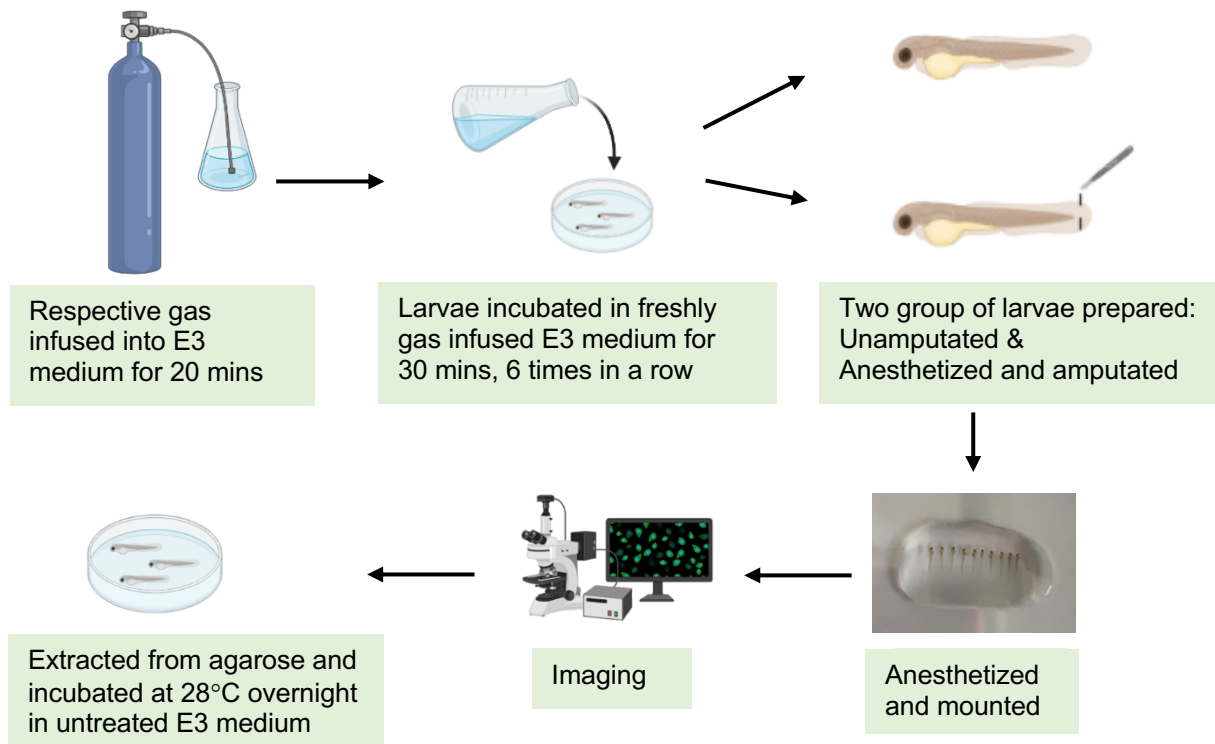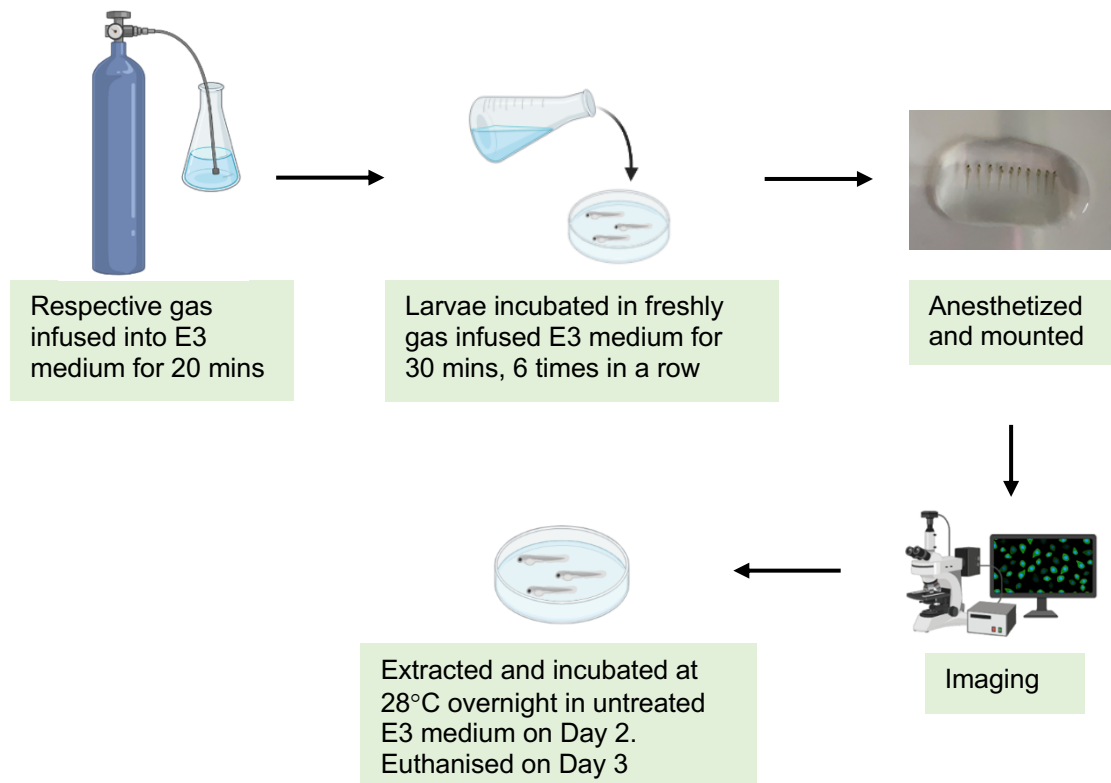
Fig. 63: Flow chart of larvae treatment by gas diffusion.
The 3 day post-fertilised larvae were treated by gas infused E3 medium prior to amputation, mounting and imaging from day 1-3. The larvae were euthanized after imaging on Day 3. Image created using BioRender.com.

7.5.6 Zebrafish larvae electromagnetic fields radiation treatment

The 3 dpf stage larvae were separated into two groups which are unamputated and amputated to observe the tissue development of intact-fin and tissue re-growth rate of amputated-fin of zebrafish larvae. The 3 dpf stage larvae were radiated for 30 minutes twice with an hour interval period to avoid temperature shoot-up of the E3 medium which may cause thermal shock. The 3 dpf larvae were exposed to EMF on Day 1 before amputation and imaging, then on Day 2 and Day 3 at the age of 4 dpf and 5 dpf, respectively, were exposed to EMF radiation before imaging. A 100 mL flask, fully filled with approximately 120 mL E3 medium to completely immerse the Tesla oscillator handheld-antenna into the medium to achieve equilibrium and also to avoid the E3 medium temperature from increasing. 15 larvae were transferred into each conical flask. The Tesla oscillator antenna was covered by a 17 mL thin-wall borosilicate test tube which was used as a shield to protect the larvae from possible direct electric current or thermal shock. The oscilloscope sensor has confirmed that the EMF waves radiated by the Tesla oscillator do travel through the borosilicate test tube and liquid medium to reach the larvae. The temperature of the E3 medium in 100 mL flasks with larvae was monitored during the Tesla oscillator radiation treatment and confirmed the temperature of the E3 medium does not elevate more than 1.0 °C. The WLAN radiation setup also used the same procedure where 100 mL flasks filled with 120 mL E3 medium were placed next to the WLAN router which transferring the signal to a handphone that was kept in the next room. The WLAN radiation is expected to be more intense when the signal receiving device is located further away. The WLAN radiation treatment was carried out for 3 hours continuously on day 1, day 2 and day 3 because WLAN is expected to radiate low intense radiation due to lower energy input, also WLAN radiation does not influence the temperature of the E3 medium in the flask. The untreated larvae were also incubated in a 100 mL flask containing 120 mL E3 medium for 2 hours in total before being mounted with agarose. The untreated larvae were kept in a separate room to avoid the influence of the Tesla oscillator and WLAN radiation effect. The larvae samples will be mounted with 5% low-melting agarose to immobilise the larvae on an adhesion microscopic slide prior to imaging on day 1 to day 3. The larvae will be extracted from the agarose gel and transferred into a petri dish containing untreated fresh E3 medium upon imaging on Day 1 and Day 2. The petri dish was kept in an incubator overnight at a temperature of 27.5-28 °C. On Day 3, the imaged larvae will be euthanised.
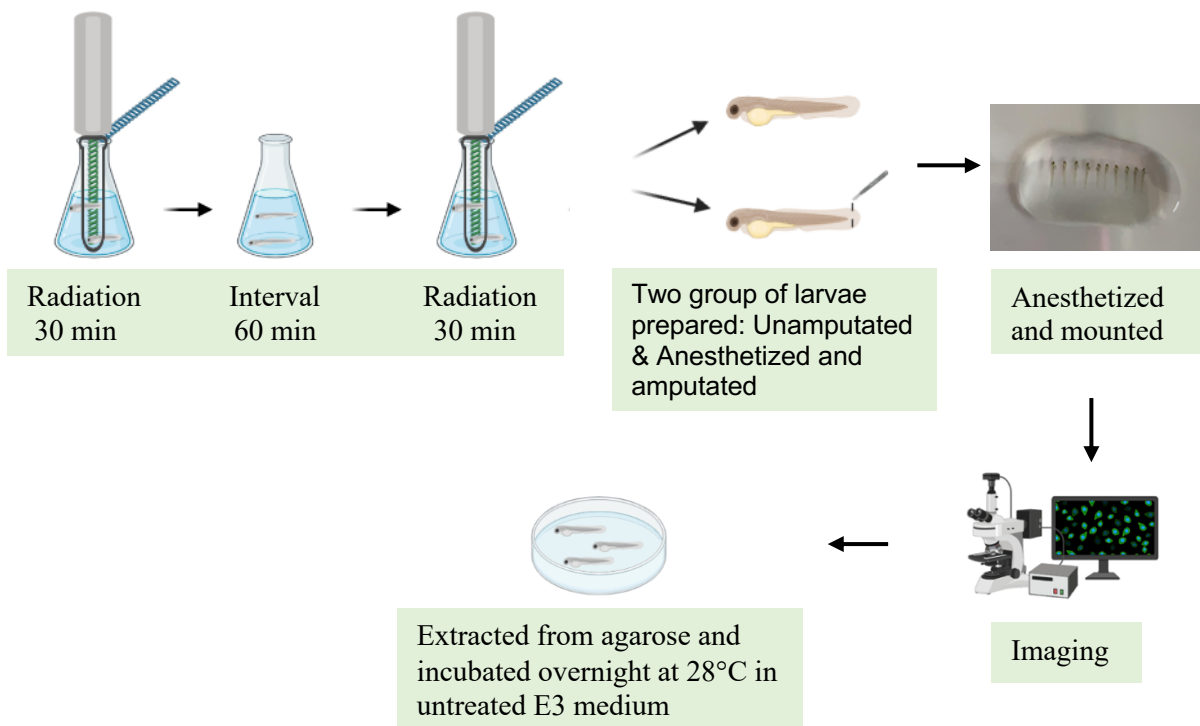
Day 1

Day 2 & Day 3
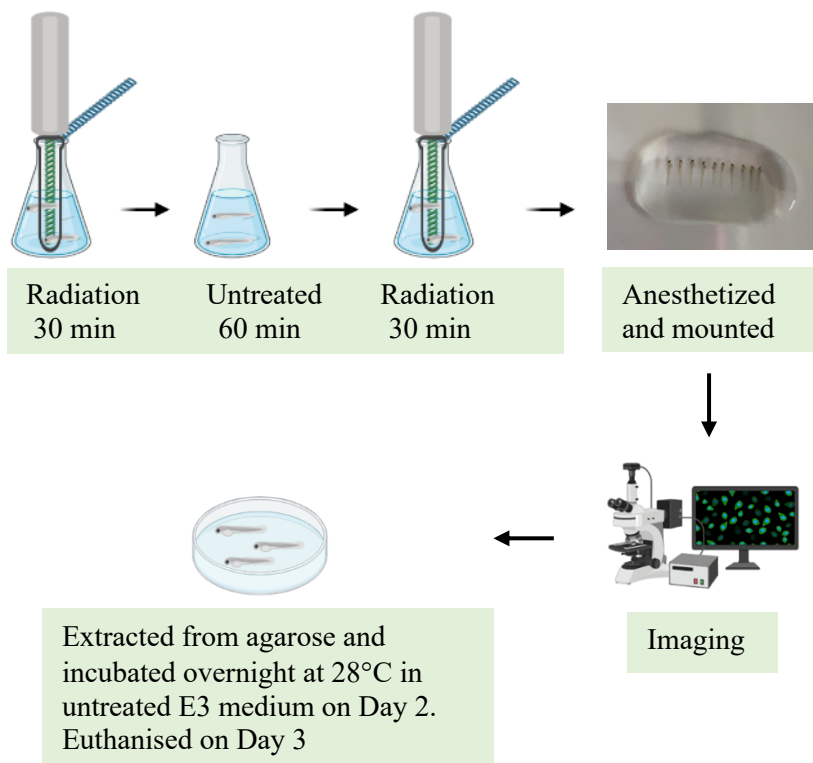
Fig. 64: Flow chart of larvae treatment by EMF radiation.
The 3 day post-fertilised larvae were treated by EMF radiation prior to amputation, mounting and imaging from day 1-3. The larvae were euthanized after imaging on Day 3. Image created using BioRender.com.

7.6 *Chlorella vulgaris* (Microalga) cell culture analysis methods and treatments

7.6.1 *Chlorella vulgaris* cell culture preparation

The freshwater microalga *Chlorella vulgaris* was kindly provided by Posten's Research Group, Institute of Process Engineering in Life Sciences, Karlsruhe Institute of Technology (KIT). 20 mL of *C. vulgaris* strain stock culture was added into 1 L of BBM medium to make a new *C. vulgaris* culture. The cell density of the new culture measured at Abs_{750} is to be ~0.1. The 100 mL flasks filled with 50 mL *C. vulgaris* culture were placed on a shaker at 200 rpm with a bottom-illuminator (0.13A, 12V) for 24 hours of light supply for optimum cell growth.

7.6.2 *Chlorella vulgaris* cell density measurement

The cell density is measured by spectrophotometer with 1 mL cuvette filled with 1 mL of *C. vulgaris* cell culture measured at Abs_{750}, repeated 3 times. The *C. vulgaris* cell culture was treated for a maximum of 4 weeks and the cell density was measured 2-3 times a week. The cell density was measured at 750 nm which is above chlorophyll maxima absorption. The wavelength between 600-680 nm is associated with chlorophyll absorption and has the possibility of interference with the cell density measurement done based on the cell turbidity principle.

7.6.3 *Chlorella vulgaris* dry weight measurement

The dry weight of *C. vulgaris* cell culture was estimated by collecting 2 mL of cell culture on the last day to harvest *C. vulgaris* culture. The *C. vulgaris* cell culture was centrifuged at 4500 rpm for 5 min at 4 °C in a sterile 2 mL reaction tube. The pellet was then gently washed with 2 mL of distilled water to remove culture medium salts. The sample was again pelleted at 4500 rpm for 5 min at 4 °C and the supernatant was carefully discarded. The pellet was kept in a freezer at -80 °C for 5 minutes. The freeze-dried sample was fixed to the lyophilizer overnight to completely remove the moist before weighing the sample (sample + reaction tube). The empty reaction tube will be weighed earlier before filling up with the cell culture.

Dry weight = (Dried sample + reaction tube) – empty reaction tube

7.6.4 *Chlorella vulgaris* cell disruption by French pressure cell press

On the last day of *C. vulgaris* cell culture treatment, the cells were harvested. *C. vulgaris* culture was transferred into a 50 mL falcon tube and centrifuged at 4500 rpm for 5 min at 4 °C to remove the culture medium (BBM). The pellet was then gently washed with another 20 mL of distilled water to remove culture medium salts and stored at -20 °C overnight. The *C. vulgaris* cell was added with 10 mL of distilled water and mixed well before being disrupted with the French pressure cell press at 1100 psi pressure.

7.6.5 *Chlorella vulgaris* chlorophyll quantification

Chlorophyll pigment was extracted from *C. vulgaris* using by 90% methanol mixture condition. Total chlorophyll (Chlorophyll a and chlorophyll b) content in harvested *C. vulgaris* cells was quantified as suggested by Lichtenthaler and Buschmann in 2001[211]. The French pressed samples were normalised according to the cell density ratio at Abs_{750}. 200 µL of normalised French pressed sample was mixed with 1800 µL of 100% methanol in a 2 mL reaction tube to make a 90% methanol condition. Two tubes were prepared for each treated sample. The tubes with samples were incubated on a heat block at 45 °C for 20 minutes. Next, the samples were vortex for 20 minutes at RT before centrifuge at 11000 rpm for 5 minutes at 4 °C. The assay was executed in darkness/minimum light conditions as chlorophyll is a light-sensitive compound. A 0.5 mL of supernatant/extracted chlorophyll was carefully transferred into 3 wells of 24 well-plates without carrying any cells along. The blank will be 0.5 mL of diluted 90% methanol. Measurement of the spectra was carried out using a Tecan-microplate reader with 24 well-plates. The absorbance of the samples was measured at 652, 665 and 750 nm, while the concentration of chlorophyll pigments was determined by using the equations below and followed the absorption coefficients as suggested for 90% methanol solvent by Lichtenthaler and Buschmann[211]. The absorption value at 750 nm was only to determine that the measured sample is cell-free, $Abs_{750} < 0.005$ confirms no interference by contaminant cells.

C_a = Chlorophyll a (µg/mL) = $16.82_{A665} - 9.28_{A652}$
C_b = Chlorophyll b (µg/mL) = $36.92_{A652} - 16.54_{A665}$

7.6.6 *Chlorella vulgaris* protein quantification

The protein concentration extracted from *C. vulgaris* was determined using Roti®-Nanoquant reagent by Roth. The French pressed samples were normalised according to the cell density ratio at Abs_{750}. 2 mL of normalised French pressed samples were transferred into a 2 mL reaction tube and then incubated on a heat block at 80 °C for 20 minutes. Two tubes were prepared for each treated sample. Next, the samples were vortex for 20 minutes at RT before centrifuge at 11000 rpm for 5 minutes at 4 °C. A 400 µL of supernatant/extracted protein was carefully transferred into a 2 mL reaction tube without carrying any cells along. 10 mL of Roti®-Nanoquant reagent is added to 40 mL of distilled water, diluted by 1:5 to a working solution. 400 µL of protein extraction is mixed with 1600 µL of working solution in a 2 mL reaction tube. A 0.5 mL of protein mixture solution was transferred into 3 wells of 24 well-plates. The blank will be 0.5 mL of the diluted working solution. Measurement of the spectra was carried out using a Tecan-microplate reader with 24 well-plates. The absorbance of the samples was measured at 450, 590 and 750 nm. The quotient of Abs_{590}/Abs_{450} is compared against the BSA standard curve to determine the protein concentration according to the Roti®-Nanoquant manual[212]. The BSA standard curve was prepared using Roti®-Nanoquant reagent at concentrations of 0, 20, 40, 60, 80 and 100 µg/mL (Fig. 65).

[Protein (µg/mL)] = Abs_{590}/Abs_{450}
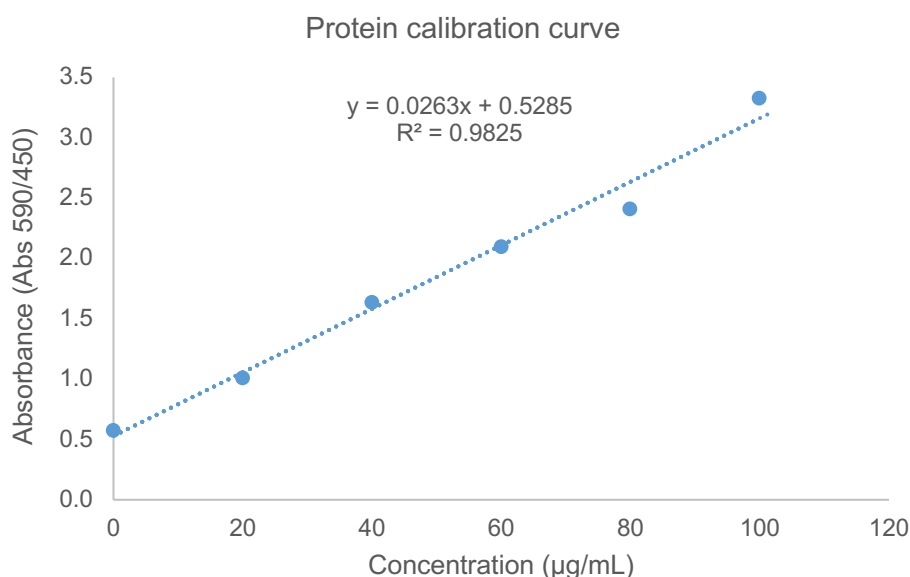
Fig. 65: Protein standard curve using bovine serum albumin (BSA). The BSA standard curve was prepared at concentrations of 0, 20, 40, 60, 80 and 100 µg/mL.

7.6.7 *Chlorella vulgaris* starch quantification

50 mg of anthrone powder mixed with 50 mL of 95% conc. H_2SO_4 acid to make 10 mM concentration of anthrone reagent. The starch concentration extracted from *C. vulgaris* were determined by anthrone reaction. 2 mL reaction tube with approximately 0.1 g of fresh cell upon normalised was added with 2 mL of 80% ethanol and heated on a heat block at 60°C for 15 minutes then centrifuged at 4500 rpm for 5 min at 4 °C, this step was repeated thrice in order to remove interfering substances such as pigments, soluble sugars and lipids, and to gelatinize starch granules. The removal of interfering substances is extremely important to avoid influencing colourimetric readings. Two tubes were prepared for each treated sample. Then the centrifuged pellets were rinsed with distilled water to remove the remaining ethanol. Subsequently, the *C. vulgaris* starch was extracted and hydrolyzed with 1.1% hydrochloric acid (22 µL of 1M HCl into 1978 µL distilled water containing pellet) and heated on a heat block at 95°C for 30 minutes. The solubilized starch solution was then centrifuged and precipitates removed. 700 µL of solubilized starch solution were transferred into a 2 mL reaction tube and mixed with 1400 µL of prepared 10 mM anthrone reagent. Next, the samples were placed on the ice for 5 minutes to cool down the mixture. A 0.5 mL of solubilised starch mixture solution was transferred into 3 wells of 24 well-plates. The blank will be 0.5 mL of the prepared anthrone reagent. Measurements of spectra were carried out using Tecan-spectrometer with 24 well-plates at 625 nm. The Abs_{625} is compared against the standard curve to determine the starch concentration. The starch standard curve was prepared using soluble starch powder diluted at concentrations of 0, 10, 20, 40, 60, 80 and 100 mg/mL (Fig. 66). The method was adapted with slight modification[213–215].
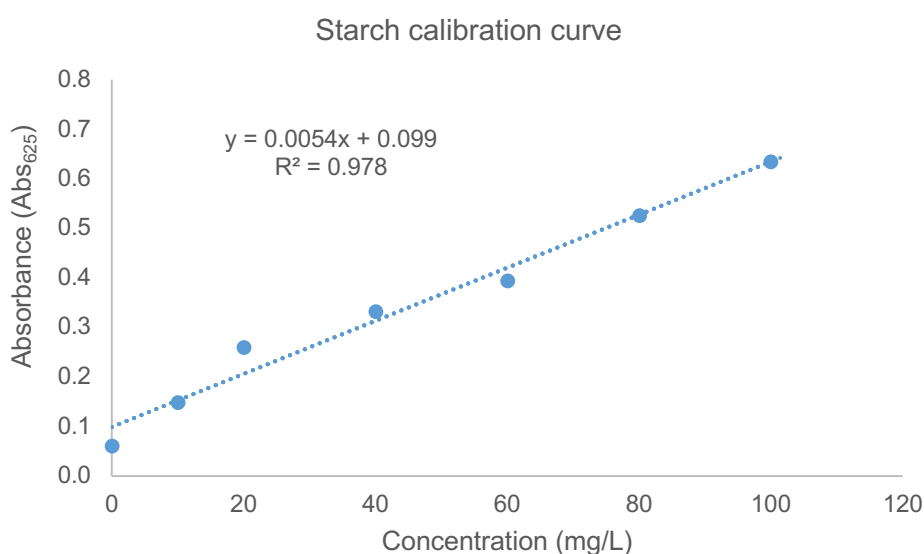
Fig. 66: Starch standard curve using soluble starch powder.
The soluble starch standard curve was prepared at concentrations of 0, 10, 20, 40, 60, 80 and 100 mg/mL.

7.6.8 *Chlorella vulgaris* gas treatment

7.6.8.1 *Chlorella vulgaris* direct-gas treatment method

Seven pairs of 100 mL flasks with 50 mL *C. vulgaris* culture which has an almost similar absorbance value (Abs_{750} = ~0.1) were prepared to begin the experiment. Each pair of flasks with *C. vulgaris* culture was bubbled through directly with different compositions of gases including, H_2, N_2, O_2, H_2-O_2 gas mixture, Brown's gas and 1 pair of flasks with *C. vulgaris* culture were kept untreated would be the control. While the second control will be 1 pair of flasks bubbled through by an air compressor to rule out the direct agitation of the *C. vulgaris* cell culture. The *C. vulgaris* cell culture was bubbled through for 30 minutes twice a day 5 times/week for approximately 4 weeks. The *C. vulgaris* culture flasks were placed on a shaker (200 rpm) with a bottom-illuminator (0.13A, 12V) for 24 hours for optimum cell growth. The *C. vulgaris* cell growth density was measured a minimum 2-3 times per week to follow the growth trend.

| Gas bubbled 30 mins | Incubation 60 mins | Gas bubbled 30 mins | UV-vis spectrophotometer measurement 2-3 times/week | Incubated on bottom-illuminated shaker all-day |
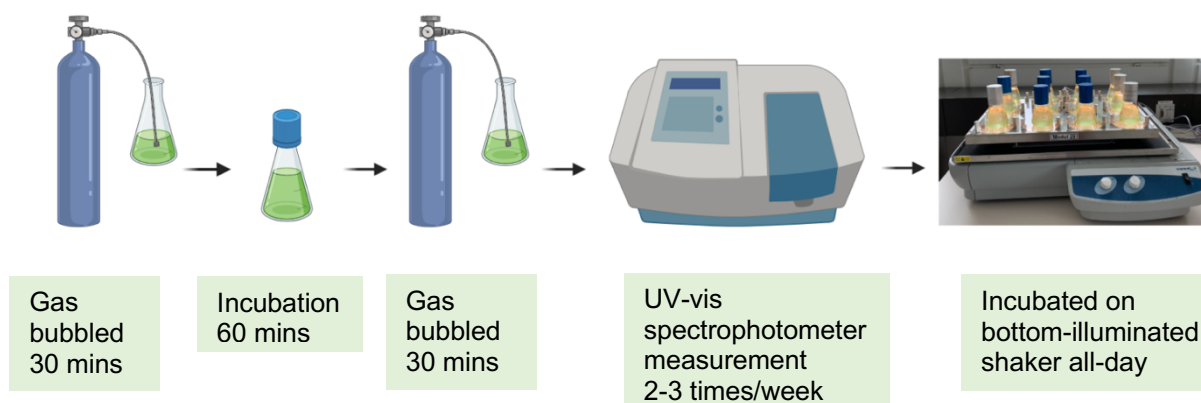
Fig. 67: Flow chart of *Chlorella vulgaris* cell culture by direct-gas treatment.
The treated *C. vulgaris* cell culture density was measured and continued incubating on the bottom-illuminated shaker all-day. Culture bubbled with respective gas for 30 minutes 2 times/day; 5 times/week for 4 weeks. Image created using BioRender.com.

7.6.8.2   *Chlorella vulgaris* medium gas pre-treatment method

Seven 100 mL flasks with 40 mL *C. vulgaris* culture which has an almost similar absorbance value (Abs_{750} = ~0.5) were prepared to begin the experiment. The pre-treatment method requires a *C. vulgaris* cell culture with a larger cell density. Each flask with *C. vulgaris* culture was treated with 5 different gas conditions (H_2, N_2, O_2, H_2-O_2 gas mixture and Brown's gas). The untreated and air bubbled *C. vulgaris* cell culture will be the main controls. Untreated condition to rule out pre-agitation of medium effects to *C. vulgaris* cell while air bubbled to

compare the effect of bubbling a medium prior to mixing the *C. vulgaris* cells. In order to evaluate the influence of the gases without overlay by agitation effects, the 40 mL of *C. vulgaris* culture was centrifuged at 4500 rpm for 5 minutes at 4 °C to avoid cell disruption but only to separate the culture medium from *C. vulgaris* cells. The separated supernatant was infused with Air, H_2, N_2, O_2, H_2-O_2 gas mixture and Brown's gas for 30 minutes before incubating the *C. vulgaris* cells back into the respective gas infused medium. Then the *C. vulgaris* cell culture flasks were placed on a shaker (200 rpm) with bottom-illuminator (0.13A, 12V) for 24 hours for optimum cell growth. The *C. vulgaris* cell culture was only treated once per day 5 times/week for approximately 2-3 weeks with respective gases. The treatment period was minimised with the gas pre-treatment method to avoid unwanted stress to the cell due to frequent centrifugation. The *C. vulgaris* cell growth density was measured a minimum 2-3 times per week to follow the growth trend.

| *C. vulgaris* cells culture centrifuged to separate the medium | Gas infused for 30 mins into medium then transfer the cells into medium | UV-vis spectrophotometer measurement 2-3 times/week | Incubated on bottom-illuminated shaker all-day |
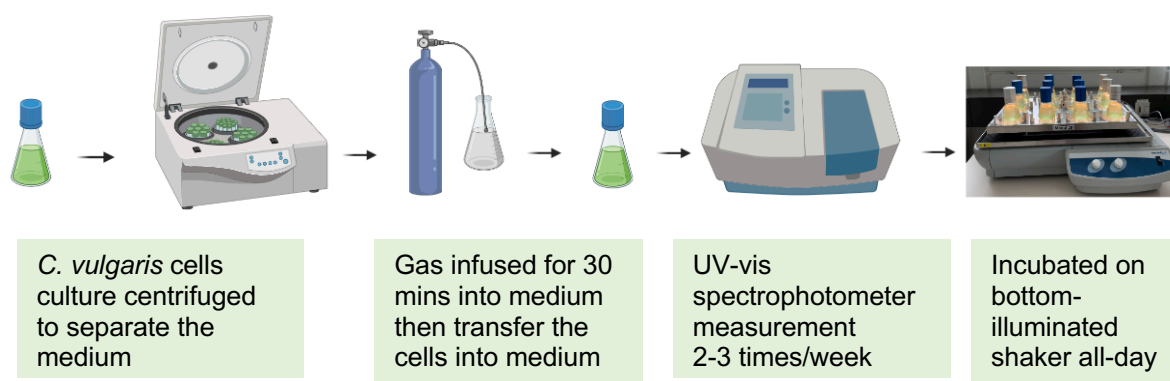
Fig. 68: Flow chart of *Chlorella vulgaris* cell culture by the gas pre-treatment medium. The treated *C. vulgaris* cell culture density was measured and continued incubating on the bottom-illuminated shaker all-day. Culture medium separated from *C. vulgaris* cells were bubbled with respective gas for 30 minutes once/day; 5 times/week for 2-3 weeks. Image created using BioRender.com.

7.6.9 *Chlorella vulgaris* electromagnetic fields radiation treatment

Three pairs of 100 mL flasks with 120 mL *C. vulgaris* culture which has an almost similar absorbance value (Abs_{750} = ~0.1) were prepared to begin the experiment. A large amount of *C. vulgaris* culture medium is essential to completely immerse the Tesla oscillator handheld-antenna into the medium to achieve equilibrium and also to avoid the culture medium temperature from increasing (Fig. 69). The Tesla oscillator antenna was covered by a 17 mL thin-wall borosilicate test tube which was used as a shield to protect the *C. vulgaris* cell from possible direct electric current. The *C. vulgaris* cell culture was radiated by the Tesla oscillator antenna for 30 minutes twice with 2 hours interval period to avoid temperature shoot-up of the BBM culture medium which may cause thermal shock. The temperature of the culture medium was monitored during the Tesla oscillator radiation treatment and confirmed the temperature

of the E3 medium does not elevate more than 1.0 °C. The WLAN radiation setup also used the same procedure where two 100 mL flasks filled with 120 mL *C. vulgaris* cell cultures were placed next to the WLAN router which transferred the signal to a handphone that was kept in the next room. The WLAN radiation treatment was carried out for 3 hours continuously because WLAN is expected to radiate low intense radiation due to lower energy input, also WLAN radiation does not influence the temperature of the culture medium in the flask. The untreated *C. vulgaris* cell culture flasks were the control, kept in a separate room to avoid the influence of the Tesla oscillator and WLAN radiation effect. The *C. vulgaris* cell cultures were treated 5 times/week for approximately 4 weeks, the culture flasks were placed on a shaker (200 rpm) with bottom-illuminator (0.13A, 12V) for 24 hours for optimum cell growth. The *C. vulgaris* cell growth density was measured a minimum 2-3 times per week to follow the growth trend.
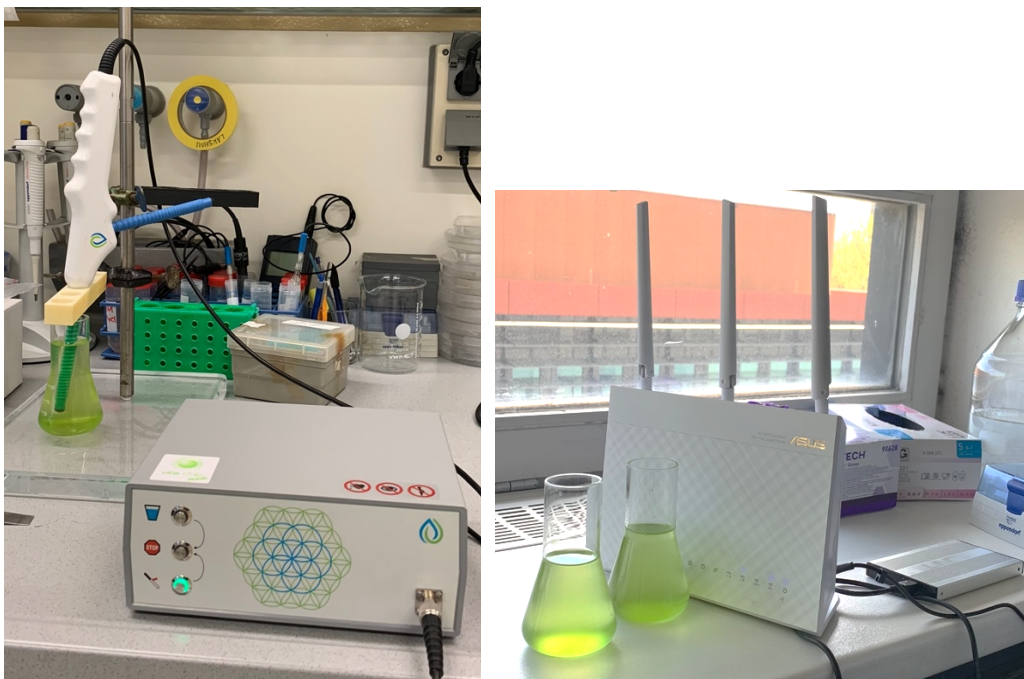
Fig. 69: The *Chlorella vulgaris* cell culture treated by EMF radiation.
The Tesla oscillator generates 144 MHz frequency and WLAN transfer signal at 5GHz frequency.
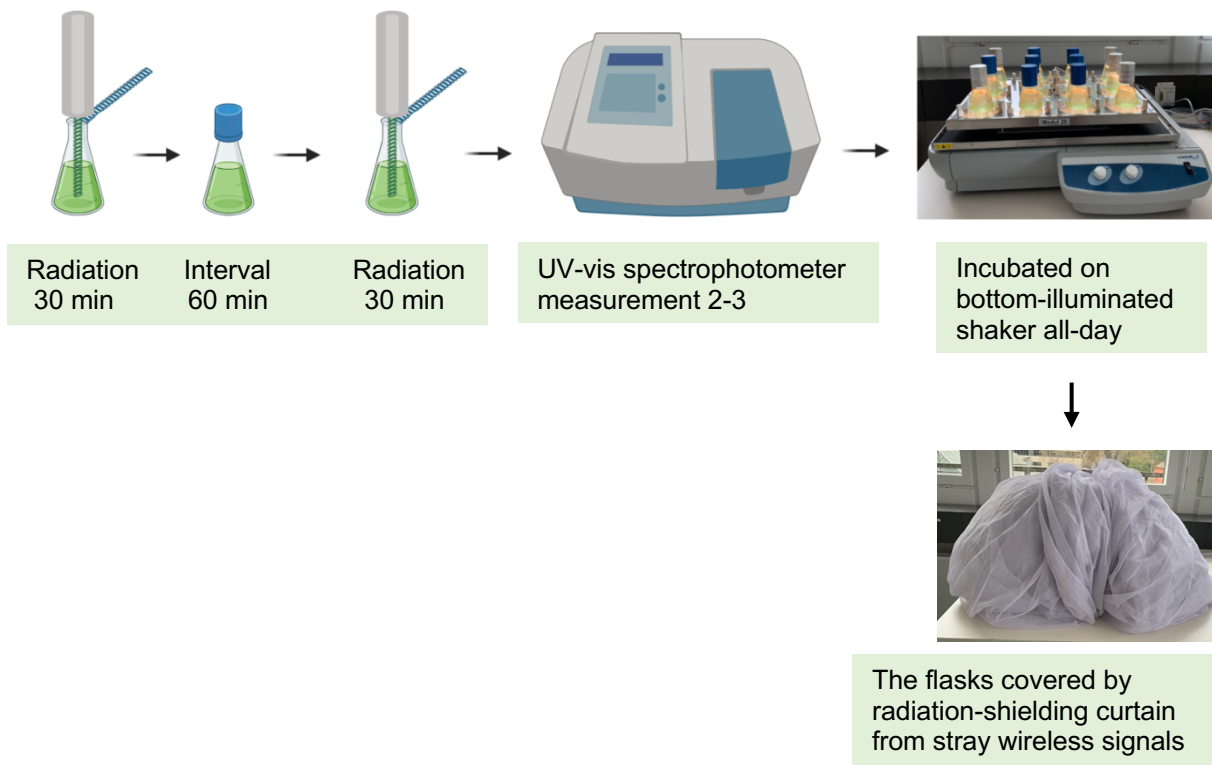
Fig. 70: Flow chart of *Chlorella vulgaris* cell culture by Tesla oscillator radiation treatment.
The treated *C. vulgaris* cell culture density was measured and continued incubating on the bottom-illuminated shaker all-day. Culture radiated by Tesla oscillator ("health-promoting" radiation device) for 30 minutes 2 times/day; 5 times/week for 4 weeks.
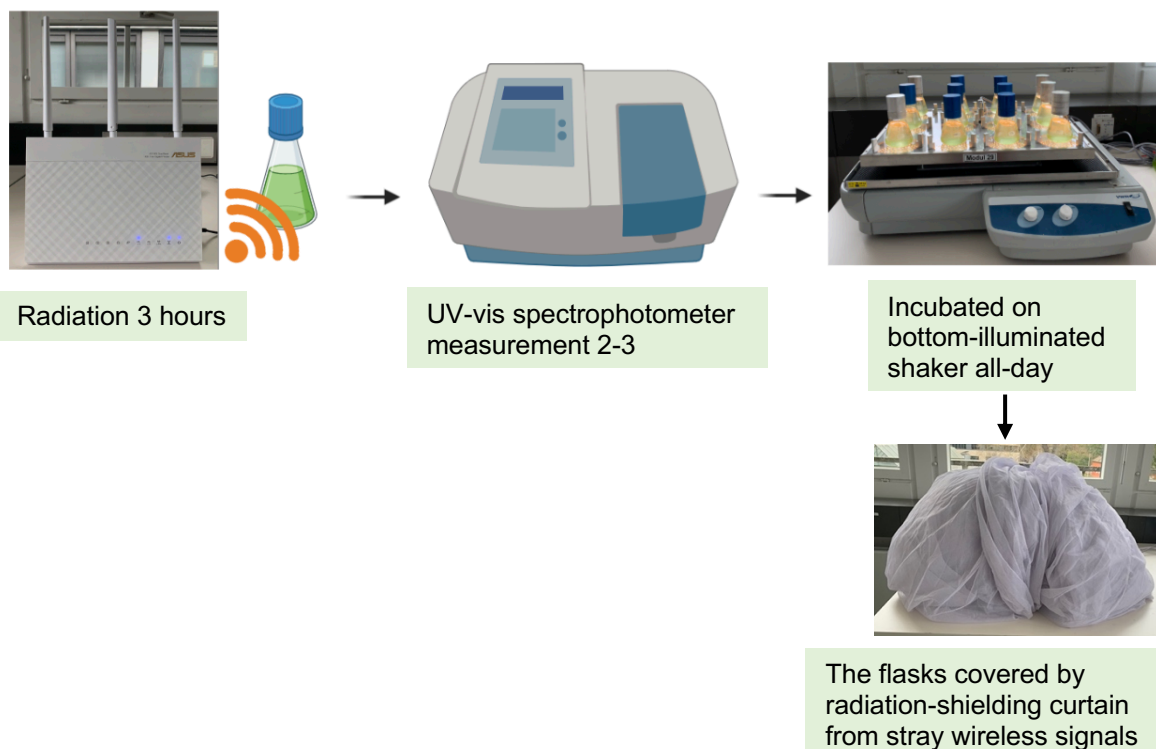
Fig. 71: Flow chart of *Chlorella vulgaris* cell culture by WLAN radiation treatment.
The treated *C. vulgaris* cell culture density was measured and continued incubating on the bottom-illuminated shaker all-day. Culture radiated by WLAN router (signalling network via radiation) for 3 hours once/day; 5 times/week for 4 weeks.

7.7   Statistical analyses

The statistical analyses were carried out using SPSS26. Data were analysed using Welch's t-test of One-Way ANOVA. Post-Hoc multiple comparison with Gomes-Howell test. Data analysed by the mean difference is significant at the 0.05 level. The fin growth difference compared between the consecutive days of treatment is expressed by a stacked bar chart to represents the proportional growth of larvae in the first 24 hours (Day2 - Day1) and 48 hours (Day3 - Day2) which contribute to the total growth of zebrafish larvae fin-area. The error bar represents the standard deviation (S.D) of total larvae's fin-growth per condition. Results for the neutrophil count are expressed by a line graph as means ± S.D. for each experiment. All tables were prepared in Excel (Microsoft). A value of $p < 0.05$ was considered statistically significant.

8. References

1. Kurokawa, R., Hirano, S., Ichikawa, Y., Matsuo, G. & Takefuji, Y. Preventing explosions of hydrogen gas inhalers. *Med Gas Res* **9**, 160–162 (2019).
2. Hydrogen for health: H2 nano V2 molecular hydrogen water bottle with PEM dual chamber nano technology. https://hydrogen4health.com/h2-nanov2-hydrogen-water-bottle/?ref=thf. *Developed by Myogenic Solutions* (2022).
3. Ohta, S. Will the hydrogen therapy be approved shortly? *Ann Transl Med* **8**, 264–264 (2020).
4. Gharib, B. *et al.* Anti-inflammatory properties of molecular hydrogen: investigation on parasite-induced liver inflammation. *Comptes Rendus de l'Académie des Sciences - Series III - Sciences de la Vie* **324**, 719–724 (2001).
5. Hancock, J. T. & Russell, G. Downstream signalling from molecular hydrogen. *Plants* **10**, 367–379 (2021).
6. Yamamoto, R., Homma, K., Suzuki, S., Sano, M. & Sasaki, J. Hydrogen gas distribution in organs after inhalation: Real-time monitoring of tissue hydrogen concentration in rat. *Sci Rep* **9**, 1255–1263 (2019).
7. Ohsawa, I. *et al.* Hydrogen acts as a therapeutic antioxidant by selectively reducing cytotoxic oxygen radicals. *Nat Med* **13**, 688–694 (2007).
8. Guan, W.-J. *et al.* Hydrogen/oxygen mixed gas inhalation improves disease severity and dyspnea in patients with Coronavirus disease 2019 in a recent multicenter, open-label clinical trial. *J Thorac Dis* **12**, 3448–3452 (2020).
9. Xiaofeng Liang, Zijian Feng & Liming Li. National Health Commission (NHC) of the PRC, National Administration of Traditional Chinese Medicine of the PRC. Guidance for corona virus disease 2019: prevention, control, diagnosis and management. *People's Republic of China* 1–146 (2020).
10. Tsujita, A. *et al.* Quantitative determination of H2 in human blood by 22Ne-aided gas chromatography-mass spectrometry using a single quadrupole instrument. *Analytical Sciences* **36**, 1231–1236 (2020).
11. Sano, M. *et al.* Pharmacokinetics of a single inhalation of hydrogen gas in pigs. *PLoS One* **15**, 1–10 (2020).
12. Hylemon, P. B., Harris, S. C. & Ridlon, J. M. Metabolism of hydrogen gases and bile acids in the gut microbiome. *FEBS Lett* **592**, 2070–2082 (2018).
13. Jin, Q. *et al.* Hydrogen gas acts as a novel bioactive molecule in enhancing plant tolerance to paraquat-induced oxidative stress via the modulation of heme oxygenase-1 signalling system. *Plant Cell Environ* **36**, 956–969 (2013).
14. Asada, R., Saitoh, Y. & Miwa, N. Effects of hydrogen-rich water bath on visceral fat and skin blotch, with boiling-resistant hydrogen bubbles. *Med Gas Res* **9**, 68–73 (2019).
15. Li, C. *et al.* Nano-bubble hydrogen water: An effective therapeutic agent against inflammation related disease caused by viral infection in zebrafish model. *Virol Sin* **37**, 277–283 (2022).
16. Martin, W. & Müller, M. The hydrogen hypothesis for the first eukaryote. *Nature* **392**, 37–41 (1998).
17. Batyrova, K. & Hallenbeck, P. C. Hydrogen production by a Chlamydomonas reinhardtii strain with inducible expression of photosystem II. *Int J Mol Sci* **18**, 647–661 (2017).

18. Su, X., Zhao, W. & Xia, D. The diversity of hydrogen-producing bacteria and methanogens within an in situ coal seam. *Biotechnol Biofuels* **11**, 245–263 (2018).

19. Ogata, H., Lubitz, W. & Higuchi, Y. Structure and function of [NiFe] hydrogenases. *J Biochem* **160**, 251–258 (2016).

20. Ghysels, B., Godaux, D., Matagne, R. F., Cardol, P. & Franck, F. Function of the chloroplast hydrogenase in the microalga Chlamydomonas: The role of hydrogenase and state transitions during photosynthetic activation in anaerobiosis. *PLoS One* **8**, 1–8 (2013).

21. Strocchi, A. & Levitt, M. D. Maintaining intestinal H2 balance: Credit the colonic bacteria. *Gastroenterology* **102**, 1424–1426 (1992).

22. Gibson, G. R. *et al.* Alternative pathways for hydrogen disposal during fermentation in the human colon. *Gut* **31**, 679–683 (1990).

23. Wolf, P. G., Biswas, A., Morales, S. E., Greening, C. & Gaskins, H. R. H2 metabolism is widespread and diverse among human colonic microbes. *Gut Microbes* **7**, 235–245 (2016).

24. Boyle, R. Complete dictionary of scientific biography. https://www.encyclopedia.com/science/dictionaries-thesauruses-pictures-and-press-releases/boyle-robert. (2022).

25. Antoine L. Lavoisier. *Elements of chemistry in new systematic order, containing all modern discoveries, translated from the French by Robert Kerr.* (Tredition Classics, 2012).

26. 'Hydrogen' Alternative Energy. Retrieved October 27, 2022 from Encyclopedia.com: https://www.encyclopedia.com/environment/energy-government-and-defense-magazines/hydrogen.

27. Zubenko, D., Singh, S. & Rosen, B. A. Exsolution of Re-alloy catalysts with enhanced stability for methane dry reforming. *Appl Catal B* **209**, 711–719 (2017).

28. Ron Everett. Methods and systems for dissociation of water molecules using inertial-kinetic electromagnetic resonance. 1–14 (2010).

29. Schneider, J., Holzer, F., Kraus, M., Kopinke, F.-D. & Roland, U. Water dissociation in a radio-frequency electromagnetic field with ex situ electrodes—decomposition of perfluorooctanoic acid and tetrahydrofuran. *Plasma Sources Sci Technol* **22**, 5007–5015 (2013).

30. van Slyke, D. D. & Sendroy, J. Studies of gas and electrolyte equilibria in blood: XI. The solubility of hydrogen at 38° in blood serum and cells. *Journal of Biological Chemistry* **78**, 801–805 (1928).

31. Dole, M., Wilson, F. R. & Fife, W. P. Hyperbaric hydrogen Therapy: A Possible Treatment for Cancer. *Science (1979)* **190**, 152–154 (1975).

32. LeBaron, T. W., Kura, B., Kalocayova, B., Tribulova, N. & Slezak, J. A new approach for the prevention and treatment of cardiovascular disorders. molecular hydrogen significantly reduces the effects of oxidative stress. *Molecules* **24**, 2076–2102 (2019).

33. Thomas Dziubla & Allan D. Butterfield. *Oxidative stress and biomaterials.* vol. 1st Edition (2016).

34. Morelli, R., Russo-Volpe, S., Bruno, N. & lo Scalzo, R. Fenton-dependent damage to carbohydrates: Free radical scavenging activity of some simple sugars. *J Agric Food Chem* **51**, 7418–7425 (2003).

35. Skovgaard, N., Gouliaev, A., Aalling, M. & Simonsen, U. The role of endogenous H2S in cardiovascular physiology. *Curr Pharm Biotechnol* **12**, 1385–1393 (2011).

36. Janicka, M., Reda, M., Czyżewska, K. & Kabała, K. Involvement of signalling molecules NO, H2O2 and H2S in modification of plasma membrane proton pump in cucumber roots subjected to salt or low temperature stress. *Functional Plant Biology* **45**, 428–439 (2018).

37. Buxton, G. v., Greenstock, C. L., Helman, W. P. & Ross, A. B. Critical Review of rate constants for reactions of hydrated electrons, hydrogen atoms and hydroxyl radicals (·OH/·O-) in Aqueous Solution. *J Phys Chem Ref Data* **17**, 513–886 (1988).

38. Wood, K. C. & Gladwin, M. T. The hydrogen highway to reperfusion therapy. *Nat Med* **13**, 673–674 (2007).

39. Penders, J., Kissner, R. & Koppenol, W. H. ONOOH does not react with H2: Potential beneficial effects of H2 as an antioxidant by selective reaction with hydroxyl radicals and peroxynitrite. *Free Radic Biol Med* **75**, 191–194 (2014).

40. Babbs, C. F., Pham, J. A. & Coolbaugh, R. C. Lethal hydroxyl radical production in paraquat-treated plants. *Plant Physiol* **90**, 1267–1270 (1989).

41. Koppenol, W. H., Stanbury, D. M. & Bounds, P. L. Electrode potentials of partially reduced oxygen species, from dioxygen to water. *Free Radic Biol Med* **49**, 317–322 (2010).

42. Blough, N. v. & Zafiriou, O. C. Reaction of superoxide with nitric oxide to form peroxonitrite in alkaline aqueous solution. *Inorg Chem* **24**, 3502–3504 (1985).

43. Radi, R. Oxygen radicals, nitric oxide, and peroxynitrite: Redox pathways in molecular medicine. *Proceedings of the National Academy of Sciences* **115**, 5839–5848 (2018).

44. Sim, M. *et al.* Hydrogen-rich water reduces inflammatory responses and prevents apoptosis of peripheral blood cells in healthy adults: a randomized, double-blind, controlled trial. *Sci Rep* **10**, 21–30 (2020).

45. Chen, J.-B. *et al.* "Real world survey" of hydrogen-controlled cancer: a follow-up report of 82 advanced cancer patients. *Med Gas Res* **9**, 115–121 (2019).

46. Erejuwa, O. O., Sulaiman, S. A. & Ab Wahab, M. S. Evidence in support of potential applications of lipid peroxidation products in cancer treatment. *Oxid Med Cell Longev* **2013**, 1–8 (2013).

47. Hayashida, K. *et al.* Inhalation of hydrogen gas reduces infarct size in the rat model of myocardial ischemia–reperfusion injury. *Biochem Biophys Res Commun* **373**, 30–35 (2008).

48. Yamazaki, M., Kusano, K., Ishibashi, T., Kiuchi, M. & Koyama, K. Intravenous infusion of H2-saline suppresses oxidative stress and elevates antioxidant potential in Thoroughbred horses after racing exercise. *Sci Rep* **5**, 15514–15523 (2015).

49. Oharazawa, H. *et al.* Protection of the retina by rapid diffusion of hydrogen: administration of hydrogen-loaded eye drops in retinal ischemia–reperfusion injury. *Investigative Opthalmology & Visual Science* **51**, 487–492 (2010).

50. Liu, C. *et al.* Estimation of the hydrogen concentration in rat tissue using an airtight tube following the administration of hydrogen via various routes. *Sci Rep* **4**, 5485–5496 (2014).

51. Rombough, P. J. Partitioning of oxygen uptake between the gills and skin in fish larvae: a novel method for estimating cutaneous oxygen uptake. *Journal of Experimental Biology* **201**, 1763–1769 (1998).

52. Pelster, B. & Bagatto, B. Respiration. in *Fish physiology* vol. 29 289–309 (2010).

53. Iqbal, Z., Iqbal, M. S., Hashem, A., Abd_Allah, E. F. & Ansari, M. I. Plant defense responses to biotic stress and its interplay with fluctuating dark/light conditions. *Front Plant Sci* **12**, 1–22 (2021).

54. Hu, H., Li, P., Wang, Y. & Gu, R. Hydrogen-rich water delays postharvest ripening and senescence of kiwifruit. *Food Chem* **156**, 100–109 (2014).

55. Jiang, K. *et al.* Molecular hydrogen maintains the storage quality of chinese chive through improving antioxidant capacity. *Plants* **10**, 1095–1104 (2021).

56. Xu, S. *et al.* Hydrogen-rich water alleviates salt stress in rice during seed germination. *Plant Soil* **370**, 47–57 (2013).

57. Abd_Allah, E. F., Hashem, A., Alqarawi, A. A., Bahkali, A. H. & Alwhibi, M. S. Enhancing growth performance and systemic acquired resistance of medicinal plant Sesbania sesban (L.) Merr using arbuscular mycorrhizal fungi under salt stress. *Saudi J Biol Sci* **22**, 274–283 (2015).

58. Ádám, A., Nagy, Z., Kátay, G., Mergenthaler, E. & Viczián, O. Signals of systemic immunity in plants: Progress and open questions. *Int J Mol Sci* **19**, 1146–1167 (2018).

59. Engwa, G. A. Free radicals and the role of plant phytochemicals as antioxidants against oxidative stress-related diseases. in *Phytochemicals - Source of Antioxidants and Role in Disease Prevention* 49–77 (InTech, 2018). doi:10.5772/intechopen.76719.

60. El-Maarouf-Bouteau, H. & Bailly, C. Oxidative signaling in seed germination and dormancy. *Plant Signal Behav* **3**, 175–182 (2008).

61. Wang, Y., Liu, Y., Wang, S., Du, H. & Shen, W. Hydrogen agronomy: research progress and prospects. *Journal of Zhejiang University-Science B* **21**, 841–855 (2020).

62. Cui, W., Gao, C., Fang, P., Lin, G. & Shen, W. Alleviation of cadmium toxicity in Medicago sativa by hydrogen-rich water. *J Hazard Mater* **260**, 715–724 (2013).

63. Chen, M. *et al.* Hydrogen-rich water alleviates aluminum-induced inhibition of root elongation in alfalfa via decreasing nitric oxide production. *J Hazard Mater* **267**, 40–47 (2014).

64. Zhao, G. *et al.* Hydrogen-rich water prepared by ammonia borane can enhance rapeseed (Brassica napus L.) seedlings tolerance against salinity, drought or cadmium. *Ecotoxicol Environ Saf* **224**, 1–11 (2021).

65. Hu, H., Zhao, S., Li, P. & Shen, W. Hydrogen gas prolongs the shelf life of kiwifruit by decreasing ethylene biosynthesis. *Postharvest Biol Technol* **135**, 123–130 (2018).

66. Zhang, J., Zhang, G., Lan, H., Qu, J. & Liu, H. Synergetic hydroxyl radical oxidation with atomic hydrogen reduction lowers the organochlorine conversion barrier and potentiates effective contaminant mineralization. *Environ Sci Technol* **55**, 3296–3304 (2021).

67. Yu, J., Yu, Q., Liu, Y., Zhang, R. & Xue, L. Hydrogen gas alleviates oxygen toxicity by reducing hydroxyl radical levels in PC12 cells. *PLoS One* **12**, 1–12 (2017).

68. Pottosin, I., Zepeda-Jazo, I., Bose, J. & Shabala, S. An anion conductance, the essential component of the hydroxyl-radical-induced ion current in plant roots. *Int J Mol Sci* **19**, 897–907 (2018).

69. Jeong, J. B., Seo, E. W. & Jeong, H. J. Effect of extracts from pine needle against oxidative DNA damage and apoptosis induced by hydroxyl radical via antioxidant activity. *Food and Chemical Toxicology* **47**, 2135–2141 (2009).

70. Ayala, A., Muñoz, M. F. & Argüelles, S. Lipid peroxidation: Production, metabolism, and signaling mechanisms of malondialdehyde and 4-hydroxy-2-nonenal. *Oxid Med Cell Longev* **2014**, 1–31 (2014).

71. Liu, X. R., Zhang, M. M., Zhang, B., Rempel, D. L. & Gross, M. L. Hydroxyl-radical reaction pathways for the fast photochemical oxidation of proteins platform as revealed by 18o isotopic labeling. *Anal Chem* **91**, 9238–9245 (2019).

72. Zeng, J., Zhang, M. & Sun, X. Molecular Hydrogen Is Involved in Phytohormone Signaling and Stress Responses in Plants. *PLoS One* **8**, 1–10 (2013).

73. Russell, G., Zulfiqar, F. & Hancock, J. T. Hydrogenases and the role of molecular hydrogen in plants. *Plants* **9**, 1136–1146 (2020).

74. Gerschman, R., Gilbert, D. L., Nye, S. W., Dwyer, P. & Fenn, W. O. Oxygen poisoning and X-irradiation: A mechanism in common. *Science (1979)* **119**, 623–626 (1954).

75. Harman, D. Aging: A theory based on free radical and radiation chemistry. *J Gerontol* **11**, 298–300 (1956).

76.   Di Meo, S. & Venditti, P. Evolution of the knowledge of free radicals and other oxidants. *Oxid Med Cell Longev* **2020**, 1–32 (2020).

77.   Genestra, M. Oxyl radicals, redox-sensitive signalling cascades and antioxidants. *Cell Signal* **19**, 1807–1819 (2007).

78.   Nishikawa, M. & Inoue, M. Oxidative stress and tissue injury. *Masui* **57**, 321–326 (2008).

79.   D'Autréaux, B. & Toledano, M. B. ROS as signalling molecules: mechanisms that generate specificity in ROS homeostasis. *Nat Rev Mol Cell Biol* **8**, 813–824 (2007).

80.   Paola Rosanna, D. & Salvatore, C. Reactive Oxygen Species, Inflammation, and Lung Diseases. *Curr Pharm Des* **18**, 3889–3900 (2012).

81.   Bates, J. T. *et al.* Reactive oxygen species generation linked to sources of atmospheric particulate matter and cardiorespiratory effects. *Environ Sci Technol* **49**, 13605–13612 (2015).

82.   Romashko, J. *et al.* MAPK pathways mediate hyperoxia-induced oncotic cell death in lung epithelial cells. *Free Radic Biol Med* **35**, 978–993 (2003).

83.   Birben, E., Sahiner, U. M., Sackesen, C., Erzurum, S. & Kalayci, O. Oxidative stress and antioxidant defense. *World Allergy Organization Journal* **5**, 9–19 (2012).

84.   Kellner, M. *et al.* ROS signaling in the pathogenesis of acute lung injury (ALI) and acute respiratory distress syndrome (ARDS). *Adv Exp Med Biol.* **967**, 105–137 (2017).

85.   Manach, C., Scalbert, A., Morand, C., Rémésy, C. & Jiménez, L. Polyphenols: food sources and bioavailability. *Am J Clin Nutr* **79**, 727–747 (2004).

86.   Baiano, A. & del Nobile, M. A. Antioxidant compounds from vegetable matrices: Biosynthesis, occurrence, and extraction systems. *Crit Rev Food Sci Nutr* **56**, 2053–2068 (2016).

87.   Francenia Santos-Sánchez, N., Salas-Coronado, R., Villanueva-Cañongo, C. & Hernández-Carlos, B. Antioxidant compounds and their antioxidant mechanism. in *Antioxidants* (IntechOpen, 2019). doi:10.5772/intechopen.85270.

88.   Shiva Kumar, S. & Himabindu, V. Hydrogen production by PEM water electrolysis – A review. *Mater Sci Energy Technol* **2**, 442–454 (2019).

89.   Mefford, J. T. *et al.* Water electrolysis on La1−xSrxCoO3−δ perovskite electrocatalysts. *Nat Commun* **7**, 11053–11064 (2016).

90.   Fabbri, E. & Schmidt, T. J. Oxygen evolution reaction: The enigma in water electrolysis. *ACS Catal* **8**, 9765–9774 (2018).

91.   Dragoslav Dobraš, Žarko Petrović & Zdravko Božičković. Brown's gas: Heat source for welding. in *https://www.researchgate.net/publication/294260575* 1–7 (11th International Conference on Accomplishments in Electrical and Mechanical Engineering and Information Technology – DEMI, 2016).

92.   Nécropotame. Diagram of the electrolysis of water. https://en.m.wikipedia.org/wiki/File:Schemas_electrolyse_h2o.svg. *Wikimedia Commons* (2005).

93.   Mohaupt, E. & Madl, P. Brown's gas for health: Background, observations and medical data. *Water (Basel)* **11**, 109–131 (2020).

94.   Santilli, R. A new gaseous and combustible form of water. *Int J Hydrogen Energy* **31**, 1113–1128 (2006).

95.   Kadeisvili, J. Rebuttal of J.M. Calo's comments on R.M. Santilli's HHO paper. *Int J Hydrogen Energy* **33**, 918–921 (2008).

96.   George Wiseman. What is Brown's Gas (BG)? *https://eagle-research.com/q-what-is-browns-gas-bg/* (2019).

97.   Teixeira, F. L., Moreira, F. J. S. & Pereira-Filho, O. M. C. Electromagnetic wave propagation. in *Encyclopedia of RF and Microwave Engineering* (John Wiley & Sons, Inc., 2005). doi:10.1002/0471654507.eme098.

98. Kenneth R. Spring, Shinya Inoué, Brian O. Flynn, Robert T. Sutter & Michael W. Davidson. Electromagnetic wave propagation. *https://www.olympus-lifescience.com/en/microscope-resource/primer/java/polarizedlight/emwave/* (2022).

99. Emmanuel.boutet. A diagram of electric and magnetic fields in an electromagnetic wave.https://commons.wikimedia.org/wiki/File:Onde_electromagnetique.svg. *Wikimedia Commons* (2007).

100. Ching, Y. Y., Rahman, T. A. & Kim, M. C. Wireless industry emission: Electromagnetic field monitoring and analysis. ARPN journal of engineering and applied sciences. **10**, 9800–9807 (2015).

101. Davis, D., Sears, M. E., Miller, A. B. & Bray, R. *Microwave/radiofrequency radiation and human health*. vol. 1 (Oxford University Press, 2017).

102. World Health Organisation (WHO). Radiation: Ionizing radiation. https://www.who.int/news-room/questions-and-answers/item/radiation-ionizing-radiation. (2020).

103. Feychting, M. & Ahlbom, A. Childhood leukemia and residential exposure to weak extremely low frequency magnetic fields. *Environ Health Perspect* **103**, 59–62 (1995).

104. National Cancer Institute (NCI). Electromagnetic fields and cancer . *https://www.cancer.gov/about-cancer/causes-prevention/risk/radiation/electromagnetic-fields-fact-sheet* (2022).

105. McBride, W. H. & Schaue, D. Radiation-induced tissue damage and response. *J Pathol* **250**, 647–655 (2020).

106. Horst Frank. Electromagnetic Wave Spectrum. https://commons.wikimedia.org/wiki/File:Electromagnetic_spectrum_-eng.svg#mw-jump-to-license. *Wikimedia Commons* (2006).

107. Barker A. T, Jalinous R & Freeston I. L. Non-invasive magnetic stimulation of human motor cortex. *The Lancet* 1106–1107 (1985).

108. Markov, M. S. Expanding use of pulsed electromagnetic field therapies. *Electromagn Biol Med* **26**, 257–274 (2007).

109. Hu, H. *et al.* Promising application of pulsed electromagnetic fields (PEMFs) in musculoskeletal disorders. *Biomedicine & Pharmacotherapy* **131**, 1–8 (2020).

110. Wang, S., Manudhane, A., Ezaldein, H. H. & Scott, J. F. A review of the FDA's 510(k) approvals process for electromagnetic devices used in body contouring. *Journal of Dermatological Treatment* **30**, 727–729 (2019).

111. Andrade, R. *et al.* Pulsed electromagnetic field therapy effectiveness in low back pain: A systematic review of randomized controlled trials. *Porto Biomed J* **1**, 156–163 (2016).

112. Guo, L., Kubat, N. J. & Isenberg, R. A. Pulsed radio frequency energy (PRFE) use in human medical applications. *Electromagn Biol Med* **30**, 21–45 (2011).

113. Ranieri, D., Cucina, A., Bizzarri, M., Alimandi, M. & Torrisi, M. R. Microgravity influences circadian clock oscillation in human keratinocytes. *FEBS Open Bio* **5**, 717–723 (2015).

114. Tran, D. *et al.* Cellular transduction of mechanical oscillations in plants by the plasma-membrane mechanosensitive channel MSL10. *Proceedings of the National Academy of Sciences* **118**, 1–7 (2021).

115. He, L., Wang, X., Tang, H. L. & Montell, D. J. Tissue elongation requires oscillating contractions of a basal actomyosin network. *Nat Cell Biol* **12**, 1133–1142 (2010).

116. Balaji, R. *et al.* Calcium spikes, waves and oscillations in a large, patterned epithelial tissue. *Sci Rep* **7**, 42786–42800 (2017).

117. Huuskonen, H., Lindbohm, M.-L. & Juutilainen, J. Teratogenic and reproductive effects of low-frequency magnetic fields1This is the third in a series of four papers, the

first of which was published in Mutation Res. 387 (1997) pp. 165–171.1. *Mutation Research/Reviews in Mutation Research* **410**, 167–183 (1998).

118. Kim, J. H. *et al.* Exposure to RF-EMF alters postsynaptic structure and hinders neurite outgrowth in developing hippocampal neurons of early postnatal mice. *Int J Mol Sci* **22**, 5340–5359 (2021).

119. BERENIS Secretariat. The Swiss expert group on electromagnetic fields and non-ionising radiation: Newsletter Nr. 28. *Swiss Tropical and Public Health Institute Department of Epidemiology and Public Health. Environmental Exposures and Health Unit* 1–4 (2022).

120. Bernard Pietsch, German Besler & Berthold Czink. Tesla oscillator from Wassermatrix AG: Elemental power of water for our cells. *https://wasserurkraft.de/#wasservitalisierer* (2020).

121. Peter C. Dartsch. Tesla Oscillator – Investigations on Its Beneficial Cell Effects. *Jpn J Med (Lond)* **4**, 495–499 (2021).

122. Kehayas, E. *et al.* Packet-format and network-traffic transparent optical signal processing. *Journal of Lightwave Technology* **22**, 2548–2556 (2004).

123. Foster, K. R. & Moulder, J. E. Wi-Fi and health. *Health Phys* **105**, 561–575 (2013).

124. Bundesamt für Strahlenschutz. Electromagnetic fields. Scientifically discussed biological and health effects of high frequency fields. https://archiv.bge.de/archiv/www.endlager-konrad.de/EN/topics/emf/hff/effect/hff-discussed/hff-discussedb4fd.html?nn=6013030. (2017).

125. Colin Blackman & Simon Forge. *5G Deployment: State of play in Europe, USA and Asia. Policy Department for Economic, Scientific and Quality of Life Policies, Directorate-General for Internal Policies, European Parliament.* (2019).

126. Urey, H. C. & Lavin, G. I. Reactions of dissociated water vapor. *J Am Chem Soc* **51**, 3290–3293 (1929).

127. Urey, H. C. & Lavin, G. I. Some reactions of atomic hydrogen. *J Am Chem Soc* **51**, 3286–3290 (1929).

128. Mukasa, S., Nomura, S., Toyota, H., Maehara, T. & Yamashita, H. Internal conditions of a bubble containing radio-frequency plasma in water. *Plasma Sources Sci Technol* **20**, 4020–4028 (2011).

129. Maehara, T. *et al.* Influence of conductivity on the generation of a radio frequency plasma surrounded by bubbles in water. *Plasma Sources Sci Technol* **20**, 4016–4024 (2011).

130. Maehara, T. *et al.* Radio Frequency Plasma in Water. *Jpn J Appl Phys* **45**, 8864–8868 (2006).

131. Howe, K. *et al.* The zebrafish reference genome sequence and its relationship to the human genome. *Nature* **496**, 498–503 (2013).

132. Harvie, E. A. & Huttenlocher, A. Neutrophils in host defense: new insights from zebrafish. *J Leukoc Biol* **98**, 523–537 (2015).

133. Zon, L. I. & Peterson, R. T. In vivo drug discovery in the zebrafish. *Nat Rev Drug Discov* **4**, 35–44 (2005).

134. Li, L., Jin, H., Xu, J., Shi, Y. & Wen, Z. Irf8 regulates macrophage versus neutrophil fate during zebrafish primitive myelopoiesis. *Blood* **117**, 1359–1369 (2011).

135. Ablain, J., Durand, E. M., Yang, S., Zhou, Y. & Zon, L. I. A CRISPR/Cas9 vector system for tissue-specific gene disruption in zebrafish. *Dev Cell* **32**, 756–764 (2015).

136. Strecker, R., Seiler, T.-B., Hollert, H. & Braunbeck, T. Oxygen requirements of zebrafish (Danio rerio) embryos in embryo toxicity tests with environmental samples. *Comparative Biochemistry and Physiology Part C: Toxicology & Pharmacology* **153**, 318–327 (2011).

137. Kawakami, A., Fukazawa, T. & Takeda, H. Early fin primordia of zebrafish larvae regenerate by a similar growth control mechanism with adult regeneration. *Developmental Dynamics* **231**, 693–699 (2004).

138. Gilbert SF. Early Development in Fish. in *Developmental Biology* (Sunderland (MA): Sinauer Associates, 2000).

139. Warga, R. M. & Kimmel, C. B. Cell movements during epiboly and gastrulation in zebrafish. *Development* **108**, 569–580 (1990).

140. Kawasaki, T., Maeno, A., Shiroishi, T. & Sakai, N. Development and growth of organs in living whole embryo and larval grafts in zebrafish. *Sci Rep* **7**, 16508–16519 (2017).

141. Gerhard, G. S. *et al.* Life spans and senescent phenotypes in two strains of Zebrafish (Danio rerio). *Exp Gerontol* **37**, 1055–1068 (2002).

142. Indian Institute of Science Education and reserach Bhopal. Life cycle in zebrafish. https://commons.wikimedia.org/wiki/File:Life_cycle.png. *Wikimedia Commons* (2014).

143. Lam, S. H., Chua, H. L., Gong, Z., Lam, T. J. & Sin, Y. M. Development and maturation of the immune system in zebrafish, Danio rerio: a gene expression profiling, in situ hybridization and immunological study. *Dev Comp Immunol* **28**, 9–28 (2004).

144. Sant, K. E. & Timme-Laragy, A. R. Zebrafish as a model for toxicological perturbation of yolk and nutrition in the early embryo. *Curr Environ Health Rep* **5**, 125–133 (2018).

145. Beijerinck, M. W. Culturversuche mit Zoochlorellen, Lichenengonidien und anderen niederen Algen. *Bot. Zeitung* **48**, 781–785 (1890).

146. Safi, C., Zebib, B., Merah, O., Pontalier, P.-Y. & Vaca-Garcia, C. Morphology, composition, production, processing and applications of Chlorella vulgaris: A review. *Renewable and Sustainable Energy Reviews* **35**, 265–278 (2014).

147. Nam, S.-H., Lee, J. & An, Y.-J. Quantitative assessment of photosynthetic activity of Chlorella (Class Trebouxiophyceae) adsorbed onto soil by using fluorescence imaging. *Environmental Pollution* **254**, 112942–112953 (2019).

148. Gojo, R., Suzuki, H. & Tezuka, T. Near-UV radiation promotes growth of Chlorella. *Environ Sci* **11**, 189–198 (2004).

149. Zhang, W. *et al.* Toxicity assessment of Chlorella vulgaris and Chlorella protothecoides following exposure to Pb(II). *Environ Toxicol Pharmacol* **36**, 51–57 (2013).

150. Shchemelinina, T. N., Anchugova, E. M., Kotova, O. B. & Shushkov, D. A. The analcime-bearing rock immobilized microalgae: Stress resistance, psychrotolerance, phenol removal. *Bioresour Technol* **322**, 124560–124569 (2021).

151. Li, T., Zheng, Y., Yu, L. & Chen, S. High productivity cultivation of a heat-resistant microalga Chlorella sorokiniana for biofuel production. *Bioresour Technol* **131**, 60–67 (2013).

152. Yamamoto, M., Fujishita, M., Hirata, A. & Kawano, S. Regeneration and maturation of daughter cell walls in the autospore-forming green alga Chlorella vulgaris (Chlorophyta, Trebouxiophyceae). *J Plant Res* **117**, 257–264 (2004).

153. Kawakami, A., Fukazawa, T. & Takeda, H. Early fin primordia of zebrafish larvae regenerate by a similar growth control mechanism with adult regeneration. *Developmental Dynamics* **231**, 693–699 (2004).

154. Mathias, J. R. *et al.* Resolution of inflammation by retrograde chemotaxis of neutrophils in transgenic zebrafish. *J Leukoc Biol* **80**, 1281–1288 (2006).

155. de Oliveira, S., Rosowski, E. E. & Huttenlocher, A. Neutrophil migration in infection and wound repair: going forward in reverse. *Nat Rev Immunol* **16**, 378–391 (2016).

156. Phillipson, M. & Kubes, P. The neutrophil in vascular inflammation. *Nat Med* **17**, 1381–1390 (2011).

157. Olajire, A. A., O. A. J. Kinetic Study of Decolorization of Methylene Blue with Sodium Sulphite in Aqueous Media: Influence of Transition Metal Ions. *J Phys Chem Biophys* **2**, 136–142 (2014).

158. Kohen, R. & Nyska, A. Invited review: Oxidation of biological systems: oxidative stress phenomena, antioxidants, redox reactions, and methods for their quantification. *Toxicol Pathol* **30**, 620–650 (2002).

159. Clift, D., Richendrfer, H., Thorn, R. J., Colwill, R. M. & Creton, R. High-throughput analysis of behavior in zebrafish larvae: Effects of feeding. *Zebrafish* **11**, 455–461 (2014).

160. Sant, K. E. & Timme-Laragy, A. R. Zebrafish as a Model for Toxicological Perturbation of Yolk and Nutrition in the Early Embryo. *Curr Environ Health Rep* **5**, 125–133 (2018).

161. Brinkmann, V. *et al.* Neutrophil extracellular traps kill bacteria. *Science (1979)* **303**, 1532–1535 (2004).

162. Forrester, S. J., Kikuchi, D. S., Hernandes, M. S., Xu, Q. & Griendling, K. K. Reactive Oxygen Species in Metabolic and Inflammatory Signaling. *Circ Res* **122**, 877–902 (2018).

163. Jenne, C. N., Liao, S. & Singh, B. Neutrophils: multitasking first responders of immunity and tissue homeostasis. *Cell Tissue Res* **371**, 395–397 (2018).

164. Xu, S. *et al.* Prolonged neutrophil retention in the wound impairs zebrafish heart regeneration after cryoinjury. *Fish Shellfish Immunol* **94**, 447–454 (2019).

165. Vieira, W. A., Wells, K. M. & McCusker, C. D. Advancements to the Axolotl Model for Regeneration and Aging. *Gerontology* **66**, 212–222 (2020).

166. Strecker, R., Seiler, T.-B., Hollert, H. & Braunbeck, T. Oxygen requirements of zebrafish (Danio rerio) embryos in embryo toxicity tests with environmental samples. *Comparative Biochemistry and Physiology Part C: Toxicology & Pharmacology* **153**, 318–327 (2011).

167. Uemoto, T., Abe, G. & Tamura, K. Regrowth of zebrafish caudal fin regeneration is determined by the amputated length. *Sci Rep* **10**, 649–660 (2020).

168. Shang, E. H. H. & Wu, R. S. S. Aquatic hypoxia Is a teratogen and affects fish embryonic development. *Environ Sci Technol* **38**, 4763–4767 (2004).

169. Jonz, M. G. & Nurse, C. A. Ontogenesis of oxygen chemoreception in aquatic vertebrates. *Respir Physiol Neurobiol* **154**, 139–152 (2006).

170. Kannan, S., Pang, H., Foster, D. C., Rao, Z. & Wu, M. Human 8-oxoguanine DNA glycosylase increases resistance to hyperoxic cytotoxicity in lung epithelial cells and involvement with altered MAPK activity. *Cell Death Differ* **13**, 311–323 (2006).

171. Rahman, I., Biswas, S. K. & Kode, A. Oxidant and antioxidant balance in the airways and airway diseases. *Eur J Pharmacol* **533**, 222–239 (2006).

172. Mantell, L. L., Horowitz, S., Davis, J. M. & Kazzaz, J. A. Hyperoxia-induced cell death in the lung-the correlation of apoptosis, necrosis, and inflammation. *Ann N Y Acad Sci* **887**, 171–180 (1999).

173. Papaiahgari, S., Kleeberger, S. R., Cho, H.-Y., Kalvakolanu, D. v. & Reddy, S. P. NADPH Oxidase and ERK Signaling Regulates Hyperoxia-induced Nrf2-ARE Transcriptional Response in Pulmonary Epithelial Cells. *Journal of Biological Chemistry* **279**, 42302–42312 (2004).

174. Pittman, K. & Kubes, P. Damage-Associated Molecular Patterns Control Neutrophil Recruitment. *J Innate Immun* **5**, 315–323 (2013).

175. Zhou, W. *et al.* Neutrophil-specific knockout demonstrates a role for mitochondria in regulating neutrophil motility in zebrafish. *Dis Model Mech* **11**, 33027–33058 (2018).

176. Frangogiannis, N. G. & Entman, M. L. Chemokines in Myocardial Ischemia. *Trends Cardiovasc Med* **15**, 163–169 (2005).

177. Halliwell, B. Reactive species and antioxidants. Redox biology is a fundamental theme of aerobic life. *Plant Physiol* **141**, 312–322 (2006).

178. Frangogiannis, N. G. *et al.* Resident Cardiac Mast Cells Degranulate and Release Preformed TNF-α, Initiating the Cytokine Cascade in Experimental Canine Myocardial Ischemia/Reperfusion. *Circulation* **98**, 699–710 (1998).

179. Ma, Y. *et al.* Temporal neutrophil polarization following myocardial infarction. *Cardiovasc Res* **110**, 51–61 (2016).

180. Lai, S.-L. *et al.* Reciprocal analyses in zebrafish and medaka reveal that harnessing the immune response promotes cardiac regeneration. *Developmental Biology. eLife* **6**, 25605–25630 (2017).

181. Fedrowitz, M. & Löscher, W. Gene expression in the mammary gland tissue of female Fischer 344 and Lewis rats after magnetic field exposure (50 Hz, 100 μT) for 2 weeks. *Int J Radiat Biol* **88**, 425–429 (2012).

182. Lupke, M. *et al.* Gene expression analysis of ELF-MF exposed human monocytes indicating the involvement of the alternative activation pathway. *Biochimica et Biophysica Acta (BBA) - Molecular Cell Research* **1763**, 402–412 (2006).

183. Chen, G., Lu, D., Chiang, H., Leszczynski, D. & Xu, Z. Using model organism Saccharomyces cerevisiae to evaluate the effects of ELF-MF and RF-EMF exposure on global gene expression. *Bioelectromagnetics* **33**, 550–560 (2012).

184. Huwiler, S. G. *et al.* Genome-wide transcription analysis of Escherichia coli in response to extremely low-frequency magnetic fields. *Bioelectromagnetics* **33**, 488–496 (2012).

185. Zhao, M. *et al.* Electrical signals control wound healing through phosphatidylinositol-3-OH kinase-γ and PTEN. *Nature* **442**, 457–460 (2006).

186. Shiurba, R. *et al.* Evidence that far-infrared radiation promotes growth of Xenopus laevis. *Advances in Space Research* **23**, 2041–2044 (1999).

187. Tokalov, S. v. & Gutzeit, H. O. The heat shock-induced cell cycle arrest is attenuated by weak electromagnetic fields. *Cell Prolif* **36**, 101–111 (2003).

188. Xu, S. *et al.* Cell type-dependent induction of DNA damage by 1800 MHz radiofrequency electromagnetic fields does not result in significant cellular dysfunctions. *PLoS One* **8**, 54906–54915 (2013).

189. Schuermann, D. & Mevissen, M. Manmade Electromagnetic Fields and Oxidative Stress—Biological Effects and Consequences for Health. *Int J Mol Sci* **22**, 3772–3805 (2021).

190. Powell, R. J. & Hill, R. T. Rapid Aggregation of Biofuel-Producing Algae by the Bacterium Bacillus sp. Strain RP1137. *Appl Environ Microbiol* **79**, 6093–6101 (2013).

191. Xu, L., Weathers, P. J., Xiong, X.-R. & Liu, C.-Z. Microalgal bioreactors: Challenges and opportunities. *Eng Life Sci* **9**, 178–189 (2009).

192. Vian, A. *et al.* Plants Respond to GSM-Like Radiations. *Plant Signal Behav* **2**, 522–524 (2007).

193. Roux, D. *et al.* Electromagnetic fields (900 MHz) evoke consistent molecular responses in tomato plants. *Physiol Plant* **128**, 283–288 (2006).

194. Tkalec, M., Malarić, K. & Pevalek-Kozlina, B. Exposure to radiofrequency radiation induces oxidative stress in duckweed Lemna minor L. *Science of The Total Environment* **388**, 78–89 (2007).

195. Tkalec, M., Malarić, K. & Pevalek-Kozlina, B. Influence of 400, 900, and 1900 MHz electromagnetic fields onLemna minor growth and peroxidase activity. *Bioelectromagnetics* **26**, 185–193 (2005).

196. Sharma, V. P., Singh, H. P., Batish, D. R. & Kohli, R. K. Cell Phone Radiations Affect Early Growth of Vigna radiata (Mung Bean) through Biochemical Alterations. *Zeitschrift für Naturforschung C* **65**, 66–72 (2010).

197. Jinapang, P., Prakob, P., Wongwattananard, P., Islam, N. E. & Kirawanich, P. Growth characteristics of mung beans and water convolvuluses exposed to 425-MHz electromagnetic fields. *Bioelectromagnetics* **31**, 519–527 (2010).

198. Senavirathna, M. D. H. J. & Asaeda, T. Radio-frequency electromagnetic radiation alters the electric potential of Myriophyllum aquaticum. *Biol Plant* **58**, 355–362 (2014).

199. Sharma, V. P., Singh, H. P., Kohli, R. K. & Batish, D. R. Mobile phone radiation inhibits Vigna radiata (mung bean) root growth by inducing oxidative stress. *Science of The Total Environment* **407**, 5543–5547 (2009).

200. Surducan E., Surducan V., Butiuc-Keul A. & Halgamagy A. Microwaves irradiation experiments on biological samples. *Studia Univesitas Babes-Bolyai Biologia* **58**, 83–98 (2013).

201. Senavirathna, M. D. H. J., Asaeda, T., Thilakarathne, B. L. S. & Kadono, H. Nanometer-scale elongation rate fluctuations in the Myriophyllum aquaticum (Parrot feather) stem were altered by radio-frequency electromagnetic radiation. *Plant Signal Behav* **9**, 28590–28597 (2014).

202. Chen, Y.-P., Jia, J.-F. & Han, X.-L. Weak microwave can alleviate water deficit induced by osmotic stress in wheat seedlings. *Planta* **229**, 291–298 (2009).

203. Soran, M.-L., Stan, M., Niinemets, Ü. & Copolovici, L. Influence of microwave frequency electromagnetic radiation on terpene emission and content in aromatic plants. *J Plant Physiol* **171**, 1436–1443 (2014).

204. Singh, H. P., Sharma, V. P., Batish, D. R. & Kohli, R. K. Cell phone electromagnetic field radiations affect rhizogenesis through impairment of biochemical processes. *Environ Monit Assess* **184**, 1813–1821 (2012).

205. Halgamuge, M. N., Yak, S. K. & Eberhardt, J. L. Reduced growth of soybean seedlings after exposure to weak microwave radiation from GSM 900 mobile phone and base station. *Bioelectromagnetics* **36**, 87–95 (2015).

206. Mohsenzadeh, H. Z. Electromagnetic Waves from GSM Mobile Phone Simulator and Abiotic Stress in Zea mays L. *J Nutr Food Sci* **11**, 1–5 (2015).

207. Radic, S., Cvjetko, P., Malaric, K., Tkalec, M. & Pevalek-Kozlina, B. Radio frequency electromagnetic field (900 MHz) induces oxidative damage to DNA and biomembrane in tobacco shoot cells (Nicotiana tabacum). in *2007 IEEE/MTT-S International Microwave Symposium* 2213–2216 (IEEE, 2007). doi:10.1109/MWSYM.2007.380400.

208. Afzal, M. & Mansoor, S. Effect of mobile phone radiations on morphological and biochemical parameters of mung bean (Vigna radiata) and wheat (Triticum aestivum) seedlings. *Asian Journal of Agricultural Sciences* **4**, 149–152 (2012).

209. Kouzmanova, M., Dimitrova, M., Dragolova, D., Atanasova, G. & Atanasov, N. Alterations in Enzyme Activities in Leaves after Exposure of *Plectranthus Sp.* Plants to 900 MHZ Electromagnetic Field. *Biotechnology & Biotechnological Equipment* **23**, 611–615 (2009).

210. Kumar, A., Singh, H. P., Batish, D. R., Kaur, S. & Kohli, R. K. EMF radiations (1800 MHz)-inhibited early seedling growth of maize (Zea mays) involves alterations in starch and sucrose metabolism. *Protoplasma* **253**, 1043–1049 (2016).

211. Lichtenthaler, H. K. & Buschmann, C. Extraction of phtosynthetic tissues: chlorophylls and carotenoids. Current protocols in food analytical chemistry. **1**, F4.3.1-F4.3.8 (2001).

212. Carl Roth Imprint. *ROTI®Nanoquant. Protein quantitation assay for low amount of protein. https://www.carlroth.com/medias/BA-K880-EN.pdf?context=bWFzdGVyfGluc3RydWN0aW9uc3w2ODA2NDd8YXBwbGljYXRpb2 4vcGRmfGluc3RydWN0aW9ucy9oMzEva2E0aGQxLzkwMzg2MTU2NDIxNDIucGRmfGZlN*

*ThkYWE0MjNiNTI3ZDRjZGIzODE5MzExOWEyOTZmYjdhOGM4NmNjNDAyMDRkO
GJhODcyOTMxYWFiYzcxZTM.* (2021).

213. Brányiková, I. *et al.* Microalgae-novel highly efficient starch producers. *Biotechnol Bioeng* **108**, 766–776 (2011).

214. Oren, R. *et al.* Performance of two Picea abies (L.) Karst. stands at different stages of decline. *Oecologia* **75**, 25–37 (1988).

215. Fernandes, B. *et al.* Starch determination in Chlorella vulgaris: A comparison between acid and enzymatic methods. *J Appl Phycol* **24**, 1203–1208 (2012).

9. Appendices

9.1 Gas saturation determination in gas infused E3 and BBM medium
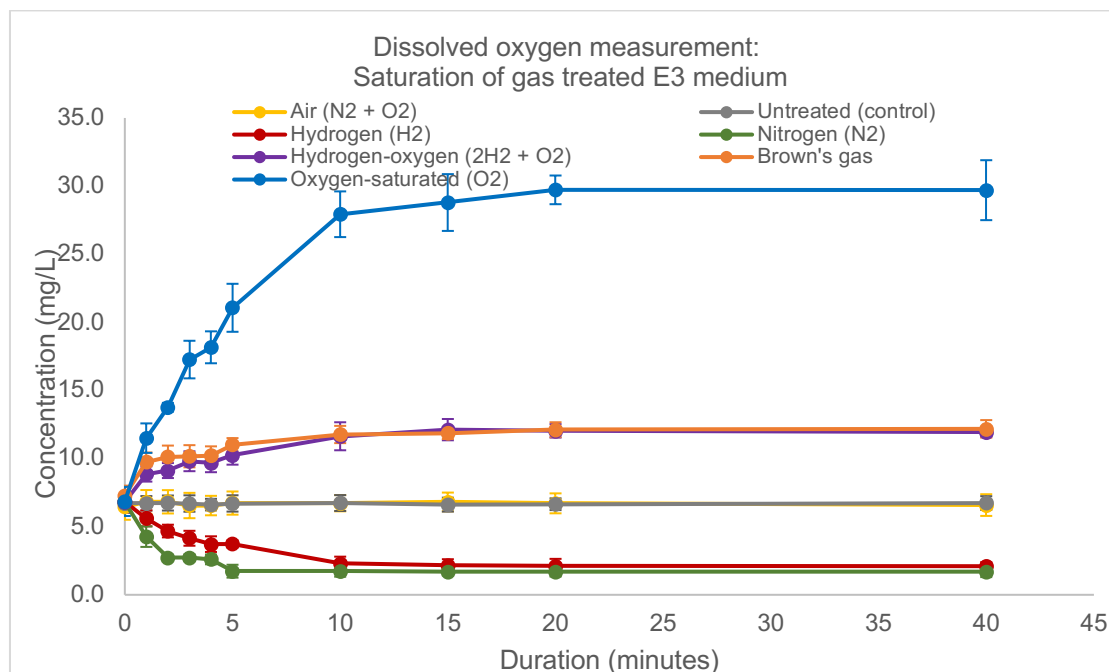
Fig. S1: Saturation curve for dissolved oxygen concentration of gas infused E3 medium.
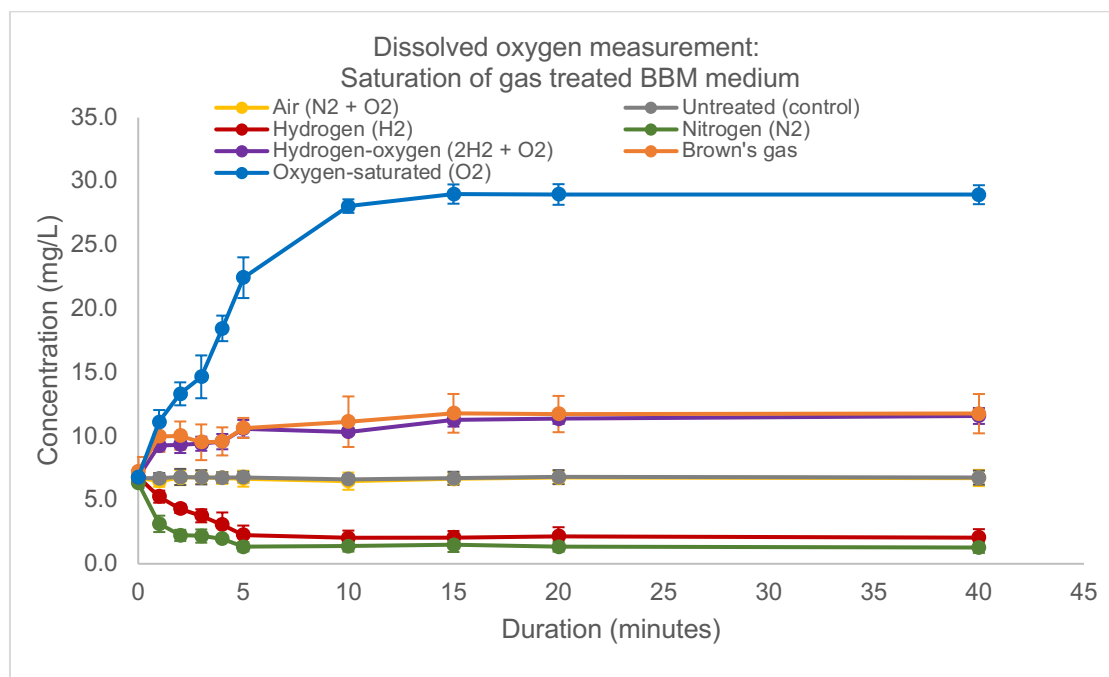
Fig. S2: Saturation curve for dissolved oxygen concentration of gas infused BBM medium.
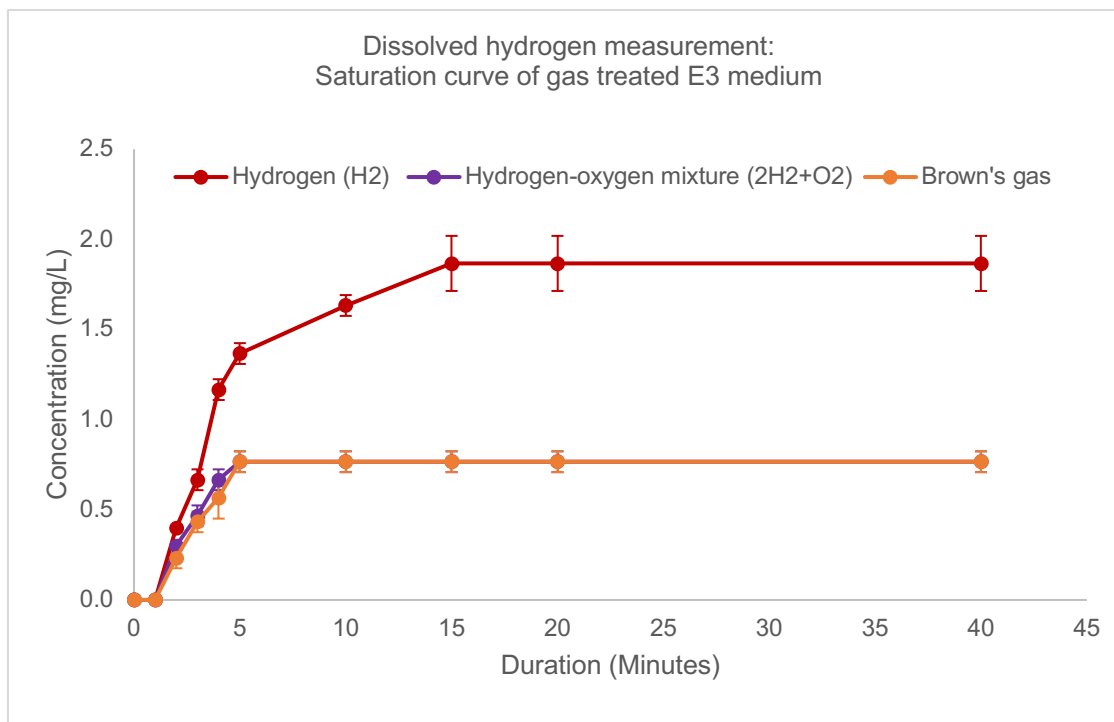
Fig. S3: Saturation curve for dissolved hydrogen concentration of gas infused E3 medium.
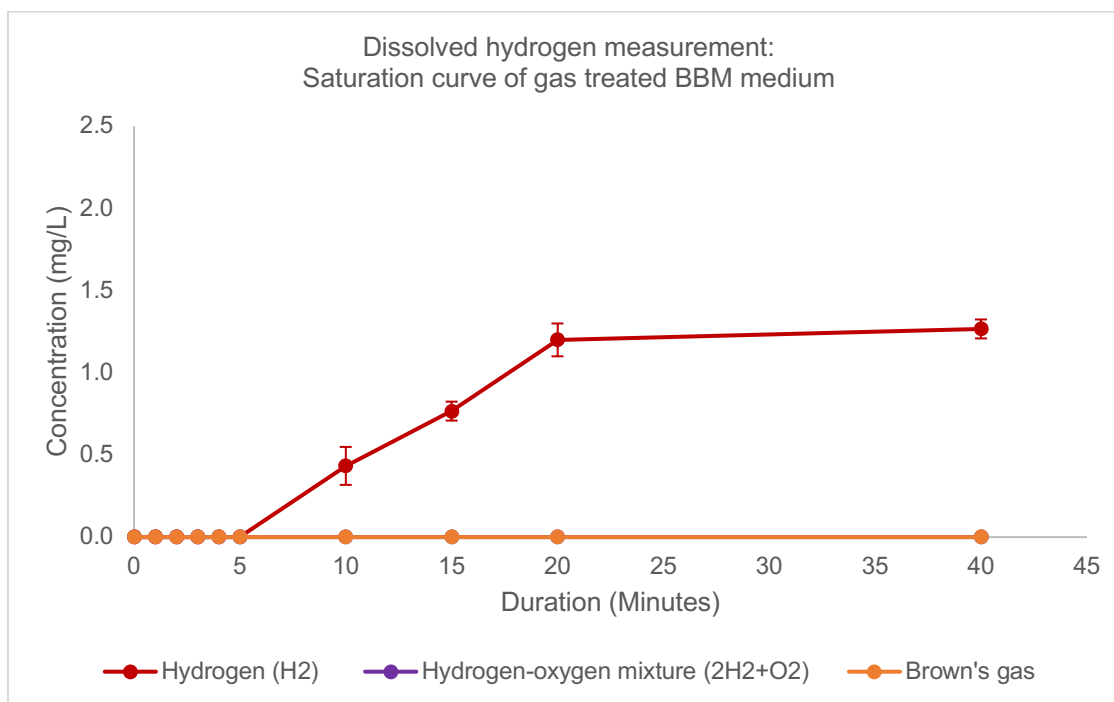
Fig. S4: Saturation curve for dissolved hydrogen concentration of gas infused BBM medium.
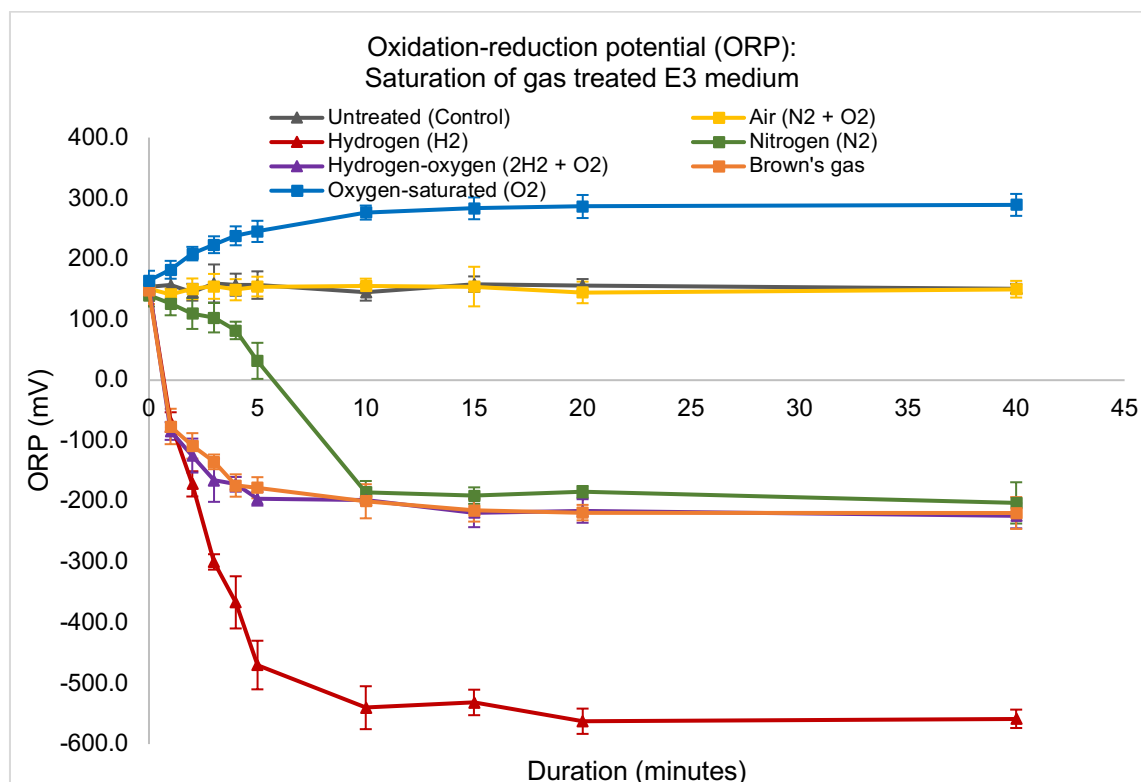
Fig. S5: Oxidation-reduction potential (ORP) of gases achieving saturation in gas infused E3 medium
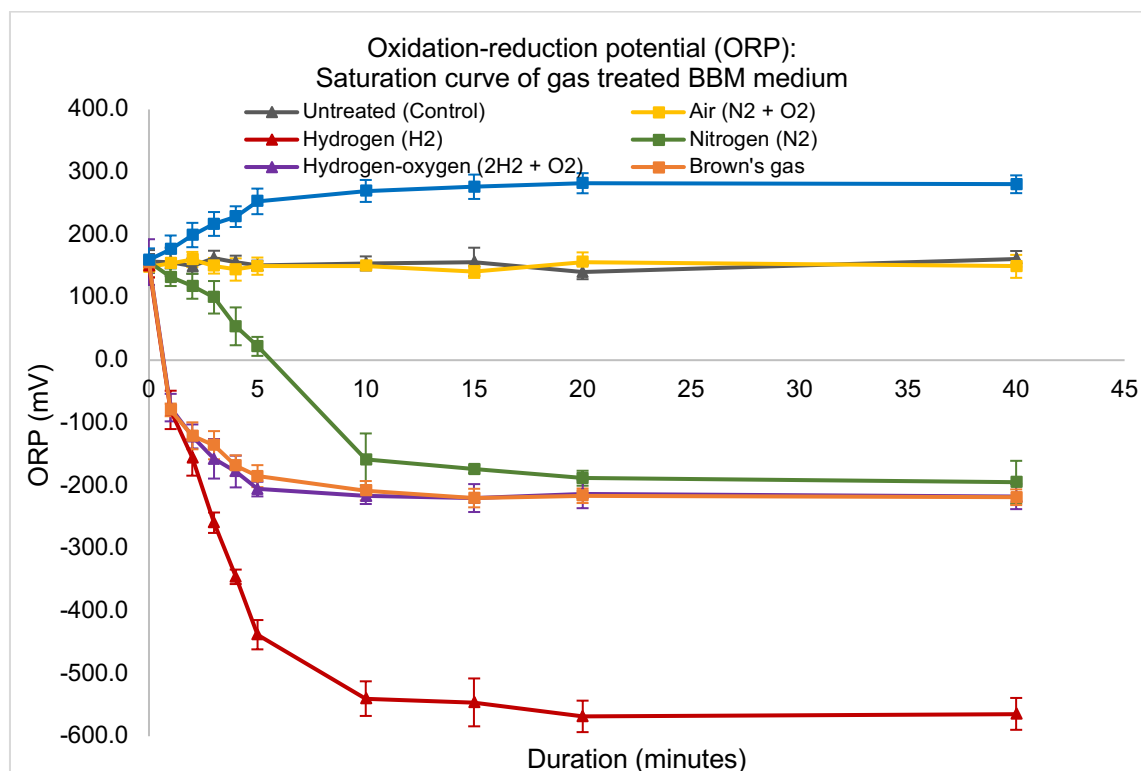
Fig. S6: Oxidation-reduction potential (ORP) of gases achieving saturation in gas infused BBM medium

9.2 Gas desaturation determination in gas infused E3 and BBM medium
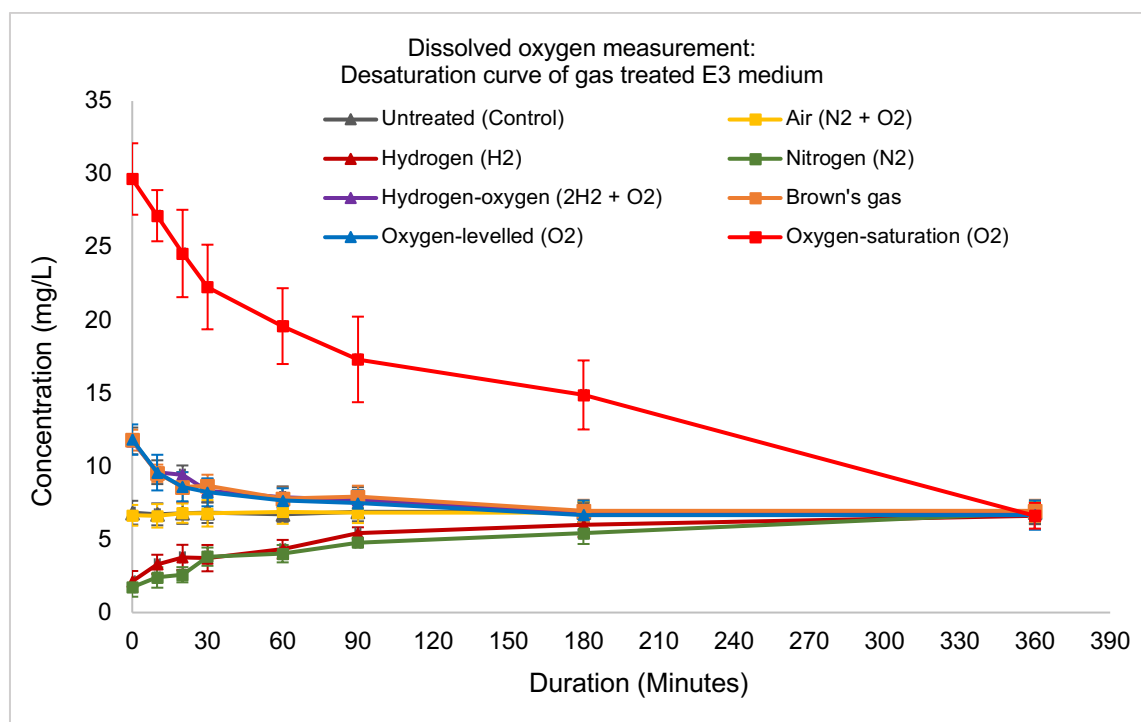
Fig. S7: Desaturation curve for dissolved oxygen concentration of gas infused E3 medium.
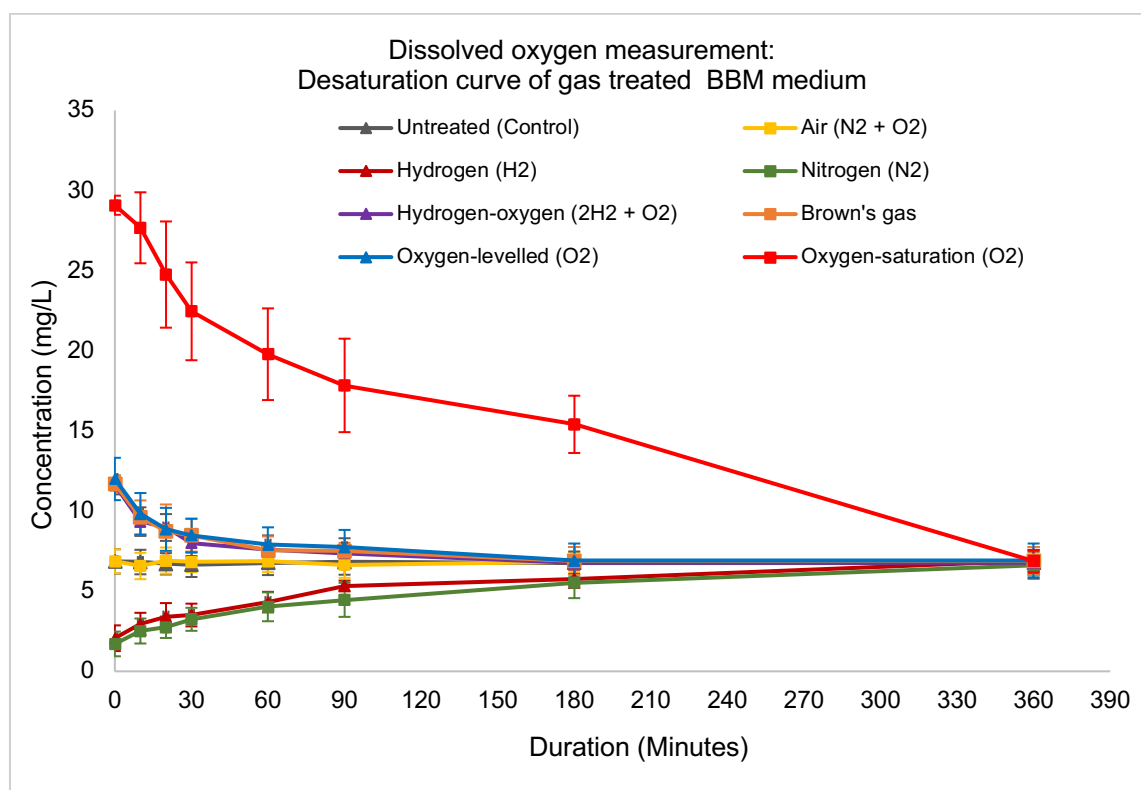
Fig. S8: Desaturation curve for dissolved oxygen concentration of gas infused BBM medium.
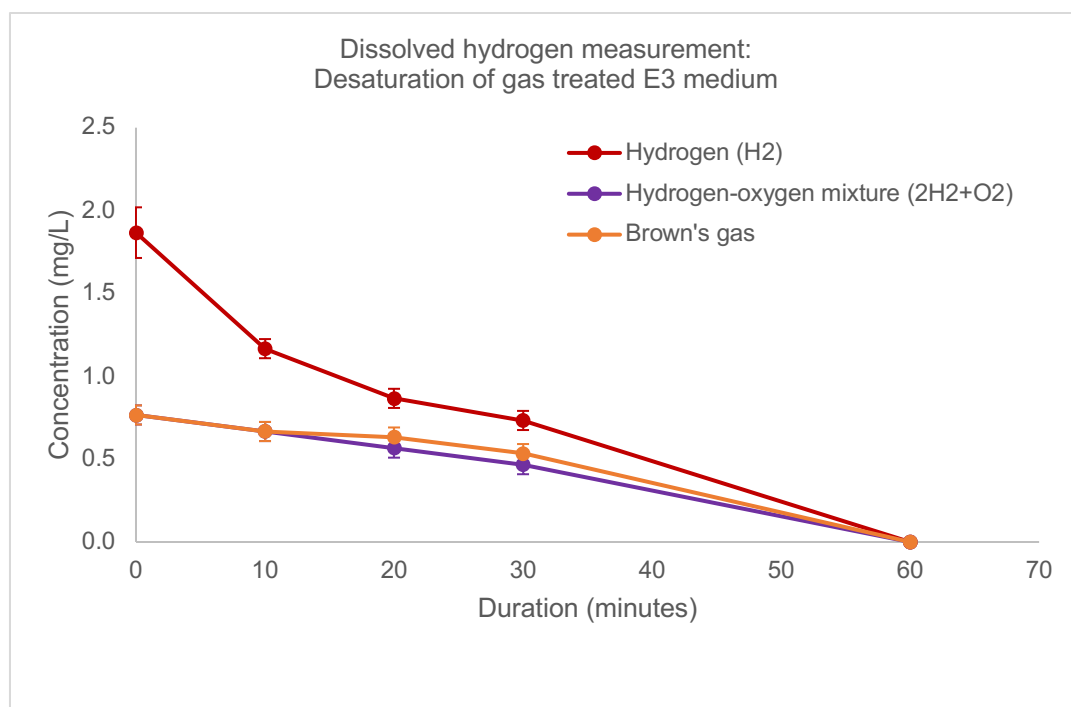
Fig. S9: Desaturation curve for dissolved hydrogen concentration of gas infused E3 medium.
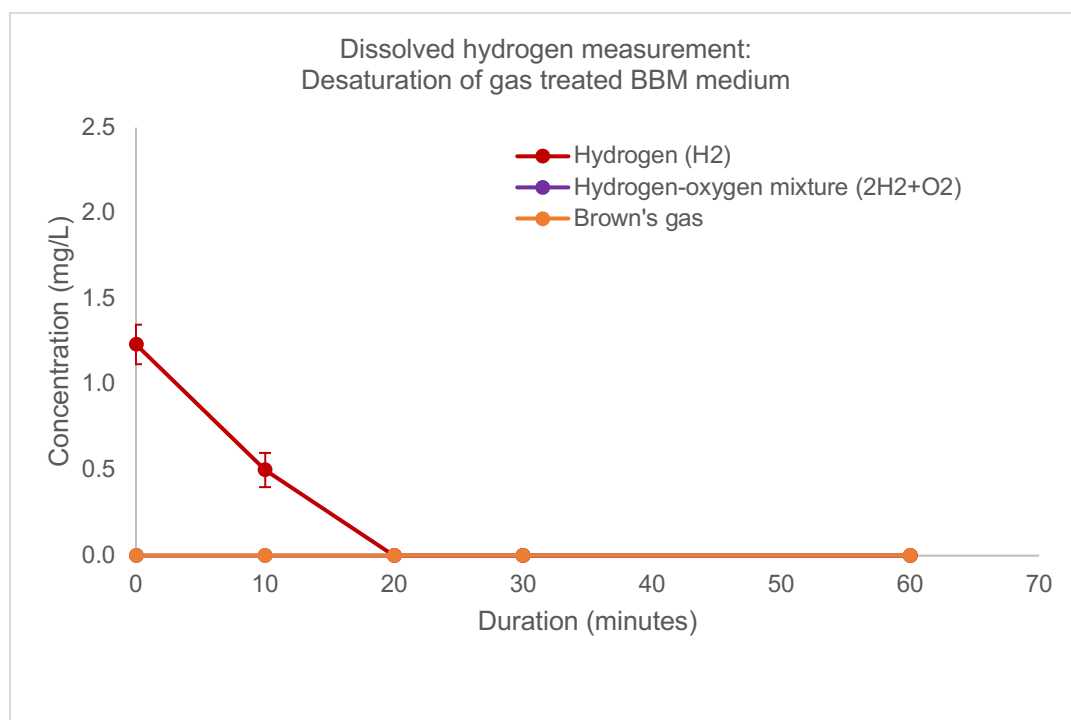
Fig. S10: Desaturation curve for dissolved hydrogen concentration of gas infused BBM medium.
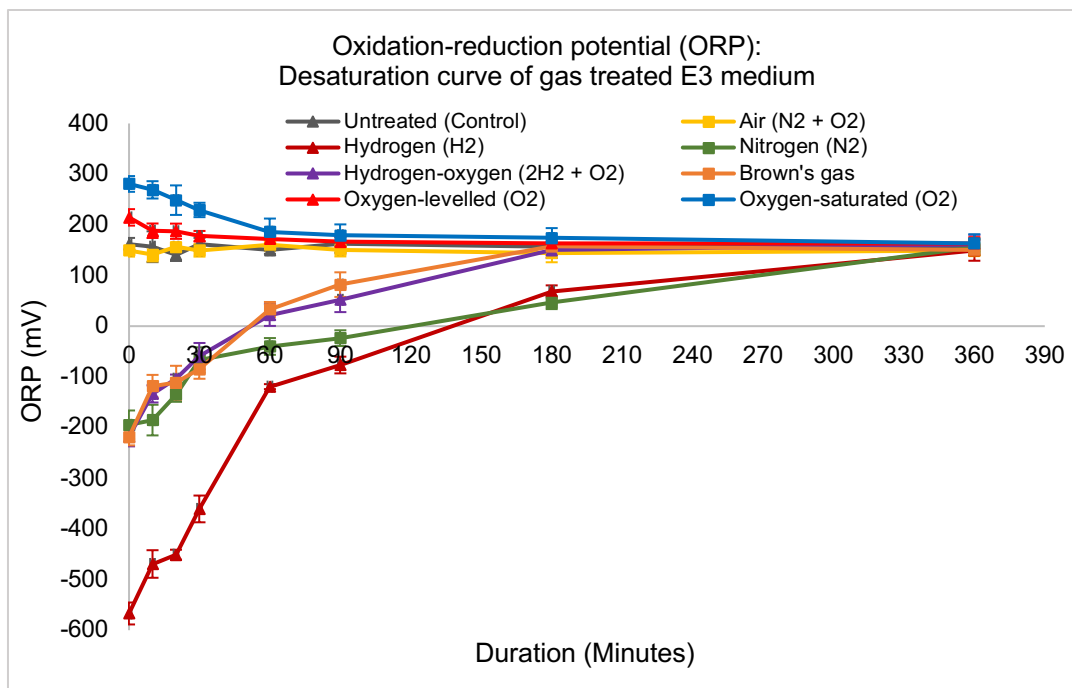
Fig. S11: Oxidation-reduction potential (ORP) of desaturation of E3 medium
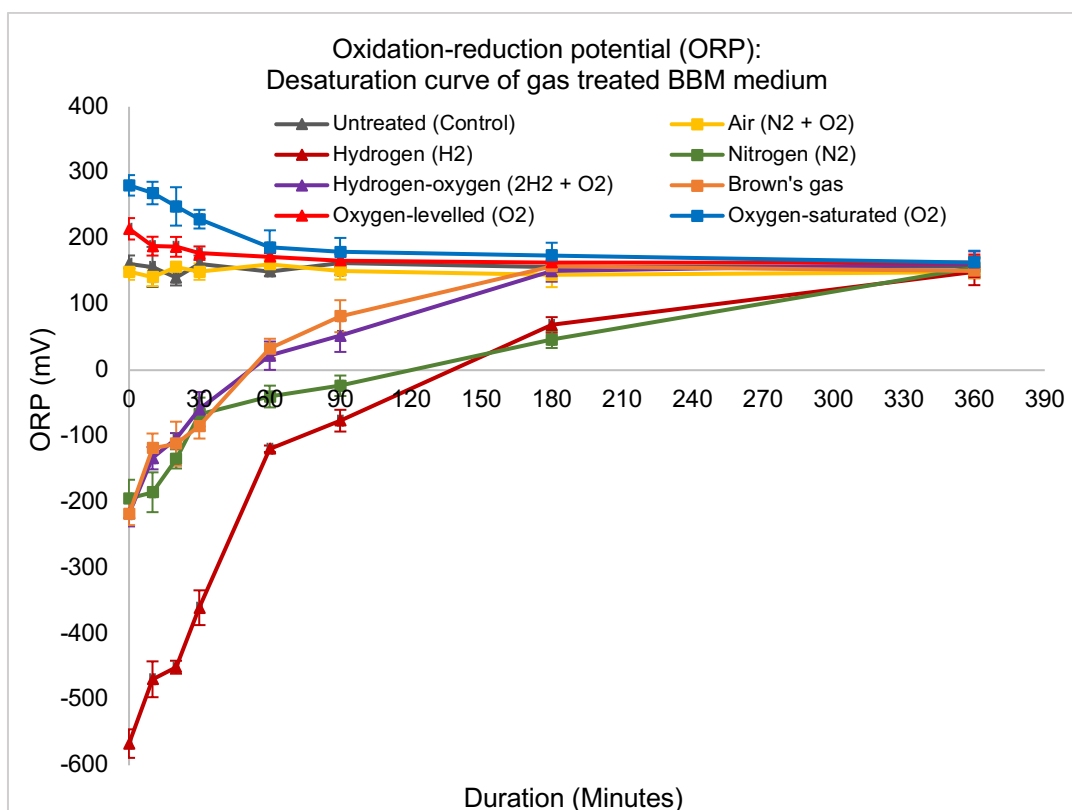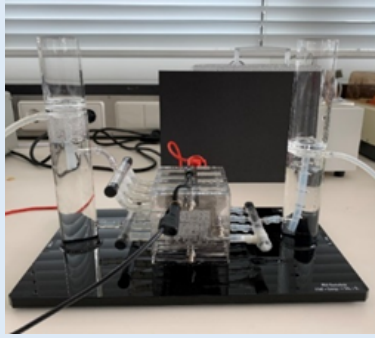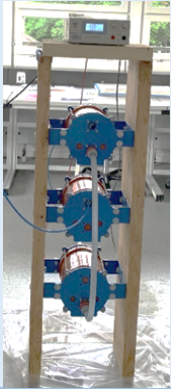
Fig. S12: Oxidation-reduction potential (ORP) of desaturation of E3 medium

9.3 The additional devices used for the comparison study

Table S1: The different types of electrolysis devices.
The concentration of O_2, concentration of H_2 and the ORP values of treated medium is shown here together with the producing devices. (Dissolved hydrogen, DH; dissolved oxygen, DO; oxidation-reduction potential, ORP)

Instruments/devices	Images	Medium analysis
Proton exchange membrane (PEM) water electrolysis Provides: hydrogen (H_2) and oxygen (O_2)		H_2 saturated medium DH: 1.5 mg/L, 0.74 mM DO: 2.0 - 2.3 mg/L, 0.06 - 0.07 mM ORP: - 475 mV O_2 saturated medium DH: 0 mg/L DO: 29.0 mg/L, 0.91 mM ORP: +290 mV $2H_2 + O_2$ saturated medium DH: 0.8 mg/L, 0.40 mM DO: 11.7 mg/L, 0.37 mM ORP: -206 mV
Proton exchange membrane (PEM) water electrolysis Provides: hydrogen (H_2) and oxygen (O_2)		H_2 saturated medium DH: 1.6 - 2.0 mg/L, 0.79 - 1.0 mM DO: 2.0 mg/L, 0.06 mM ORP: - 560 mV O_2 saturated medium DH: 0 mg/L DO: 29.0 mg/L, 0.91 mM ORP: +290 mV $2H_2 + O_2$ saturated medium DH: 0.8 mg/L, 0.40 mM DO: 11.7 mg/L, 0.37 mM ORP: -206 mV
Alkaline water electrolysis with intercalated electrodes Provides: Brown's gas		Brown's gas saturated medium DH: 0.8 mg/L, 0.40 mM DO: 11.7 mg/L, 0.37 mM ORP: -219 mV

9.4 Bioactive compound analysis of *Chlorella vulgaris* cell culture by gas direct treatment: Chlorophyll, protein and starch content
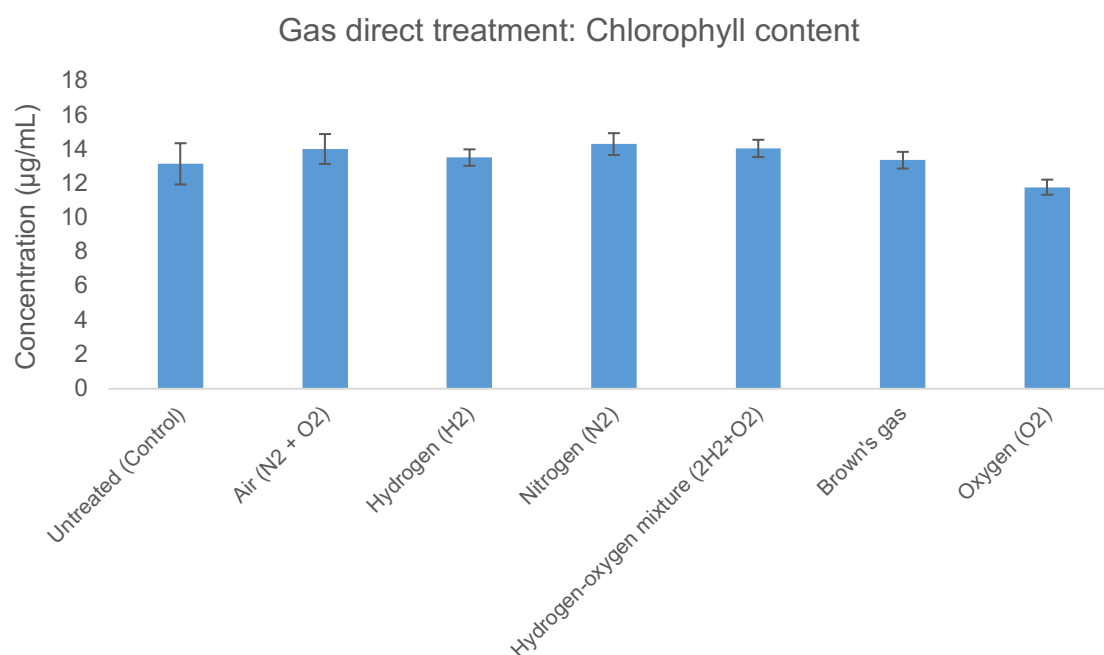
Fig. S13: Chlorophyll quantification of direct-gas treated *Chlorella vulgaris* culture.
The different gas treated cell cultures harvested and absorbance measured at OD_{665} and OD_{652} to confirm the chlorophyll content in *Chlorella vulgaris* cell culture. The value expressed by Mean ± S.D.
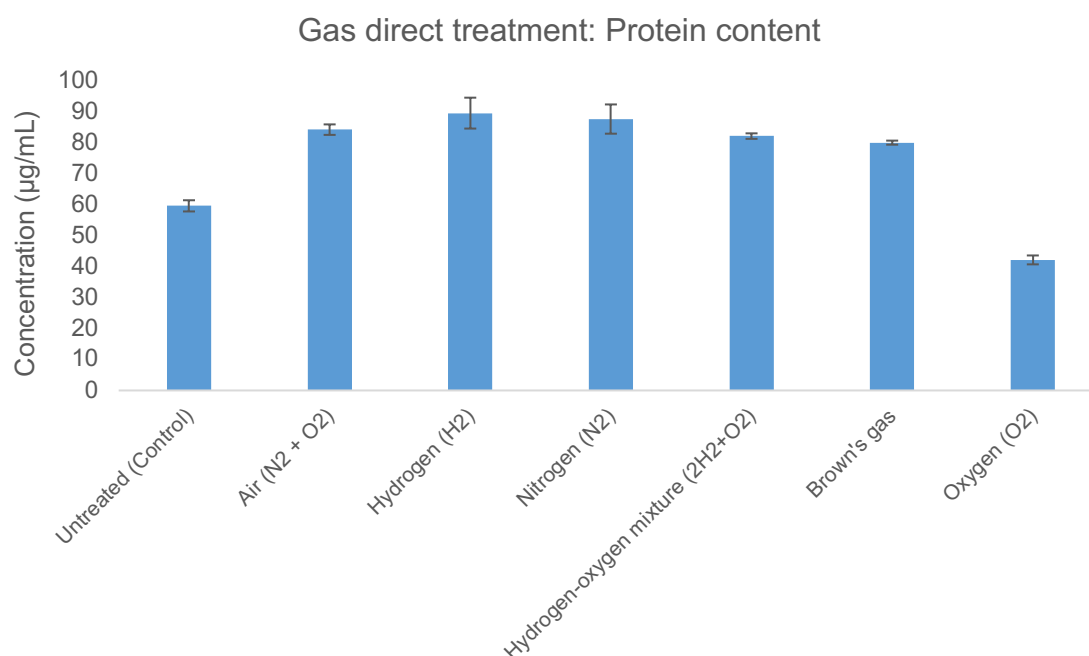
Fig. S14: Protein quantification of direct-gas treated *Chlorella vulgaris* culture.
The different gas treated cell cultures harvested and absorbance measured at OD_{590}/OD_{450} and compared with BSA standard curve to confirm the protein content in *Chlorella vulgaris* cell culture. The value expressed by Mean ± S.D.
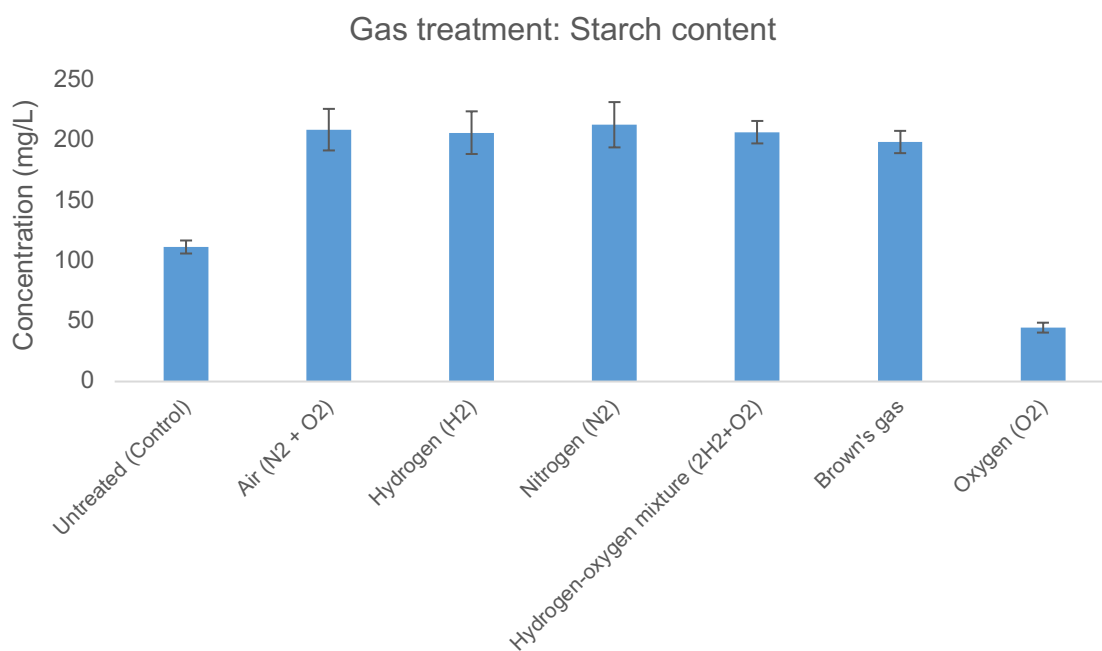
Fig. S15: Starch quantification of direct-gas treated *Chlorella vulgaris* culture.
The different gas treated cell culture harvested and absorbance measured at OD_{625} and compared with starch standard curve to confirm the starch content in *Chlorella vulgaris* cell culture. The value expressed by Mean ± S.D.

9.5   Statistical analyses data

The statistical analyses were carried out using SPSS26. Data were analysed using Welch's t-test of One-Way ANOVA. Post-Hoc multiple comparison with Gomes-Howell test. Data analysed by the mean difference is significant at the 0.05 level. The *p*-value for each analysis presented here.

Air and Untreated: Intact and Amputated fin growth analysis

ANOVA

		Sum of Squares	df	Mean Square	F	Sig.
Intact-fin (Fin area difference (µm^2))	Between Groups	139920.500	1	139920.500	.005	.946
	Within Groups	165301179	6	27550196.6		
	Total	165441100	7			
Amputated-fin (Fin area difference (µm^2))	Between Groups	147968.000	1	147968.000	.005	.946
	Within Groups	179989158	6	29998193.0		
	Total	180137126	7			

Descriptives

		N	Mean	Std. Deviation	Std. Error	95% Confidence Interval for Mean Lower Bound	95% Confidence Interval for Mean Upper Bound	Minimum	Maximum
Intact-fin (Fin area difference (µm^2))	Air (N2 + O2)	4	20425.75	6012.643	3006.322	10858.29	29993.21	16359	29345
	Untreated	4	20690.25	4352.989	2176.495	13763.67	27616.83	16249	26150
	Total	8	20558.00	4861.527	1718.809	16493.66	24622.34	16249	29345
Amputated-fin (Fin area difference (µm^2))	Air (N2 + O2)	4	36412.5000	4726.14843	2363.07422	28892.1432	43932.8568	32129.00	41804.00
	Untreated	4	36140.5000	6136.76682	3068.38341	26375.5346	45905.4654	30933.00	44592.00
	Total	8	36276.5000	5072.85670	1793.52569	32035.4857	40517.5143	30933.00	44592.00

Air and Untreated: Neutrophil count analysis

ANOVA

		Sum of Squares	df	Mean Square	F	Sig.
Neutrophil count 0.5 hpa	Between Groups	1.966	1	1.966	.262	.627
	Within Groups	45.079	6	7.513		
	Total	47.045	7			
Neutrophil count 3 hpa	Between Groups	4.205	1	4.205	4.137	.088
	Within Groups	6.098	6	1.016		
	Total	10.303	7			
Neutrophil count 24 hpa	Between Groups	.700	1	.700	.359	.571
	Within Groups	11.711	6	1.952		
	Total	12.411	7			
Neutrophil count 48 hpa	Between Groups	.018	1	.018	.015	.907
	Within Groups	7.409	6	1.235		
	Total	7.428	7			

Descriptives

		N	Mean	Std. Deviation	Std. Error	95% Confidence Interval for Mean Lower Bound	Upper Bound	Minimum	Maximum
Neutrophil count 0.5 hpa	Air (N2 + O2)	4	4.4475	2.90499	1.45250	-.1750	9.0700	2.13	8.69
	Untreated	4	3.4560	2.56657	1.28329	-.6280	7.5400	1.00	6.89
	Total	8	3.9518	2.59243	.91656	1.7844	6.1191	1.00	8.69
Neutrophil count 3 hpa	Air (N2 + O2)	4	6.5868	.11272	.05636	6.4074	6.7661	6.50	6.75
	Untreated	4	8.0368	1.42125	.71062	5.7752	10.2983	6.89	10.11
	Total	8	7.3118	1.21320	.42893	6.2975	8.3260	6.50	10.11
Neutrophil count 24 hpa	Air (N2 + O2)	4	3.6843	1.40850	.70425	1.4430	5.9255	2.38	5.63
	Untreated	4	4.2758	1.38555	.69277	2.0710	6.4805	2.56	5.44
	Total	8	3.9800	1.33152	.47076	2.8668	5.0932	2.38	5.63
Neutrophil count 48 hpa	Air (N2 + O2)	4	3.8315	1.10741	.55370	2.0694	5.5936	2.25	4.81
	Untreated	4	3.7355	1.11509	.55754	1.9612	5.5098	2.44	5.17
	Total	8	3.7835	1.03010	.36420	2.9223	4.6447	2.25	5.17

Air, Nitrogen, Oxygen-levelled and Oxygen-saturated: Intact and Amputated fin growth analysis

Multiple Comparisons

Games-Howell

Dependent Variable	(I) Treatment	(J) Treatment	Mean Difference (I-J)	Std. Error	Sig.	95% Confidence Interval Lower Bound	Upper Bound
Intact-fin (Fin area difference (μm^2))	Air (N2 + O2)	Nitrogen (N2)	9598.000*	707.254	<.001	7023.83	12172.17
		O2-levelled (O2)	3104.500	1058.547	.105	-728.95	6937.95
		O2-saturated (O2)	5249.250*	949.014	.007	1911.30	8587.20
	Nitrogen (N2)	Air (N2 + O2)	-9598.000*	707.254	<.001	-12172.17	-7023.83
		O2-levelled (O2)	-6493.500*	960.245	.008	-10341.53	-2645.47
		O2-saturated (O2)	-4348.750*	837.959	.017	-7569.00	-1128.50
	O2-levelled (O2)	Air (N2 + O2)	-3104.500	1058.547	.105	-6937.95	728.95
		Nitrogen (N2)	6493.500*	960.245	.008	2645.47	10341.53
		O2-saturated (O2)	2144.750	1149.995	.335	-1871.16	6160.66
	O2-saturated (O2)	Air (N2 + O2)	-5249.250*	949.014	.007	-8587.20	-1911.30
		Nitrogen (N2)	4348.750*	837.959	.017	1128.50	7569.00
		O2-levelled (O2)	-2144.750	1149.995	.335	-6160.66	1871.16
Amputated-fin (Fin area difference (μm^2))	Air (N2 + O2)	Nitrogen (N2)	14230.2500*	1649.26064	.008	6585.8616	21874.6384
		O2-levelled (O2)	7917.00000*	1764.50067	.036	774.8769	15059.1231
		O2-saturated (O2)	9811.75000*	1788.71212	.016	2716.8695	16906.6305
	Nitrogen (N2)	Air (N2 + O2)	-14230.250*	1649.26064	.008	-21874.6384	-6585.8616
		O2-levelled (O2)	-6313.2500*	746.12386	.004	-9349.9852	-3276.5148
		O2-saturated (O2)	-4418.5000*	801.70397	.020	-7744.0594	-1092.9406
	O2-levelled (O2)	Air (N2 + O2)	-7917.0000*	1764.50067	.036	-15059.1231	-774.8769
		Nitrogen (N2)	6313.25000*	746.12386	.004	3276.5148	9349.9852
		O2-saturated (O2)	1894.75000	1017.90531	.334	-1636.6272	5426.1272
	O2-saturated (O2)	Air (N2 + O2)	-9811.7500*	1788.71212	.016	-16906.6305	-2716.8695
		Nitrogen (N2)	4418.50000*	801.70397	.020	1092.9406	7744.0594
		O2-levelled (O2)	-1894.75000	1017.90531	.334	-5426.1272	1636.6272

*. The mean difference is significant at the 0.05 level.

Air, Nitrogen, Oxygen-levelled and Oxygen-saturated: Neutrophil count analysis

Multiple Comparisons

Games–Howell

Dependent Variable	(I) Treatment	(J) Treatment	Mean Difference (I–J)	Std. Error	Sig.	95% Confidence Interval Lower Bound	95% Confidence Interval Upper Bound
Neutrophil count 0.5 hpa	Air (N2 + O2)	Nitrogen (N2)	−1.74450	2.00887	.821	−9.0242	5.5352
		O2–levelled (O2)	−.63825	2.01011	.988	−7.9194	6.6429
		O2–saturated (O2)	−3.85725	2.00353	.322	−11.1307	3.4162
	Nitrogen (N2)	Air (N2 + O2)	1.74450	2.00887	.821	−5.5352	9.0242
		O2–levelled (O2)	1.10625	1.58443	.894	−4.3786	6.5911
		O2–saturated (O2)	−2.11275	1.57607	.573	−7.5688	3.3433
	O2–levelled (O2)	Air (N2 + O2)	.63825	2.01011	.988	−6.6429	7.9194
		Nitrogen (N2)	−1.10625	1.58443	.894	−6.5911	4.3786
		O2–saturated (O2)	−3.21900	1.57766	.272	−8.6806	2.2426
	O2–saturated (O2)	Air (N2 + O2)	3.85725	2.00353	.322	−3.4162	11.1307
		Nitrogen (N2)	2.11275	1.57607	.573	−3.3433	7.5688
		O2–levelled (O2)	3.21900	1.57766	.272	−2.2426	8.6806
Neutrophil count 3 hpa	Air (N2 + O2)	Nitrogen (N2)	−8.75525*	1.46764	.020	−15.1950	−2.3155
		O2–levelled (O2)	−4.62850*	.49355	<.001	−6.3944	−2.8626
		O2–saturated (O2)	−7.19625	2.22161	.126	−17.4588	3.0663
	Nitrogen (N2)	Air (N2 + O2)	8.75525*	1.46764	.020	2.3155	15.1950
		O2–levelled (O2)	4.12675	1.44062	.167	−2.4679	10.7214
		O2–saturated (O2)	1.55900	2.60141	.928	−7.9445	11.0625
	O2–levelled (O2)	Air (N2 + O2)	4.62850*	.49355	<.001	2.8626	6.3944
		Nitrogen (N2)	−4.12675	1.44062	.167	−10.7214	2.4679
		O2–saturated (O2)	−2.56775	2.20386	.682	−12.9593	7.8238
	O2–saturated (O2)	Air (N2 + O2)	7.19625	2.22161	.126	−3.0663	17.4588
		Nitrogen (N2)	−1.55900	2.60141	.928	−11.0625	7.9445
		O2–levelled (O2)	2.56775	2.20386	.682	−7.8238	12.9593
Neutrophil count 24 hpa	Air (N2 + O2)	Nitrogen (N2)	−3.86675	1.66139	.248	−11.0614	3.3279
		O2–levelled (O2)	−.18225	.66397	.992	−2.4855	2.1210
		O2–saturated (O2)	−.46450	.69044	.904	−2.8546	1.9256
	Nitrogen (N2)	Air (N2 + O2)	3.86675	1.66139	.248	−3.3279	11.0614
		O2–levelled (O2)	3.68450	1.65056	.274	−3.5618	10.9308
		O2–saturated (O2)	3.40225	1.66139	.320	−3.7924	10.5969
	O2–levelled (O2)	Air (N2 + O2)	.18225	.66397	.992	−2.1210	2.4855
		Nitrogen (N2)	−3.68450	1.65056	.274	−10.9308	3.5618
		O2–saturated (O2)	−.28225	.66397	.972	−2.5855	2.0210
	O2–saturated (O2)	Air (N2 + O2)	.46450	.69044	.904	−1.9256	2.8546
		Nitrogen (N2)	−3.40225	1.66139	.320	−10.5969	3.7924
		O2–levelled (O2)	.28225	.66397	.972	−2.0210	2.5855
Neutrophil count 48 hpa	Air (N2 + O2)	Nitrogen (N2)	−2.89300*	.55428	.011	−4.8932	−.8928
		O2–levelled (O2)	.12375	.52835	.995	−1.8566	2.1041
		O2–saturated (O2)	−.83925	.54662	.482	−2.8304	1.1519
	Nitrogen (N2)	Air (N2 + O2)	2.89300*	.55428	.011	.8928	4.8932
		O2–levelled (O2)	3.01675*	.40998	.001	1.5850	4.4485
		O2–saturated (O2)	2.05375*	.43327	.013	.5529	3.5546
	O2–levelled (O2)	Air (N2 + O2)	−.12375	.52835	.995	−2.1041	1.8566
		Nitrogen (N2)	−3.01675*	.40998	.001	−4.4485	−1.5850
		O2–saturated (O2)	−.96300	.39957	.176	−2.3528	.4268
	O2–saturated (O2)	Air (N2 + O2)	.83925	.54662	.482	−1.1519	2.8304
		Nitrogen (N2)	−2.05375*	.43327	.013	−3.5546	−.5529
		O2–levelled (O2)	.96300	.39957	.176	−.4268	2.3528

*. The mean difference is significant at the 0.05 level.

Air, Hydrogen, Hydrogen-oxygen mixture and Brown's gas: Intact and Amputated fin growth analysis

Multiple Comparisons

Games–Howell

Dependent Variable	(I) Treatment	(J) Treatment	Mean Difference (I–J)	Std. Error	Sig.	95% Confidence Interval	
						Lower Bound	Upper Bound
Intact–fin (Fin area difference (µm^2))	Air (N2 + O2)	Hydrogen (H2)	−7986.000*	2524.882	.044	−15758.45	−213.55
		Brown's gas	−2791.333	2169.438	.591	−9441.53	3858.86
		Hydrogen–oxygen(H2–O2)	−2489.667	2077.439	.642	−8893.61	3914.28
	Hydrogen (H2)	Air (N2 + O2)	7986.000*	2524.882	.044	213.55	15758.45
		Brown's gas	5194.667	2425.673	.210	−2335.53	12724.87
		Hydrogen–oxygen(H2–O2)	5496.333	2343.754	.160	−1859.84	12852.51
	Brown's gas	Air (N2 + O2)	2791.333	2169.438	.591	−3858.86	9441.53
		Hydrogen (H2)	−5194.667	2425.673	.210	−12724.87	2335.53
		Hydrogen–oxygen(H2–O2)	301.667	1955.662	.999	−5692.72	6296.06
	Hydrogen–oxygen(H2–O2)	Air (N2 + O2)	2489.667	2077.439	.642	−3914.28	8893.61
		Hydrogen (H2)	−5496.333	2343.754	.160	−12852.51	1859.84
		Brown's gas	−301.667	1955.662	.999	−6296.06	5692.72
Amputated–fin (Fin area difference (µm^2))	Air (N2 + O2)	Hydrogen (H2)	−12575.667*	2031.28095	<.001	−18985.7492	−6165.5841
		Brown's gas	−5189.66667	2230.86499	.172	−12350.9058	1971.5725
		Hydrogen–oxygen(H2–O2)	−5263.33333	2156.28958	.145	−12141.9715	1615.3049
	Hydrogen (H2)	Air (N2 + O2)	12575.6667*	2031.28095	<.001	6165.5841	18985.7492
		Brown's gas	7386.00000	2584.30854	.070	−543.5998	15315.5998
		Hydrogen–oxygen(H2–O2)	7312.33333	2520.21364	.065	−407.3915	15032.0581
	Brown's gas	Air (N2 + O2)	5189.66667	2230.86499	.172	−1971.5725	12350.9058
		Hydrogen (H2)	−7386.00000	2584.30854	.070	−15315.5998	543.5998
		Hydrogen–oxygen(H2–O2)	−73.66667	2683.67903	1.000	−8287.0649	8139.7315
	Hydrogen–oxygen(H2–O2)	Air (N2 + O2)	5263.33333	2156.28958	.145	−1615.3049	12141.9715
		Hydrogen (H2)	−7312.33333	2520.21364	.065	−15032.0581	407.3915
		Brown's gas	73.66667	2683.67903	1.000	−8139.7315	8287.0649

*. The mean difference is significant at the 0.05 level.

Air, Hydrogen, Hydrogen-oxygen mixture and Brown's gas: Neutrophil count analysis

Multiple Comparisons

Games–Howell

Dependent Variable	(I) Treatment	(J) Treatment	Mean Difference (I–J)	Std. Error	Sig.	95% Confidence Interval Lower Bound	95% Confidence Interval Upper Bound
Neutrophil count 0.5 hpa	Air (N2 + O2)	Hydrogen (H2)	.66667	1.13039	.933	−2.8609	4.1943
		Brown's gas	−1.00000	1.58114	.919	−5.9282	3.9282
		Hydrogen–oxygen(H2–O2)	−.16667	1.07755	.999	−3.5954	3.2621
	Hydrogen (H2)	Air (N2 + O2)	−.66667	1.13039	.933	−4.1943	2.8609
		Brown's gas	−1.66667	1.44145	.669	−6.3654	3.0321
		Hydrogen–oxygen(H2–O2)	−.83333	.85959	.769	−3.4750	1.8084
	Brown's gas	Air (N2 + O2)	1.00000	1.58114	.919	−3.9282	5.9282
		Hydrogen (H2)	1.66667	1.44145	.669	−3.0321	6.3654
		Hydrogen–oxygen(H2–O2)	.83333	1.40040	.930	−3.8348	5.5015
	Hydrogen–oxygen(H2–O2)	Air (N2 + O2)	.16667	1.07755	.999	−3.2621	3.5954
		Hydrogen (H2)	.83333	.85959	.769	−1.8084	3.4750
		Brown's gas	−.83333	1.40040	.930	−5.5015	3.8348
Neutrophil count 3 hpa	Air (N2 + O2)	Hydrogen (H2)	1.16667	1.86934	.921	−5.1050	7.4383
		Brown's gas	.50000	2.20227	.996	−6.3027	7.3027
		Hydrogen–oxygen(H2–O2)	.66667	2.32618	.991	−6.4635	7.7969
	Hydrogen (H2)	Air (N2 + O2)	−1.16667	1.86934	.921	−7.4383	5.1050
		Brown's gas	−.66667	1.54200	.971	−5.6736	4.3403
		Hydrogen–oxygen(H2–O2)	−.50000	1.71432	.991	−6.1712	5.1712
	Brown's gas	Air (N2 + O2)	−.50000	2.20227	.996	−7.3027	6.3027
		Hydrogen (H2)	.66667	1.54200	.971	−4.3403	5.6736
		Hydrogen–oxygen(H2–O2)	.16667	2.07230	1.000	−6.1929	6.5262
	Hydrogen–oxygen(H2–O2)	Air (N2 + O2)	−.66667	2.32618	.991	−7.7969	6.4635
		Hydrogen (H2)	.50000	1.71432	.991	−5.1712	6.1712
		Brown's gas	−.16667	2.07230	1.000	−6.5262	6.1929
Neutrophil count 24 hpa	Air (N2 + O2)	Hydrogen (H2)	1.33333	.98883	.556	−1.6964	4.3630
		Brown's gas	1.16667	1.03548	.683	−2.0181	4.3514
		Hydrogen–oxygen(H2–O2)	.66667	1.22020	.945	−3.1784	4.5118
	Hydrogen (H2)	Air (N2 + O2)	−1.33333	.98883	.556	−4.3630	1.6964
		Brown's gas	−.16667	1.07755	.999	−3.4672	3.1339
		Hydrogen–oxygen(H2–O2)	−.66667	1.25610	.949	−4.5835	3.2502
	Brown's gas	Air (N2 + O2)	−1.16667	1.03548	.683	−4.3514	2.0181
		Hydrogen (H2)	.16667	1.07755	.999	−3.1339	3.4672
		Hydrogen–oxygen(H2–O2)	−.50000	1.29314	.979	−4.5010	3.5010
	Hydrogen–oxygen(H2–O2)	Air (N2 + O2)	−.66667	1.22020	.945	−4.5118	3.1784
		Hydrogen (H2)	.66667	1.25610	.949	−3.2502	4.5835
		Brown's gas	.50000	1.29314	.979	−3.5010	4.5010
Neutrophil count 48 hpa	Air (N2 + O2)	Hydrogen (H2)	2.00000	.62361	.050	−.0024	4.0024
		Brown's gas	1.50000	.85959	.354	−1.1495	4.1495
		Hydrogen–oxygen(H2–O2)	1.16667	.79232	.487	−1.2590	3.5924
	Hydrogen (H2)	Air (N2 + O2)	−2.00000	.62361	.050	−4.0024	.0024
		Brown's gas	−.50000	.73409	.901	−2.9269	1.9269
		Hydrogen–oxygen(H2–O2)	−.83333	.65405	.603	−2.9519	1.2852
	Brown's gas	Air (N2 + O2)	−1.50000	.85959	.354	−4.1495	1.1495
		Hydrogen (H2)	.50000	.73409	.901	−1.9269	2.9269
		Hydrogen–oxygen(H2–O2)	−.33333	.88192	.981	−3.0414	2.3748
	Hydrogen–oxygen(H2–O2)	Air (N2 + O2)	−1.16667	.79232	.487	−3.5924	1.2590
		Hydrogen (H2)	.83333	.65405	.603	−1.2852	2.9519
		Brown's gas	.33333	.88192	.981	−2.3748	3.0414

Air, Nitrogen, Hydrogen: Intact and Amputated fin growth analysis

Multiple Comparisons

Games–Howell

Dependent Variable	(I) Treatment	(J) Treatment	Mean Difference (I–J)	Std. Error	Sig.	95% Confidence Interval	
						Lower Bound	Upper Bound
Intact–fin (Fin area difference (µm^2))	Air (N2 + O2)	Nitrogen (N2)	4094.000	1504.833	.073	−447.34	8635.34
		Hydrogen (H2)	−9652.500*	1669.881	<.001	−14369.51	−4935.49
	Nitrogen (N2)	Air (N2 + O2)	−4094.000	1504.833	.073	−8635.34	447.34
		Hydrogen (H2)	−13746.500*	1037.980	<.001	−16705.77	−10787.23
	Hydrogen (H2)	Air (N2 + O2)	9652.500*	1669.881	<.001	4935.49	14369.51
		Nitrogen (N2)	13746.500*	1037.980	<.001	10787.23	16705.77
Amputated–fin (Fin area difference (µm^2))	Air (N2 + O2)	Nitrogen (N2)	7499.83333	6222.27996	.477	−9586.4496	24586.1163
		Hydrogen (H2)	−10713.0000	7687.36326	.386	−32385.4080	10959.4080
	Nitrogen (N2)	Air (N2 + O2)	−7499.83333	6222.27996	.477	−24586.1163	9586.4496
		Hydrogen (H2)	−18212.8333	7940.10352	.108	−40357.3130	3931.6463
	Hydrogen (H2)	Air (N2 + O2)	10713.00000	7687.36326	.386	−10959.4080	32385.4080
		Nitrogen (N2)	18212.83333	7940.10352	.108	−3931.6463	40357.3130

*. The mean difference is significant at the 0.05 level.

Air, Nitrogen, Hydrogen: Neutrophil count analysis

Multiple Comparisons

Games-Howell

Dependent Variable	(I) Treatment	(J) Treatment	Mean Difference (I-J)	Std. Error	Sig.	95% Confidence Interval	
						Lower Bound	Upper Bound
Neutrophil count 0.5 hpa	Air (N2 + O2)	Nitrogen (N2)	-1.54333	1.05944	.358	-4.5492	1.4626
		Hydrogen (H2)	.07833	1.24115	.998	-3.3261	3.4827
	Nitrogen (N2)	Air (N2 + O2)	1.54333	1.05944	.358	-1.4626	4.5492
		Hydrogen (H2)	1.62167	1.01437	.297	-1.2360	4.4793
	Hydrogen (H2)	Air (N2 + O2)	-.07833	1.24115	.998	-3.4827	3.3261
		Nitrogen (N2)	-1.62167	1.01437	.297	-4.4793	1.2360
Neutrophil count 3 hpa	Air (N2 + O2)	Nitrogen (N2)	-2.12000	2.53391	.696	-9.9403	5.7003
		Hydrogen (H2)	2.84167	2.48597	.528	-5.0003	10.6836
	Nitrogen (N2)	Air (N2 + O2)	2.12000	2.53391	.696	-5.7003	9.9403
		Hydrogen (H2)	4.96167*	.89851	<.001	2.4623	7.4611
	Hydrogen (H2)	Air (N2 + O2)	-2.84167	2.48597	.528	-10.6836	5.0003
		Nitrogen (N2)	-4.96167*	.89851	<.001	-7.4611	-2.4623
Neutrophil count 24 hpa	Air (N2 + O2)	Nitrogen (N2)	-1.27000	.88697	.367	-3.7566	1.2166
		Hydrogen (H2)	.72000	1.07482	.786	-2.2286	3.6686
	Nitrogen (N2)	Air (N2 + O2)	1.27000	.88697	.367	-1.2166	3.7566
		Hydrogen (H2)	1.99000	.93023	.140	-.6377	4.6177
	Hydrogen (H2)	Air (N2 + O2)	-.72000	1.07482	.786	-3.6686	2.2286
		Nitrogen (N2)	-1.99000	.93023	.140	-4.6177	.6377
Neutrophil count 48 hpa	Air (N2 + O2)	Nitrogen (N2)	-1.38167	.78721	.234	-3.5473	.7839
		Hydrogen (H2)	1.50833	.59929	.081	-.1965	3.2132
	Nitrogen (N2)	Air (N2 + O2)	1.38167	.78721	.234	-.7839	3.5473
		Hydrogen (H2)	2.89000*	.67071	.007	.9457	4.8343
	Hydrogen (H2)	Air (N2 + O2)	-1.50833	.59929	.081	-3.2132	.1965
		Nitrogen (N2)	-2.89000*	.67071	.007	-4.8343	-.9457

*. The mean difference is significant at the 0.05 level.

Air, Oxygen-levelled, Hydrogen-oxygen mixture and Brown's gas: Intact and Amputated fin growth analysis

Multiple Comparisons

Games-Howell

Dependent Variable	(I) Treatment	(J) Treatment	Mean Difference (I-J)	Std. Error	Sig.	95% Confidence Interval	
						Lower Bound	Upper Bound
Intact-fin (Fin area difference (μm^2))	Air (N2 + O2)	Oxygen-levelled (O2)	2871.167	1764.270	.424	-2990.81	8733.14
		Brown's gas	-2791.333	2169.438	.591	-9441.53	3858.86
		Hydrogen-oxygen(H2-O2)	-2489.667	2077.439	.642	-8893.61	3914.28
	Oxygen-levelled (O2)	Air (N2 + O2)	-2871.167	1764.270	.424	-8733.14	2990.81
		Brown's gas	-5662.500*	1619.108	.037	-10963.52	-361.48
		Hydrogen-oxygen(H2-O2)	-5360.833*	1493.587	.030	-10180.03	-541.64
	Brown's gas	Air (N2 + O2)	2791.333	2169.438	.591	-3858.86	9441.53
		Oxygen-levelled (O2)	5662.500*	1619.108	.037	361.48	10963.52
		Hydrogen-oxygen(H2-O2)	301.667	1955.662	.999	-5692.72	6296.06
	Hydrogen-oxygen(H2-O2)	Air (N2 + O2)	2489.667	2077.439	.642	-3914.28	8893.61
		Oxygen-levelled (O2)	5360.833*	1493.587	.030	541.64	10180.03
		Brown's gas	-301.667	1955.662	.999	-6296.06	5692.72
Amputated-fin (Fin area difference (μm^2))	Air (N2 + O2)	Oxygen-levelled (O2)	9969.16667*	1855.96730	.002	4199.8432	15738.4901
		Brown's gas	-5189.66667	2230.86499	.172	-12350.9058	1971.5725
		Hydrogen-oxygen(H2-O2)	-5263.33333	2156.28958	.145	-12141.9715	1615.3049
	Oxygen-levelled (O2)	Air (N2 + O2)	-9969.1667*	1855.96730	.002	-15738.4901	-4199.8432
		Brown's gas	-15158.833*	2448.91058	<.001	-22740.2299	-7577.4368
		Hydrogen-oxygen(H2-O2)	-15232.500*	2381.17390	<.001	-22577.2939	-7887.7061
	Brown's gas	Air (N2 + O2)	5189.66667	2230.86499	.172	-1971.5725	12350.9058
		Oxygen-levelled (O2)	15158.8333*	2448.91058	<.001	7577.4368	22740.2299
		Hydrogen-oxygen(H2-O2)	-73.66667	2683.67903	1.000	-8287.0649	8139.7315
	Hydrogen-oxygen(H2-O2)	Air (N2 + O2)	5263.33333	2156.28958	.145	-1615.3049	12141.9715
		Oxygen-levelled (O2)	15232.5000*	2381.17390	<.001	7887.7061	22577.2939
		Brown's gas	73.66667	2683.67903	1.000	-8139.7315	8287.0649

*. The mean difference is significant at the 0.05 level.

Air, Oxygen-levelled, Hydrogen-oxygen mixture and Brown's gas: Neutrophil count analysis

Multiple Comparisons

Games–Howell

Dependent Variable	(I) Treatment	(J) Treatment	Mean Difference (I–J)	Std. Error	Sig.	95% Confidence Interval	
						Lower Bound	Upper Bound
Neutrophil count 0.5 hpa	Air (N2 + O2)	Oxygen–levelled (O2)	.00000	1.19722	1.000	–3.6858	3.6858
		Brown's gas	–1.00000	1.58114	.919	–5.9282	3.9282
		Hydrogen–oxygen(H2–O2)	–.16667	1.07755	.999	–3.5954	3.2621
	Oxygen–levelled (O2)	Air (N2 + O2)	.00000	1.19722	1.000	–3.6858	3.6858
		Brown's gas	–1.00000	1.49443	.906	–5.7665	3.7665
		Hydrogen–oxygen(H2–O2)	–.16667	.94575	.998	–3.1092	2.7758
	Brown's gas	Air (N2 + O2)	1.00000	1.58114	.919	–3.9282	5.9282
		Oxygen–levelled (O2)	1.00000	1.49443	.906	–3.7665	5.7665
		Hydrogen–oxygen(H2–O2)	.83333	1.40040	.930	–3.8348	5.5015
	Hydrogen–oxygen(H2–O2)	Air (N2 + O2)	.16667	1.07755	.999	–3.2621	3.5954
		Oxygen–levelled (O2)	.16667	.94575	.998	–2.7758	3.1092
		Brown's gas	–.83333	1.40040	.930	–5.5015	3.8348
Neutrophil count 3 hpa	Air (N2 + O2)	Oxygen–levelled (O2)	–1.83333	1.90467	.774	–8.1229	4.4563
		Brown's gas	.50000	2.20227	.996	–6.3027	7.3027
		Hydrogen–oxygen(H2–O2)	.66667	2.32618	.991	–6.4635	7.7969
	Oxygen–levelled (O2)	Air (N2 + O2)	1.83333	1.90467	.774	–4.4563	8.1229
		Brown's gas	2.33333	1.58465	.494	–2.7290	7.3957
		Hydrogen–oxygen(H2–O2)	2.50000	1.75278	.521	–3.2039	8.2039
	Brown's gas	Air (N2 + O2)	–.50000	2.20227	.996	–7.3027	6.3027
		Oxygen–levelled (O2)	–2.33333	1.58465	.494	–7.3957	2.7290
		Hydrogen–oxygen(H2–O2)	.16667	2.07230	1.000	–6.1929	6.5262
	Hydrogen–oxygen(H2–O2)	Air (N2 + O2)	–.66667	2.32618	.991	–7.7969	6.4635
		Oxygen–levelled (O2)	–2.50000	1.75278	.521	–8.2039	3.2039
		Brown's gas	–.16667	2.07230	1.000	–6.5262	6.1929
Neutrophil count 24 hpa	Air (N2 + O2)	Oxygen–levelled (O2)	.00000	.78881	1.000	–2.4954	2.4954
		Brown's gas	1.16667	1.03548	.683	–2.0181	4.3514
		Hydrogen–oxygen(H2–O2)	.66667	1.22020	.945	–3.1784	4.5118
	Oxygen–levelled (O2)	Air (N2 + O2)	.00000	.78881	1.000	–2.4954	2.4954
		Brown's gas	1.16667	.89753	.589	–1.7407	4.0740
		Hydrogen–oxygen(H2–O2)	.66667	1.10554	.928	–3.0440	4.3773
	Brown's gas	Air (N2 + O2)	–1.16667	1.03548	.683	–4.3514	2.0181
		Oxygen–levelled (O2)	–1.16667	.89753	.589	–4.0740	1.7407
		Hydrogen–oxygen(H2–O2)	–.50000	1.29314	.979	–4.5010	3.5010
	Hydrogen–oxygen(H2–O2)	Air (N2 + O2)	–.66667	1.22020	.945	–4.5118	3.1784
		Oxygen–levelled (O2)	–.66667	1.10554	.928	–4.3773	3.0440
		Brown's gas	.50000	1.29314	.979	–3.5010	4.5010
Neutrophil count 48 hpa	Air (N2 + O2)	Oxygen–levelled (O2)	.16667	.60093	.992	–1.8111	2.1445
		Brown's gas	1.50000	.85959	.354	–1.1495	4.1495
		Hydrogen–oxygen(H2–O2)	1.16667	.79232	.487	–1.2590	3.5924
	Oxygen–levelled (O2)	Air (N2 + O2)	–.16667	.60093	.992	–2.1445	1.8111
		Brown's gas	1.33333	.71492	.327	–1.0859	3.7526
		Hydrogen–oxygen(H2–O2)	1.00000	.63246	.446	–1.0997	3.0997
	Brown's gas	Air (N2 + O2)	–1.50000	.85959	.354	–4.1495	1.1495
		Oxygen–levelled (O2)	–1.33333	.71492	.327	–3.7526	1.0859
		Hydrogen–oxygen(H2–O2)	–.33333	.88192	.981	–3.0414	2.3748
	Hydrogen–oxygen(H2–O2)	Air (N2 + O2)	–1.16667	.79232	.487	–3.5924	1.2590
		Oxygen–levelled (O2)	–1.00000	.63246	.446	–3.0997	1.0997
		Brown's gas	.33333	.88192	.981	–2.3748	3.0414

Untreated, Tesla oscillator and WLAN: Intact and Amputated fin growth analysis

Multiple Comparisons

Games-Howell

Dependent Variable	(I) Treatment	(J) Treatment	Mean Difference (I–J)	Std. Error	Sig.	95% Confidence Interval	
						Lower Bound	Upper Bound
Intact–fin (Fin area difference (µm^2))	Control (Untreated)	Tesla Oscillator (Sine wave)	7792.600*	2163.042	.017	1610.68	13974.52
		WLAN (Pulse wave)	275.600	2236.735	.992	–6117.58	6668.78
	Tesla Oscillator (Sine wave)	Control (Untreated)	–7792.600*	2163.042	.017	–13974.52	–1610.68
		WLAN (Pulse wave)	–7517.000*	2205.417	.023	–13824.73	–1209.27
	WLAN (Pulse wave)	Control (Untreated)	–275.600	2236.735	.992	–6668.78	6117.58
		Tesla Oscillator (Sine wave)	7517.000*	2205.417	.023	1209.27	13824.73
Amputated–fin (Fin area difference (µm^2))	Control (Untreated)	Tesla Oscillator (Sine wave)	5422.40000	2759.03771	.183	–2465.9203	13310.7203
		WLAN (Pulse wave)	–204.60000	3298.38168	.998	–9858.0405	9448.8405
	Tesla Oscillator (Sine wave)	Control (Untreated)	–5422.40000	2759.03771	.183	–13310.7203	2465.9203
		WLAN (Pulse wave)	–5627.00000	3358.17711	.276	–15394.0262	4140.0262
	WLAN (Pulse wave)	Control (Untreated)	204.60000	3298.38168	.998	–9448.8405	9858.0405
		Tesla Oscillator (Sine wave)	5627.00000	3358.17711	.276	–4140.0262	15394.0262

*. The mean difference is significant at the 0.05 level.

Untreated, Tesla oscillator and WLAN: Neutrophil count analysis

Multiple Comparisons

Games-Howell

Dependent Variable	(I) Treatment	(J) Treatment	Mean Difference (I–J)	Std. Error	Sig.	95% Confidence Interval	
						Lower Bound	Upper Bound
Neutrophil count 0.5 hpa	Control (Untreated)	Tesla Oscillator (Sine wave)	–.64800	1.52894	.907	–5.0890	3.7930
		WLAN (Pulse wave)	–1.10200	1.52127	.757	–5.5276	3.3236
	Tesla Oscillator (Sine wave)	Control (Untreated)	.64800	1.52894	.907	–3.7930	5.0890
		WLAN (Pulse wave)	–.45400	1.28937	.934	–4.1384	3.2304
	WLAN (Pulse wave)	Control (Untreated)	1.10200	1.52127	.757	–3.3236	5.5276
		Tesla Oscillator (Sine wave)	.45400	1.28937	.934	–3.2304	4.1384
Neutrophil count 3 hpa	Control (Untreated)	Tesla Oscillator (Sine wave)	–7.74200*	1.64619	.004	–12.4470	–3.0370
		WLAN (Pulse wave)	–2.11400	1.56862	.411	–6.6144	2.3864
	Tesla Oscillator (Sine wave)	Control (Untreated)	7.74200*	1.64619	.004	3.0370	12.4470
		WLAN (Pulse wave)	5.62800*	1.53898	.016	1.2202	10.0358
	WLAN (Pulse wave)	Control (Untreated)	2.11400	1.56862	.411	–2.3864	6.6144
		Tesla Oscillator (Sine wave)	–5.62800*	1.53898	.016	–10.0358	–1.2202
Neutrophil count 24 hpa	Control (Untreated)	Tesla Oscillator (Sine wave)	–1.82600	3.66284	.874	–12.5865	8.9345
		WLAN (Pulse wave)	.95200	3.25279	.954	–9.4662	11.3702
	Tesla Oscillator (Sine wave)	Control (Untreated)	1.82600	3.66284	.874	–8.9345	12.5865
		WLAN (Pulse wave)	2.77800	2.39195	.513	–4.4233	9.9793
	WLAN (Pulse wave)	Control (Untreated)	–.95200	3.25279	.954	–11.3702	9.4662
		Tesla Oscillator (Sine wave)	–2.77800	2.39195	.513	–9.9793	4.4233
Neutrophil count 48 hpa	Control (Untreated)	Tesla Oscillator (Sine wave)	–1.44600	2.10099	.777	–7.5252	4.6332
		WLAN (Pulse wave)	.50200	1.84605	.960	–5.2122	6.2162
	Tesla Oscillator (Sine wave)	Control (Untreated)	1.44600	2.10099	.777	–4.6332	7.5252
		WLAN (Pulse wave)	1.94800	1.52669	.452	–2.5902	6.4862
	WLAN (Pulse wave)	Control (Untreated)	–.50200	1.84605	.960	–6.2162	5.2122
		Tesla Oscillator (Sine wave)	–1.94800	1.52669	.452	–6.4862	2.5902

*. The mean difference is significant at the 0.05 level.